UNIVERSITE DE LIMOGES

ECOLE DOCTORALE Biologie - Santé

FACULTE DE PHARMACIE

Laboratoire de Chimie des Substances Naturelles EA1069

Thèse

pour obtenir le grade de

DOCTEUR DE L'UNIVERSITÉ DE LIMOGES

Discipline / Spécialité : Chimie Théorique

présentée et soutenue par

Florent DI MEO

le 27 Novembre 2012

Molecular and supramolecular highlights on reactivity and optoelectronics of natural polyphenols

JURY :

Rapporteurs
    Pr. Juan Carlos SANCHO-GARCIA   Universidad de Alicante, España
    Dr. Jérôme CORNIL   Université de Mons, Belgique
Examinateurs
    Pr. Olivier DANGLES   Université d'Avignon, France
    Pr. Jean-Luc DUROUX   (Directeur de thèse)   Université de Limoges, France
    Dr. Patrick TROUILLAS   (Directeur de thèse)   Université de Limoges, France
    Dr. Roberto IMPROTA   Instituto Biostrutture e Bioimmagini - CNR, Napoli Italia

Membre invité
    Dr. Christophe Hano   Université d'Orléans, France

A Sandrine,

Grand-Mère, Grand-Père, Pépé et Henri

Remerciements

Ce travail a été effectué dans l'équipe de Biophysique de la Faculté de Pharmacie de Limoges appartenant au Laboratoire de Chimie des Substances Naturelles (LCSN) – EA1069. Le financement de cette thèse a été assuré par la Région Limousin, l'ex-EA4021, l'EA1069, COST et l'AVRUL.

Je tiens tout d'abord à remercier le Pr. **Jean-Luc Duroux** pour m'avoir accueilli au sein de son laboratoire. Je tiens à lui exprimer toute ma gratitude pour sa disponibilité, sa compréhension. Merci pour m'avoir fourni un cadre idéal pour l'ensemble de mes études ainsi que pour la codirection de cette présente thèse.

Des remerciements particuliers et non sans-émotions vont au Dr. **Patrick Trouillas**. Comme je l'ai précisé il y a trois ans dans un autre manuscrit, sa patience, sa générosité, sa disponibilité, sa gentillesse et sa compréhension (non, il n'y pas de « rayer la mention inutile ») m'ont permis de prendre confiance en moi. Toutes ses qualités humaines ont été un plus loin d'être négligeable dans l'accomplissement personnel de cette thèse. Son expertise scientifique et sa volonté de toujours comprendre les phénomènes dans leur ensemble m'ont toujours permis de garder un pied sur terre et de ne pas tomber dans les méandres d'un calcul CCSDT/CBS (Oui, oui, sans perturbation sur les triples !) sur un protéine en solvant explicite. Voilà des années que j'ai eu la chance de travailler avec toi. Quand je fais un bilan, j'estime avoir été extrêmement chanceux d'avoir eu un codirecteur de thèse comme toi, car en tant d'années, les accrochages de la vie se comptent uniquement sur les doigts d'une main, ce qui est quand même exceptionnel compte tenu de mon caractère ! Une reconnaissance qui perdura tout au long de ma carrière (d'éleveur de chèvres en Patagonie), et un Bravo pour m'avoir supporté. Je n'ai pas de mot assez fort et assez complet pour t'exprimer le respect et la reconnaissance que j'ai pour toi.

Mi más sincero agradecimiento a Pr. **Juan Carlos Sancho García** (Universidad de Alicante, España) por aceptar revisar esta tesis. Así como un enorme agradecimiento por la invitación y bienvenida al laboratorio de investigación en Química Cuántica de la Universidad de Alicante. Agradezco infinitamente por su ejemplo, sus consejos, su asistencia y principalmente su bondad. Además, mi última visita a Alicante me permitió mantener mi chancletas un mes más!

Je tiens également à sincèrement remercier Dr. **Jérôme Cornil** (Université de Mons, Belgique) pour avoir accepté d'être rapporteur de ces travaux de thèse. Je tiens également à vous exprimer ma gratitude pour vos conseils, votre soutien scientifique depuis le début du projet cinétique. (je tiens à rajouter également les deux mots « Nonante » et « Septante » pour montrer que ce paragraphe est écrit en Belge).

Je tiens à remercier le Pr. **Olivier Dangles** (Université d'Avignon, France) pour avoir accepté de juger les présents travaux de thèse. C'est un honneur pour moi de vous avoir dans mon jury. Je tiens à vous remercier d'avoir toujours apporté cet œil d'expérimentateur lors de nos projets collaboratifs.

Ringrazio il Dr. **Roberto Improta** (IBB-CNR, Napoli, ITALIA). È un onore avervi sul mio giuria e vi ringrazio di cuore di giudicare il mio lavoro di tesi.

Je remercie également Dr. **Christophe Hano** pour avoir accepté d'assister à cette thèse et de la juger en tant que membre invité.

Je tiens à sincèrement remercier le Pr. **Roberto Lazzaroni** (Université de Mons, Belgique) pour m'avoir toujours accueilli à bras ouverts au sein de son laboratoire et avoir toujours

apporté votre expertise scientifique dans nos projets. Vous avez été mon premier contact avec la « collaboration scientifique » et je me souviens encore l'accueil chaleureux, humain. Premier contact qui m'a également permis de m'initier aux joies de la bière belge, et ça, ça n'a pas de prix. Merci du fond du cœur. (« Nonante » et « septante » doivent une nouvelle fois apparaître).

Je tiens ensuite à remercier tous les membres du Laboratoire de Biophysique, ses anciens et ses invités permanents. Parmi eux, merci au Dr. **Claude Calliste** pour votre gentillesse, votre bonne humeur durant toutes ses années. Merci au Dr. **Serge Battu** pour votre objectivité, votre humour et votre soutien durant toutes mes longues études. Je tiens à remercier particulièrement le (depuis peu) Dr. **Gabin Fabre**, notre nouveau doctorant. Tu m'as tiré vers le haut grâce à ta capacité de recul, ta gentillesse et ta soif d'apprendre. J'ai particulièrement apprécié nos discussions scientifiques, informatiques et « geeks ». Un énorme merci à toi. Je tiens également à encourager et remercier **Imene** pour ton courage et ton aide apportée lors de la relecture. De sincères remerciements vont à **Thomas** (ainsi qu'à **Claire** et **Colin** en même temps !) pour avoir été là pour m'aider en tant que collègue et ami. Merci également au Dr. **El Hassane Anouar** et Dr. **Pavlina Kosinova** (les anciens). Merci à **Nicolas** pour ton aide à la recherche de coquilles. Merci notamment à **Gaelle** pour ces petites madeleines et autres recettes toujours appréciées !

Mes remerciements vont à l'ensemble de l'équipe EA1069 et ses membres. Des remerciements particuliers **Lamia** et ton soutien sans faille et ses moments d'humanité, pour **PH**, **PAF** et **Benj** pour ces bons moments passés ensemble, notamment à Egletons (*NB :* moment un peu plus court le premier soir pour PH… on se comprend…).

Je tiens également à remercier tous mes collègues et amis de la pause café sur le parvis de la Faculté *i.e.*, **Youn'** (surtout quand on discute avec convictions), **Pierre** (que j'aime les pauses café à 13h30 en été), **Steph'** (le reproducteur), **Laurent**, **Nico**, **Aurore**, **Marcela**, **Ludo**, **Elodie**, **Barbara** (pas les oreilles, non pas les oreilles, par contre, la tête tu peux), **Mathilde, Yohann, Thomas, Hussein, Bassel** et ceux que j'ai oublié en écrivant ces remerciements (Je m'en excuse, il est tard).

Merci à toute l'équipe de l'UMONS, anciens ou non pour leur accueil fantastique, notamment **Maxime**, **Claire**, **Mike** et **Chinh**. Un grand merci à **Vincent** et **Yohann** pour leur aide et leurs conseils (alors, on l'a finalement eu ce λ_s - Cf Chapitre III).

Grazie al Pr. **Osvaldo Failla** (Universita degli studi Milano) per il suo aiuto sull'evoluzione delle piante (Capitolo I).

Je tiens à remercier de tout mon cœur ma Famille. Je tiens à exprimer ma reconnaissance à **mes parents**. Qui aurait cru, il y a 12 ans de cela, que je ferai deux thèses ! Cependant, vous avez toujours été là, vous m'avez toujours soutenu malgré mon caractère ! Cette thèse est pour moi une facon de vous remercier pour tout ce que vous m'avez apporté jusque-là, et, malheureusement pour vous, ce n'est pas encore fini. Je tiens également à remercier ma sœur **Chrystel** (oui, je sais l'écrire), mon frère **Alain-Nicolas** et mon cousin **Thierry**, pour votre écoute et votre soutien inconditionnel. Merci à **Emilie** pour avoir supporté un an de vie commune en espérant qu'elle ne soit pas traumatisée à vie. Je tiens également à remercier également mes oncles et tantes **Michèle** (planteur, planteur !), **Nadia**, **Patricia**, **Jacky**, **Jean-Philippe** et **Bruno** ainsi que mes cousins **Aurélien** et **Ludivine**.

J'en profite également pour remercier, même si ils en ont et n'en auront jamais conscience, l'ensemble de mes neveux et nièces qui ont réussi à me faire tout oublier quand je les voyais seulement me sourire, **Timothée**, **Téo**, **Lilia** et **Evelie**.

Merci également à tous ceux qui m'ont toujours soutenu. Une mention spéciale pour les plows-naab **Alexis** et **Pierrot**, ainsi qu'à **Rémi** pour votre écoute, pour avoir toujours été là quand vous le pouviez.

Grazie a **Luca** per il tuo aiuto! Gracias a **Omar** por tu ayuda!

Come si dice in francese, la migliora por ultima. Un ringraziamento speciale a te, **Laura**, per avermi sostenuto nonostante le mie nevrosi e paure, cercando di aiutarmi come meglio era possibile. Posso vedere che 1000 km non sono sufficienti a scoraggiarti. Grazie mille.

Acronyms

AF	Adduct formation
ASC	Apparent Surface Charge
ATP	Adenosine triphosphate
CASPT2	Complete Active Space Second Perturbation Theory
CASSCF	Complete Active Space Self Consistent Field
C-atom	Carbon atom
CC	Coupled Cluster
CC2	Second-order approximate coupled cluster singles and doubles
CD	Circular Dichroism
CI	Configuration Interaction
COSMO	COnductor-like Screening Model
CPD	Cyclobutane Pyrimidine Dimers
CT	Charge Transfer
DFT	Density Functional Theory
DFT-D	Dispersion-corrected DFT
DNA	DesoxyriboNucleic Acid
ES	Excited State
ES-CT	Excited State Charge Transfer
GB	Generalized Born
GEA	Gradient Expansion Approximation
GS	Ground State
GS-CT	Ground State Charge Transfer
HAT	H-Atom Transfer
H-atom	Hydrogen atom
HF	Hartree-Fock
HK	Hohenberg-Kohn
HOMO	Highest Occupied Molecular Orbital
IEFPCM	Integral Equation Formalism Polarizable Continuum Model
INDO	Intermediate Neglect of Differential Overlap
IP	Ionization Potential
IR	Infrared
KS	Kohn-Sham
l.h.s.	left hand side
LCAO	Linear Combination of Atomic Orbital
LDA	Local Density Approximation
LSDA	Local Spin Density Approximation
LUMO	Lowest Unoccupied Molecular Orbital
MI	Molecular Interaction
MO	Molecular Orbital
MP	Møller-Plesset
MP1	First-Order Møller-Plesset
MP2	Second-Order Møller-Plesset

MP3	Third-Order Møller-Plesset
MP4	Fourth-Order Møller-Plesset
MPE	Multipole Expansion
N-atom	Nitrogen atom
NMR	Nuclear Magnetic Resonance
O-atom	Oxigen atom
PA	pyrrazolidine alkaloids
PCET	Proton-Coupled Electron Transfer
PCM	Polarizable Continuum Model
PT	Perturbation Theory
r.h.s.	right hand side
RNS	Reactive Nitrogen Species
ROS	Reactive Oxygen Species
SCF	Self Consistent Field
SCRF	Self-Consistent Reaction Field
SCS	Spin-component-scaled
SIC	Self-Interaction Correction
SIE	Self-Interaction Error
SOD	SuperOxide Dismutase
SOMO	Single Occupied Molecular Orbital
SOS	Scaled-Opposite-Spin
SS-PCM	State-Specific Polarizable Continuum Model
TCA	Tricarboxylic acid
TD	Time Dependent
TD-DFT	Time Dependent Density Functional Theory
UEG	Uniform Electron Gas
UV	Ultraviolet
UV/Vis	Ultraviolet/Visible
Vis	Visible
XC	Exchange-Correlation
ZINDO	Zerner's Intermediate Neglect of Differential Overlap

Contents

8

Introduction

Nature, mainly plants, has provided a fantastic "armamentarium" of natural drugs for animals and human. Most of the current drugs originate from plant metabolites (*e.g.*, aspirin, paclitaxel, bromocryptine). Starting from natural compounds pharmaceutical companies have developed new powerful derivatives and it seems that they abandoned the search for new natural drugs. Due to the numerous potential biological activities of plants, academic groups efficiently continue this research.

Among natural compounds, polyphenols (*e.g.*, flavonoids, stilbenoids, lignans and depsides) are powerful antioxidants. Some of them efficiently protect against oxidative stress and the UV aggressions are also responsible for *e.g.*, liver and cardiac diseases, cancers or Alzheimer's disease. Being widely distributed in fruit (*e.g.*, apples, kiwis and grapes), vegetables (*e.g.*, tomatoes, broccoli and onions), spices (*e.g.*, curcumins, paprika and cacao) and beverages (*e.g.*, wine, tea and beers), they are of major importance in human diets, together with vitamins.

Due to their π-conjugated system, polyphenols absorb UV-visible light and some of them are responsible for plant colours. The UV light absorption capacity, together with the antioxidant capacity, make polyphenols good candidate as UV-screen and anti-age agents. For several reasons, the interest of cosmological companies is still rather limited, making this field of research very prospective and wide open for future developments. Due to their visible light absorption properties, some polyphenols are responsible for plant colours (*e.g.*, blue to purple in berries, grape and flowers). This property is highly related to organoleptic properties so it is important for food industries, being the first feelings of consumers. They are of course responsible for visual appeal but may also influence the other senses, mainly taste. The different colours of polyphenols are attributed to single molecules or interacting complexes (copigmentation).

In parallel to the numerous industrial developments in the field of polyphenols, a deep understanding of their behaviours has been the subject of numerous fundamental studies. In this quest for finding new molecules and rationalizing their biological activities, theoretical chemistry has recently appeared as a powerful tool to support, and even predict, experimental data.

Theoretical chemistry allows understanding biological, physical and chemical phenomena at the atomic scale. It provides electronic and molecular orbital pictures for a deep understanding of the processes. All new innovations related with supercomputers together with intensive improvements of theoretical models have significantly broadened the fields of investigation for theoretical chemistry.

The present work is a theoretical study of the two main properties of polyphenols, namely (i) UV-visible absorption properties and the corresponding pigmentation and copigmentation, and (ii) antioxidant properties and all relative oxidative processes.

Chapter I presents plants as a machinery to produce natural compounds. Section A is a brief overview of the plant armamentarium (*i.e.*, second metabolites including polyphenols, terpenoids and alkaloids). Section B discusses on the plant response to sunlight, mainly focusing on pigmentation. Section C carefully defines oxidative stress and the natural antioxidants.

Chapter II aims at describing the basic concepts of quantum chemistry methods used in this PhD. Section A is a reminding on the Hartree-Fock model and further improvements are detailed including Møller-Plesset and coupled-cluster methods. Section B describes basements and refinements of density functional theory (DFT). The last section describes electronic spectroscopy from the physical-chemistry point of view; the time-dependent DFT framework is briefly discussed.

Chapter III presents the theoretical results related to the UV-visible properties of polyphenols. The UV-visible absorption causes electronic transition from the ground state to excited states. Based on a joint experimental and theoretical study (Section A), this capacity to absorb UV-visible light is discussed for a series of single polyphenols extracted from lichens. In Section B, a theoretical methodology is proposed to fully rationalize the copigmentation process for a model system, namely anthocyanin:flavonol, in which the former partner is the pigment and the latter is the copigment. Section C is an extrapolation of this methodology to larger and more realistic copigmentation systems; this theoretical study supports the experimental work performed by a group dealing with grape and wine pigments in Porto.

Chapter IV deals with oxidative processes. An antioxidant is efficient if (i) it efficiently decreases the oxidative stress and (ii) it is "inactive" after the reaction. The efficiency has been widely studied in the literature and in our group from the thermodynamic point of view. However, the theoretical viewpoint of free-radical-scavenging kinetics is not fully elucidated yet (and appears challenging!). Section A presents theoretical methods aiming at rationalizing the physico-chemical parameters of free radical scavenging kinetics. All mechanisms of action are discussed in details. After the free-radical-scavenging action, natural compounds may lead to original compounds by oxidative coupling. In collaboration with a Malaysian group, the oxidative coupling of stilbenoids is discussed from a theoretical study, supporting experimental observations already published (Section B). Again, in this case, the quantum methodology appears crucial.

Chapter I. Nature, a fantastic machinery to create original compounds

"Nature" comes from the Latin "*natura*" which means "essential qualities, innate dispositions", but this word has several meanings. The broadest sense refers to the physical world, our universe, going from subatomic to astronomical scales. It encompasses things and beings, *i.e.* reality.

To most people, "Nature" refers to the non-human world, especially plants. Plants are eukaryotic multicellular organisms, being able to use light for the synthesis of organic compounds and production of energy (namely photosynthesis). The almost infinite variety of natural compounds increases the capacity of plants to adapt to their environment.

Despite a growing scientific interest for natural compounds their roles and mechanisms of action still requires gaining into knowledge. The huge diversity of their chemical structures allows a broad range of biological activities in cells (*i.e.*, plant, insect and human cells). There exist naturally-derived drugs (*e.g.*, morphine, bromocryptine) which are widely used in human medicine, however the lack of knowledge concerning their mechanisms of action is a limiting factor for their extensive development.

Section A. Plant chemistry: how can Nature create original compounds?

Organisms are classified into different kingdoms. Originally, in ancient Greece, Aristotle separated all living things into plants and animals. The former referred to all the organisms having motion too slow for human sight. Later, this simple classification of plants appeared not accurate enough because many organisms unrelated to modern plants were included in the plant kingdom such as fungi.

At the beginning of the XXth century, the plant kingdom was divided into three groups: i) cyanobacteria which are prokaryotic organisms (cell without nucleus) capable of photosynthesis, ii) thallophytic organisms including algae, fungi and lichens and iii) cormophytes or evolved plants. This definition was then revised so that fungi have been excluded and have been classified in their own kingdom.[1]

Cyanobacteria are plant precursors; they appeared on Earth 3.8 billion years ago. They were the first organisms able to use light to produce energy through photosynthesis. Their cells are prokaryotic (*i.e.,* without nucleus) and photosynthesis occurs directly in the cytoplasm.

Plants have always evolved and adapted to abiotic or biotic aggressions. The former include all physical phenomena (*e.g.* temperature, light, pressure) whereas the latter refer to organisms living with or against plants (*e.g.*, fungi, herbivores, insects). The most important changes occurred when the ancestral aquatic plants left seas and oceans about 510 million ago and became land plants. Self-evolution occurred but also the symbiosis with fungi had participated in the adaptation to this new environment.

The plant evolution is due to the ability of plants to alter their physiology and/or morphology in response to changes in environmental conditions. As a consequence, they continuously produced new metabolites, increasing adaptability. Photosynthesis originates plant metabolism since it allows the synthesis of organic compounds. This process transforms carbon dioxide (CO_2) into organic compounds using "chemical energy". It also requires water, *e.g.* to incorporate hydrogen atoms.

When submitted to light, water is transformed into dioxygen and energy (Eq. (I.1a)).

$$H_2O \rightarrow O_2 + \text{Chemical Energy } (NADH, H^+ - NADPH_2) \qquad (I.1a)$$
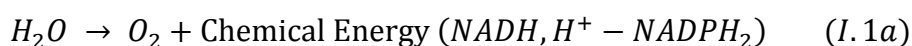
Organisms are able to store and transfer energy *e.g.*, via bond formation and bond cleavage. For example, this energy is used to transform CO_2 into sugar during photosynthesis (Eq. (I.1b)).

$$CO_2 + \text{Chemical Energy} \rightarrow C_6H_{12}O_6 + H_2O \quad (I.1b)$$
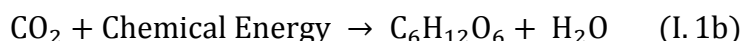
This process produces the very first primary metabolites (*e.g.*, sugars and amino-acids), which in turn enter into the machinery which produce secondary metabolites, so-called because they are biosynthesized using primary metabolites. The huge diversity of chemical structures (more than one hundred thousand[2]) emphasizes the impressive number of protective and adaptive functions.[3]

1. Primary metabolites essential for life

Dewick defines the primary metabolism as "the pathways for generally modifying and synthesising carbohydrates, proteins, fats, and nucleic acids found to be essentially the same in all organisms apart from minor variations".[4] It produces metabolites that are vital to sustain life including carbohydrates, amino-acids and lipids.[5]

1.1. Carbohydrates

Carbohydrates are universally present in organisms. Their chemical structure is made of tetrahydropyrane or tetrahydrofurane moieties substituted by many alcohol groups.

1.1.1. A brief overview of carbohydrates

These compounds are simple carbohydrates or polymers. Glucose (see Fig. I.1) is the firstly formed and the most important simple carbohydrate in plants. Its biosynthesis is possible thanks to the biotransformation of carbon dioxide and water by photosynthesis (Eqs. (I.1b)). It is widely distributed in its native form as a series of different isomers[1] (*e.g.* fructose, mannose, galactose). Some carbohydrates are universal and present in all plants (*e.g.* D-glucose, see Fig.

---

[1] Chemical structures of simple carbohydrates mainly differ by their (i) heterocyclic structure (*i.e.*, pyranne of furanne) and the stereochemistry of chiral carbons

I.1a) whereas others are specific to a plant family (*e.g.* fructose mainly isolated from fruit-bearing plants, see Fig. I.1b).

(a)   (b)
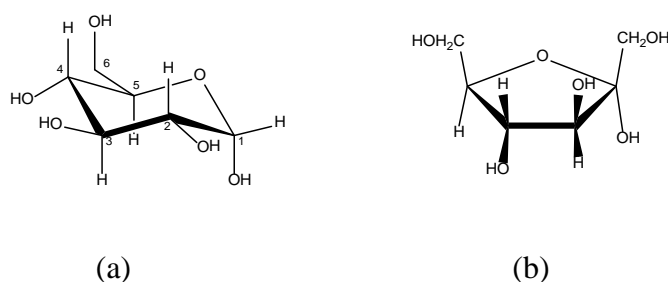
Figure I.1. Structure of (a) α-glucose and (b) α-fructose

Carbohydrate polymers may also exist. Whatever their chemical structure, there are always originated from glucose. The polymers are divided into two subgroups depending on whether they are bound to non-carbohydrate compounds or not. Different glucose polymers can be described depending on (i) their stereochemistry, (ii) the position of the inter-glycosidic bond, (iii) their size and (iv) fork positions. The biological and chemical properties of these polymers may be totally different even if they are all constituted by glucose moieties. For example, amylum and cellulose differ mainly by the stereochemistry of atom C1 (Fig. I.1a). The former is the natural substrate of digestive human enzymes (*e.g.* amylase) whereas the latter resists the entire human digestive process. This resistance is used by nutritionists since it allows equilibrating digestive cycles (lengthening the short intestinal transit or shortening the long one).

Disaccharides are also widely observed in plants. Sucrose is the best known disaccharide, especially among children. Isolated mainly from *Beta vulgaris* L. or *Saccharum officinarum* L., it is widely used to sweeten food.

Carbohydrates are vital for living cells; they provide energy to cells by different chemical transformations. This process is performed by the biological machinery involving proteins, enzymes and complex chemical reactions such as glycolysis or the Krebs cycle. Glucose is a direct substrate whereas polysaccharides are sugar stored in cells.

Carbohydrates are also important as they are often bound to secondary metabolites, which deeply modify their electronic, chemical and biological properties. Some of these complexes, so-called glycosides are discussed in the manuscript.

1.1.2. Importance in secondary metabolism: synthesis of pyruvate

Carbohydrates originate other primary metabolites (amino acids) and all secondary metabolites. Glucose or more generally carbohydrate metabolism (glycolysis) provides all compounds required for their biosynthesis *e.g.*, pyruvate.[6, 7]

Pyruvate provides shikimate using the pentose-P pathway. Shikimate then can be transformed into either aminoacids or polyphenols (Fig. I.2). Pyruvate is also the source of terpenoids either after condensation with another glycolysis metabolite (glyceraldehyde-3-phosphate) or after its transformation into acetylCoA. This compound is as important as pyruvate since it may provide (i) alkaloids using the tricarboxylic acid (TCA) cycle, (ii) terpenoids and (iii) polyphenols after condensation in polyacetates or (iv) amino acids using the Krebs cycle (Fig. I.2).[7]
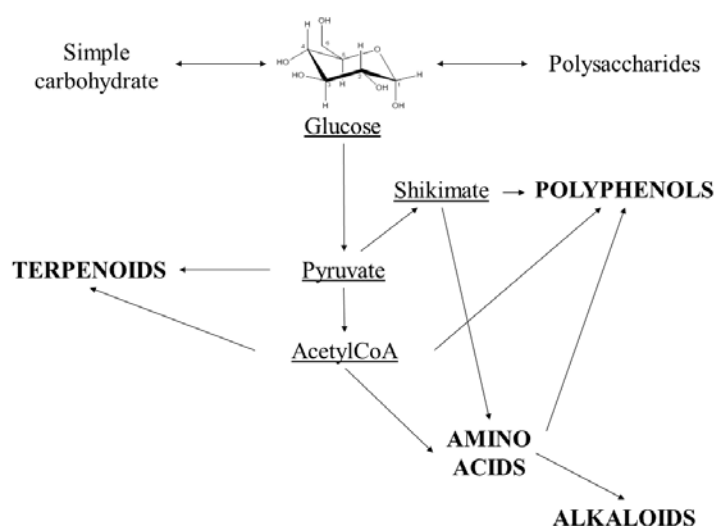
Figure I.2. Importance of glucose in plant secondary metabolism[2]

1.2. Amino acids

Amino acids are chemically described by the presence of both carboxylic and amine moieties. There exist more than three hundred different amino acids in the plant kingdom.

---

[2] Further information about chemical process are available in refs 5 and 6.

1.2.1. Standard amino acids

Only twenty two are so-called standard or proteinogenic amino acids since they are the main constituents of proteins or peptides.[8] Carboxylic and amine moieties are bound to the same carbon implying a chiral centre except for the simplest one, *i.e.* glycine (Fig. I.3). Concerning protein constitution, amino acids belong mainly to the so-called L-group[3].

Standard amino acids can be divided depending on the chemical properties of the side chain. The side chain can be aromatic (*e.g.* phenylalanine, tryptophan), acidic (*e.g.* glutamate), cyclic (*e.g.* prolin) or aliphatic (*e.g.* isoleucine, (Fig I.3)). The protein structure and properties strongly depend on the proportion of a particular type of amino acids. For example, amino acids that are H-bond donors or acceptors are often observed in α-helix substructures of proteins.[8]

Some of amino acids are so-called essential because the human body is not able to synthesize them and are only issued from diet including plant food.

Standard amino acids in plants come from the pyruvate metabolism. Shikimate can be transformed into chorismate which provides aromatic amino acids (*i.e.* tryptophan, tyrosine and phenylalanine). Other amino acids come from the transformation of acetylCoA through the classical and well-known Krebs cycle[4].[6, 7]

Beside the structure of proteins, amino acids allow the formation of specific secondary metabolites. Aromatic amino acids can be chemically and enzymatically modified into polyphenols such as coumarins or quinonic compounds. Alkaloids mainly come from amino acids.

---

[3] The L-group refers to Fisher's representation which implies the amino moiety on the left.

[4] The Krebs cycle is obviously well-known and well-described by biologists.
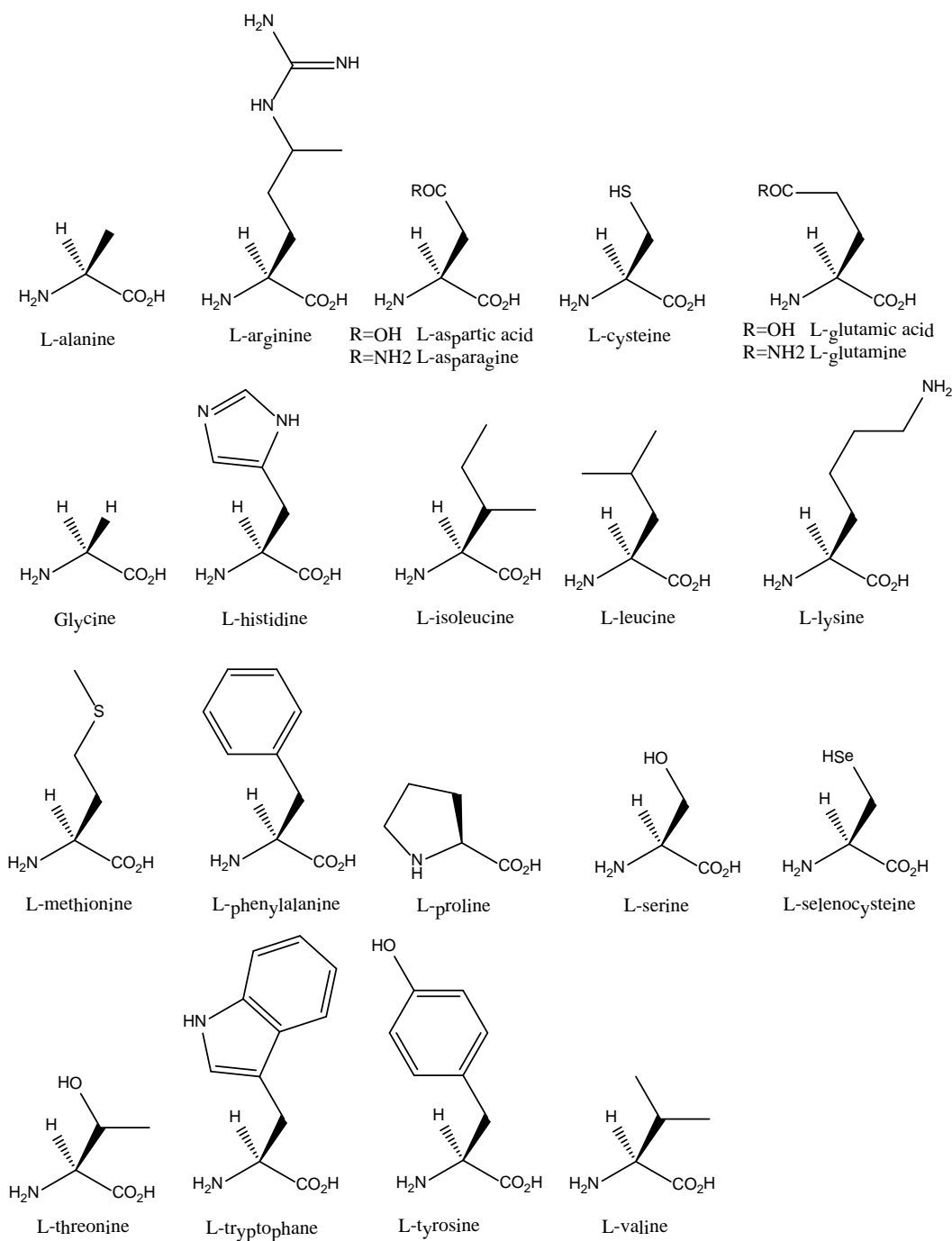
Figure I.3. Important amino acids

1.2.2. Non-standard amino acids

Non-standard amino acids are original compounds produced by plants that are not considered as secondary metabolites since they are close enough to the amino acid structure. They mostly derive from standard amino acids. Cysteine derivatives are often isolated from Brassicaceae (*e.g.* cysteine sulfoxide analogues). The presence of selenium in plants allows the

formation of selenium amino acid derivatives. Some original structures are also observed in plants such as aliphatic cyclic amino acid derived or not from proline.

The role of these compounds is still under debate. Different hypotheses propose to better understand the reasons for their biosynthesis. High toxicity in predator organism is often highlighted, which thus implies that their biosynthesis is an evolution against predators. They are also accumulated in seeds, suggesting nitrogen storage. They may also participate in the preservation of the species since they can inhibit germination of other flower species.

2. Secondary metabolites

Secondary metabolites are mainly divided into three groups according to their chemical structures and biosynthesis: (i) polyphenols, (ii) terpenoids and (iii) alkaloids. The huge diversity of these groups prevents from an exhaustive description of their synthesis, chemical structures and properties. This manuscript aims at giving an overview of the origin of secondary metabolites, mainly focusing on polyphenols.

2.1. Polyphenols

Polyphenols have become popular and well-known compounds in particular for their healthy properties, which are used as commercial promotion (*e.g.* tea, wines, fruit juices rich in polyphenols, anti-wrinkle creams). However it must be stressed that they constitute a large family of compounds. They exhibits many properties, e.g., being either healthy or toxic, some of them being coloured or others colourless, glycosides or aglycones, small or big… Here we propose to briefly introduce their chemical structures, distribution and role in plants

2.1.1. A simple chemical structure for a huge diversity of compounds

Polyphenols are organic compounds possessing at least one phenol moiety in their chemical structures. Depending on their chemical skeleton and substitution, they belong to different sub-classes including simple phenols, phenolic acids, flavonoids, stilbenoids, coumarins, depsidoids and lignanes.

They are also defined according to their biosynthesis. They are formed from two main biochemical pathways: the (i) shikimate and (ii) polyacetate pathways. These two biosynthetic

pathways differ from the chemical reactions and enzymes, subsequently providing different structures of polyphenols.[7]

(i)   The shikimate pathway is common to the synthesis of some amino acids (*e.g.* tyrosine, phenylalanine and tryptophane). It starts from the 4-phosphoerythrose and phosphoenolpyruvate Claisen-type condensation. Then, shikimate is formed using multiple enzymatic systems (*e.g.* synthase, dehydroquinase). Shikimate is transformed into chorismate, the key molecule of metabolic crossroads, leading to aromatic amino acids, cinnamates, coumarins or quinones (Fig. I.4).

(ii)   The polyacetate pathway is common with the primary metabolism and terpenoid synthesis. Polyphenol formation is possible thanks to the multiple Claisen condensations of activated acetylCoA molecules. Acetate polymers are then cyclized following different ways to yield acylphenols, lactones, chromones, phenolic acids or flavonoids (Fig. I.4).
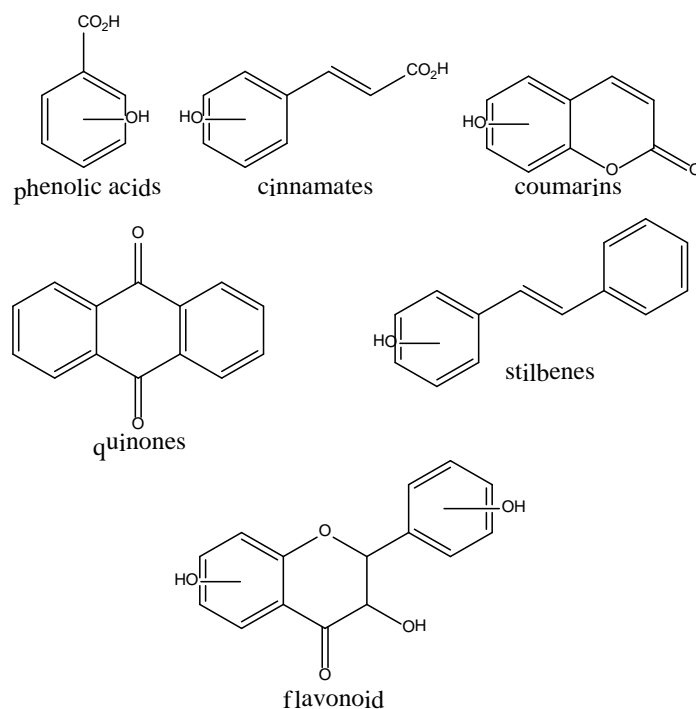
Figure I.4. Examples of polyphenol structures

2.1.2. Variability of distribution

Polyphenols are widely distributed in the plant kingdom. They can be divided into two main categories: (i) water-soluble polyphenols found in plant stems, fruit and roots (ii) fat-soluble polyphenols mainly found in seeds. Over the past decades, polyphenol contents have been widely studied in human diet (Table I.1).

The heterogeneity of polyphenol contents over the plant kingdom is so huge that to draw an exhaustive list is unfeasible. The distribution represents an active field of research based on the isolation, synthesis, characterization, biosynthesis and epigenetic of polyphenols. The variability of the environment, the co-existence with neighbouring organisms and aggression exposure strongly modify polyphenol proportion in *e.g.*, fruit, chocolate and vegetables (Table I.1). The variability of polyphenol distribution in grape wine has been extensively studied.[9, 11]

Table I.1. Polyphenol content in common (a) beverages (mg/100 mL) and (b) foods (mg/100 mg fresh weighted). Data obtained from Ref. 10.

(a)

Beverages		Plant family	Number of compounds	Total polyphenol content	Most important polyphenols (mean content in mg/100 mL)
Beer	*Dark*	-	25	41.6	Vanillic acid (0.17); Isoxanthohumol (0.12); Syringic acid (0.11); Ferulic acid (0.09)
	Blond	-	69	27.83	4-Hydroxybenzoic acid (0.96); Tyrosol (0.32); Feruclic acid (0.26); Gallic acid 3-*O*-gallate (0.26)
Wine	*Red*	Vitaceae	108	215.48	Malvidin 3-*O*-glucoside (9.97); Procyanidin dimer B3 (9.47); Procyanidin dimer B4 (7.29); (+)-Catechin (6.81)
	Rosé	Vitaceae	40	82.21	3-Caffeoylquinic acid (4.08); Gallic acid (1.04); (+)-Catechin (0.91); Hydroxytyrosol (0.61)
	White	Vitaceae	72	32.1	Caffeoyl tartaric acid (2.15); Gentisic acid (1.82); (+)-Catechin (1.08); (-)-Epicatechin (0.95)
Rhum	-	-	6	-	Ellagic acid (0.21); Vanillin (0.08); Gallic acid (0.06); syringaldehyde (0.04)
Chocolate	*Milk*	Sterculiaceae	18	1859.88	(-)-Epicatechin (70.36); Cinnamtannin A2 (53.83); Procyanidin dimer B2 (36.50); Procyanidin trimer C1 (26.00)
Coffee	*Arabica*	Rubiaceae	12	-	Caffeoylquinic acid isomers (62.09); Feruloylquinic acid isomers (17.9); Dicaffeoylquinic acid isomers (7.72); Catechol (0.54)
	Robusta	Rubiaceae	8	-	Caffeoylquinic acid isomers (144.52); Feruloylquinic acid isomers (46.62); Dicaffeoylquinic acid isomers (13.47)
Herb infusion	*German camomile*	Asteraceae	11	22.8	(-)-Epicatechin 3-*O*-gallate (0.78); (-)-Epigallocatechin 3-*O*-gallate (0.78); (+)-gallocatechin 3-*O*-gallate (0.36); (+)-catechin 3-*O*-gallate (0.09)
	Lemon verbena	Verbenaceae	2	-	Verbascoside (39.40); Luteolin 7-*O*-diglucuronide (10.60)
	Peppermint	Lamiaceae	11	30.8	(-)-Epicatechin 3-*O*-gallate (9.24); (+)-catechin 3-*O*-gallate (0.45) (+)-Catechin (0.30); (-)-Epigallocatechin (0.24)
Tea	*Black*	Theaceae	59	104.48	(+)-Gallocatechin (14.01); 5-Galloylquinic acid (11.57); (-)-Epigallocatechin 3-*O*-gallate (9.12) (-)-Epicatechin 3-*O*-gallate (7.34)
	Green	Theaceae	11	61.86	(-)-Epigallocatechin 3-*O*-gallate (27.16); (-)-Epigallocatechin (19.68); 5-Galloylquinic acid (9.41); (-)-Epicatechin (7.93)
	Oolong	Theaceae	15	-	(-)-Epigallocatechin 3-*O*-gallate (17.89); (-)-Epigallocatechin (9.65); (-)-Epicatechin 3-*O*-gallate (4.99); 5-Galloylquinic acid (4.34)

(b)

	Food	Plant family	Number of compounds	Total polyphenol content	Most important polyphenols (mean content in mg/100g FW)
Chocolate	*Dark*	Sterculiaceae	19	-	(-)-Epicatechin (70.36); Cinnamtannin A2 (53.83); Procyanidin dimer B2 (36.50); Procyanidin trimer C1 (26.00)
Fruits	*Black rasperry*	Rosaceae	14	980	Hydroxybenzoic acids (38.00); Quercetin 3-*O*-rutinoside (19.00)
	Blackberry	Rosaceae	88	569.43	Cyanidin glucosides (172.59); Ellagic acid (43.67); (-)-Epicatechin (11.48); Gallic acid (4.67)
	Lemon[5]	Rutaceae	12	59.80	Eriodictyol (17.60); Hesperetin (17.10); Luteolin (1.27); Naringenin (0.55)
	Lime[6]	Rutaceae	7	-	Hesperetin (43.00); Naringenin (3.40); Quercetin (0.40)
	Orange[6]	Rutaceae	18	278.59	Hesperetin (33.60); Naringenin (11.22); Kaempferol (0.10)
Vegetable	*Red chili pepper[6]*	Solanaceae	2	326.39	Quercetin (2.92); Luteolin (1.89)
	Black olive	Oleaceae	43	117.17	Oleuropein aglycon (81.82); Cyanidin 3-*O*-rutinoside (72.35); Oleuropein (72.02); Verbascoside (68.08)
	Cherry tomato[6]	Solanaceae	12	-	5-Caffeoylquinic acid (3.74); Quercetin 3-*O*-rutinoside (3.33); Keampferol (0.007); Quercetin (0.0005)
	Red onions	Alliaceae	22	-	Quercetin glucosides (150.07); Delphinidin 3-glocusyl-glucoside (43.71); Isorhamnetin 4'-*O*-glucoside (6.00); Protocatechuic acid (2.00)

2.1.3. Role of polyphenols in plant from the co-evolution point of view

The huge chemical diversity of polyphenols is responsible for a wide range of roles in plants, most of them being not fully elucidated.

(a)   (b)
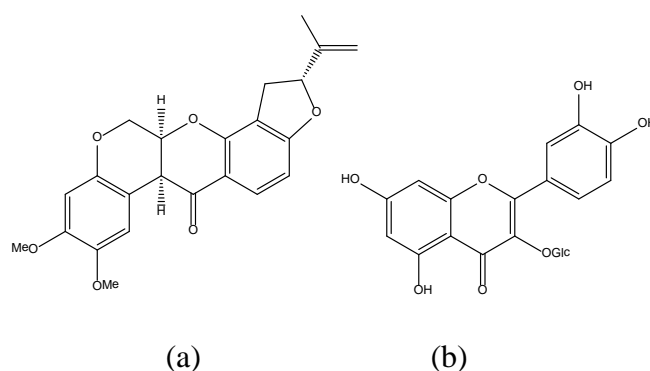
Figure I.5. Structure of (a) rotenone and (b) quercetin 3-*O*-glucoside

---

[5] Polyphenol content has been performed after hydrolysis.

Flavonoids (and other polyphenols) are known to protect plants against herbivores. This role can be divided into different actions. Lipid-soluble flavonoids in leaves can form the resin that deters insects from feeding. This resin can also bind protein forming flavonoid-based tannins that are unpalatable to herbivores (*e.g.* rotenoid isoflavonoid family, see Fig. I.5a). They can also be phagostimulant to insects. The taste of flavonoids may be associated either with attraction or with herbivore repellence. For example, quercetin-3-*O*-glucoside (Fig. I.5b) (*e.g.* in sunflower, *Helianthus annus* L.) is phagoactive (*i.e.*, having appealing taste) with some insects such as the western corn rootworm (*Diabrotica virgifera*). Note that this correlation is strongly dependent on the animal-flower couple. They can also be directly toxic to herbivores.[9, 12]

2.2. Terpenoids

Terpenoids are mainly associated to flavour and perfume. Most of them are specific to the plant kingdom and probably constitute the most important group of secondary metabolites. More than 20,000 different compounds have been isolated. Some of them originate steroid compounds.[7]

Terpenoids directly derive from acetylCoA (Fig. I.2). AcetylCoA is transformed into the 5-atom isoprenyl moiety which is the key compound of terpenoid biosynthesis. All terpenoids are produced by the head-to-tail condensation of isoprenyl moieties. The π-bonds and spatial arrangements of the isoprenic polymer allow regioselective rearrangements. Terpenoids are divided into different families depending on the number of isoprenic units (Fig. I.6):[7]

(i) Monoterpenoids are constituted of two isoprenic units, *i.e.* 10-atom basis structure. They are volatile and known for their perfume (*e.g.* menthol, α-pinene, see Table I.2). Some of them act as pollinator attractants and others can help mediate tritrophic interaction such as E-β-ocimene.[6] The stereochemistry is particularly important in these compounds since it modulates flavour *e.g.*, (*S*)- and (*R*)-limonene provide orange or lemon flavours, respectively (table. I.2).

(ii) Sesquiterpenoids constitute the largest family. They have a C_{15}-basis structure (Table I.2). They are also volatile and play an important role in plant-animal interactions.[6]

(iii) Diterpenoids have a 20-atom basis structure and are mainly implicated in plant growth (*e.g.* the giberreline family). It must be stressed that paclitaxel is a well-

known member of this family, being widely used in chemotherapy as an antineoplastic drug.

(iv) Higher terpenoids (*e.g.* triterpenoids, steroids and carotenoids) have different functions in plants *e.g.* UV protection, microbial action against aggression or in modification of animal growth.
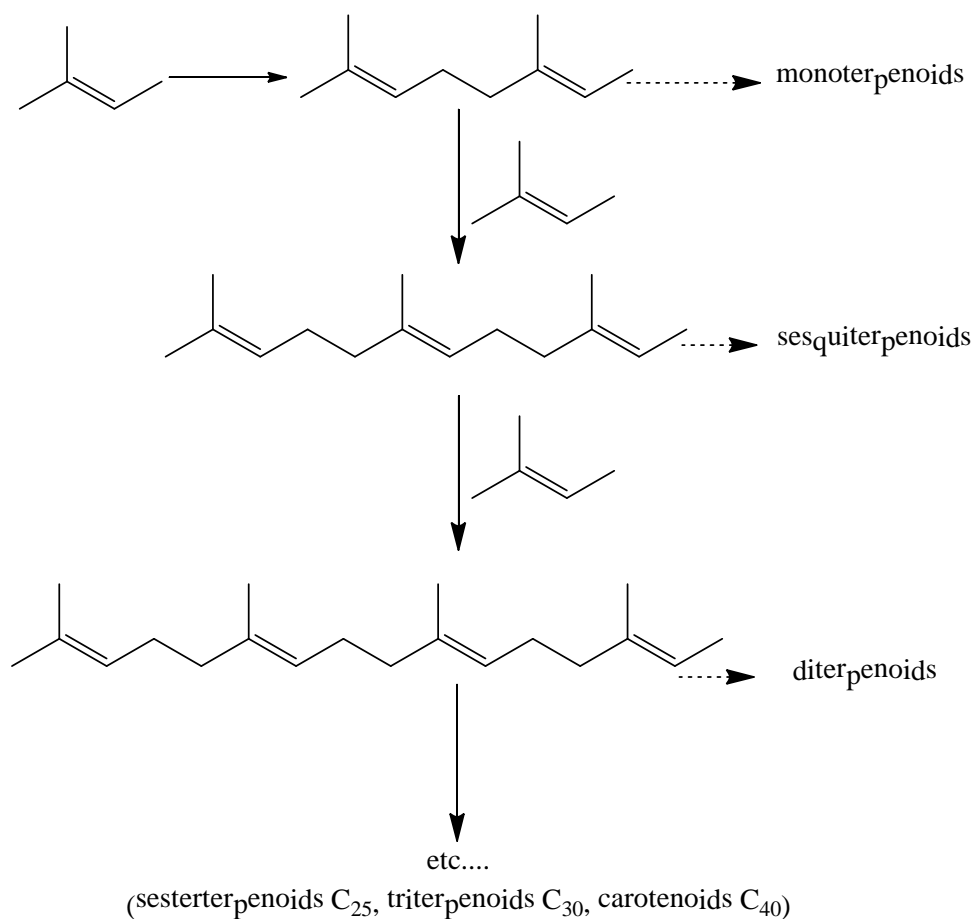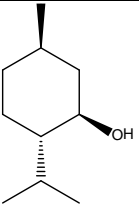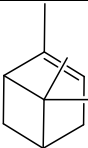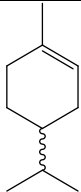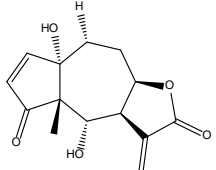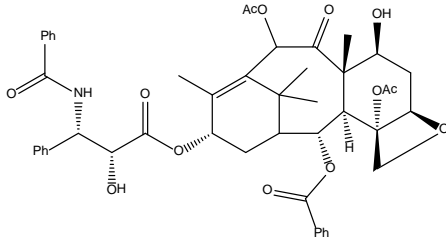
Figure I.6. Biosynthetic scheme of terpenoids

Table I.2. Examples of terpenoids

Group	Example		
Monoterpenoid	 (-)-menthol	 a-pinene	 limonene
Sesquiterpenoids	 arnifoline		
Diterpenoids	 paclitaxel		

2.3. Alkaloids
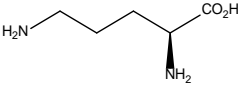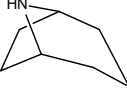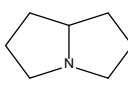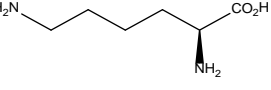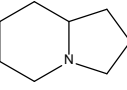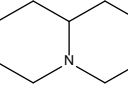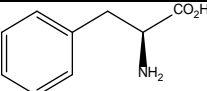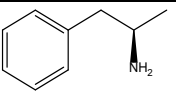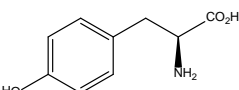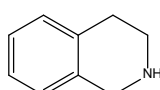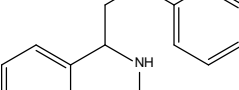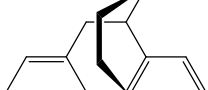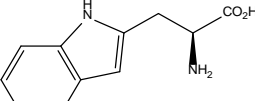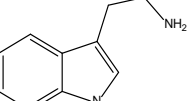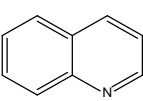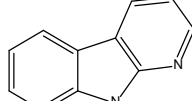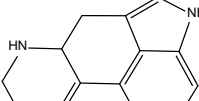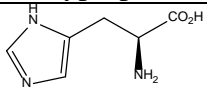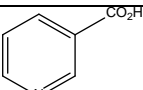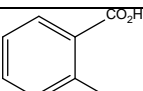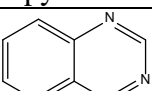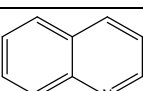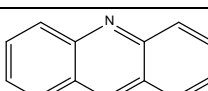
Some alkaloid derivatives (*e.g.*, morphine, cocaine and nicotine) are known for their deleterious effects. However, again due to the large variety of chemical structures, addiction is far from the only property of alkaloids. They consist of a heterocyclic nitrogen-containing skeleton. As for terpenoids and polyphenols, they present a huge diversity of structures and activities.

In addition to their chemical structure, they can be defined by the biosynthetic pathway since real alkaloids come from the transformation of specific L-amino acids[6] or specific nitrogen-containing compounds (anthranilic acid, nicotinic acid or purine nucleotides). Table I.3 provides a relevant (but not exhaustive) overview of different structures and their origins. It

---

[6] They include lysine, ornithine, phenylalanine, tyrosine, tryptophane and histidin.

must be stressed that alkaloids are present in only 20% of plants, contrary to polyphenols and terpenoids.[6, 7]

Table I.3. Biosynthetic origin of alkaloids and structure examples (Compiled from Refs 4 and 6)

Precursors	Alkaloids classes		
L-ornithine	pyrrolidine	tropane	pyrrolizidine
L-lysine	piperidine	indolizidine	quinolizidine
L-phenylalanine	ephedra		
L-tyrosine	tetrahydro-isoquinoline	phenethyliso-quinoline	morphanes
L-tryptophane	indole	quinoline	pyrroloindole / ergot
L-histidine	imidazole		
Nicotinic acid	pyridine		
Anthranilic acid	quinazoline	quinoline	acridine

They are widely used as therapeutic compounds (*e.g.* morphine as an analgesic, atropine as an anticholinergic and ergot derivatives in migraine treatment). The chemical analogy with natural amino acids in animals explains that a competition exists between natural ligands and alkaloids. In plants, most of the known properties of alkaloids are related to the protection from herbivores and neighbouring plants. For example, hyoscamine and hyoscine (Fig. I.7) are

potentially toxic for animals since they compete with endogenous compounds.[6] Senecionine and triangularine (in Senecioneae and Boraginaceae, respectively) are known as strong feeding deterrents for most herbivores, liver-toxic for vertebrates and mutagenic for insects.[13, 14]
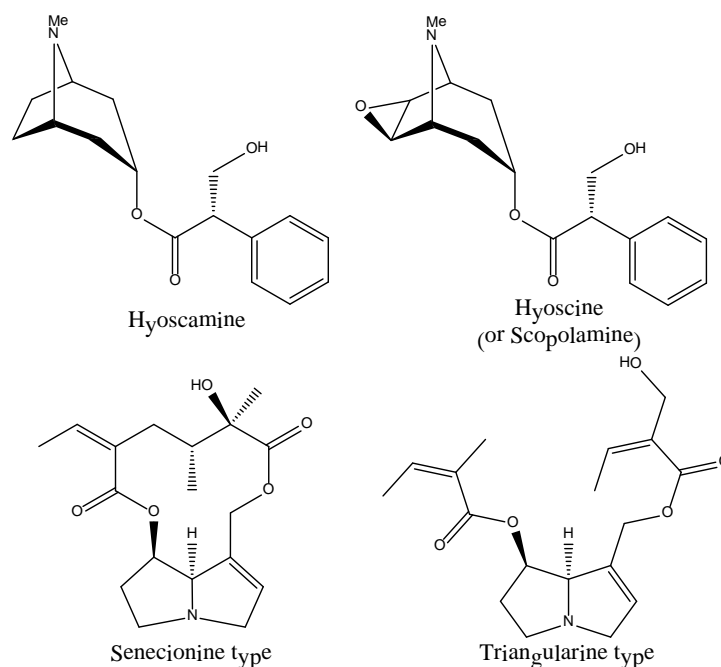
Figure I.7. Examples of alkaloids involved in plant defence mechanisms

This section clearly demonstrates the large diversity of compounds produced by plants in particular for the sake of their self-protection against abiotic or biotic stresses. The following two sections focus on two important stresses, light and oxidative stress.

Section B. Light absorption and colouration of plants

1. Molecules of the plant response to light exposure

The main source of light for plants is sun. The radiations cover not only the visible range (400 – 800 nm) but also the whole electromagnetic spectrum. The atmosphere stops most of toxic wavelengths including partly those of the UV range. This range is subdivided as UV-A (400-315 nm), UV-B (315-280 nm) and UV-C (280-100 nm). The most energetic and toxic radiations are UV-C absorbed by the ozone layer (when it is not destroyed) in the Earth stratosphere. UV-B are toxic but partially stopped, while UV-A are less toxic but 95% are transmitted by the atmosphere. Plant colouration is an external indicator of the chemical plant response to sunlight exposure.

1.1. Light effects on plants

1.1.1. Benefits of Lights

The main beneficial effects are attributed to the visible domain. These effects significantly differ with the wavelength, depending on the photoreceptor sensitivity; *e.g.*, cryptochromes are blue-light photoreceptors[15, 16] and phototropin is a blue-light and UV-A photoreceptor[17]. The light-induced excitation of the photoreceptor is transferred to a chromophore (*e.g.*, flavin-adenin dinucleotide (FAD) in blue-light photoreceptors). Electron transfer can then occur from the chromophore to (i) a redox or (ii) an intramolecular partner. It finally activates complicated redox signalling pathways inducing specific plant metabolism.[16]

UV-A and blue-light radiations play a determining role in plant elongation, anthocyanin production, phototropism, chloroplast migration, stomatal opening and sensitivity of flowering to photoperiod.[16, 17] High blue-light exposure mainly improves leaf growth but decreases hypocotyl. Hypocotyl elongation is related to helio/phototropism *i.e.*, when plant do not catch enough light, it elongates stems towards light. Blue-sensible cryptochromes may also play an important role in plant circadian rhythm (*i.e.*, day/night alternation). They were first found in *Arabidopsis*, ferns and algae but they are not specific of the plant kingdom since they are also characterized in insect and mammalian phylogenetic.

Green-light responses have been shown to be opposed to blue-light responses. Green radiation can be seen as a control in plant morphology under blue-light. For example, blue- and green-light responses are inverted with respect to stem elongation and flowering.[18-20]

Red radiations can be divided into two categories: (i) red and (ii) far red (end of the visible spectrum) lights. They play a determining role in seed germination, inhibition the hypocotyl and stem elongations, leaf developments and induction of genes required for photosynthesis. Even if red and far-red light effects have been studied for many years,[21] their roles are not completely elucidated. Red and far-red light effects are mainly mediated by phytochromes photoreceptors. Phytochrome is activated by red light and can be converted back to its initial form by far-red light.[22] Far-red light also plays an important role in UV-protection since it can reverse UV-B pathological effects.[23]

1.1.2. Harmful effects of light

Harmful effects of light are mainly attributed to high energetic UV light. UV-B and UV-C radiations are extremely harmful for all organisms whereas UV-A has both beneficial and harmful effects. UV effects can be divided into two groups, namely DNA damage and alteration of physiological processes.[23] It must be stressed that harmful effects are mainly due to UV-B since UV-C are absorbed by the ozone layer.

1.1.2.1. DNA damages

UV-B and UV-C effects are related to direct DNA damage (Fig. I.8).[24] When a UV photon is absorbed by DNA, the subsequent electronic rearrangement enables chemical reactions and the formation of photoproducts The two main types of photoproducts are the *cys-syn* cyclobutane pyrimidine dimers (CPD) and the 6,4-bispyrimidine photoproducts ([6-4] photoproducts, Fig. I.9) These dimerizations have been widely studied in the literature from both experimental and theoretical points of view.[24, 25] The CPD formation is one order of magnitude higher than the [6,4] photoproduct formation.[26-29] The [6,4] photoproduct formation requires a specific spatial DNA rearrangement (*i.e.*, unwinding and base rotation) decreasing their occurrence.[24] Others photoproducts (*e.g.*, pyrimidine monoadducts, purines and furocumarins) are also observed under UV radiations but at lower occurrence; they are

mainly produced when a photoactivated nucleic acid reacts with another type of biological compounds.
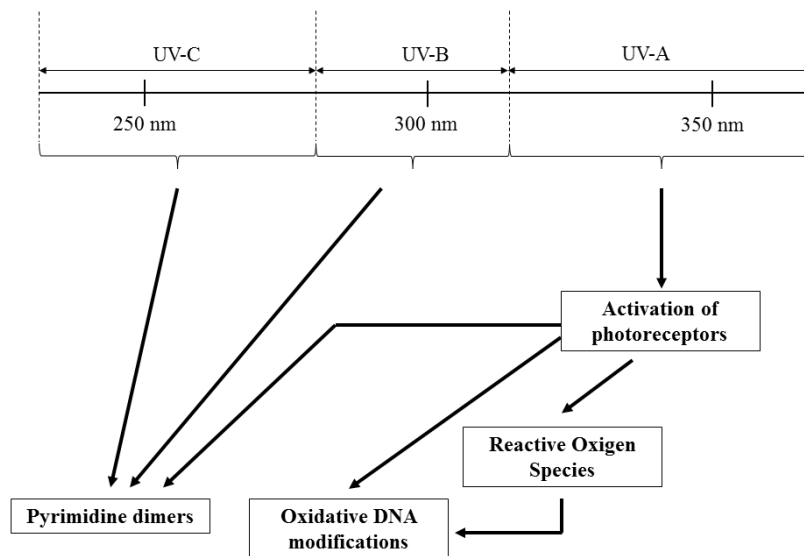
Figure I.8 Pathways of DNA damages provided by UV radiations (adapted from Ref. 23)

UV light including UV-A can induce indirect effects on DNA. Light exposure induces the formation of free radicals, mainly hydroxyl and singlet oxygen. This initiates oxidative processes providing several reactive oxygen species (ROS) which can alter DNA structures.[7] Another hypothesis is the modification of the Ca^{2+} metabolism, activating intracellular enzymes such as nucleases inducing DNA damage.[30] These processes mainly induce oxidative DNA derivatives such as 8-oxoguanine or formamidopyrimidine.[31]

---

[7] ROS formation and effects are discussed in Section C.
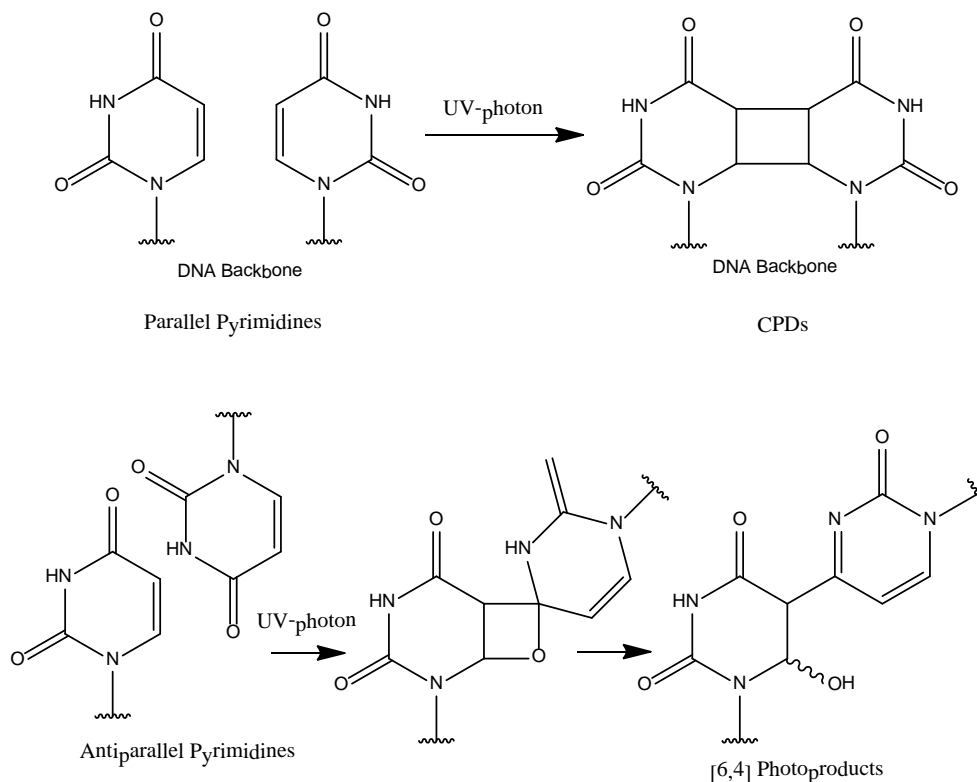
Figure I.9 Photoproduct provided by UV-photon excitation

DNA modifications originate a wide variety of cell modifications. The main effect is mutagenicity inducing the non-recognition of certain DNA sequences, preventing the biosynthesis of vital proteins. Even if some DNA damages can be repaired, others are part of the heritage information. UV-induced mutations can cause chromosomal aberrations in all plant organs (*e.g.*, root, leave) or the inhibition of the production of secondary metabolites (*e.g.*, anthocyanidins).

1.1.2.2. Alteration of physiological processes

Except DNA alteration, it is impossible to classify all the different metabolisms affected by UV light. Some are provided by the direct alteration of metabolic constituents (*e.g.*, proteins, membrane) while others remain to be elucidated (*e.g.*, alteration of protein activity from DNA mutation or direct structure alteration). Moreover, results are sometimes contradictory due to *e.g.*, different methods of investigation. However, a consensus has been proposed to elucidate at least potential targets of UV,[32] which can be divided into different function categories as described in Fig. I.10.

Photosynthetic machinery:
- Inactivation of photosystems
- Inactivation of enzymes
- Inactivation of Carotenoid biosynthesis
- Alteration of chloroplast structure
- Decrease of photosynthetic biosynthesis

Structure alteration:
- Membrane alteration
- Organite degradation (e.g., chloroplaste)

UV

Oxidative stress:
- ROS formation
- Increase of endogenous antioxidant systems (e.g., ascorbate, glutathione, enzymes…)

Cell communications:
- Alteration of phytohormones (e.g., photooxidation)

Secondary metabolism:
- Regulation of polyphenol synthesis
- Accumulation of alkaloids, waxes and polyamines
- Activation of UV photoreceptor

Figure I.10. Overview of the UV effects on the cell components

1.2. Optically-active secondary metabolites

Secondary metabolites (*e.g.*, terpenoids including carotenoids and polyphenols) play a determinant role in the protection against light.

1.2.1. Carotenoids

Carotenoids gather hundreds of tetraterpenic molecules (*e.g.*, lycopene, β-carotene or capsorubine, Fig. I.11).[7] The chemical structures contain eight isoprenic units. Two main groups are defined according to the absence or presence of at least either one O-atom (hydroxy or keto group) (carotenes or xanthophylls, respectively). Their optical properties are attributed to the presence of the highly π-conjugated system favouring (sun)light absorption.

Carotenoids are responsible for the red-orange colour of several plants including carrots, mango, kaki and tomatoes (in a more or less extend depending on the variety). These compounds are not synthesized by animals but play an important role in their photochemical processes such as vision.
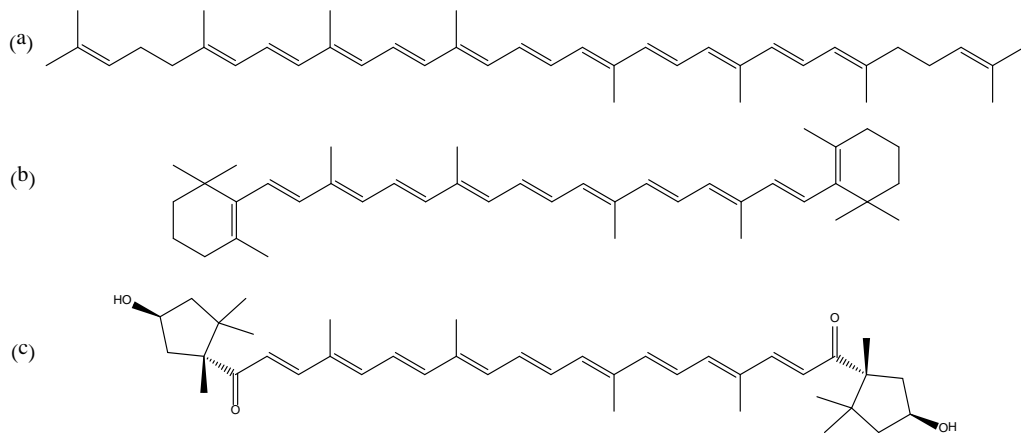
Figure I.11. Chemical structures of (a) lycopene, (b) *β*-carotene and (c) capsorubine.

Carotenoids are mainly involved in the photoreceptors of plant cells. They play an important role, keeping intact the double-helix structures of proteins by forming a cross-brace (Fig. I.12).[33] They play a dual photochemical role: (i) light-harvesting and (ii) protection.
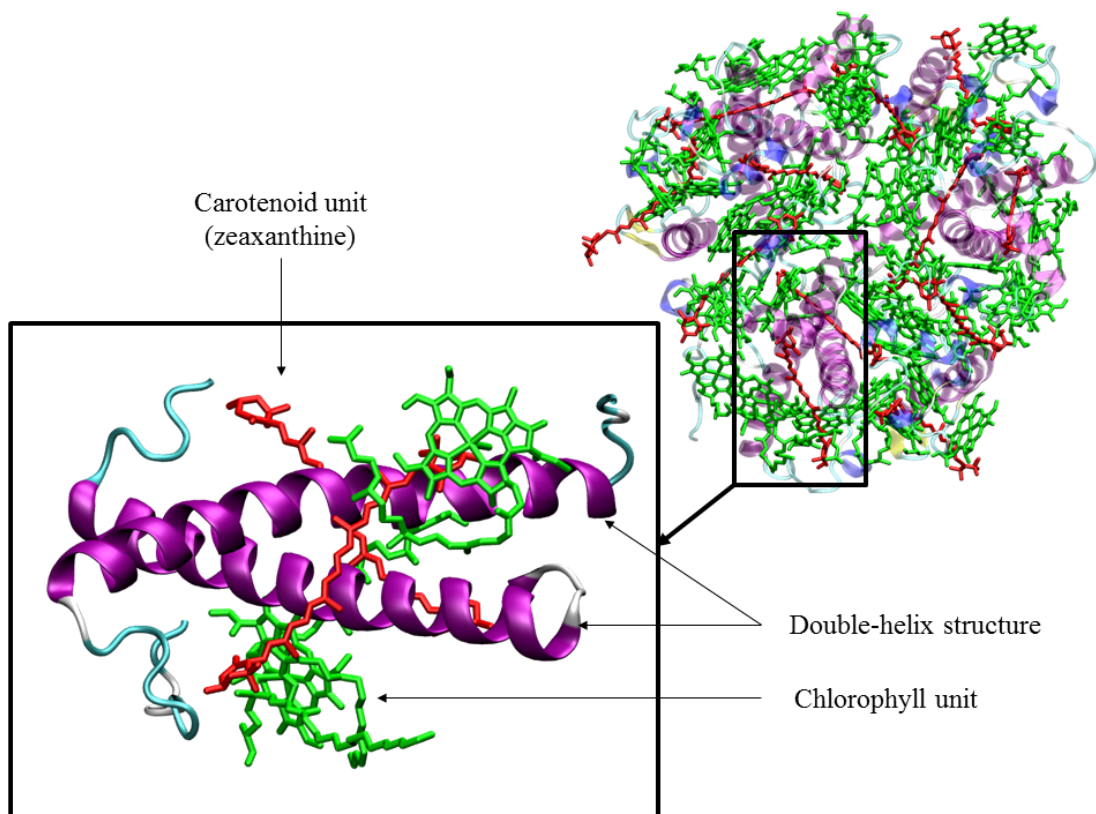
Figure I.12. X-ray structure of the cross-brace formed between carotenoids and proteins, here the LHC-II photosystem.

The former role (light-harvesting) is explained by their capacity to absorb light. Moreover, long-range interactions may exist between carotenoids (*e.g.*, zeaxanthine) and cholorophyll, which allow charge and energy transfers between both compounds,[33] the energy transfer being a singlet-singlet exchange reaction. This contribution is however minor in photosynthesis.

The photoprotective function is the most important role of carotenoids. The sunlight excess with respect to the part used by photosynthesis may excite chlorophyll into the triplet state. This metastable triple-state can be stabilized by energy transfer to the surrounding molecular oxygen, inducing the formation of singlet oxygen $^1O_2$. This species is involved in oxidative stress (see Section C) and provides severe damages to cell components. Carotenoids (*e.g.*, violaxanthin, antheraxanthin) can convert the chlorophyll triplet state by energy transfer. This so-called triplet quenching is a triplet-triplet transfer. The carotenoids then enter into a chemical reaction process.[34] When light absorption decreases, epoxyde xanthophylls are regenerated by an auto-regenerative-enzyme process present in plant cells (*e.g.*, NADPH/H$^+$, Fig. I.13).

Auxiliary enzymatic systems allow the xanthophyll epoxidation being not overwhelmed (Fig. I.13). The close-association between chlorophyll and carotenoids is called the dynamic photoinhibition.
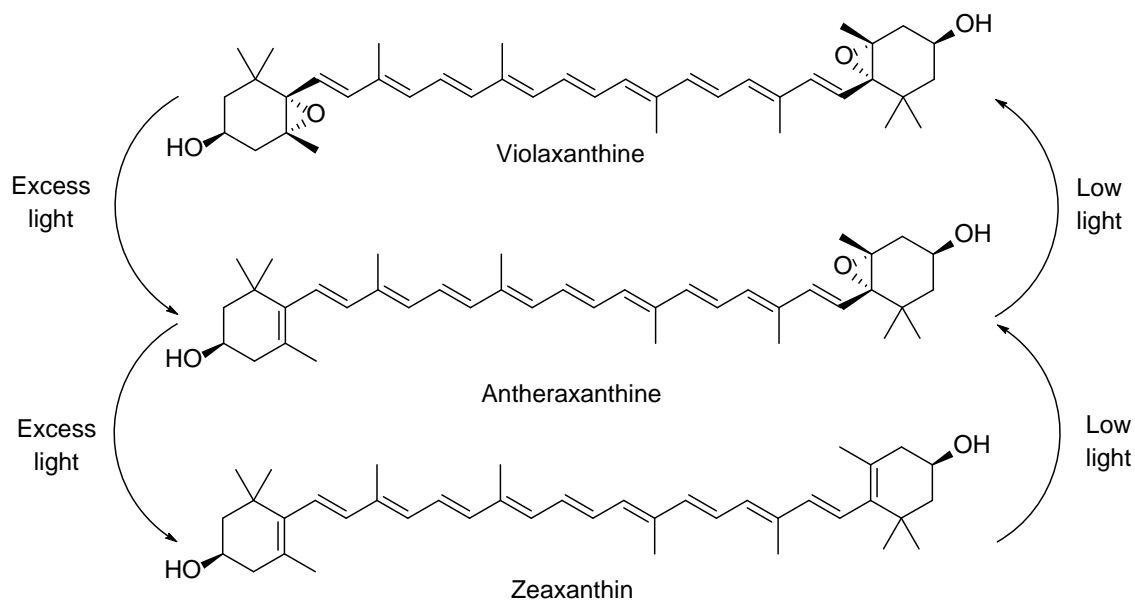
Figure I.13. Xanthophyll cycle

1.2.2. Flavonoids

The crucial role of flavonoids in light protection is attributed to two main groups of compounds (i) anthocyanins and (ii) other flavonoids.

1.2.2.1. *Anthocyanidins and their derivatives*

Anthocyanidins are polyhydroxy and/or polymethoxy derivatives of the 2-phenylbenzopyrylium cation, *i.e.*, the so-called flavylium cation. More than twenty anthocyanidins are known but only six play an important role from the food chemistry point of view.[35, 36] They differ in the number of OH or OMe groups on the skeleton (Table. I.4).[36]

There exist around one thousand anthocyanins (i.e., anthocyanidin 3-*O*-glycosides) including anthocyanidins and their glycosylated derivatives. They are widely distributed in flower-bearing plants and are responsible for the red, blue and purple colours in flowers (*e.g.*, orchids, roses and tulips), fruit (*e.g.*, most of berries, grapes, apples and plums), vegetables

(*e.g.*, oignons, rheum and aubergines) and leaves (artichoke and tobacco). They are mainly located in vacuoles[8].

Table I.4. Substitution pattern of most important anthocyanidins and their corresponding colours.

Anthocyanidin	3	5	7	3'	4'	5'	Colour
Cyanidin	OH	OH	OH	OH	OH	H	Orange-red
Malvidin	OH	OH	OH	OMe	OH	OMe	Bluish Red
Peonidin	OH	OH	OH	OMe	OH	H	Red
Delphinidin	OH	OH	OH	OH	OH	OH	Bluish Red
Petunidin	OH	OH	OH	OMe	OH	OH	Bluish Red
Pelargonidin	OH	OH	OH	H	OH	OH	Orange

In principle anthocyanins are not relevant candidates as UV-filters, since in most red-leafed species they are mainly located in the internal tissues. This prevents efficient filter actions even if the compounds have the intrinsic capacity to absorb UV light.[9, 12] Actually, anthocyanins play an important role in the photoinhibition process of carotenoids, acting somehow in synergy. During a long light exposure jointly with other stresses (*e.g.*, heat or cold), the photoinhibition of xanthophyll cycle (Fig. I.13) can be saturated leading to the so-called chronic photoinhibition. The most harmful consequence of the chronic photoinhibition is the generation of ROS leading to irreversible and necrotic lesions in plants. Anthocyanins are able to absorb green light, thus desexciting chlorophyll from the triplet-state, under prolonged exposure. A high level of anthocyanins enables to depopulate the chlorophyll triple state, in place of carotenoids.

1.2.2.2. Colourless flavonoids
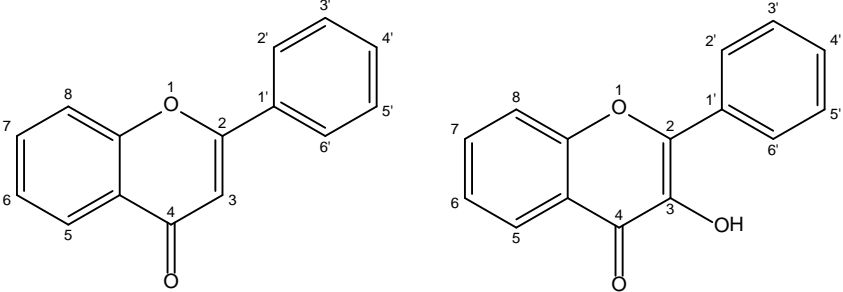
Unlike anthocyanidins, colourless and yellow flavonoids (*e.g.*, flavones, chalcones, flavonols) are the major actors of UV-protection. Plants often respond to UV radiation by the

---

[8] Vacuole is a typical structure of plant and fungal cells. They are essentially enclosed compartments containing mainly water, inorganic and organic compounds. They play an important role in *e.g.*, the storage of specific organic compounds, the hydrostatic pressure and pH maintaining.

activation of flavonoid biosynthesis.[9] At 370 nm, about 98% of UV radiation is absorbed by flavonoids.[12]

Among flavonoids, flavones and flavonols (Table I.5) strongly absorb UV light. They are mainly accumulated in the outermost layer, providing an effective UV-filter barrier. A depletion of flavonol in *Arabidopsis* mutants causes a slower growth under UV-B radiation.[9] Recently, some studies on specific species (*e.g.*, *Petunia*, *Arabidopsis*, *Vicia fabia*) rationalized flavonoid biosynthesis with respect to UV radiations.[9] These researches have evidenced that UV light favours the biosynthesis of flavonoids with a high level of hydroxylation (*e.g.*, quercetin instead of kaempferol, isoorientin instead of isovitexin, Table I.5). The presence of several OH groups significantly modifies UV/Vis absorption spectra; the higher the number of OH groups, the higher the UV-absorption.[37]

Table I.5. Substitution pattern of most important flavones and flavonols.

Flavone				Flavonols		
Family	Compound	5	6	7	3'	4'
Flavone	Isovitexin	OH	Glucose	OH	H	OH
	Isoorientin	OH	Glucose	OH	OH	OH
Flavonols	Kaempferol	OH	H	OH	H	OH
	Quercetin	OH	H	OH	OH	OH

2. Colour modulation: pigmentation and copigmentation

2.1. The paradox of anthocyanidins

Anthocyanins constitute the most important class of natural pigments. *Vitis* species (especially, *V. vinifera*) is the most important source of anthocyanins. Grape chemistry is an active field of research in which the understanding of colour is crucial. Anthocyanin profiles

guide the differences between all varieties of red and white wines.[36, 38] The hydroxyl or methoxyl substituents on the flavylium skeleton significantly modify the absorption properties of anthocyanins and thus of the colour of wine. Cyanidin, malvidin and peonidin provide orange, bluish red and red, respectively (See Table I.4). The flavylium cation form is highly unstable under natural conditions, being mainly sensitive to pH and temperature.[9]

2.1.1.1. pH effect

Anthocyanins provide a broad range of colours, possibly covering almost the entire visible spectrum from pH 1 to 14. The cationic form is mainly stable under very acidic pH conditions. A pH increase causes structural modifications involving several chemical equilibria (Fig. I.14). The red colour of anthocyanins is mainly attributed to the flavylium cation (AH+) which prevails at pH lower than 4. When pH is ranging from 4 to 6, at least one of the acidic groups of AH^+ (mainly 7, 4' and 5) is deprotonated, thus giving a mixture of neutral tautomeric quinoidal bases A, providing purple. At pH higher than 6, a second deprotonation forms the blue-anionic-quinoidal bases A^-. Besides the fast deprotonation, AH^+ can also undergo hydration at position 2 forming the colourless hemiketal B (Fig. I.14). The hemiketal B form is also in equilibrium with the s-*cis* and s-*trans* chalcones C (Fig. I.14). It must be stressed that deprotonation products are actually kinetics products while chalcones are thermodynamics products.

---

[9] It must be stressed that anthocyanins are also sensible to chemical species present in vacuoles (*e.g.*, oxygen, enzyme).
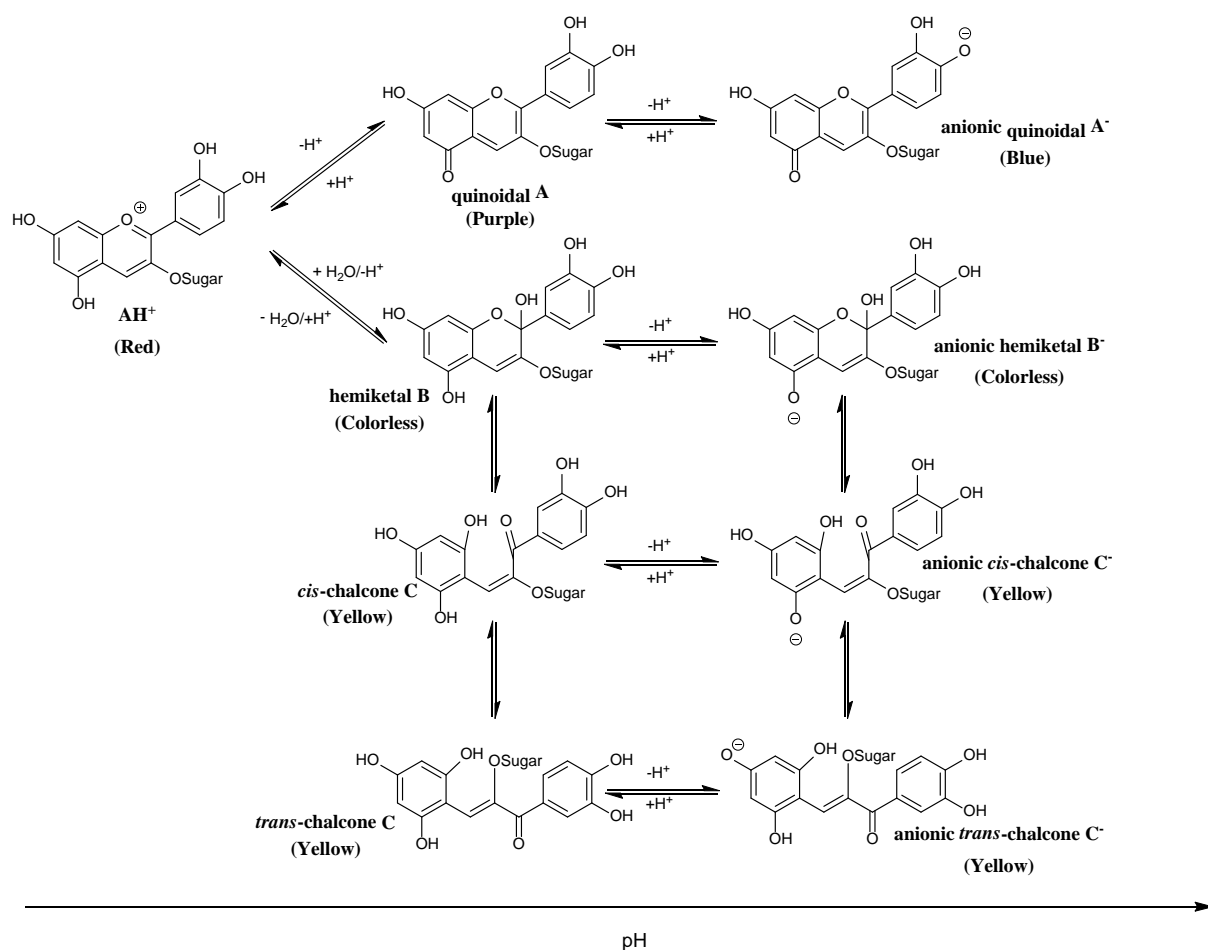
Figure I.14. Impact of pH on anthocyanins in aqueous solution.

2.1.1.2. Thermal degradation

Temperature is an important external factor leading to degradation products and thus to colour modification. Heating up to 95°C induces chemical transformations, mainly on the C-ring, leading to chalcone glycosides (Fig. I.15). Long heating periods initiate deglycosylation, and the corresponding aglycones can afterwards be degraded into phenolic acids or aldehydes (Fig. I.15).[36, 39]
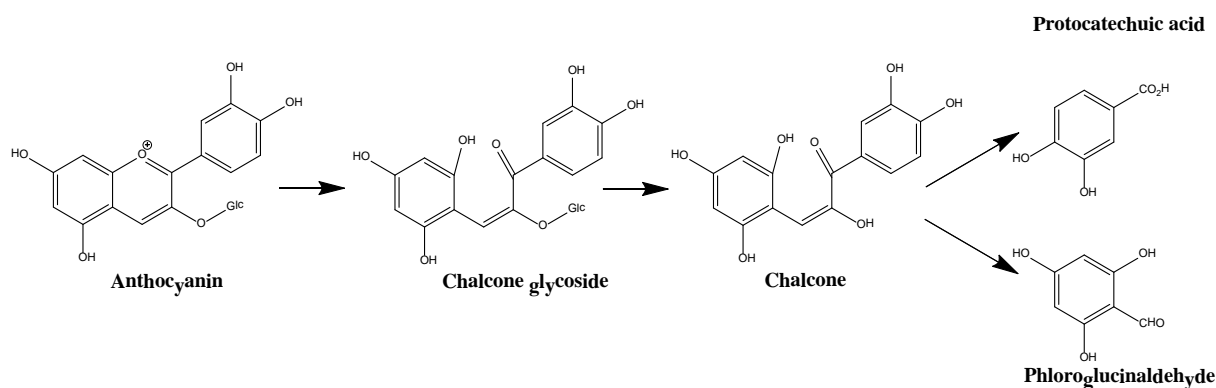
Figure I.15. Thermal degradation of 3-*O*-methylcyanidin

2.2. Copigmentation

According to pH conditions in plant vacuole (pH *ca.* 5), anthocyanins should be in non-coloured forms. Nevertheless, the persistence of bright colours suggests stabilization processes. Anthocyanin colours can be stabilized by the complexation (copigmentation) with other natural compounds, so-called copigments (or pigment cofactors). The copigmentation process allows preserving the flavylium cations and pH- and temperature-dependent colour degradations. This colour modulation by copigmentation was already observed in 1916 by Willstätter and Zollinger.[36, 40] It had only been associated to grape wine until it was described in different flower petals in 1931.[41]

Copigmentation is mainly experimentally studied by UV/visible spectroscopy since copigmentation is related to (i) bathochromic shifts of the maximum absorption wavelengths of anthocyanins, $\Delta\lambda_{max}$ and (ii) hyperchromic effects. The higher the bathochromic shift, the higher the copigmentation effect. Other experiments are useful to rationalize copigmentation such as nuclear magnetic resonance (NMR) or circular dichroism (CD) giving a structural picture of the copigmentation complexes.

The self-association has also been suggested when the concentration of anthocyanins is relatively important in the solution.[36, 42] It has been suggested as a strong factor in wine aging.[38] For some pigments, the copigmentation process can be driven by metal binding,

leading to supramolecular assemblies.[43] In some specific cases (e.g., acylated glycosides), intramolecular copigmentation (*i.e.*, intramolecular interactions) is also favoured.

In 1982, Brouillard *et al.* proposed that the driving force for copigmentation complexation was non-covalent interactions including dispersive, electrostatic and H-bonding.[44] The contributions of each type of interactions strongly depend on the chemical structure of both pigment and co-pigment. However the different contributions are not perfectly known and understood for most of pigment/copigments systems.

2.3. Brief overview of possible co-pigments

Copigments are usually colourless or provide yellow to yellowish colours. A broad range of natural compounds may play such a role as far as they present an extended π-delocalization in their chemical structure.

The most known copigments are flavonoids in which flavonols, flavones and flavanones have been widely studied.[36] Among them, the rutin and quercetin have a strong copigmentation capacity (in this case, the bathochromic shifts have been assessed at 30 and 28 nm). Due to a less extended π-conjugated system, flavan-3-ols such as catechin or epicatechin are less efficient copigments.

Phenolic acids are also copigments. With these copigments, hyperchromicity is high (about 70%) while bathochromic shifts are weak.[42] Sinapic and ferulic acids were found as the most efficient phenolic acid copigments.

Some "exotic" copigments were also proposed in the literature, including alkaloids (*e.g.*, caffeine, 20 and 68% hyperchromicity) and amino-acids (*e.g.*, tryptophane, proline, arginine).[42] Although alkaloids present aromatic rings, this is not the case for amino-acids such as arginine, for which dispersive interactions are unlikely but strong electrostatic or H-bonding interactions probably occur.

The different copigments often act in competition in the process of copigmentation complexation. Recently, an anti-copigmentation phenomenon was proposed in which a given copigment B was proposed to replace the initial copigment A when the intermolecular

interactions were more favourable with the "new" one. Anti-copigmentation occurs if the presence of copigment A induces colour loss.[45]

Section C. Oxidative stress and natural antioxidants

The previous sections dealt with the plant abilities to create original compounds in order to adapt to their environment. Among the external aggressions, oxidative stress is probably the most important. Plants also fight this stress producing natural antioxidants, mainly secondary metabolites. Oxidative stress affects both plants and animals, most of antioxidants present in humans directly come from plant consumption. The other antioxidants are endogenously produced.

1. Oxidative Stress

Oxidative stress is defined as the massive liberation of free radicals and related reactive species in the organism. Free radicals can be produced endogenously, mainly by enzymes (*e.g.*, of the inflammatory process), or exogenously (*e.g.*, UV light, radiotherapy, smoking, pollution). Free radicals are atoms or molecules possessing a single electron in their outer shell (*i.e.*, valence shell) and are chemically quoted $R^\bullet$. The unpaired electron provides a high reactivity against neighbouring molecules. They may react with biological molecules including DNA, proteins and lipids.

In living organisms, most of the free radicals are oxygen-centred (*e.g.*, superoxide anion $O_2^{\bullet-}$, hydroxyl radical $^\bullet OH$, alkoxyl radical $RO^\bullet$ and peroxil radicals $ROO^\bullet$) and are so-called reactive oxygen species (ROS). From the biological point of view, it must be stressed that ROS also include few closed-shell molecules (*e.g.*, singlet oxygen $^1O_2$ and hydrogen peroxide H_2O_2).

1.1. A list of reactive oxygen species

1.1.1. Singlet oxygen
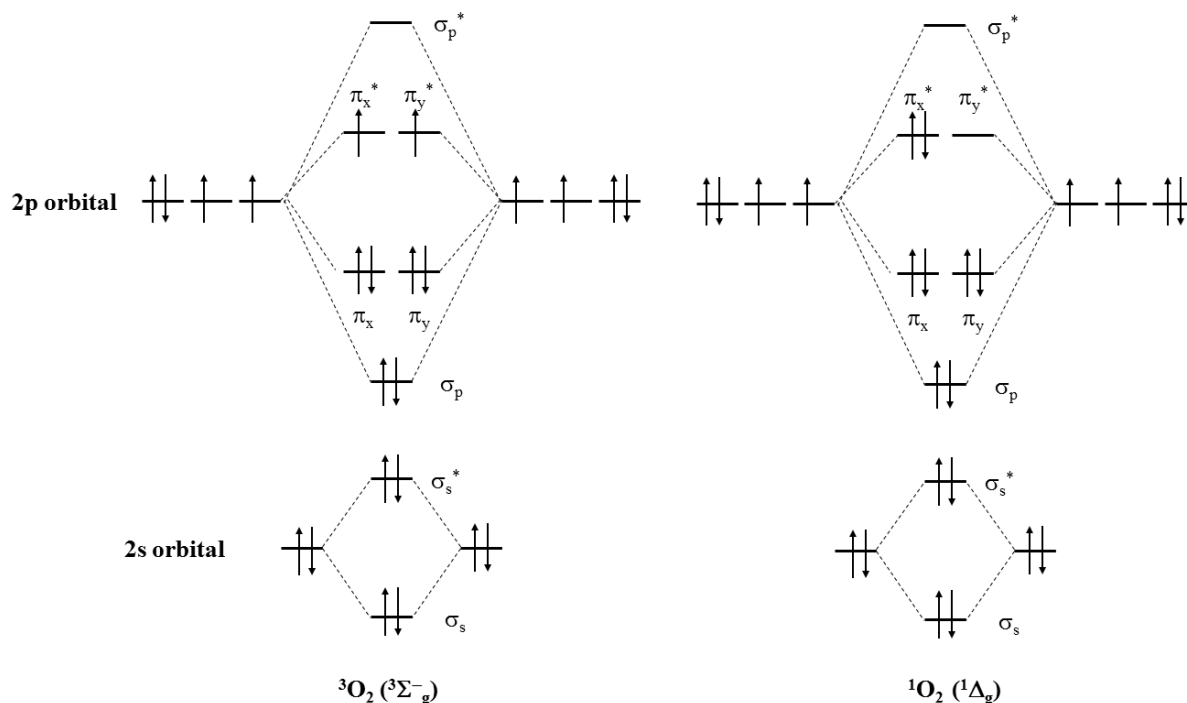
Figure I.16. LCAO scheme of triplet and singlet molecular oxygen

The most stable form of molecular oxygen in nature is the triplet state $^3O_2$. The transformation into the metastable singlet $^1O_2$, in the $^1\Delta_g$ form, is possible *e.g.*, under UV sunlight excitation (Fig. I.16).[10] $^1O_2$ is less stable than $^3O_2$ by 22.5 kcal.mol^{-1} demonstrating a much higher reactivity.[46] $^1O_2$ is capable to oxidize and denature many biological compounds.

1.1.2. Superoxide anion

The superoxide anion $O_2^{\bullet-}$ is formed by several enzymatic systems including oxidases (*e.g.*, NADPH oxidase in lipid bilayer membrane, cytochrome oxidase in mitochondrial respiratory chain complex), transferring one electron from the enzymatic cofactor to $^3O_2$ (Eq. (I.2)):

---

[10] The $^1\Sigma^+_g$ form of singlet oxygen also exists but quickly relaxes into the $^1\Delta_g$ form.

$$\text{O}_2 + \text{e}^- \xrightarrow{\textit{Oxidase}} \text{O}_2^{\bullet-} \qquad\qquad \text{(I.2)}$$
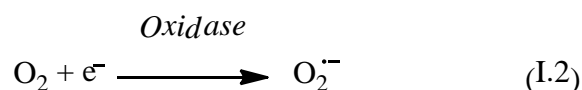
Its lifetime is very short due to a relatively high reactivity. It reacts so quickly with the direct environment (solvent molecules) that it cannot be considered as a direct source of the degradation of biological compounds. It is a major intermediate for the production of several other ROS.

1.1.3. Hydrogen peroxide

The disproportionation of $\text{O}_2^{\bullet-}$ may occur under acidic conditions. The reaction is catalysed by superoxide dismutase (SOD) leading to hydrogen peroxide H_2O_2.

$$2\text{O}_2^- + 2\text{H}^+ \xrightarrow{\textit{SOD}} \text{H}_2\text{O}_2 + \text{O}_2 \qquad \text{(I.3)}$$
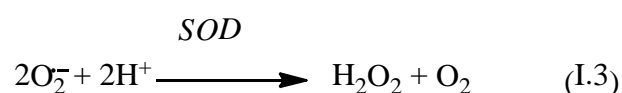
H_2O_2 is not strictly a free radical and is much more stable than a sheer free radical. It is however considered as a ROS. It can cross lipid bilayer membranes and plays an important role as a vector of oxidative stress.

Hydrogen peroxide may react with chloride anions in intracellular media leading to hypochlorous acid HOCl. This acid reacts with amine moieties of biological compounds (*e.g.*, proteins) denaturing them.[47] It also reacts with hydrogen peroxide leading to singlet oxygen $^1\text{O}_2$.

$$\text{H}_2\text{O}_2 + \text{HOCl} \longrightarrow \text{HCl} + {}^1\text{O}_2 + \text{H}_2\text{O} \qquad\qquad \text{(I.4)}$$

1.1.4. Hydroxyl radical

The very slow reaction between $\text{O}_2^{\bullet-}$ and H_2O_2 (Haber-Weiss reaction) forms the very toxic free hydroxyl radical $^{\bullet}\text{OH}$:

$$\text{H}_2\text{O}_2 + \text{O}_2^- + \text{H}^+ \longrightarrow {}^{\bullet}\text{OH} + \text{O}_2 + \text{H}_2\text{O} \qquad \text{(I.5)}$$
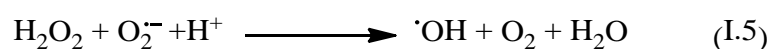
Hydrogen peroxide may also be reduced into $^{\bullet}OH$ by the oxidation of transition metals such as ferrous ions (namely, Fenton's reaction):

$$H_2O_2 + Fe^{2+} \longrightarrow {}^{\bullet}OH + {}^{-}OH + Fe^{3+} \qquad (I.6)$$
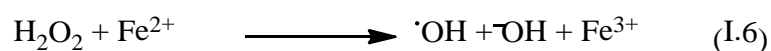
This is by far the most reactive and toxic ROS, with a 10^{-9} s half-life. It reacts non-specifically with all neighbouring compounds (*e.g.*, DNA and proteins). It is also the initiator of lipid peroxidation resulting in the degradation of lipid bilayer membranes.[48]

1.1.5. Peroxyl radicals

Peroxyl radicals, $ROO^{\bullet}$, play a major role in the lipid peroxidation process. They are formed by the addition of molecular oxygen to carbon-centred free radicals $R^{\bullet}$.

$$O_2 + R^{\bullet} \longrightarrow ROO^{\bullet} \qquad (I.7)$$

When R refers to a lipid, the carbon-centred free radical is quoted $L^{\bullet}$ and the corresponding peroxyl is quoted $LOO^{\bullet}$. It must be stressed that the addition of singlet oxygen on fatty acid lead to the closed-shell hydroperoxide compounds LOOH. Their oxidation by metal forms peroxyl radicals:

$$^{1}O_2 + LH \longrightarrow LOOH \qquad (I.8)$$

$$LOOH + M^{n+} \longrightarrow LOO^{\bullet} + H^{+} + M^{(n-1)+} \qquad (I.9)$$
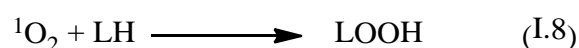
1.1.6. Alkoxyl radicals

The degradation of peroxyl radicals following a Fenton-like (Eq. I.6) reaction leads to the highly reactive alkoxyl radicals, e.g.:

$$ROOH + Fe^{2+} \longrightarrow RO^{\bullet} + {}^{-}OH + Fe^{3+} \qquad (I.10)$$

1.1.7. Other radicals

Carbon-centred radicals classically quoted L$^\bullet$ are usually formed during the lipid peroxidation process (see Section 1.2.1). It must be stressed that the smallest carbon-centred radicals $^\bullet CH_2OH$ and $^\bullet CH_2CH_3OH$ are produced during methanol and ethanol intoxication, jointly with the $CH_3O^\bullet$ and $CH_3CH_2O^\bullet$ free radicals, respectively.

Reactive nitrogen species (RNS) are also produced in the organism from ROS. They result from the reaction between nitric oxide NO$^\bullet$ and $O_2^{\bullet-}$ leading to the highly reactive peroxynitric anion ONOO$^-$.

$$O_2^{\bullet-} + NO^\bullet \longrightarrow ONOO^- \qquad (I.11)$$

This anion is less reactive than ROS but induces selective oxidation of biomolecules.[46]

1.2. Oxidative stress processes

1.2.1. Lipid peroxidation

Lipids are main components of the cell membranes in animals and plants. Their oxidation by free radicals (lipid peroxidation) is responsible for important membrane degradation and disorganization, often inducing the decrease of membrane fluidity.

Lipid peroxidation is a three-stage process. The initiation stage is almost systematically attributed to $^\bullet$OH radicals. It attacks lipid chains by H-atom transfer (HAT) leading to L$^\bullet$ radicals. Propagation consists first of the addition of molecular oxygen onto L$^\bullet$ (reaction I.7) to form the peroxyl radical LOO$^\bullet$, then of HAT from chain to chain to propagate the LOO$^\bullet$ free radical (Fig. I.17). The reaction is finally completed when *e.g.*, two radicals combined leading to closed-shell species (Fig. I.17).
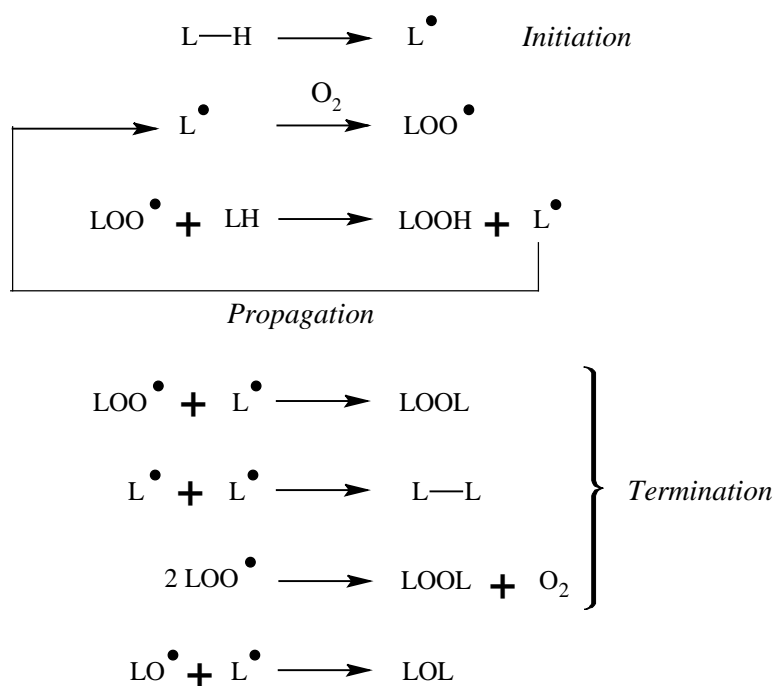
Figure I.17. Lipid peroxidation process

1.2.2. DNA oxidation

According to Doll and Peto, most of the cancer cases are related to life-style.[49] The most known external factors of risk are (i) cigarette smoking, (ii) alcohol drinking and (iii) fatty diet. Oxidative stress is highly induced by these three factors. It plays an important role in the carcinogenesis process. ROS bombard DNA about 10^4 times a day per cell. The high reactivity of ROS allows particular reactions with the π-conjugated systems of DNA (*e.g.*, pyrimidine and purine moiety). Two scenarios are possible when a base of DNA is oxidized by ROS:

(i) The alteration is located on an intron of DNA. In this case, the mutation will be silent.

(ii) The alteration is located on an exon of DNA and may lead to permanent modifications of DNA if it is not repair by specific cellular mechanisms.

1.2.3. Protein oxidation

All amino acids are sensitive to the direct reaction with ROS. Sulphur amino acids such as cysteine and methionine appear to be the most sensitive residues to oxidation. The oxidation of

cysteine and methionine leads to disulphide and methionine sulphoxide, respectively.[50] The oxidations of arginine and lysine lead to aldehyde derivatives (glutamic and aminoadipic semialdehydes, respectively), aldehydes being well-known to be highly reactive with amino residues NH_2. Adducts are also formed by the attack of ${}^{\bullet}OH$ onto the aromatic rings of phenylalanine and tyrosine.[51]

The consequences of protein oxidation are driven by (i) the targeted amino acids, (ii) the protein function and (iii) the location. For example, when the carotenoid-chlorophyll system in plant cell is overwhelmed, the photosystem is oxidized by singlet oxygen and free radicals, decreasing the photosynthesis yield. Another example in the animal kingdom is the oxidation of β-amyloid in brain cells that was suggested as one of the etiologies of Alzheimer's disease.[52]

2. Natural antioxidants: a plant response to oxidative stress

All living organisms from both the plant and animal kingdoms have developed many protective systems against oxidative stress. The so-called antioxidant systems are defined as "species enabled to decrease oxidative stress in organism". Antioxidants can be divided into four main families: (i) antioxidant enzymes, (ii) metal-chelating systems, (iii) inhibitors of prooxidant enzymes and (iii) free radical scavengers. In this manuscript, we will focus on point (iii) since numerous secondary metabolites are powerful free radical scavengers.

2.1. Chemical requirements for efficient free radical scavenging

An efficient free radical scavenger has the capacity to transfer an electron to the free radical that is then transformed in a closed-shell system (*i.e.*, without unpaired electron). The electron transfer occurs either alone or accompanied by a proton (H-atom transfer, HAT). The electron donor capacity is mainly driven by three intrinsic chemical parameters:

(i)   The presence of H-atom or electron donor moieties.
(ii)   The capacity of the antioxidant to delocalize the single electron after the free radical scavenging reaction, allowing the formation of a relatively stable radical. The higher the π-conjugation along the molecule, the higher the free radical scavenging.

(iii)   The capacity to react directly with free radicals by addition processes, leading to stable adducts.

Over the past decade, physico-chemical parameters have been used to assess the free radical scavenging potential. The capacity of HAT from a **X-H** compound to a free radical is related to the bond dissociation enthalpy (BDE), calculated as follow:

$$BDE(\text{X} - \mathbf{H}) = \ H^{298}[\text{X}\mathbf{H}] - (H^{298}[\text{X}^{\bullet}] + H^{298}[\text{H}^{\bullet}]) \quad (\text{I.}\,12)$$

The lower the BDE of the corresponding moiety, the easier the X-**H** bond cleavage and the more important its role in the free radical scavenging. The electron donor capacity can also be intrinsically assessed with the ionization potential (IP) of the free radical scavenger. The lower the IP, the easier the abstraction of an electron and the more important the free radical scavenging. Other physico-chemical intrinsic parameters (*e.g.*, molecular orbital delocalization and spin density) exist that correlate with the free radical scavenging capacity of natural compounds. By gathering all these physico-chemical parameters, structure activity relationship can be established.

2.2. Natural terpenoid and polyphenol antioxidants

The plant kingdom probably provides the widest armamentarium of antioxidants. Most of them are terpenoids or polyphenols. Few alkaloids can also act as antioxidants (*e.g.*, caffeine, theobromine).

2.2.1. Terpenoids

It is impossible to provide an exhaustive list of terpenoid antioxidants and their mechanisms of action. In this section, we propose key examples. Most of these examples are known as vitamins. Humans cannot synthetize them and these compounds are provided by food.

2.2.1.1. Vitamin E

Vitamin E corresponds to eight different compounds depending on the substitution pattern and the presence of double bonds (Fig. I.18), the most important being α-tocopherol. They are fat-soluble vitamins mainly provided by plant oil (*e.g.*, wheat germ, sunflower, olive and palm

oils). They play an important role in the inhibition of lipid peroxidation, as free radical scavengers. The chromane moiety allows easy HAT reaction thanks to π-conjugation from the OH group to the intracyclic O-atom. The carbon chain increases lipophilicity thus favouring lipid bilayer penetration and direct action in cell membranes during lipid peroxidation. α-Tocopherol is an antioxidant of reference to be compared with new antioxidants.
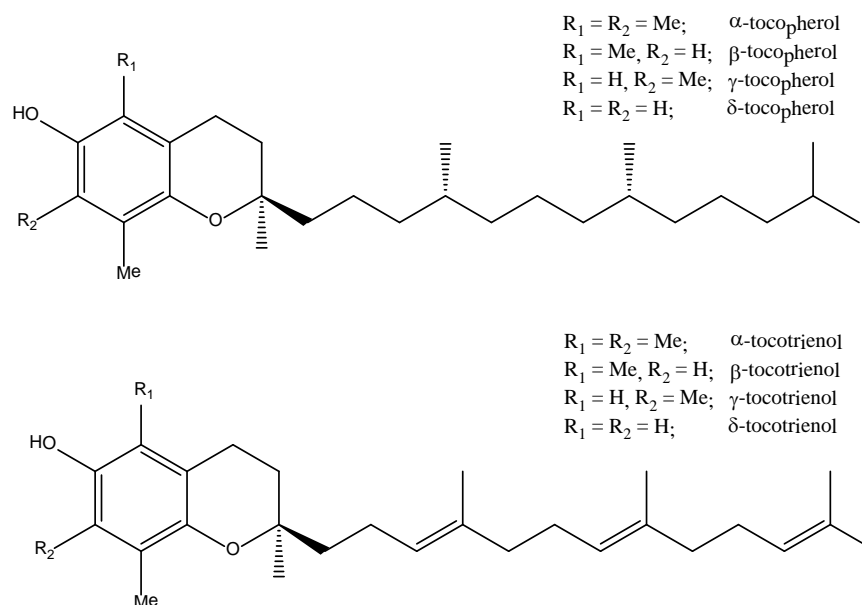
Figure I.18. Chemical structures of vitamins E

2.2.1.2. *Vitamin C*

Even if vitamin C, also known as ascorbic acid (Fig. I.19), is not a terpenoid, its antioxidant activity is related to that of vitamin E. Vitamin C can be extracted from many fruit-bearing plants such as oranges, lemons or strawberries. In contrast to vitamin E, vitamin C is not soluble in lipids and thus cannot act directly on lipid peroxidation. Vitamin C is able to scavenge free radical initiating this process but is also well-known to regenerate vitamin E by HAT.
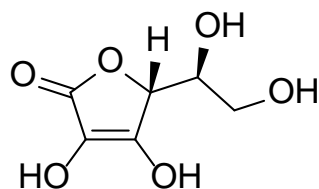
Figure I.19. Chemical structure of reduced vitamin C

2.2.1.3. β-carotene

Surprisingly, β-carotene (Fig. I.20) is a good natural antioxidant even in absence of OH group. It is mainly provided by carrot, pumpkin or sweet potato. The antioxidant activity of β-carotene is due to (i) its high lipophilicity allowing the penetration into cell membranes and (ii) its high π-conjugated system that allows adduct formation with peroxyl free radicals. However, it has been shown that it can act as lipid peroxidation inhibitor only at low oxygen partial pressure. Indeed, it has been showned that β-carotene may be oxidized as a fatty acid when oxygen partial pressure increases, causing thus pro-oxidant effects.[46]
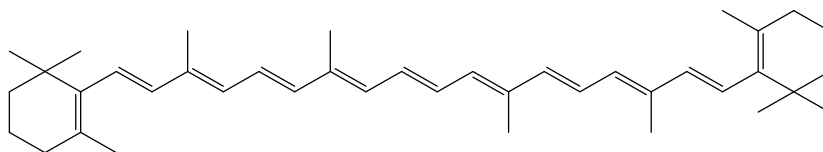
Figure I.20. Chemical structure of β-carotene

2.2.1.4. Curcumin

Curcumin (Fig. I.21) is a yellow-orange pigment derived from the rhizome of *Curcuma longa*. Its structure provides all key parameters to be an efficient antioxidant candidate (*i.e.*, presence of OH groups and an extended π-conjugated system for an efficient HAT). However, the free radical scavenging capacity has been attributed not only to the phenol OH group but also to CH_2 group from the different tautomeric forms in equilibrium (Fig I.21). The phenol OH group provides the most important contribution. However, *e.g.*, under alkaline conditions, the CH_2 moiety may scavenge DPPH (2,2-diphenyl-1-picrylhydrazyl) by sequential-proton loss electron transfer (SPLET).[53]
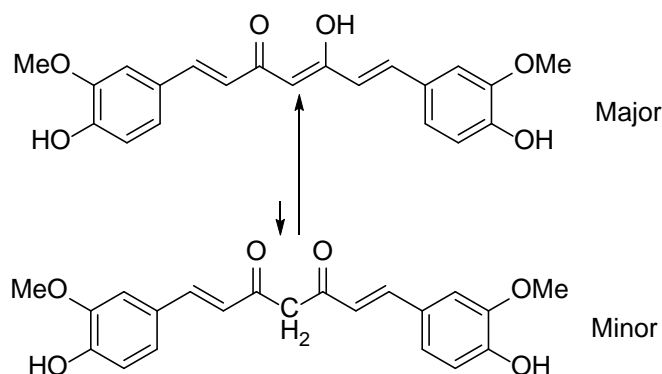
Figure I.21. Tautomeric chemical structures of curcumin.

2.2.2. Polyphenols

Over the past decade, the antioxidant activity of numerous polyphenols has been widely studied. The structure activity relationship (SAR) has been elucidated according to different chemical parameters including the number of OH group, O-H BDE, IP and π-conjugation. It must be stressed that the SAR of polyphenols had only been investigated from a thermodynamic point of view.[11] The following sections give a non-exhaustive overview of the theoretical SARs as established in our lab.

2.2.2.1. Flavonols and flavones

Flavonols (Fig. I.22) are known as powerful free radical scavengers. The B-ring plays an important role in free radical scavenging, mainly in the presence of the ortho-dihydroxyphenyl structure (namely catechol). The B-ring catechol moiety allows dramatically increasing the electron and H-atom donor capacities. The former capacity is related to the mesomeric electron donor property (+M) of OH groups. The latter is related to the stabilization of the formed phenoxyl radical, by H-bonding and π-conjugation from the B-ring to the C-ring (due to the presence of the 2,3-double bond). The BDEs of the 4'-OH group are 82.8 and 87.7 kcal.mol^{-1} for quercetin and kaempferol, respectively (Fig. I.22a&b). For most of flavonols, the A-ring is of minor importance, the 5-OH being engaged in a strong intra molecular H-bonding interaction and the 7-OH does not directly participate in the free radical scavenging.[54] In the rare presence of an extra OH group at C6, the moiety is active. In flavonols, the 3-OH group also

---

[11] The kinetic point of view is consciously discarded since it is studied in chapter 4.

plays a major role: (i) a direct role since the 3-OH group is coupled to the π-electron system, so the corresponding phenoxyl radical is well stabilized and the BDE is low; (ii) an indirect role since the 3-OH group allows a better π-delocalization by +M mesomeric effect, thus lowering BDEs of the B-ring (quercetin *vs.* luteolin see Fig. I.22a and c, respectively).
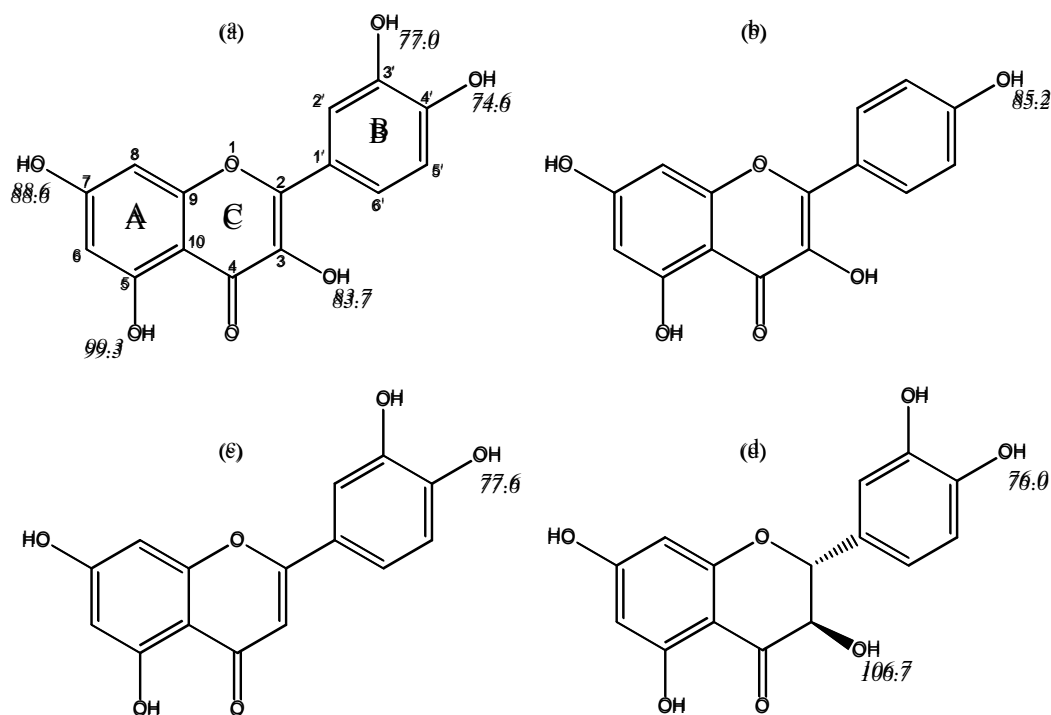
Figure I.22. Chemical structures and BDEs of interest (in kcal.mol^{-1}) of (a) quercetin and (b) kaempferol, (c) luteolin and (d) taxifolin

2.2.2.2. Dihydroflavonols and Flavanones

In this case again, the B-ring, mainly the catechol moiety, strongly participates in the free radical scavenging. Comparing dihydroflavonols (*e.g.*, taxifolin see Fig. I.22d) and flavonols (*e.g.*, quercetin see Fig. I.22a) allows to rationalize the role of the 2,3-double bond which extend π-delocalisation over the molecule. It has a direct influence on BDEs of the OH groups of the B-ring (*e.g.*, 4'-OH group), which are lower in taxifolin than in quercetin. In the former case, the phenoxyl radical is less π-conjugated.[54, 55] Moreover in the absence of the 2,3-double bond (taxifolin), the 3-OH group is not coupled to the π-electron system, thus becoming totally inactive.

Flavan-3-ols such as (+)-catechin or (-)-epicatechin do not present the 2,3-double bond nor the C4 keto group (Fig. I.23a&b). Again the B-ring plays a major role in their well-known powerful free radical scavenging capacity. Due to the absence of the 2,3-double bond it is however less active in vitro than quercetin. It is interesting to note that while most of polyphenols are naturally linked to sugar moieties (glycosides), catechin derivatives are not (aglycons).
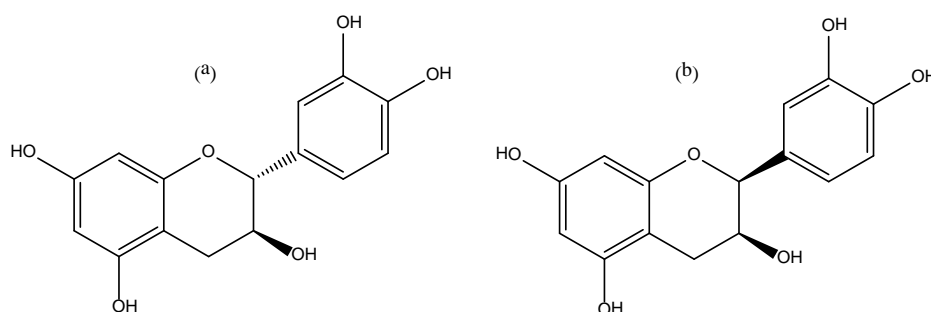
Figure I.23. Chemical structures of (a) (+)-catechin and (b) (-)-epicatechin

2.2.2.4. *Other polyphenols*

The antioxidant activities of chalcones were studied from both theoretical and experimental points of view. Structural analogies with flavonoids have been highlighted such as the presence of the catechol moiety and the presence of a double bond allowing an extended π-delocalization.[56]

The antioxidant activities of two flavonolignans (silybin and dehydrosilybin, Fig. I.24a&b) and their derivatives were studied in a joint experimental and theoretical study.[57] Dehydrosilybin and silybin differ by the presence or absence of the 2,3-double bond, respectively. BDE calculations and DPPH free radical scavenging measurements have confirmed the importance of the coupled 2,3-enol system. Dehydrosilybin appears more efficient to scavenge free radicals than silybin. In this case, the 3-OH group is shown as the most active group. The activity of dehydrosilybin is improved by replacing the 19-methoxy moiety by a hydroxyl group (compound 19-nordehydrosilybin). 19-Nordehydrosilybin exhibits a much higher free radical scavenging activity thanks to the presence of this catechol moiety (Fig. I.24c).
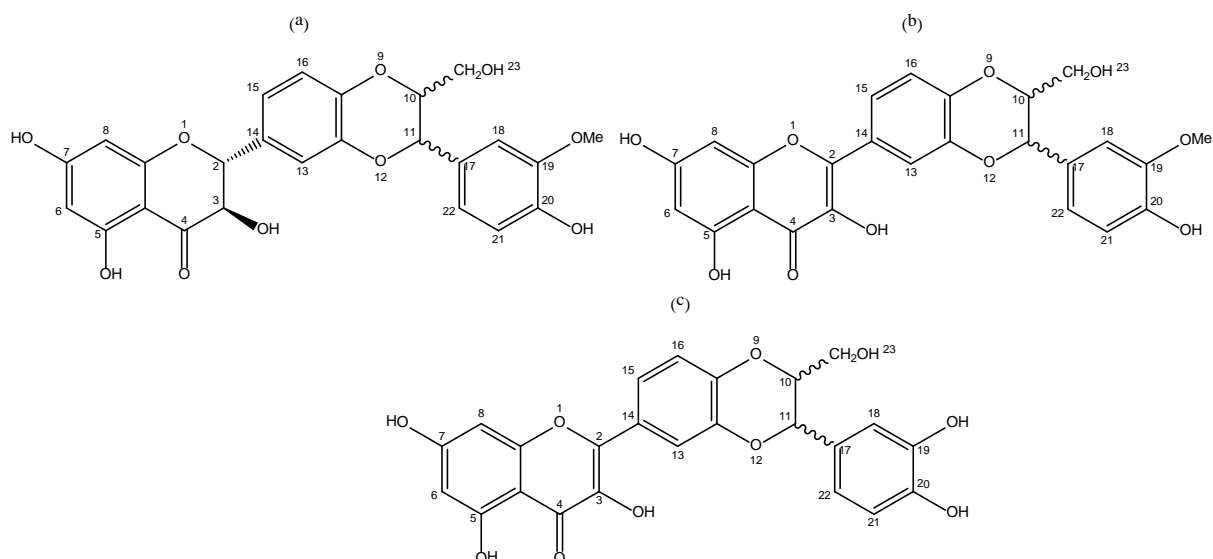
Figure I.24. Chemical structures of (a) silybin, (b) dehydrosilybin and (c) 19-nordehydrosilybin

Recently, the free radical scavenging capacity of a series of guaiacol oligomers, with increasing unit number (Fig. I.25) was elucidated from both theoretical and experimental points of view.[58]
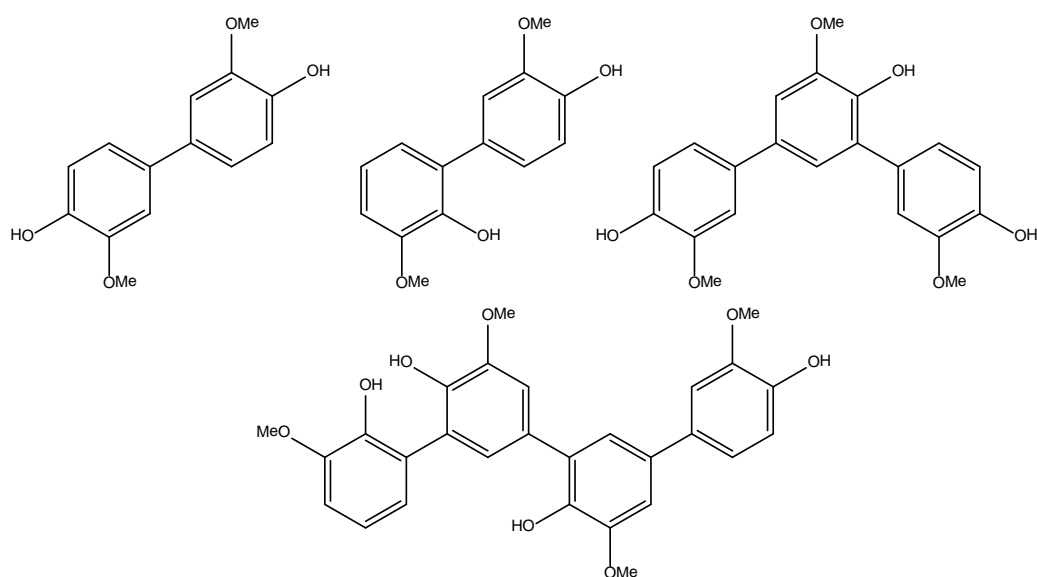
Figure I.25. Examples of guaiacol oligomers

The following conclusions were achieved: guaiacol dimers and trimers both present better free radical scavenging capacities than the stand-alone guaiacol. This increase of capacity is correlated to the increase of π-conjugation and the number of OH groups. No linear relationship

between the activity and the number of units was observed and the free radical capacity somehow saturate for the guaiacol tetramers.[58] In these systems, double HAT is crucial as the phenoxyl radical formed after the first HAT can easily undergo a second HAT leading to stable quinone forms (Fig. I.26).
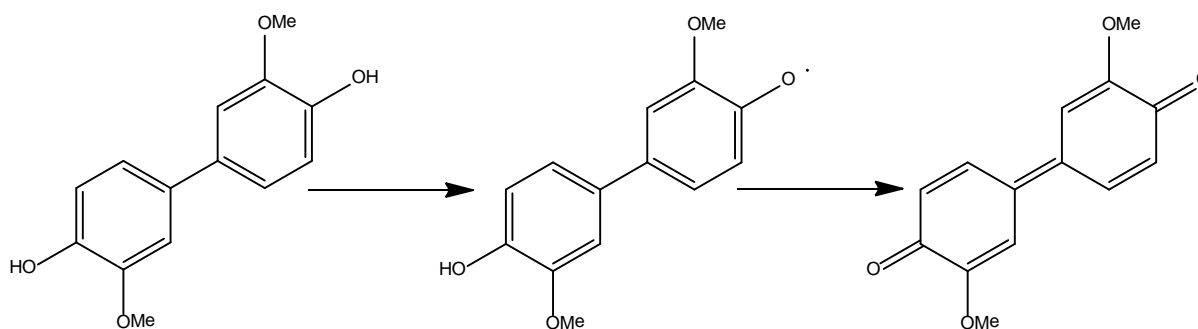
Figure I.26. Example of double HAT in guaiacol dimer

2.2.2.5. Polyphenol metabolites

The abundance of polyphenols in our diet has been clearly proven but the *in vivo* antioxidant activity strongly differs between the various polyphenols. The most abundant and/or active polyphenols are not necessarily the best absorbed.[59, 60] It is now clearly admitted that few polyphenols are absorbed by the organism in their native form and only in low concentration (< 1 µM).

Flavan-3-ols such as (+)-catechin and (-)-epicatechin are mainly transformed into methylether metabolites.[61] The methylation often occurs on the catechol moiety that may dramatically decreases the *in vivo* free radical scavenging activity**.**

Quercetin metabolites can be separated into conjugated (*i.e.*, methylated, sulphated and glucuronides) and cleaved into quercetin derivatives by intestinal microflora (Fig. I.27).[61, 62] In one hand, the literature has reported more than twenty different conjugated quercetin compounds in which the 3'-*O*- and 4'-*O*-methylated, the 4'-*O*-sulphated and 3-*O*-glucuronide quercetin are the most representative. *In vitr*o studies showed that conjugated metabolites exhibit free radical scavenging activities at least twice lower than the aglycone form of quercetin. In the other hand, cleaved quercetin metabolites exhibit far lower *in vitro* free radical scavenging activities (from 2 to 10 times lower than the native quercetin).[62] It must be stressed that the most active cleaved metabolites are still those having the catechol moiety (*i.e.*,

2-(3,4-dihydroxyphenyl)acetic and 3-(3,4-dihydroxy)propionic acids).[62] Quercetin metabolites are less active but still exhibit significant free radical scavenging activities.

Compound	n	R₁	R₂
3-(3-hydroxyphenyl)acetic acid	1	H	OH
2-(3,4-dihydroxyphenyl)acetic acid	1	OH	OH
2-(4-hydroxy-3-methoxyphenyl)acetic acid	1	OH	OMe
3-(4-hydroxyphenyl)propionic acid	2	H	OH
3-(3,4-dihydroxyphenyl)propionic acid	2	OH	OH

Compound	R₁	R₂
4-hydroxybenzoic acid	H	OH
3,4-dihydroxybenzoic acid	OH	OH
4-hydroxy-3-methoxybenzoic acid	OMe	OH
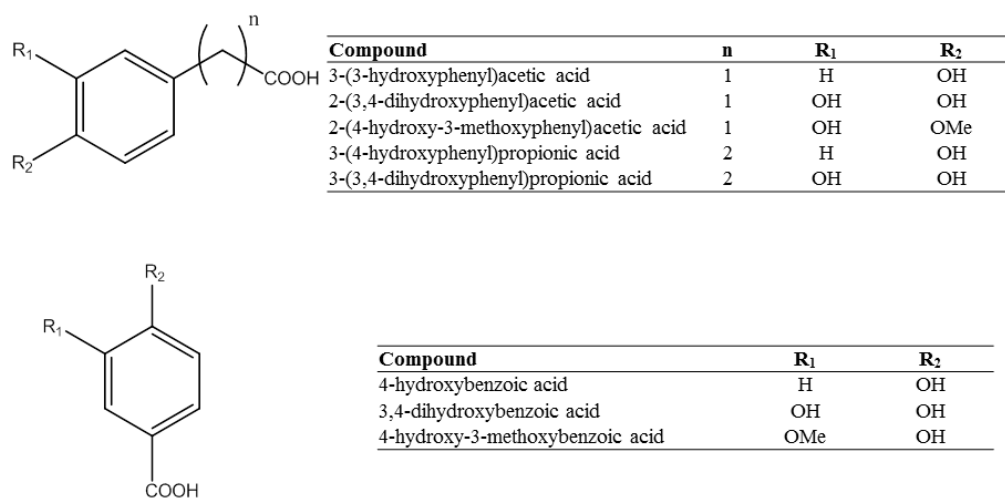
Figure I.27. Examples of bacterial quercetin metabolites

There exist analogies between the metabolism of quercetin and that of other flavonols. Nonetheless, each metabolism pathway has its own specificities and must be carefully studied. *E.g.*, silybin is well absorbed in the gastrointestinal tract. It has been proven that the most important liver metabolite of silybin is the *O*-demethylated silybin (namely 19-norsilybin).[63] 19-Norsilybin possesses the catechol moiety which enhances the free radical scavenging activity as observed with the 19-nor-2,3-dehydrosilybin.[57]

2.3. Mechanisms of the free radical scavenging

Most of the natural antioxidants contain a phenol moiety and are thus usually quoted as ArOH. There exist four different mechanisms of free radical scavenging. The first three are better described in Chapter III.

2.3.1. H-atom transfer

In this pathway, the free radical is reduced by the transfer by HAT from the antioxidant (ArO-**H**) to the free radical (R•):

$$\text{ArO-}\mathbf{H} + \text{R}^\bullet \longrightarrow \text{ArO}^\bullet + \text{R-}\mathbf{H} \qquad (\text{I.13})$$

This reaction yields the phenoxyl radical ArO$^\bullet$ which can be stabilized by (i) π-delocalization, (ii) further HAT, leading to quinones or (iii) reaction with other radicals, leading to closed-shell systems (when ArO$^\bullet$ reacts with another ArO$^\bullet$, dimers are formed).[64, 65]

The O-H BDE (bond dissociation enthalpy) is a relevant intrinsic thermodynamic parameter to assess and predict free radical scavenging by HAT.

When a H-bonding pre-reaction complex (with the lone pair of the O-atom of the free radical) is formed, the HAT mechanism involves a proton transfer, five electrons playing a major role in the transition state.[66] This is the mechanism which is described for polyphenols and so-called proton-coupled electron transfer, HAT(PCET).

2.3.2. Electron Transfer – Proton Transfer (ET-PT)

This mechanism is a two-step mechanism; the first step being electron transfer (ET) from the antioxidant to the free radical leading to a radical-cation ArOH$^{+\bullet}$, the second step is a proton transfer (PT):

$$\text{ArOH} + \text{R}^\bullet \longrightarrow \text{ArOH}^{+\bullet} + \text{R}^- \qquad (\text{I.14a})$$

$$\text{ArO}\mathbf{H}^{+\bullet} + \text{R}^- \longrightarrow \text{ArO}^\bullet + \text{R-}\mathbf{H} \qquad (\text{I.14b})$$

The driving force of ET-PT is electron transfer. This property can be evaluated by the ionization potential (IP).

2.3.3. Sequential Proton Loss Electron Transfer (SPLET)

SPLET is a three-step mechanism.

$$\text{ArO-}\mathbf{H} \longrightarrow \text{ArO}^- + \mathbf{H}^+ \qquad (\text{I.15a})$$

$$\text{ArO}^- + \text{R}^{\bullet} \longrightarrow \text{ArO}^{\bullet} + \text{R}^- \qquad (\text{I.15b})$$

$$\text{R}^- + \text{H}^+ \longrightarrow \text{R-}\mathbf{H} \qquad (\text{I.15c})$$

First, the antioxidant is deprotonated, which is highly sensitive to pH. This deprotonation drastically activates the antioxidant to favour electron transfer.[67] This mechanism highly depends on the polarity of the solvent due to the ionic pair formed during this mechanism.

2.3.4. Adduct formation

The last free radical scavenging reaction consists of the addition of the free radical to the antioxidant. This leads to more or less stable products. It must be stressed that this reaction is a minor route with polyphenols. The hydroxyl radical is a good candidate to undergo such adduct formations:

$$\text{ArOH} + {}^{\bullet}\text{OH} \longrightarrow [\text{ArOH--OH}]^{\bullet} \longrightarrow \text{Stable Products} \qquad (\text{I.16})$$

This mechanism is relatively specific and is mainly observed in solution rich in very reactive species *e.g.*, radiolysis solutions. Adduct formation is favoured on aromatic rings *e.g.*, caffeine[68] (Fig. I.28) and double bonds *e.g.*, ferulic acid (Fig. I.29).[69]
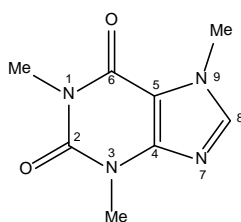
Figure I.28. Chemical Structure of caffeine
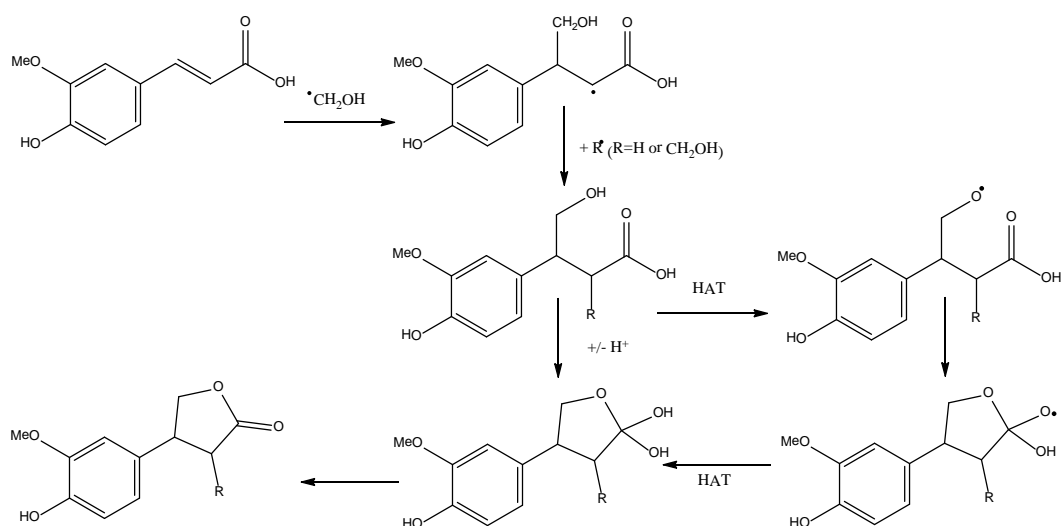
Figure I.29. Adduct formation from ferulic acid, under radiolysis conditions.

Bibliography

[1]   Whittaker, R.H., *New concepts of kingdoms or organisms. Evolutionary relations are better represented by new classifications than by the traditional two kingdoms.* Science, 1969. **163**: p. 150-160.

[2]   Hadacek, F., *Secondary metabolites as plant traits: Current assessment and future perspective.* Critical Reviews in Plant Sciences, 2002. **21**: p. 273-322.

[3]   Edreva, A.*, et al.*, *Stress-protective role of secondary metabolites: diversity of functions and mechanisms.* General and Applied Plant Physiology, 2008. **34**: p. 67-78.

[4]   Dewick, P.M., *Secondary Metabolism: The Building Blocks and Construction Mechanisms*, in *Medicinal Natural Products*2001, John Wiley & Sons, Ltd. p. 7-34.

[5]   Bolton, M.D., *Primary metabolism and plant defense--fuel for the fire.* Molecular Plant-Microbe Interactions, 2009. **22**: p. 487-497.

[6]   Bernards, M.A., *Plant natural products: a primerThe present review is one in the special series of reviews on animal–plant interactions.* Canadian Journal of Zoology, 2010. **88**: p. 601-614.

[7]   Bruneton, J., *Pharmacognosie, phytochimie, plantes medicinales*1999, Cachan, [S.l.]: Éditions médicales internationales Editions Technique & Documentation*'.

[8]   Creighton, T.E., *Proteins : structures and molecular principles*1993, New York: W.H. Freeman.

[9]   Andersen, Ø.M. and K.R. Markham, *Flavonoids : chemistry, biochemistry, and applications*2006, Boca Raton, FL: Taylor&Francis.

[10]   *The Phenol-Explorer database*. Available from: http://www.phenol-explorer.eu.

[11]   Neveu, V.*, et al.*, *Phenol-Explorer: an online comprehensive database on polyphenol contents in foods.* Database, 2010: p. No pp. given.

[12]   Harborne, J.B., T.J. Mabry, and H. Mabry, *The Flavonoids*1975, London: Chapman & Hall.

[13]   Esch, H.*, et al.*, *Phytochrome-controlled phototropism of protonemata of the moss ceratodon purpureus: physiology of the wild type and class 2 ptr-mutants.* Planta, 1999. **209**: p. 290-298.

[14]   Cheng, D., K. Vrieling, and P.G. Klinkhamer, *The effect of hybridization on secondary metabolites and herbivore resistance: implications for the evolution of chemical diversity in plants.* Phytochemistry Reviews, 2011. **10**: p. 107-117.

[15]   Gressel, J., *BLUE LIGHT PHOTORECEPTION.* Photochemistry and Photobiology, 1979. **30**: p. 749-754.

[16]   Cashmore, A.R.*, et al.*, *Cryptochromes: blue light receptors for plants and animals.* Science, 1999. **284**: p. 760-765.

[17]   Briggs, W.R. and J.M. Christie, *Phototropins 1 and 2: versatile plant blue-light receptors.* Trends in Plant Science, 2002. **7**: p. 204-210.

[18]   Bouly, J.P.*, et al.*, *Cryptochrome blue light photoreceptors are activated through interconversion of flavin redox states.* Journal of Biological Chemistry, 2007. **282**: p. 9383-9391.

[19]   Folta, K.M., *Green light stimulates early stem elongation, antagonizing light-mediated growth inhibition.* Plant Physiology, 2004. **135**: p. 1407-1416.

[20]   Zhang, T., S.A. Maruhnich, and K.M. Folta, *Green light induces shade avoidance symptoms.* Plant Physiology, 2011. **157**: p. 1528-1536.

[21]   Miller, C.O., *Similarity of Some Kinetin and Red Light Effects.* Plant Physiol, 1956. **31**: p. 318-319.

[22]   Reed, J.W.*, et al.*, *Mutations in the gene for the red/far-red light receptor phytochrome B alter cell elongation and physiological responses throughout Arabidopsis development.* Plant Cell, 1993. **5**: p. 147-157.

[23]   Stapleton, A.E., *Ultraviolet Radiation and Plants: Burning Questions.* Plant Cell, 1992. **4**: p. 1353-1358.

[24]   Pfeifer, G.P., *Formation and processing of UV photoproducts: effects of DNA sequence and chromatin environment.* Photochemistry and Photobiology, 1997. **65**: p. 270-283.

[25]   Blancafort, L. and A. Migani, *Modeling thymine photodimerizations in DNA: mechanism and correlation diagrams.* Journal of the American Chemical Society, 2007. **129**: p. 14540-14541.

[26]   Douki, T.*, et al.*, *Formation of the main UV-induced thymine dimeric lesions within isolated and cellular DNA as measured by high performance liquid chromatography-tandem mass spectrometry.* Journal of Biological Chemistry, 2000. **275**: p. 11678-11685.

[27]   Marguet, S. and D. Markovitsi, *Time-resolved study of thymine dimer formation.* Journal of the American Chemical Society, 2005. **127**: p. 5780-5781.

[28]   Schreier, W.J.*, et al.*, *Thymine dimerization in DNA is an ultrafast photoreaction.* Science, 2007. **315**: p. 625-629.

[29]   Durbeej, B. and L.A. Eriksson, *On the formation of cyclobutane pyrimidine dimers in UV-irradiated DNA: why are thymines more reactive?* Photochemistry and Photobiology, 2003. **78**: p. 159-167.

[30]   Kielbassa, C., L. Roza, and B. Epe, *Wavelength dependence of oxidative DNA damage induced by UV and visible light.* Carcinogenesis, 1997. **18**: p. 811-816.

[31]   Kawanishi, S., Y. Hiraku, and S. Oikawa, *Mechanism of guanine-specific DNA damage by oxidative stress and its role in carcinogenesis and aging.* Mutation Research, 2001. **488**: p. 65-76.

[32]   Rozema, J.*, et al.*, *UV-B as an environmental factor in plant life: stress and regulation.* Trends in Ecology and Evolution, 1997. **12**: p. 22-28.

[33] Kuhlbrandt, W., D.N. Wang, and Y. Fujiyoshi, *Atomic model of plant light-harvesting complex by electron crystallography.* Nature, 1994. **367**: p. 614-621.

[34] Wright, A.H.*, et al.*, *The interrelationship between the lower oxygen limit, chlorophyll fluorescence and the xanthophyll cycle in plants.* Photosynthesis Research, 2011. **107**: p. 223-235.

[35] Francis, F.J., *Food colorants: anthocyanins.* Critical Reviews in Food Science and Nutrition, 1989. **28**: p. 273-314.

[36] Rein, M., *Copigmentation reactions and color stability of berry anthocyanins*, in *Department of Applied Chemistry and Microbiology*2005, University of Helsinki. p. 88.

[37] Anouar, E.H.*, et al.*, *UV/Visible spectra of natural polyphenols: A time-dependent density functional theory study.* Food Chemistry, 2012. **131**: p. 79-89.

[38] Rustioni, L.*, et al.*, *Bunch exposure to direct solar radiation increases ortho-diphenol anthocyanins in Northern Italy climatic condition.* Journal Internation des Sciences de la Vigne et du Vin, 2011. **45**: p. 85-99.

[39] Sadilova, E., R. Carle, and F.C. Stintzing, *Thermal degradation of anthocyanins and its impact on color and in vitro antioxidant capacity.* Molecular Nutrition & Food Research, 2007. **51**: p. 1461-1471.

[40] Willstatter, R. and E.H. Zollinger, *Anthocyans. XVI. Anthocyans of the grape and of the bilberry. II.* Journal of the Chemical Society, Abstract, 1916. **112**: p. 47-48.

[41] Robinson, G.M. and R. Robinson, *A survey of anthocyanins. I.* Biochemical Journal, 1931. **25**: p. 1687-1705.

[42] Boulton, R., *The Copigmentation of Anthocyanins and Its Role in the Color of Red Wine: A Critical Review.* American Journal of Enology and Viticulture, 2001. **52**: p. 67-87.

[43] Yoshida, K., M. Mori, and T. Kondo, *Blue flower color development by anthocyanins: from chemical structure to cell physiology.* Natural Product Reports, 2009. **26**: p. 884-915.

[44] Markakis, P. and Editor, *Anthocyanins as Food Colors*1982: Academic Press. 263 pp.

[45] Rustioni, L.*, et al.*, *Copigmentation and anti-copigmentation in grape extracts studied by spectrophotometry and post-column-reaction HPLC.* Food Chemistry, 2012. **132**: p. 2194-2201.

[46] Bourgeois, C.F., *Antioxidant vitamins and health : cardiovascular disease, cancer, cataracts, and aging*2003, New York: HNB Pub.

[47] Babior, B.M., *Oxidants from phagocytes: agents of defense and destruction.* Blood, 1984. **64**: p. 959-966.

[48] Gutteridge, J.M., *Free radicals in disease processes: a compilation of cause and consequence.* Free Radical Research Communications, 1993. **19**: p. 141-158.

[49]   Doll, R. and R. Peto, *The Causes of Cancer: Quantitative Estimates of Avoidable Risks of Cancer in the United States Today.* Journal of the National Cancer Institute, 1981. **66**: p. 1192-1308.

[50]   Berlett, B.S. and E.R. Stadtman, *Protein oxidation in aging, disease, and oxidative stress.* Journal of Biological Chemistry, 1997. **272**: p. 20313-20316.

[51]   Trouillas, P., J. Bergès, and C. Houée-Lévin, *Toward understanding the protein oxidation processes: •OH addition on tyrosine, phenylalanine, or methionine?* International Journal of Quantum Chemistry, 2011. **111**: p. 1143-1151.

[52]   Varadarajan, S.*, et al.*, *Review: Alzheimer's amyloid beta-peptide-associated free radical oxidative stress and neurotoxicity.* Journal of Structural Biology, 2000. **130**: p. 184-208.

[53]   Galano, A.*, et al.*, *Role of the reacting free radicals on the antioxidant mechanism of curcumin.* Chemical Physics, 2009. **363**: p. 13-23.

[54]   Trouillas, P.*, et al.*, *A theoretical study of the conformational behavior and electronic structure of taxifolin correlated with the free radical-scavenging activity.* Food Chemistry, 2004. **88**: p. 571-582.

[55]   Trouillas, P.*, et al.*, *A DFT study of the reactivity of OH groups in quercetin and taxifolin antioxidants: The specificity of the 3-OH site.* Food Chemistry, 2006. **97**: p. 679-688.

[56]   Kozlowski, D.*, et al.*, *Density Functional Theory Study of the Conformational, Electronic, and Antioxidant Properties of Natural Chalcones.* Journal of Physical Chemistry A, 2007. **111**: p. 1138-1145.

[57]   Trouillas, P.*, et al.*, *Mechanism of the Antioxidant Action of Silybin and 2,3-Dehydrosilybin Flavonolignans: A Joint Experimental and Theoretical Study.* Journal of Physical Chemistry A, 2008. **112**: p. 1054-1063.

[58]   Anouar, E.*, et al.*, *Free Radical Scavenging Properties of Guaiacol Oligomers: A Combined Experimental and Quantum Study of the Guaiacyl-Moiety Role.* Journal of Physical Chemistry A, 2009. **113**: p. 13881-13891.

[59]   Manach, C.*, et al.*, *Polyphenols: food sources and bioavailability.* American Journal of Clinical Nutrition, 2004. **79**: p. 727-747.

[60]   Hollman, P.C.H., *Absorption, Bioavailability, and Metabolism of Flavonoids.* Pharmaceutical Biology, 2004. **42**: p. 74-83.

[61]   Spencer, J.P.E., *Metabolism of Tea Flavonoids in the Gastrointestinal Tract.* Journal of Nutrition, 2003. **133**: p. 3255S-3261S.

[62]   Dueñas, M.*, et al.*, *Antioxidant properties of major metabolites of quercetin.* European Food Research and Technology, 2011. **232**: p. 103-111.

[63]   Jančová, P.*, et al.*, *Silybin Is Metabolized by Cytochrome P450 2C8 in Vitro.* Drug Metabolism and Disposition, 2007. **35**: p. 2035-2039.

[64]   Kosinova, P., *et al.*, *Dimerisation process of silybin-type flavonolignans: insights from theory.* ChemPhysChem, 2011. **12**: p. 1135-1142.

[65]   Velu, S.S., *et al.*, *Regio- and Stereoselective Biomimetic Synthesis of Oligostilbenoid Dimers from Resveratrol Analogues: Influence of the Solvent, Oxidant, and Substitution.* Chemistry – A European Journal, 2008. **14**: p. 11376-11384.

[66]   Litwinienko, G. and K.U. Ingold, *Solvent Effects on the Rates and Mechanisms of Reaction of Phenols with Free Radicals.* Accounts of Chemical Research, 2007. **40**: p. 222-230.

[67]   Zhang, H.-Y. and H.-F. Ji, *How vitamin E scavenges DPPH radicals in polar protic media.* New Journal of Chemistry, 2006. **30**: p. 503-504.

[68]   León-Carmona, J.R. and A. Galano, *Is Caffeine a Good Scavenger of Oxygenated Free Radicals?* Journal of Physical Chemistry B, 2011. **115**: p. 4538-4546.

[69]   Anouar, E., *et al.*, *New aspects of the antioxidant properties of phenolic acids: a combined theoretical and experimental approach.* Physical Chemistry Chemical Physics, 2009. **11**: p. 7659-7668.

Chapter II. Theoretical chemistry methods to tackle chemical and optical issues

The basements of theoretical chemistry are known for a century. Over the past decades, the fantastic evolution of computer facilities has allowed somewhat democratization. The diversity of theoretical methods is huge, however two main formalisms exist based on either nuclei or electrons:

(i)   Molecular mechanics focuses on nuclei applying the classical (Newton) laws of physics. In this case, atoms and bonds are modelled as charged balls and springs, respectively. These methods are mainly applied to big molecular systems (*e.g.*, DNA, proteins, membranes and polymers).

(ii)   Quantum chemistry focuses on electrons. It aims at solving the Schrödinger equation. Quantum chemistry is originally dedicated to small molecular systems and all phenomena implying electronic behaviours (*e.g.*, reactivity, UV/Vis absorption properties). Only this formalism is described in the present manuscript.

Quantum mechanical methods can be divided into three sub-families: (i) Hartree-Fock (HF) and post-HF methods, (ii) semi-empirical methods and (iii) methods based on the density functional theory (DFT). In this chapter, Section A is a brief reminding of the theory of HF and two post-HF (MP2 and CCSD(T)) methods. Section B presents DFT methods focusing on the last refinements. Section C describes UV/Visible absorption properties and the theoretical approaches dedicated to these properties, in particular the time dependent DFT (TD-DFT) framework.

Section A. Hartree-Fock approximation and beyond

1. Reminding on Hartree-Fock approximation

1.1. The Schrödinger equation and the Born-Oppenheimer approximation

The Schrödinger equation describes the energy and motion of electrons and nuclei.[1, 2] For a molecular system, the time-independent non-relativistic Schrödinger equation is given by:

$$\widehat{\mathcal{H}}\Psi = E\Psi \qquad (\text{II}.\,1)$$

where $\mathcal{H}$, Ψ and E are the Hamiltonian operator, the wave function and the energy of the system, respectively. The Hamiltonian operator includes all the different interactions for a system with N-electrons and M-nuclei. It is given in atomic units as follows:

$$\widehat{\mathcal{H}} = -\sum_{i=1}^{N}\frac{1}{2}\nabla_i^2 - \sum_{A=1}^{M}\frac{1}{2M_A}\nabla_i^2 - \sum_{i=1}^{N}\sum_{A=1}^{M}\frac{Z_A}{r_{iA}} + \sum_{i=1}^{N}\sum_{j>i}^{N}\frac{1}{r_{ij}} + \sum_{A=1}^{M}\sum_{B>A}^{M}\frac{Z_AZ_B}{r_{AB}} \qquad (\text{II}.\,2)$$

where M_A, Z_A are the mass and the charge of nucleus, respectively. r_{iA}, r_{ij} and r_{AB} are nucleus-electron, electron-electron and nucleus-nucleus distances, respectively. The first two terms are the kinetic operators for electrons T_{elec} and nuclei T_N, respectively. The last three terms are the electron-nucleus (V_{eN}), electron-electron (V_{ee}) and nucleus-nucleus (V_{NN}) potentials, respectively.

There are too many variables in Eq. (II.2) to be exactly solved for $N > 1$. Born and Oppenheimer suggested to separate electrons and nuclei;[2, 3] nucleus motions are neglected since nuclei are much heavier than electrons. It means that the electronic wave function depends only on the positions of nuclei and not on their momenta. The electronic Schrödinger equation is given by:

$$\widehat{\mathcal{H}}_{elec}\Psi_{elec} = \Psi_{elec}E_{elec} \qquad (\text{II}.\,3)$$

where the electronic Hamiltonian is defined by :

$$\hat{\mathcal{H}}_{elec} = -\sum_{i=1}^{N} \frac{1}{2}\nabla_i^2 - \sum_{i=1}^{N}\sum_{A=1}^{M} \frac{Z_A}{r_{iA}} + \sum_{i=1}^{N}\sum_{j>i}^{N} \frac{1}{r_{ij}} \qquad (\text{II.}\,4)$$

The total energy is obtained by adding the constant nuclear repulsion for fixed nuclei to the solved electronic energy (E_{elec}):

$$E = E_{elec} + \sum_{A=1}^{M}\sum_{B>A}^{M} \frac{Z_A Z_B}{r_{AB}} \qquad (\text{II.}\,5)$$

The nucleus motion within the Born-Oppenheimer approximation may be solved by describing vibration, rotation and translation of a molecule within the harmonic approximation.[12] For the sake of readability, the "$_{elec}$" is now dropped.

1.2. Hartree-Fock approximation

The electrons are described by their positions r_i and their spins ω_t. Within the molecular orbital (MO) theory, an electron is described by a spin-orbital wave function $\chi(x_i)$ which is given by:

$$\chi(x_i) = \begin{cases} \varphi(r_i)\alpha(\omega_i) \\ \quad \text{or} \\ \varphi(r_i)\beta(\omega_i) \end{cases} \qquad (\text{II.}\,6)$$

where $\varphi(r_i)$ is the spatial orbital, $\alpha(\omega_i)$ and $\beta(\omega_i)$ are the function corresponding to spin up and spin down, respectively. In the following, spatial and spin coordinates are denoted collectively by x_i.

The electronic wave function Ψ of a N-electron system is quoted $\Psi(x_1, x_2, \dots, x_N)$. In HF model, the best approximation of the electronic wave function Ψ is a Slater determinant which satisfies both Schrödinger equation and the anti-symmetry principle[13]:

---

[12] Vibrations, rotations and translations can be solved by (i) normal mode analysis and (ii) following potential energy surfaces

[13] The antisymmetry principle is the general statement of the Pauli principle stipulating that two electrons having the same spin cannot (i) be at the same place and (ii) have the same energy.

$$\Psi(x_1, x_2, \ldots, x_N) = \frac{1}{\sqrt{N!}} \begin{vmatrix} \chi_i(x_1) & \chi_j(x_1) & \cdots & \chi_k(x_1) \\ \chi_i(x_2) & \chi_j(x_2) & \cdots & \chi_k(x_2) \\ \vdots & \vdots & \ddots & \vdots \\ \chi_i(x_N) & \chi_j(x_N) & \cdots & \chi_k(x_N) \end{vmatrix} \qquad (II.7)$$

When inserted Eq. (II.7) in Eq. (II.3) and applying the variational principle on the energy, we obtain the HF equations. At this stage a polyelectronic problem must be solved. The HF approximation proposes to replace this complicated many-electron problem by a one-electron problem in which electron-electron repulsion is treated in an average way. That is, the electron does not see all the different electrons separately, but sees an average potential field, which is due to the other electrons. Within this approximation the HF equations are derived as:

$$\hat{f}(i)\chi(x_i) = \varepsilon_i \chi(x_i) \qquad (II.8)$$

where $f(i)$ is an effective one-electron operator and ε_i is the energy of a given spin-orbital $\chi(x_i)$. The mono-electronic Fock operator is given by:

$$\hat{f}_i = -\frac{1}{2}\nabla_i^2 - \sum_{A=1}^{M}\frac{Z_A}{r_{iA}} + v_i^{HF} = H_i^c + v_i^{HF} \qquad (II.9)$$

where H_i^c is the monoelectronic core operator that includes kinetics and electron-nuclei interactions; v_i^{HF} is also a monoelectronic operator describing electron-electron interaction within the HF approximation, it is given by:

$$\hat{v}_i^{HF} = \sum_{j \neq i}^{N}\left(J_j(i) - K_j(i)\right) \qquad (II.10)$$

where $J_j(i)$ and $K_j(i)$ are the Coulomb repulsion and the exchange term, respectively. The latter satisfies the indiscernibility principle and is a pure quantum contribution, corresponding the correlation of motion for electrons having parallel spins. The HF Hamiltonian is defined for an N-electron system by:

$$\hat{\mathcal{H}}_{HF} = \sum_i^N f_i = \sum_i^N H_i^c + \sum_i^N \sum_{j>i}^N \left(J_j(i) - K_j(i)\right) \qquad (II.11)$$

The HF energy (E_{HF}) is obtained by solving HF equations, on the basis of N-occupied spin-orbitals.

1.3. Hartree-Fock limit or the correlation energy

Considering an electron interacting with an electron cloud easily underlines the main limit of the HF approximation, namely electron correlation cannot be fully taken into account. The correlation energy is a rather complex concept. Several philosophies tried and distinguished the different correlations but no global definition has been fully convincing. The most general definition of the correlation effect can be described as follow: in a two-electron system, the position and the spin of electron 1 is related to the position and the spin of electron 2. HF theory partially includes correlation effects as Coulomb J and exchange K contributions are explicitly defined (see Eq. (II.11)).[14] All the other correlation contributions are not taken into account (mainly correlation attributed to two electrons having antiparallel spins). Actually the correlation energy (E_{corr}) usually refers to all the contributions that are not taken into account within the HF formalism. It is given by:

$$E_{corr} = E_{exact} - E_{HF} \qquad (\text{II}.12)$$

where E_{exact} is the exact electronic energy (not known) for the exact wave function (not known) and E_{HF} is the HF energy derived from Eqs. (II.8-11).

2. Post Hartree-Fock methods: how to include correlation energy

The evaluation of E_{corr} is the main objective of post-HF methods. They improve the HF model by expressing E_{corr} to approach the exact energy E_{exact}.

---

[14] In some case, confusion in correlation definitions arises from the Fermi and Coulomb correlations. Those correlations are taken into account into HF theory since the former is related to the exchange potential (to follow the anti-symmetric principle of the wave function) and the latter is related to the Coulomb repulsion. In other words, those correlations differ from E_{corr} in Eq. (II.12).

2.1. The perturbation Møller-Plesset methods

2.1.1. Introduction to the perturbation theory

The perturbation theory is a mathematical method to find an approximate solution to an equation which cannot be solved exactly. The main philosophy is to add a small term to the mathematical description of the problem. The resulting sum should then describe the exact unsolvable problem.

To picture this philosophy in the quantum mechanical background, let us take the Rayleigh-Schrodinger equation in which the Hamiltonian is perturbed by an operator V:[3]

$$\widehat{\mathcal{H}}|\Phi_i\rangle = \mathcal{E}_i|\Phi_i\rangle = \left(\widehat{\mathcal{H}}_0 + \lambda\widehat{V}\right)|\Phi_i\rangle = \mathcal{E}_i|\Phi_i\rangle \qquad \text{(II. 13)}$$

where λ is the perturbation factor; for $\lambda = 0$, the perturbation is zero whereas the perturbation is maximum for $\lambda = 1$. The exact eigenvalues and eigenfunctions are expanded as Taylor series:

$$\mathcal{E}_i = E_i^{(0)} + \lambda E_i^{(1)} + \lambda^2 E_i^{(2)} + \cdots \qquad \text{(II. 14a)}$$

$$|\Phi_i\rangle = \left|\Psi_i^{(0)}\right\rangle + \lambda\left|\Psi_i^{(1)}\right\rangle + \lambda^2\left|\Psi_i^{(2)}\right\rangle + \cdots \qquad \text{(II. 14b)}$$

where $E_i^{(n)}$ are the nth-order energy. For $\lambda = 0$ the Taylor series is:

$$|\Phi_i\rangle = \left|\Psi_i^{(0)}\right\rangle \qquad \text{(II. 15)}$$

By including Eqs. (II.14) in (II.13), we obtain by, identification up, to the second order (*i.e.*, λ^2):

$$n = 0 \quad \widehat{\mathcal{H}}_0\left|\Psi_i^{(0)}\right\rangle = E_i^{(0)}\left|\Psi_i^{(0)}\right\rangle \qquad \text{(II. 16a)}$$

$$n = 1 \quad \widehat{\mathcal{H}}_0\left|\Psi_i^{(1)}\right\rangle + \widehat{V}\left|\Psi_i^{(0)}\right\rangle = E_i^{(0)}\left|\Psi_i^{(1)}\right\rangle + E_i^{(1)}\left|\Psi_i^{(0)}\right\rangle \qquad \text{(II. 16b)}$$

$$n = 2 \quad \widehat{\mathcal{H}}_0\left|\Psi_i^{(2)}\right\rangle + \widehat{V}\left|\Psi_i^{(1)}\right\rangle = E_i^{(0)}\left|\Psi_i^{(2)}\right\rangle + E_i^{(1)}\left|\Psi_i^{(1)}\right\rangle E_i^{(2)}\left|\Psi_i^{(0)}\right\rangle \qquad \text{(II. 16c)}$$

Left-multiplying by $\Psi_i^{(0)}$ and integrating II.16b and II.16c, we obtain the first and second order corrections to energy, respectively:

$$E_i^{(1)} = \left\langle \Psi_i^{(0)} \middle| \hat{V} \middle| \Psi_i^{(0)} \right\rangle \qquad (\text{II. 17a})$$

$$E_i^{(2)} = \left\langle \Psi_i^{(0)} \middle| \hat{V} \middle| \Psi_i^{(1)} \right\rangle \qquad (\text{II. 17a})$$

The first-order corrected wave function $\Psi_i^{(1)}$ is defined by a linear combination of $\Psi_i^{(n)}$ taking the intermediary normalization theorem[15] into account:

$$\begin{cases} \Psi_i^{(1)} = \displaystyle\sum_n c_{ni}^{(1)} \Psi_n^{(0)} & (\text{II. 18a}) \\ \left\langle \Psi_i^{(0)} \middle| \Psi_i^{(1)} \right\rangle = 0 & (\text{II. 18b}) \end{cases}$$

If the wave functions are real, the general result for the second-order energy can be demonstrated to be:[3]

$$E_i^{(2)} = \sum_n \frac{\left| \left\langle \Psi_i^{(0)} \middle| \hat{V} \middle| \Psi_n^{(0)} \right\rangle \right|^2}{E_i^{(0)} - E_n^{(0)}} \qquad (\text{II. 19})$$

where $\Psi_n^{(0)}$ is defined in Eq. (II.18a) and E_n^0 its energy.

2.1.2. Møller-Plesset methods

2.1.2.1. The equations

The Møller-Plesset (MP) theory corrects the HF Hamiltonian $\mathcal{H}_0$ in a perturbative way, the perturbation being given by:[3, 4]

---

[15] The intermediary normalization theorem states that Φ_i is written to satisfy that $\left\langle \Psi_i^{(0)} \middle| \Phi_i \right\rangle = 1$. Thereby, by developing Φ_i, it can be demonstrated that Eq. (II.18b) is true. The complete demonstration is available in Ref. 3.

$$\lambda \hat{V} = \hat{\mathcal{H}} - \hat{\mathcal{H}}_0 = \frac{1}{2} \sum_i \sum_j \frac{1}{r_{ij}} - \sum_i \hat{v}_i^{HF} \qquad \text{(II. 20)}$$

Using the HF Hamiltonian from Eq. (II.20), one can solve and obtain the different energies:

$$E_0^{(0)} = E_{HF} + E_{ee} \qquad \text{(II. 21)}$$

where E_{ee} is the electron-electron term already included in E_{HF} (i.e., the Coulomb and Exchange terms).

$$E_0^{(1)} = -E_{ee} \qquad \text{(II. 22)}$$

Therefore the truncated first-order Møller-Plesset (MP1) method is useless since it provides the HF energy:

$$E_{MP1} = E_0^{(0)} + E_0^{(1)} = E_{HF} \qquad \text{(II. 23)}$$

The second-order Møller-Plesset (MP2) energy is obtained from Eq. (II.19). The $\Psi_i^{(0)}$ wave function is defined by the ground-state HF Slater determinant. The $\Psi_n^{(0)}$ wave function is here defined by the double-electron excited wave function Ψ^D. It can be demonstrated that the single-electron excitation wave function Ψ^S is forbidden due to Brillouin's theorem.[16] The second order energy is thus described:

$$E_0^{(2)} = \sum_{\substack{Possible \\ diexcitations}} \frac{\left| \left\langle \Psi_{HF} \middle| \sum_{j>i} \frac{1}{r_{ij}} \middle| \Psi^D \right\rangle \right|^2}{E_0^0 - E_0^D} = \sum_{s>r} \sum_{b>a} \frac{|\langle ab||rs \rangle|^2}{(\varepsilon_r - \varepsilon_a) + (\varepsilon_s - \varepsilon_b)} \qquad \text{(II. 24)}$$

where a and b refer to the spin-orbitals of electrons 1 and 2 for the ground state, while r and s are those of the excited state. The MP2 energy is given by the sum of Eqs. (II.21,22&24) and provide very reliable results with respect to experimental data.

---

[16] Taking single-electron or higher excitation wave function provide zero since the perturbation operator is bielectronic. The mathematical demonstration is available in Ref. 3.

The computational time of MP2 calculations varies as a N^5 function (N being the number of basis functions). The system size is still limited. Nowadays, MP2 allows tackling molecular systems containing up to thirty atoms, at a reasonable time. Moreover MP2 is not as accurate as high level theory (*e.g.*, CCSD(T), see Section 2.2) or for some systems even faster computational methods as DFT.[5] MP2 mainly fails at assessing (i) atomization energy, (ii) dispersion interactions, and (iii) complicated correlation problems (*e.g.*, biradicals, transition states and metal containing systems). Furthermore, convergence problems in MP2 calculations appear when using large basis sets. When using small basis sets (*e.g.*, 6-31+G(d,p)), these problems are avoided but accuracy then appears very limited.

The third order Møller-Plesset (MP3) method does not improve the results while dramatically increasing computational time. MP4 is much better and allow reaching high accuracy level; nonetheless the computational time evolving in this case as a N^7 function, this method is limited to very small molecular systems. Recently, MP2 has been improved to overcome its own limitations. Here we present the most known MP2 refinements, namely spin-component-scaled (SCS)-MP2 methods.

2.1.3.   SCS-MP2 methods

Following Eq. (II.24), the MP2 correlation energy $E_{corr,MP2}$ can be decomposed into the components of spin-paired ($E^{\uparrow\downarrow}$) and spin-unpaired ($E^{\uparrow\uparrow}$ or $E^{\downarrow\downarrow}$) double-excited electron systems. It must be stressed that the spin-unpaired contributions account half up-up ($\uparrow\uparrow$) and half down-down ($\downarrow\downarrow$) double excitations:[5]

$$E_{corr,MP2} = E_0^{(2)} = \frac{1}{2}E^{\uparrow\uparrow} + \frac{1}{2}E^{\downarrow\downarrow} + E^{\uparrow\downarrow} \qquad (\text{II.}25)$$

Classical MP2 underestimates the energy of the spin-paired electron contribution while that of spin-unpaired electrons is overestimated. In 2003, Grimme parameterized MP2[17] by scaling each contribution within the SCS-MP2 refinement:

---

[17] Thereby, SCS-MP2 and derivative methods no longer belong to *ab initio* methods

$$E_{corr,SCS-MP2} = E_0^{(2)} = c^{\uparrow\uparrow}\left(\frac{1}{2}E^{\uparrow\uparrow} + \frac{1}{2}E^{\downarrow\downarrow}\right) + c^{\uparrow\downarrow}E^{\uparrow\downarrow} \qquad \text{(II.26)}$$

where $E_{corr,SCS-MP2}$ is the SCS-MP2 correlation energy, $c^{\uparrow\downarrow}$ and $c^{\uparrow\uparrow}$ are the scaling factors for spin-paired and spin-unpaired electron contributions, respectively. In the initial SCS-MP2, Grimme proposed 6/5 and 1/3, respectively (See Table II.1).[5]

Many algorithm complications have appeared by taking the spin-unpaired contribution into account. In 2004, Jung *et al.* proposed to improve SCS-MP2 by neglecting the spin-unpaired (parallel) contribution (*i.e.*, $c^{\uparrow\uparrow} = 0$) and a new $c^{\uparrow\downarrow}$ parameter of 1.3 was proposed, leading to the scaled-opposite-spin-MP2 (SOS-MP2) method.[6]

These SCS-MP2 methods can be parameterized for specific chemical purposes. For example, Hobza's group proposed SCS-MI-MP2[18] or SCS-S66-MP2 methods to describe long-range interactions.[7] The different $c^{\uparrow\downarrow}$ and $c^{\uparrow\uparrow}$ values are given in Table II.1.

Table II.1. Antiparallel $c^{\uparrow\downarrow}$ and parallel $c^{\uparrow\uparrow}$ spin component factors for SCS-MP2-type methods.

Method	$c^{\uparrow\downarrow}$	$c^{\uparrow\uparrow}$
MP2	1.00	1.00
SCS-MP2	1.20	0.33
SOS-MP2	1.30	0.00
SCS-MI-MP2[a]	0.17	1.75
SCS-S66-MP2[a]	0.14	1.88

[a] with cc-pVTZ basis set

2.2. Coupled-Cluster methods: the high-level weapon of single determinant post-HF methods

Coupled-cluster (CC) methods belong the most elegant post-HF methods. These methods do use neither the variational nor the perturbation principles. The exact wave function Φ_0 (within the basis set approximation) is defined by using the exponential operator:[2, 3]

---

[18] « MI » stands for molecular interaction.

$$\Phi_0 = e^{\hat{T}}\Psi_0 \qquad (II.27)$$

where $\hat{T}$ is the so-called transition operator associated with electronic excitations. The general expression is given by:

$$\hat{T} = \hat{T}_1 + \hat{T}_2 + \cdots + \hat{T}_n \qquad (II.28)$$

where $\hat{T}_n$ is the *n*-excitation operator generating all possible determinants having n-excitation from the ground state wavefunction. For example, $\hat{T}_1$ and $\hat{T}_2$ are defined by using the mono- and bi-excited wave functions (*i.e.*, Ψ_a^r and Ψ_{ab}^{rs}, respectively):

$$\hat{T}_1\Psi_0 = \sum_a^{occ}\sum_r^{virt} t_a^r \Psi_a^r \qquad (II.29a)$$

$$\hat{T}_2\Psi_0 = \sum_{\substack{a,b \\ b>a}}^{occ}\sum_{\substack{r,s \\ s>r}}^{virt} t_{ab}^{rs} \Psi_{ab}^{rs} \qquad (II.29b)$$

where t_a^r and t_{ab}^{rs} are the amplitude. The sums in Eqs. (II.29) run over occupied and virtual spin-orbitals.

The use of the exponential operators in Eq. (II.27) is particularly brilliant as it can be easily developed as a Taylor expansion:

$$e^{\hat{T}} = 1 + \hat{T} + \frac{1}{2!}\hat{T}^2 + \frac{1}{3!}\hat{T}^3 + \cdots + \frac{1}{n!}\hat{T}^n = \sum_{i=0}^{n} \frac{\hat{T}^i}{i!} \qquad (II.30)$$

For example, when taking mono-, bi- and tri-excitation (*i.e.*, S, D and T for single, double and triple) contributions, the exponential operator becomes:

$$e^{\hat{T}_1+\hat{T}_2+\hat{T}_3} = e^{\hat{T}}_{SDT} = 1 + \underbrace{\hat{T}_1}_{S} + \underbrace{\left(\hat{T}_2 + \frac{\hat{T}_1^2}{2}\right)}_{D} + \underbrace{\left(\hat{T}_3 + \frac{\hat{T}_1\hat{T}_2}{2} + \frac{\hat{T}_2\hat{T}_1}{2} + \frac{\hat{T}_1^3}{6}\right)}_{T} \qquad (II.31)$$

where $\hat{T}_2$ refers to pure double excitations (*i.e.*, with correlated electrons) whereas $\hat{T}_1{}^2$ refers to the double application of the monoexcitation operator $\hat{T}_1$.

The CC energy E_{CC} can be obtained from CC-Schrödinger equation:

$$\hat{\mathcal{H}}\Phi_0 = E_{CC}\Phi_0 \qquad (\text{II.32})$$

and:

$$\langle\Psi_0|\hat{\mathcal{H}}|\Phi_0\rangle = E_{CC}\langle\Psi_0|\Phi_0\rangle \qquad (\text{II.33})$$

By using Eqs. (II.33) and the intermediate normalization principle, the CCSD energy E_{CCSD} is given by:

$$E_{CCSD} = \langle\Psi_0|\hat{\mathcal{H}}|\Psi_0\rangle + \langle\Psi_0|\hat{\mathcal{H}}|\hat{T}_1\Psi_0\rangle + \left\langle\Psi_0\left|\hat{\mathcal{H}}\right|\left(\hat{T}_2 + \frac{\hat{T}_1^2}{2}\right)\Psi_0\right\rangle \qquad (\text{II.34})$$

where the first term is the HF energy, the second term is null depending on Brillouin's theorem and the third term is the CC correlation energy $E_{corr,CCSD}$. By using Eqs. (II.33&34), the CC correlation energy is given by:

$$E_{corr,CCSD} = \sum_{a,b,r,s} (t_{ab}^{rs} + t_a^r t_b^s - t_a^s t_b^r)\langle\Psi_0|\hat{\mathcal{H}}|\Psi_{ab}^{rs}\rangle \qquad (\text{II.35})$$

Table II.2. CC methods and corresponding operators.

Method	Operator $\hat{T}$	Comment
CCD	$\hat{T} = \hat{T}_2$	Only double excitations
CCSD	$\hat{T} = \hat{T}_1 + \hat{T}_2$	As expansive as CCD with better results
CCSDT	$\hat{T} = \hat{T}_1 + \hat{T}_2 + \hat{T}_3$	Very expensive….
CCSD(T)	$\hat{T} = \hat{T}_1 + \hat{T}_2 + PT(\hat{T}_3)$	The tri-excitation term is treated by perturbation theory: the current "golden" method.

CC methods differ in the excitations taken into account (Table II.2). Currently, the CCSD(T) method with the *ad equate* basis set is considered as the "golden" standard. It allows reaching high accuracy providing the best results concerning ground-state calculations. However, the corresponding calculation time is dramatically increased with respect to other methods (following a N^7 law). A full study at this level of theory is limited to very small systems (up to

~15 atoms). Nevertheless, this method is often used as reference to validate *e.g.*, "single point" energy calculation.

Section B. Density functional theory as an alternative to post-HF methods

1. Electron density definition

Post-HF methods often reach good accuracy but at a dramatic computational cost. Currently, only relative small systems can be studied. DFT has been developed to account correlation energy at much lower computational cost. DFT is the best balance between computational time and accuracy that allows dealing with much bigger systems than with post-HF methods.

The wave function used in HF theory is not an observable and does not directly correspond to any physical data in its native form. However the probability of finding the N-electrons of a system in a given volume $d\tau = dx_1 dx_2 \dots dx_N$ is:

$$\Psi^*(x_1, x_2, \dots x_N)\Psi(x_1, x_2, \dots x_N)dx_1 dx_2 \dots dx_N$$

The electronic density of one electron at a spatial position r_1 is defined as follows:

$$\rho(r_1) = N \int \dots \int \Psi^*(x_1, x_2, \dots x_N)\Psi(x_1, x_2, \dots x_N)ds_1 dx_2 \dots dx_N \qquad (\text{II}.36)$$

The electron density is an observable and can be experimentally measured by *e.g.*, X-ray diffraction. It can be extended to the pair density, which is defined as the probability to find two electrons at two different locations r_1 and r_2 with spin s_1 and s_2 in two volume elements dr_1 and dr_2:

$$\rho_2(x_1, x_2) = \frac{N(N-1)}{2} \int \dots \int \Psi^*(x_1, x_2, \dots x_N)\Psi(x_1, x_2, \dots x_N)dx_3 \dots dx_N \qquad (\text{II}.37)$$

This density accounts for spin s_1 and s_2 to agree with Pauli's principle. This quantity is also in direct relation with electron correlation.

2. DFT: the electron density replacing the wave function

The electronic Hamiltonian operator (Eq. (II.4)) can be reformulated as follows:

$$\hat{\mathcal{H}}_{elec} = -\underbrace{\sum_{i=1}^{N}\frac{1}{2}\nabla_i^2}_{\hat{T}} - \underbrace{\sum_{i=1}^{N}\sum_{A=1}^{M}\frac{Z_A}{r_{iA}}}_{V_{eN}=V_{ext}} + \underbrace{\sum_{i=1}^{N}\sum_{j>i}^{N}\frac{1}{r_{ij}}}_{V_{ee}} \qquad (\text{II.}38)$$

where $\hat{T}$ corresponds to the kinetic operator, $V_{ext}(r)$ is related to the external potential corresponding to the electron-nuclei contribution and the last term V_{ee} is related to the electron-electron interactions.

2.1. Hohenberg-Kohn theorems

The Hohenberg-Kohn (HK) theorems are the pillars of the DFT formalism.

2.1.1. The first HK theorem

In their paper published in Physical Review, Hohenberg and Kohn state that the external potential $v_{ext}(r)$ is determined, within a trivial constant, by the electron density $\rho(r)$.[8] In turn, the electron density $\rho(r)$ gives the number of electrons and thus fixes the non-degenerate ground-state wave function. In other terms, the electronic density of an electronic system, in its fundamental state, totally determines $v_{ext}(r)$ and $\hat{\mathcal{H}}$, and subsequently all related electronic properties (*e.g.*, kinetic energy, potential energy and total energy).

So, in the DFT formalism, the electronic energy is given by:

$$E = T[\rho(r)] + V_{ext}[\rho(r)] + V_{ee}[\rho(r)] \qquad (\text{II.}39a)$$

$$E = T[\rho(r)] + \int v_{ext}(r)\rho(r)dr + V_{ee}[\rho(r)] \qquad (\text{II.}39b)$$

The T and V_{ee} functionals are universally valid since they do not depend on the number of electrons N, the position and the nature of nuclei. The case of the external functional $v_{ext}(r)$ is different; it is system-dependent since it depends on the nucleus-electron interactions.

2.1.2. The second HK theorem: the variational principle

The first HK theorem implies that all operators are defined as a function of the electron density function of Ψ *i.e.*, functional of $\rho(r)$. The second HK theorem deals with the exact ground state electronic density. Hohenberg and Kohn proposed to apply the well-known variational principle within the DFT context as follows:

$$E_0 \leq E[\tilde{\rho}(r)] = T[\tilde{\rho}(r)] + V_{ext}[\tilde{\rho}(r)] + V_{ee}[\tilde{\rho}(r)] \qquad (\text{II.}40)$$

where E_0 and $\tilde{\rho}(r)$ are respectively the exact energy and a trial electron density.

The exact energy E_0 related to the exact electron density $\rho_0(r)$ can be rewritten from Eq. (II.40) as:

$$E_0[\rho_0(r)] = F^{HK}[\rho_0(r)] + \int v_{ext}(r)\rho_0(r)dr \qquad (\text{II.}41)$$

where

$$F^{HK}[\rho_0(r)] = T[\rho_0(r)] + V_{ee}[\rho_0(r)] \qquad (\text{II.}42)$$

is the universal (or system-independent) Hohenberg-Kohn functional. Electron-electron interaction is split into the Coulomb (J) and the non-classical exchange & correlation (E_{ncl}) contributions:

$$F^{HK}[\rho(r)] = T[\rho_0(r)] + J[\rho_0(r)] + E_{ncl}[\rho_0(r)] \qquad (\text{II.}43)$$

where only $J[\rho_0(r)]$ is known:

$$J[\rho_0(r)] = \frac{1}{2} \iint \frac{\rho_0(r_1)\rho_0(r_2)}{r_{12}} dr_1 dr_2 \qquad (\text{II.}44)$$

The exchange part and the electronic correlation are included into the non-classical term $E_{ncl}[\rho_0(r)]$ which is often quoted $E_{XC}[\rho_0(r)]$.

The universality of the HK functional implies that it will be identically applied to hydrogenoid and proteins! Now the question is how to physically and mathematically define this functional.

According to the second HK theorem, the best electronic density and thus the exact energy is obtained by minimizing the energy with respect to the electron density.

$$E_0 = \min_{\tilde{\rho}} \left(F^{HK}[\tilde{\rho}(r)] + \int v_{ext}(r)\tilde{\rho}(r)dr \right) \qquad (II.45)$$

As for the HF formalism, the resolution of the $(E_0, \rho_0(r))$ couple is performed in DFT according to a self-consistent field (SCF) procedure.

2.2. Kohn-Sham formalism

2.2.1. The non-interacting system

In quantum mechanics, the exact ground state kinetic energy is given by:

$$T = \sum_i^N n_i \left\langle \chi_i \left| -\frac{1}{2}\nabla^2 \right| \chi_i \right\rangle \qquad (II.46)$$

where χ_i and n_i are the natural spin-orbitals and their occupation numbers, respectively. From the HK theorem, T is a functional of the total electron density that can also be expressed as:

$$\rho(r) = \sum_i^N n_i \sum_s |\chi_i(r,s)|^2 \qquad (II.47)$$

For a classical interacting system of electrons, T cannot be calculated, as there exists an infinite number of terms. In 1965 Kohn and Sham proposed to calculate a so-called KS kinetic energy T_{KS} and the density by:[9]

$$T_{KS}[\rho(r)] = \sum_i^N \left\langle \psi_i \left| -\frac{1}{2}\nabla^2 \right| \psi_i \right\rangle \qquad (II.48a)$$

$$\rho_{KS}(r) = \sum_i^N \sum_s |\psi_i(r,s)|^2 \qquad \text{(II.48b)}$$

These equations represent the specific case of Eqs. (II.46-47) in which the occupation number n_i is 1 for N KS spin-orbitals (ψ_i) and 0 for the others. Eqs. (II.48) describe exactly a non-interacting N-electron system. For such a system, the universal HK functional becomes:

$$H_{KS} = \sum_i^N -\frac{1}{2}\nabla^2 + \sum_i^N v_s(r) \qquad \text{(II.49)}$$

where $v_s(r)$ is the external potential for this system. By definition, in a non-interacting system there are no electron-electron interaction term. The corresponding non-interacting ground state wave function Ψ_{KS} is given by:[19]

$$\Psi_{KS} = \frac{1}{\sqrt{N!}} \begin{vmatrix} \psi_1(x_1) & \psi_2(x_1) & \dots & \psi_N(x_1) \\ \psi_1(x_2) & \psi_2(x_2) & \dots & \psi_N(x_2) \\ \vdots & \vdots & \ddots & \vdots \\ \psi_1(x_N) & \psi_2(x_N) & \dots & \psi_N(x_N) \end{vmatrix} \qquad \text{(II.50)}$$

where the spin-orbitals are determined in complete analogy with respect to the HF model *i.e.*, from:

$$\hat{f}^{KS}\psi_i = \varepsilon_i \psi_i \qquad \text{(II.51)}$$

where f^{KS} is the one-electron KS operator defined as:

$$\hat{f}^{KS} = -\frac{1}{2}\nabla^2 + v_s(r) \qquad \text{(II.52)}$$

---

[19] It must be stressed that the wave function and the corresponding spin-orbitals are quoted differently from Eq. (II.6) to underline the difference with respect to the HF Slater determinant model.

2.2.2. Kohn-Sham equations

At this stage, the KS kinetic functional $T_{KS}[\rho(r)]$ is still not the exact kinetic-energy. Kohn and Sham proposed to introduce the missing quantity (*i.e.*, $T_{KS}[\rho(r)] - T[\rho(r)]$) into the exchange-correlation energy functional *i.e.*, the HK functional is given by:

$$F^{HK}[\rho(r)] = T_{KS}[\rho(r)] + J[\rho(r)] + E_{XC}[\rho(r)] \qquad (\text{II.}53)$$

where the exchange-correlation energy functional is simply defined as:

$$E_{XC}[\rho(r)] \equiv (T[\rho(r)] - T_{KS}[\rho(r)]) + E_{ncl}[\rho(r)] \qquad (\text{II.}54)$$

The $E_{XC}[\rho(r)]$ is the only term for which no rigorous and exact explicit form exist.

In 1989, Parr and Yang developed the KS equations.[10] As in the HF formalism, the equations can be recast in the KS orbitals so that we obtain:

$$\left(-\frac{1}{2}\nabla^2 + \left[\int \frac{\rho(r_2)}{r_{12}} + v_{XC}(r_1) - \sum_A^M \frac{Z_A}{r_{1A}}\right]\right)\psi_i = \varepsilon_i\psi_i \quad (\text{II.}55)$$

These equations are mathematically very similar to those of HF and they are solved in a similar way using SCF procedures[20] and basis sets to develop the orbitals. Nonetheless, this is not similar at all in term of the formalism. In this case, the expression of the energy is exact but the exact form of v_{XC} is not known.

These equations are often re-written as:

$$\left(-\frac{1}{2}\nabla^2 + v_{eff}(r_1)\right)\psi_i = \varepsilon_i\psi_i \quad (\text{II.}56)$$

where $v_{eff}(r_1)$ is the effective potential which is identical to $v_s(r)$ in Eq. (II.52). It corresponds to the external potential in which the non-interacting system is moving within the KS problem.

---

[20] By knowing each contribution of Eq. (II.55), we can inject $v_s(r)$ in the one-electron equations, which in turn determine the orbitals and thus the ground-state density.

The total energy of the system in the DFT formalism is given by:

$$E[\rho] = T_s[\rho] + J[\rho] + E_{XC}[\rho] + E_{Ne} \qquad (\text{II.}\,57)$$

2.3. Exchange-correlation functionals

It is more convenient to express the functional dependence E_{XC} on the electron density and the so-called energy density ε_{XC}:

$$E_{XC}[\rho(r)] = \int \rho(r)\varepsilon_{XC}[\rho(r)]dr \qquad (\text{II.}\,58)$$

where the energy density is often split into exchange and correlation contributions allowing many different combinations of exchange and correlation functionals.

$$\varepsilon_{XC} = \varepsilon_X + \varepsilon_C \qquad (\text{II.}\,59)$$

For example, the B3P86 and B3LYP functionals have the same B3 exchange functional while the correlation functionals were developed by Perdew (P86[11]) and Lee-Yang-Parr (LYP[10]), respectively.

This section will give an overview of the philosophy of exchange-correlation developments.[12, 13] The electronic density $\rho(r)$ is now simply quoted as ρ.[21]

2.3.1. Local Density Approximation

The local density approximation (LDA) is based on the "jellium" model: a uniform electron gas (UEG) in which positive charges are spread out, assuring the neutrality. This form is mainly applicable to physics since the heterogeneity of molecules is misdescribed by UEG.

The exchange part was elucidated from the Thomas and Fermi work on UEG. Several forms of the correlation part ε_C were analytically extrapolated from numerical quantum Monte Carlo

---

[21] Except if it induces confusion.

simulations of UEG. The best known is the SVWN from Vosko and Wilk.[14] The LDA formalism largely overestimates the correlation energy while the exchange energy is underestimated. Because of its own essence, LDA preferentially provides accurate results with homogenous (*e.g.*, metal-like) rather than heterogeneous systems.

2.3.2. Local Spin Density Approximation

The LDA formalism does not explicitly include spin. When the number of α-electron (N^α) differs from the number of β-electron (N^β) (*e.g.*, in free radicals and metal-systems), spin must be taken into account explicitly. The corresponding unrestricted scheme is called local spin density approximation (LSDA or LSD) in which α- and β-electron densities (*i.e.*, ρ^α and ρ^β, respectively) are separated. Only the exchange-correlation is corrected since the kinetic and Coulomb contributions are spin-independent:

$$E_{XC}^{LDA}[\rho] \rightarrow E_{XC}^{LSDA}[\rho^\alpha, \rho^\beta] = \int \rho \varepsilon_{XC}[\rho^\alpha, \rho^\beta] \, dr \qquad (II.60)$$

LSDA models include the spin polarization function *f(ξ)*:

$$f(\xi) = \frac{(1+\xi)^{4/3} + (1-\xi)^{4/3} - 2}{2^{4/3} - 2} \; with \; \xi(r) = \frac{\rho^\alpha - \rho^\beta}{\rho^\alpha + \rho^\beta} \quad (II.61a-b)$$

This function has been included to allow the equality between LSDA and LDA energies when N^α was identical to N^β (*i.e.*, in closed-shell systems).

LSDA being still based on the UEG, it leads to significant errors for heterogeneous chemical systems. It is still more accurate for *e.g.*, electron conduction simulations and semi-conductor systems.

2.3.3. Generalized gradient Approximations

To overcome the "local" limitation (inherent to the jellium model) of LDA and LSDA models, density gradient was introduced to create non-homogeneities. The Taylor expansion is particularly well-adapted to apply the so-called gradient expansion approximation (GEA):

$$E_{XC}[\rho] = \int \rho \varepsilon_{XC}^{LDA}[\rho] dr + \sum_{\alpha} \sum_{\beta} \int C_{XC}^{\alpha,\beta}(\rho^{\alpha}, \rho^{\beta}) \frac{\nabla \rho^{\alpha}}{(\rho^{\alpha})^{2/3}} \frac{\nabla \rho^{\beta}}{(\rho^{\beta})^{2/3}} dr + \dots \qquad (II.62)$$

Such corrections had not given the expected improvements for non-homogenous systems, because losing of physical meanings in the LDA part of Eq. (II.62). Further refinements of GEA were proposed by the generalized gradient approximation (GGA) type functionals, in which the exchange-correlation functional is globally given by:

$$E_{XC}^{GGA}[\rho, \nabla \rho] = \int \varepsilon_{XC}^{GGA}[\rho^{\alpha}, \rho^{\beta}, \nabla \rho^{\alpha}, \nabla \rho^{\beta}] dr \qquad (II.63)$$

Afterwards, functionals including the second derivative of the density were also developed, namely the meta-GGA functionals:

$$E_{XC}^{m-GGA}[\rho, \nabla \rho, \nabla^2 \rho] = \int \varepsilon_{XC}^{m-GGA}[\rho, \nabla \rho, \nabla^2 \rho] dr \qquad (II.64)$$

These functionals allow reaching an acceptable accuracy for many systems. They are still used in the literature since they provide quite reliable results at a low computational time ($\sim N^3$).

2.3.4. Hybrid functionals

There were still too much limitations and inconsistencies with pure GGA and meta-GGA functionals. Researchers wondered why trying to approach the exchange contributions while the HF exchange is exact, and so to express E_{XC} as:

$$E_{XC} = E_X^{exact} + E_C^{KS} \quad where \ E_X^{exact} \equiv E_X^{HF} \qquad (II.65)$$

The results obtained with these functionals were not as good as expected *e.g.*, with respect to pure GGA functionals. The further improvements was the development of hybrid functionals, using a part of HF exchange and a part of KS exchange, correlation being obviously purely DFT:

$$E_{XC} = E_X^{HF} + z(E_{XC}^{KS} - E_X^{HF}) \quad or \ E_{XC} = aE_X^{HF} + E_{XC}^{KS}(1-a) \qquad (II.66a-b)$$

For example, B3[15] and BHandH[16] exchange functionals included 20 and 50% of HF exchange, respectively.

Recently, by using hybrid functionals within the meta-GGA framework, the so-called hybrid-meta GGA functionals were developed. For example, the MPWB1K (44% of HF exchange) functional from Truhlar's group was parameterized so that it appeared very accurate to describe activation barriers and kinetics of reactions with respect to experimental data.[17]

3. Toward the improvement of the DFT

Most of classical DFT functionals fail in different attempts including self-interaction error and the description of long-range interactions.

3.1. Self-interaction error

3.1.1. Definition

Considering a single-electron system such as hydrogen atom, the total energy E (Eq. (II.57)) must only depend on the kinetics and the external potential E_{Ne}. The (approximated) exchange-correlation and (exact) Coulomb contributions do not strictly compensate each other for one-electron system. This is an inherent artefact of the DFT formalism, in which the electron interacts with itself! This self-interaction error (SIE) is clearly exemplified on single-electron system (Table II.3) but is actually present in all many-electron cases.

Table II.3. Energy contribution (E_H) of various functionals with cc-pV5Z basis set for the H-atom. (Data from Ref. 2).

Functional/Method	E_{tot}	$J[\rho]$	$E_X[\rho]$	$E_C[\rho]$	$J[\rho]+E_{XC}[\rho]$
SVWN	-0.49639	0.29975	-0.25753	-0.03945	**0.00277**
BLYP	-0.49789	0.30747	-0.30607	0.00000	**0.00140**
B3LYP	-0.50243	0.30845	-0.30370	-0.00756	**-0.00281**
BP86	-0.50030	0.30653	-0.30479	-0.00248	**-0.00074**
BPW91	-0.50422	0.30890	-0.30719	-0.00631	**-0.00460**
HF	-0.49999	0.31250	-0.31250	0.00000	**0.00000**

3.1.2. The self-interaction correction (SIC)

In 1981, Perdew and Zunger proposed to eliminate SIE by adding an additional self-interaction correction (SIC) term, which explicitly ensure equality between $J[\rho]$ and $E_{XC}[\rho]$:[18]

$$E_{XC}^{SIC}[\rho^\alpha, \rho^\beta] = E_{XC}[\rho^\alpha, \rho^\beta] - \sum_i \sum_s (J[\rho_i^s] + E_{XC}[\rho_i^s, 0]) \qquad (II.67)$$

where the second sum runs over α- and β-spins.

These additional terms only slightly affect the total energy of multi-electronic systems with GGA functionals. Therefore, classical studies found in the literature do not account for SIC. In the results presented in Chapters III&IV, we assume that SIE is negligible. For SIC developments and applications, see *e.g.*, Heaton *et al.* (1983)[19], Cortona (1988)[20], Kummel and Perdew (2003)[21].

3.2. Long-range interaction in DFT

3.2.1. Observations

It is well-admitted that supramolecular chemistry is driven by long-range interactions. Long-range interactions are low with respect to electrostatic or covalent bonding contributions. Nevertheless, their implications in biological or nanochemical systems can be crucial (*e.g.*, secondary and tertiary structures of proteins, DNA stacking and nanocarbon assemblies). The "long-range" term obviously should imply a non-local description of the density, while most of DFT functionals are based on relatively local descriptions, even GGA functionals.

Over the past years, the "race" to propose the best model to describe these long-range interactions has become competitive. In this section, we will focus on the widely used methods proposed by Grimme.

3.2.2. The dispersion-corrected DFT or DFT-D

3.2.2.1. A semiclassical approach

The classical description of long-range interactions (van der Waals interactions) is often described by the Lennard-Jones-type potential:

$$E_{VdW} = \sum_{A}^{M-1} \sum_{B>A}^{M} \varepsilon_{AB} \left(\frac{r_{0,AB}}{R_{AB}^{12}} - \frac{r_{0,AB}}{R_{AB}^{6}} \right) \qquad (II.68)$$

where the sum runs over the M atoms of the systems, ε_{AB} and $r_{0,AB}$ are atom-couple dependent parameters and R_{AB} is the inter-atomic distance. The terms in $1/R_{AB}^{12}$ and in $1/R_{AB}^{6}$ are respectively the repulsive and attractive (dispersive) terms. A well-parameterized $1/R_{AB}^{6}$ (or R_{AB}^{-6}) term is known to accurately describe the dispersion interactions.

Coming back to quantum mechanical methods, the idea of Grimme (2004) was to simply add a carefully parameterized dispersion correction to the DFT energy E_{DFT}:[22]

$$E_{DFT-D} = E_{DFT} + E_{disp} \qquad (II.69)$$

where E_{disp} is the dispersion correction term. The main advantage of DFT-D is the absence of extra time calculation since the dispersion energy is semi-classically assessed in a post-SCF way.

Over the past decade, the dispersion correction has been the object of two main refinements. The first two DFT-D versions are based on R^{-6} decay functions (2004 and 2006), while the last version includes the higher-order dispersion terms, namely R^{-8} and R^{-10}-type decays (2010). These three versions of the DFT-D method were named DFT-D,[22] DFT-D2[23] and DFT-D3,[24] respectively.

3.2.2.2. DFT-D and DFT-D2

In DFT-D and DFT-D2 the dispersion correction is given by the following mathematical function:

$$E_{disp} = -s_6 \sum_{A}^{M-1} \sum_{B>A}^{M} \frac{C_6^{AB}}{R_{AB}^6} f_{dmp}(R_{AB}) \quad (II.70)$$

where s_6 is a functional dependent parameter that must be specifically parameterized (see Chapter IV); C_6^{AB} is the dispersion coefficient of a given AB atom pair, it is directly derived from the atomic dispersion coefficients C_6^A and C_6^B (Table II.4); $f_{dmp}(R_{AB})$ is the damping function, which avoids near-singularities (at low distances). This damping function is defined in DFT-D and DFT-D2 as followed:

$$f_{dmp}(R) = \frac{1}{1 + e^{-d\left(R/R_0 - 1\right)}} \quad (II.71)$$

where d determines the slope of the damping function; R_0 is the sum of the atomic Van der Waals (VdW) radii of both atoms involved.

Both DFT-D and DFT-D2 methods differ from the atomic and atom-paired dispersion coefficients and d (Table II.4).

Table II.4. Parameters of dispersion corrections for both DFT-D and DFT-D2 methods.

Parameter	DFT-D	DFT-D2
C_6^A	From literature[25]	$0.05 N I_p^A \alpha_p^{A^*}$
C_6^{AB}	$2\dfrac{C_6^A C_6^B}{C_6^A + C_6^B}$	$\sqrt{C_6^A C_6^B}$
d	23	20

*N equals 2, 10, 18, 36 and 54 for atoms from rows 1-5 of the periodic table, I_p^A and α_p^A are the ionization potential and static dipole polarizabilities of atom A.

The s_6 parameter is a key parameter in this formalism. It must be carefully parameterized in agreement with either (i) high level post-HF methods (*e.g.*, SCS-MI-MP2, CCSD(T) calculations) or (ii) experimental data. It must be stressed that the latter agreement is not easy to assess because interaction energies are rather difficult to experimentally measure.

DFT-D2 has allowed achieving high accuracy in the description of geometries and energies of long-range interaction systems.[23] For all results presented and discussed in Chapters III and IV, long-range interactions were evaluated according to this method.

3.2.2.3. DFT-D3: incorporation of short dispersive and three-body terms

In 2010, Grimme improved his own model by including (i) a three-body term and (ii) higher-order dispersion terms.[24] In this formalism, the dispersion energy is written as the sum of the two-body $E^{(2)}$ and three-body $E^{(3)}$ terms:

$$E_{disp} = E^{(2)} + E^{(3)} \qquad (II.72)$$

where the two-body term includes the higher n^{th}-order classical dispersion terms:

$$E^{(2)} = \sum_{A}^{M-1} \sum_{B>A}^{M} \sum_{n=6,8,10,\dots} s_n \frac{C_n^{AB}}{R_{AB}^n} f_{dmp,n} \qquad (II.73)$$

DFT-D3[24] actually only considers the extra $n = 8$ term, higher orders (mainly $n = 10$) lead to unstable results for complex systems and require much improvements. The definition of all parameters of Eq. (II.73) is related to that of Eq. (II.70), according to slight re-adjustments as quoted below. s_n factors are still functional dependent parameters. It must be stressed that s_8 is empirically calculated.

The damping function was that developed earlier by Chai and Head-Gordon (also used in the ωB97XD functional), numerically stable for all n^{th}-orders:[26]

$$f_{dmp,n}(R) = \frac{1}{1 + 6 \left(R / s_{r,n} R_{cut} \right)^{-\alpha_n}} \qquad (II.74)$$

where $s_{r,n}$ is the nth-order-dependent scaling factor of the cutoff radii and α_n is the steepness factor. It must be stressed that other damping functions may be used as *e.g.*, the Becke-Jonhson (BJ) function.[27]

Instead of using an empirically-derived interpolation formula as in DFT-D2, the atom-pair dispersion coefficients C_6^{AB} are calculated by TD-DFT. The C_8^{AB} terms are calculated from the geometrical average of atomic quantities C_8^A and C_8^B. These atomic coefficients are obtained by using multipole expansion of the atomic density.

Without entering into more details, $E^{(3)}$ is given by:

$$E^{(3)} = \sum_{A}^{M-1} \sum_{B>A}^{M-1} \sum_{\substack{C>A \\ C>B}}^{M} \frac{C_9^{ABC}(3cos\theta_a cos\theta_b cos\theta_c + 1)}{(R_{AB}R_{BC}R_{AC})^3} f_{dmp,(3)}(\bar{r}_{ABC}) \qquad (II.75)$$

where θ_a, θ_b and θ_c are the internal angles of the triangle formed by the AB, BC and AC segments. Here a ninth-order dispersion C_9^{ABC} coefficient appears in the equation, which is approximated as the geometrical average of the previously defined atom-pair dispersion coefficients:

$$C_9^{ABC} \approx -\sqrt{C_6^{AB} C_6^{AC} C_6^{BC}} \qquad (II.76)$$

3.2.3. Brief overview of the other DFT refinements dedicated to dispersion

3.2.3.1. Non Local (NL) DFT of VdW-DFs (VdW-Density Functionals)

VdW-DFs do not empirically include the dispersion energy in a post-SCF way. It is explicitly included as a new term in the exchange-correlation functional:

$$E_{XC}^{VdW-DF} = E_X^{LDA/GGA} + E_C^{LDA/GGA} + E_C^{NL} \qquad (II.77)$$

where the classical LDA or GGA functionals are used for short or medium distances and E_C^{NL} is the non-local (long-range) contribution. The NL term can be included as a "simple" double-space integral:

$$E_C^{NL} = \frac{1}{2} \iint \rho(r_1)\phi(r_1,r_2)\rho(r_2)dr_1 dr_2 \qquad (II.78)$$

in which the $\phi(r_1,r_2)$ kernel depends on two electron coordinates simultaneously, thus including non-locality. This takes dispersion effects somehow naturally *i.e.*, included via the charge density. The used kernel is also somehow related to the R^{-6} term.

The different VdW-DF methods proposed in the literature only differ in the chosen kernel $\phi(r_1,r_2)$. The most used VdW-DF functionals available are VdW-DF,[28] VdW-DF2,[29] VV09[30] and VV10[31].

3.2.3.2. *Conventional and parameterized functionals*

Several exchange-correlation functionals are parameterized to describe long-range interactions. For example, the hybrid exchange functional Becke Half&Half (BHandH where HF exchange part is 50%) is well-known to relatively well describe π-π interactions. However, it is well-admitted that BHandH provides reliable results in non-covalent systems only because of compensation of errors.

Other conventional functionals that can be used to describe dispersion at least at medium-distance range are meta-GGA Thrular's functionals. M06-2X[32] has been parameterized for this purpose and provided relatively accurate results with respect to the dispersion databases available in the literature (*e.g.*, S22[33] or S66[34]). However, the high number of parameters included in this functional provides numerical instabilities and "noisy" results (see Chapter IV).[35]

TPSS and TPSSh can also be classified in this section.[36] They provide relative accurate results at least for potential energy curves of rare gas dimers. However, they were shown to fail at describing asymptotic behaviours (*i.e.*,$R_{AB} \rightarrow \infty$).[2]

3.2.3.3. *Double hybrid (DH) functionals*

The double hybrid (DH) functionals were not necessarily designed for long-range interactions. DH functionals keep the philosophy of hybrid functional adding a post-HF PT2 contribution (w_{PT2}) to the correlation functional (*e.g.*, B2-PLYP,[37] PBE0-2[38]):

$$E_{XC}^{DH}[\rho] = w_{HF}E_X^{HF} + (1 - w_{HF})E_X^{DFT}[\rho] + w_{PT2}E_{Corr}^{PT2} + (1 - w_{PT2})E_C^{DFT}[\rho] \quad (\text{II}.79)$$

With these methods, post-HF calculations are required, thus considerably increasing computational time (up to N^5). The DFT-D should be used to accurately describe dispersion complexes.[39] It must be stressed that the DH-D2 s_6 parameter is lower than for the corresponding hybrid functional (*e.g.*, B2-PLYP and B3LYP).[39] The second-order perturbation theory thus brings a little part of dispersion.[35]

Section C. UV/Visible Spectroscopy

1. Introduction to electronic absorption in molecules

Molecular spectroscopy studies electromagnetic radiations which can be (i) emitted, (ii) absorbed or (iii) diffused by molecules. In turn, molecular properties can be obtained from spectroscopic analyses. Depending on the spectral range, specific properties are accessible. This manuscript will only deal with electronic absorption spectroscopy *i.e.*, concerning wavelength ranging from 200 to 750 nm (UV and visible light).

1.1. The UV/Visible absorption phenomenon from the electronic point of view

The timescale of electronic transitions, molecular vibrations and rotations are c.a., 1, 100 and 10^5 fs, respectively. Electronic spectroscopy processes can be elegantly summarized picturing electronic transitions between the ground state (GS) and excited state (ES) potential energy surfaces (Fig. II.1). In the 1920s, the Franck-Condon principle established that the UV/Vis absorption is fast enough to prevent geometrical rearrangement, the UV/Vis absorption being therefore assimilated to vertical transitions from GS to ESs ($S_0{\rightarrow}S_1$, $S_0{\rightarrow}S_2$ and $S_0{\rightarrow}S_3$, see Fig.II.1). The excitation energy *ΔE* of a vertical transition is given by:[22]

$$\Delta E = \frac{hc}{\lambda} \quad (\text{II.}\,80)$$

where h is the Planck constant, c the speed of light and λ the wavelength.

---

[22] It must be stressed that Eq. (II.80) can also be applied to emission phenomena (*i.e.*, fluorescence and phosphorence). The energetic differences between emission and absorption vertical transitions correspond to the Stokes shifts.

Considering a GS as singlet quoted S_0.:
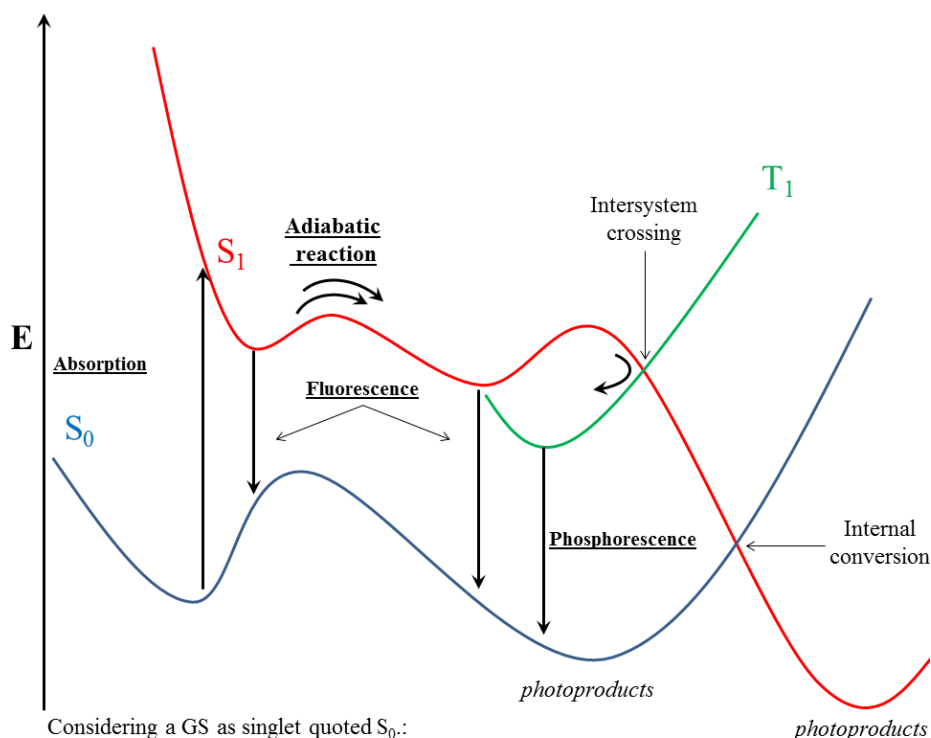
Absorption: S_0 is excited to several ESs (S_1, S_2,…).

Fluorescence: ES turns back to GS by emission of photon after relaxation

Adiabatic reaction: ES follows "excited" reactivity. Further photon emission (fluorescence) may lead to photoproducts.

Phosphorescence: ES potential energy surface has a interconical section with triplet state. A spin conversion occurs. The transition from triplet state T_1 to S_0 is called phosphorescence.

Internal conversion: ES potential energy surface cross the S0 allowing internal conversion (electronic rearrangement). It may lead to photoproduct.

Figure II.1. Schematic representation of electronic transitions between GS and ES potential energy surfaces.

Within the MO theory, an optical excitation is considered as the excitation of one electron from an occupied orbital to an unoccupied (or virtual) orbital. These electronic transitions mainly concern electrons located in frontier orbitals *i.e.*, from one of the highest occupied MOs (HOMOs, *e.g.*, $\phi_{N/2-2}$, $\phi_{N/2-1}$ and $\phi_{N/2}$ in Fig.II.2) to one of the lowest unoccupied MOs (LUMO, *e.g.*, ϕ_a in Fig.II.2). The wave functions of *e.g.*, the GS (defined in Fig. II.2) is given by $\Psi_{GS} = \left| \phi_1^2 \phi_2^2 \dots \phi_{N/2-2}^2 \phi_{N/2-1}^2 \phi_{N/2}^2 \right\rangle$.
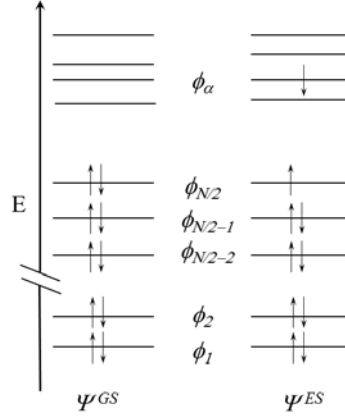
Figure II.2. Example of GS and ES schemes.

1.2. Time-dependence of electronic transition

Electronic transitions are related to the time-dependence of the wave function, which can be studied by the time-dependent (TD) Schrödinger equation:[2, 12]

$$-\frac{\hbar}{i}\frac{\partial\Psi}{\partial t} = \widehat{\mathcal{H}}\Psi \quad \text{(II.81)}$$

where $\hbar$ is the Planck constant over 2π, i the complex number and t the time.

When an electronic system is exposed to light (a time-dependent electromagnetic wave), its response can be put into equation by adding an electric perturbation to the classical Hamiltonian $\mathcal{H}^0$:[40]

$$\widehat{\mathcal{H}} = \widehat{\mathcal{H}}^0 + \varepsilon_0 e\hat{r}sin(2\pi vt) = \mathcal{H}^0 + \varepsilon_0\mu sin(2\pi vt) \quad \text{(II.82)}$$

where $e\hat{r}$ (or $\hat{\mu}$) is the electric dipole moment operator to the electric field , ε_0 and v are the amplitude and the frequency of the electric field associated to the electromagnetic radiation, respectively. The wave function may be written as a linear combination of the GS and ES wave functions dependent on time and coordinates ($\Psi_0(x,t)$ and $\Psi_{i>0}(x,t)$, respectively):

$$\Psi(x,t) = \sum_{i=0} c_i\Psi_i(x,t) \quad \text{(II.83)}$$

$\Psi_i(x, t)$ is expressed as:

$$\Psi_i(x, t) = e^{-\left(iE_i t / \hbar\right)} \Phi_i(x) \quad \text{(II.84)}$$

where $\Phi_i(x)$ is the eigenfunction of the TD-Schrödinger equation having eigenvalues E_i.

At $t = 0$, no excitation has occurred, the wave function only describes GS: $c_0 = 1$ and $c_i = 0$. At $t > 0$ (electromagnetic excitation), the coefficients c_i constantly change following the perturbation. The probability of the system to be in a given m-ES is calculated by c_m^2 corresponding to $\langle \Psi | \Psi^* \rangle$ and knowing that all states are orthogonal. To assess this probability requires solving the TD Schrödinger equation which is obtained by combining Eqs. (II.81-84):

$$-\frac{\hbar}{i}\frac{\partial}{\partial t}\sum_{k=0} c_k e^{-\left(iE_k t / \hbar\right)} \Phi_k = \left[\hat{\mathcal{H}}^0 + \varepsilon_0 \hat{\mu} sin(2\pi v t)\right]\sum_{k=0} c_k e^{-\left(iE_k t / \hbar\right)} \Phi_k \quad \text{(II.85)}$$

Eq. (II.85) is left-multiplied by Φ_m and integrated:

$$-\frac{\hbar}{i}\sum_{k=0}\frac{\partial c_k}{\partial t} e^{-\left(iE_k t / \hbar\right)} \langle \Phi_m | \Phi_k \rangle = \varepsilon_0 sin(2\pi v t)\sum_{k=0} c_k e^{-\left(iE_k t / \hbar\right)} \langle \Phi_m | \hat{\mu} | \Phi_k \rangle \quad \text{(II.86)}$$

Due to the orthogonality of wave functions, (i.e., $\langle \Phi_m | \Phi_k \rangle = \delta_{mk}$); the l.h.s. term is simplified and the equation becomes:

$$\frac{\partial c_m}{\partial t} = -\frac{i}{\hbar}\varepsilon_0 sin(2\pi v t)\sum_{k=0} c_k e^{-\left((E_m - E_k)it / \hbar\right)} \langle \Phi_m | \hat{\mu} | \Phi_k \rangle \quad \text{(II.87)}$$

The quantity c_m at time t is obtained after the integration over the time:

$$c_m(t) = -\frac{i}{\hbar}\varepsilon_0 \int_0^t \sum_{k=0} sin(2\pi v t) c_k e^{-\left((E_m - E_k)it / \hbar\right)} \langle \Phi_m | \hat{\mu} | \Phi_k \rangle \, dt$$

$$= \frac{1}{2i}\varepsilon_0 \left[\frac{e^{\frac{i}{\hbar}(E_m - E_0 + 2\pi v \hbar)t} - 1}{E_m - E_0 + 2\pi v} - \frac{e^{\frac{i}{\hbar}(E_m - E_0 - 2\pi v \hbar)t} - 1}{E_m - E_0 - 2\pi v}\right] \langle \Phi_m | \hat{\mu} | \Phi_0 \rangle \quad \text{(II.88)}$$

For a given light frequency v, the higher the c_m value, the higher the probability of the GS→ESm vertical transition.

This approach can be extrapolated to further excitations, *i.e.*, vertical transition from the ES$_m$ to a higher ES$_{m \to n}$. The complex mathematical form of c_m underlines that sequential excitations do not follow mathematical linear equations. For example, bi-photonic absorption cannot be solved by a simple GS linear-response.

Eq. (II.88) can be rewritten as follow:

$$c_m(t) = \frac{1}{2\hbar i} e_0 \left[\frac{e^{i(\omega_{m0}+\omega)t} - 1}{\omega_{m0} + \omega} - \frac{e^{i(\omega_{m0}-\omega)t} - 1}{\omega_{m0} - \omega} \right] \langle \Phi_m | \hat{\mu} | \Phi_0 \rangle \quad (\text{II}.89)$$

where $\omega_{m0} = \frac{E_m - E_0}{\hbar}$ and $\omega = 2\pi\nu$.

Eq. (II.89) includes two physical interpretations (i) the energy difference between GS and ES (*i.e.*, the term in brackets) and (ii) the properties of the MOs involved in the vertical transition (*i.e.*, the integral).[2]

1.2.1. The energetic point of view

When ω_{m0} tends to ω, the magnitude $|c_m|^2$ increases. In other terms, when the energy difference between GS and ES is close to the energy of the absorbed photon (from Eq. (II.89)), the probability of the corresponding vertical transition is close to 1. An accurate description of both GS and ES energies is thus mandatory to study electronic absorption spectroscopy.

1.2.2. The MO point of view: from mathematics to the "selection rules"

The integral term $\langle \Phi_m | \hat{\mu} | \Phi_0 \rangle$ in Eq. (II.89) is the so-called transition dipole moment. This is the key parameter to theoretically rationalize electronic spectroscopy. If this integral is zero then the vertical transition is forbidden.

The transition dipole moment can be rewritten by splitting the dipole moment operator μ into the electron and the nucleus contributions ($\hat{\mu}_e$ and $\hat{\mu}_n$, respectively):

$$M_{m0} = \langle \Phi_m | \hat{\mu}_e + \hat{\mu}_n | \Phi_0 \rangle \quad (\text{II}.90)$$

Within the Born-Oppenheimer approximation, the wave functions are:

$$\Phi_0 = \Phi_{0,e}\Phi_{0,n} \quad (II.91a)$$

$$\Phi_m = \Phi_{m,e}\Phi_{m,n} \quad (II.91b)$$

where e- and n-indexes refer to the electron and nucleus wave functions, respectively. The transition dipole moment can be developed as:

$$M_{m0} = \langle \Phi_{m,e}\Phi_{m,n}|\hat{\mu}_e + \hat{\mu}_n|\Phi_{0,e}\Phi_{0,n}\rangle$$
$$= \langle \Phi_{m,e}|\hat{\mu}_e|\Phi_{0,e}\rangle\langle \Phi_{m,n}|\Phi_{0,n}\rangle + \langle \Phi_{m,n}|\hat{\mu}_n|\Phi_{0,n}\rangle\langle \Phi_{m,e}|\Phi_{0,e}\rangle \quad (II.92)$$

The second term of the r.h.s. vanishes since the electronic wave functions are orthogonal:

$$M_{m0} = \langle \Phi_{m,e}|\hat{\mu}_e|\Phi_{0,e}\rangle\langle \Phi_{m,n}|\Phi_{0,n}\rangle \quad (II.93)$$

By including the spin parts S_m and S_0, we obtain:

$$M_{m0} = \langle \varphi_{m,e}|\hat{\mu}_e|\varphi_{0,e}\rangle\langle \Phi_{m,n}|\Phi_{0,n}\rangle\langle S_m|S_0\rangle \quad (II.94)$$

where φ refers only to the spatial part. This form of the transition dipole moment leads to the selection rules of electronic spectroscopy, which decide the allowed electronic transitions.

The first term of the r.h.s. (*i.e.*, the spatial part$\langle \varphi_{m,e}|\hat{\mu}_e|\varphi_{0,e}\rangle$) corresponds to the mathematical interpretation of the orbital selection rules *i.e.*, this integral is maximum when the transition is allowed and equal 0 when the transition is forbidden. Qualitatively, a transition is "orbitally" allowed when the orbitals involved in the transition (partially or fully) overlap. Moreover, the symmetry of the involved molecular orbital also plays a determinant role; an electronic transition is orbitally-allowed if and only if the product of the irreductible representations of both orbitals and the dipole moment ($\Gamma(\varphi_{m,e}) * \Gamma(r_e) * \Gamma(\varphi_{0,e})$) contains the totally symmetric irreductible representation of the point group of the molecule. For example, only g ↔ u transitions are allowed.

The second term $\langle \Phi_{m,n}|\Phi_{0,n}\rangle$ is the Franck-Condon factor mathematically establishing the connection between two vibrational states (possibility belonging to two different electronic states) of a vertical transition. It appears crucial when dealing with the hyperfine structure of

spectra. In this case the first two terms must be combined to establish the vibronic selection rules.

The third term $\langle S_m | S_s \rangle$ is related to the spin selection rules. Classically, a transition is allowed only between two states having the same spin multiplicity.

A spin-orbitally allowed transition has a high probability to occur; the higher the transition dipole moment, the higher this probability. Practically, the transition dipole moment is related to the oscillator strength f and thus the experimental absorbance A; so the higher the transition dipole moment, the higher the oscillator strength, the higher the absorbance (at a given concentration).

2. Time-dependent DFT

Theoretical chemists have developed methods to accurately describe excited wave functions and the corresponding energies. In this global context, the aims of quantum mechanic models are well sum up as follows: (i) "help in the assignment of experimental spectra", (ii) "increase the amount of information derived from experiments" and (iii) "shed light on the relationship between the structure of a compound and its spectral properties".[41]

Theoretical chemistry provides several methods based on the wave function theory. They are either not accurate enough (*e.g.*, the size-consistency lack of CI) or too much time-consuming (especially multi-determinant methods such as CASSCF and CASPT2). The excited-state method based on MP2, and so-called CC2, currently appears as the best compromise among wave function theories.

Computational time may be decreased by using semi-empirical models. These models are based on the wave function model in which several integrals are empirically estimated. The careful parameterization of INDO (intermediate neglect of differential overlap) for electronic spectroscopy (namely INDO/S and ZINDO/S) provides accurate results for some systems.[2]

TD-DFT has been recently developed providing accuracy at an acceptable computational time. Nowadays, TD-DFT appears again as the best compromise between computational time and accuracy. Note that TD-DFT provides the same advantages and disadvantages as DFT.

2.1. From DFT to TD-DFT

In the TD-Schrödinger framework within the DFT formalism, density is not only defined by the position r but also by the time t. Unfortunately, adding a new variable prevents the application of the second HK theorem (variational principle).

In 1984, Runge and Cross proposed to extend the first HK theorem to TD-DFT. The so-called Runge-Gross HK theorem postulates that (i) a unique density $\rho(r,t)$ determines a unique external potential $v_{ext}(r,t)$ (to within a TD constant) and (ii) as soon as the density $\rho(r,t)$ is defined, all observables can be obtained. KS orbitals can also be used in the TD-DFT framework satisfying the time-dependent equation:[12, 13]

$$i\frac{\partial}{\partial t}\psi_i(r,t) = \left\{-\frac{1}{2}\nabla_i^2 - v_{KS}(r,t)\right\}\psi_i(r,t) \qquad (II.95)$$

where the KS potential is:

$$v_{KS}(r,t) = v_{ext}(r,t) + \int \frac{\rho(r',t)}{|r-r'|}dr' + v_{XC}(r,t) \qquad (II.96)$$

The first and the second terms are the time-dependent classical external and Coulomb potentials, respectively.

In the TD-DFT framework an "action" functional is defined in place of the classical DFT-energy:

$$A[\rho(r,t)] = \int_{t_0}^{t_1} dt \left\langle \Psi(t)\left|i\frac{\partial}{\partial t} - \mathcal{H}\right|\Psi(t)\right\rangle \qquad (II.97)$$

where the stationary point of the action (*i.e.*, $\frac{\delta A[\rho(r,t)]}{\delta\rho(r,t)} = 0$) gives the exact density of the system. Here, the exchange-correlation potential is given by the derivation of the exchange-correlation part of the action ($A_{XC}[\rho(r,t)]$), contrary to the classical DFT in which $E_{XC}[\rho(r)]$ plays the central role:

$$v_{XC}(r,t) = \frac{\delta A_{XC}[\rho(r,t)]}{\delta\rho(r,t)} \qquad (II.98)$$

110

The form of the exchange-correlation potential affects directly the accuracy of TD-DFT calculations. At the time, there exists no functional specifically developed in the pure TD-DFT formalism. One of the solution is to use the time-independent functional quoted $v_{XC}^{GS}(r)$.[23] The exchange-correlation potential is thus applied at each time with the density $\rho(r,t)$ in an adiabatic way.

$$v_{XC}^{adiabatic}[\rho](r,t) = v_{XC}^{GS}[\rho](r)\big|_{\rho(r)=\rho(r,t)} \qquad (II.99)$$

Such a "local" adiabatic exchange-correlation functional mainly fails in the description of "long-range excitation" such as in ES charge transfer (ES-CT). This problem can be partly solved by splitting the $1/r_{ij}$ operator in the exchange-correlation functional into both short and long-range distance terms. This is achieved by using standard error function:

$$\frac{1}{r_{ij}} = \frac{\text{erf}(\omega r_{ij})}{r_{ij}} + \frac{\text{erfc}(\omega r_{ij})}{r_{ij}} \qquad (II.100)$$

This approach leads to the development of range separated hybrid (RSH) functionals *e.g.*, the ωB97[42] family (*e.g.*, ωB97XD[26] in Chapter IV), which is widely used in the recent literature.

2.2. Towards ES and optical properties by using TD-DFT: the linear-response

TD-DFT should define the density change under the perturbation. This perturbation related to the excitation can be expressed as a perturbation of the KS potential:

$$v_{KS}(r,t) = v_{KS}(r) + \delta v_{KS}(r,t) \qquad (II.101)$$

where $\delta v_{KS}(r,t)$ is a small perturbation. The density will thus be changed over time as:

$$\rho(r,t) = \rho(r) + \delta\rho(r,t) + \cdots \qquad (II.102)$$

---

[23] The GS-index highlights the GS property of the potential.

where the first term of the r.h.s. is the ground state density. The response is linear if and only if the perturbation is small, the r.h.s of Eq. (II.102) being reduced to the first two terms.[24]

The response of the system (*i.e.*, $\delta\rho(r,t)$) is strongly related to the KS potential perturbation $\delta v_{KS}(r,t)$:

$$\delta\rho(r,t) = \int dt' \int \chi[\rho_{GS}](r,r',t-t')\delta v_{KS}(r',t')dr' \qquad (II.103)$$

where $\chi(r,r',\omega)$ is defined here as the TD-DFT linear response (at frequency space[25]) of the GS density at point r and time t if the external potential is applied at position r' and time t'.

The ES properties only depend on (i) the GS electron density, (ii) the perturbation on KS potential $\delta v_{KS}(r,t)$ and (iii) the linear response $\chi[\rho_{GS}](r,r',t-t')$.[13] The first parameter is obtained by a classical DFT calculation, the other two are defined below.

- *Perturbation on the KS potential $\delta v_{KS}(r,t)$*

The linear change of the KS potential $\delta v_{KS}(r,t)$ is classically given from Eq. (II.101):

$$\delta v_{KS}(r,t) = \delta v_{ext}(r,t) + \int \frac{\delta\rho(r',t)}{|r-r'|}dr' + \int dt' \int \underbrace{\frac{\delta v_{xc}(r,t)}{\delta\rho(r',t')}}_{f_{xc}}\delta\rho(r',t')dr' \qquad (II.104)$$

where the exchange-correlation kernel f_{xc} is introduced. This quantity is evaluated at GS. In Eq. (II.103), the perturbation on density depends on the perturbation on the KS potential and the KS linear response. The exchange-correlation plays an important role as in time-independent DFT. By giving an *ad equate* form of the exchange-correlation kernel f_{xc} (Eq. (II.104)), the perturbed KS potential is better and thus gives a better perturbed density.

- *The TD-DFT linear response $\chi(r,r',\omega)$*

---

[24] The excitation provided by strong laser cannot be studied by linear-response (LR) TD-DFT since the perturbation is too strong. Moreover, we established in Section 1.3 that sequential excitations are not linear which can explain why the actual LR TD-DFT can neither be applied to bi-photonic absorptions.

[25] For the frequency ω related to t - t'.

The TD-DFT linear response is given by:

$$\chi(r,r',\omega) = \lim_{\eta \to 0} \sum_m \left[\frac{\langle 0|\rho(r)|m\rangle\langle m|\rho(r')|0\rangle}{\omega - \omega_q + i\eta} - \frac{\langle 0|\rho(r')|m\rangle\langle m|\rho(r)|0\rangle}{\omega + \omega_q + i\eta} \right] \quad (II.105)$$

where m refer to excited-state with energy E_m and set $|m\rangle$ and $\omega_q = E_m - E_0$. Note the similarity with the time-dependent Schrödinger formalism defined in Eq. (II.89), which is directly linked to the transition dipole moment. It must be stressed that ω_q is also related to KS orbital energies and the exchange-correlation kernel by:

$$\omega_q = \epsilon_r - \epsilon_a + \Delta f_{xc} \quad (II.106)$$

2.3. Summary

DFT and TD-DFT comparison can be sum up as follow:

Table II.5. Overview of DFT/TD-DFT differences

	DFT	TD-DFT
Schrödinger equation	$\widehat{\mathcal{H}}\Psi = E\Psi$	$-\frac{\hbar}{i}\frac{\partial \Psi}{\partial t} = \widehat{\mathcal{H}}\Psi$
The theorem	HK $v(r) \leftrightarrow \rho(r)$	Runge-Gross HK $v(r,t) \leftrightarrow \rho(r,t)$
The functional of interest	$E[\rho(r)]$	$A[\rho(r,t)]$
The variational principle	$\frac{\delta E[\rho(r)]}{\delta\rho(r)} = 0$	$\frac{\delta A[\rho(r,t)]}{\delta\rho(r,t)} = 0$
Exchange-correlation potential	$v_{xc}(r) = \frac{\delta E[\rho(r)]}{\delta\rho(r)}$	$v_{xc}(r,t) = \frac{\delta A[\rho(r,t)]}{\delta\rho(r,t)}$
Orbitals	KS	KS + Linear Response

As the information required to evaluate the optical properties comes from the ground state density, TD-DFT calculations must start by a classical single point calculation at ground state. Following Eqs. (II. 101-105), the key points to establish excitation energies and orbitals are:

- To have an accurate description of the GS density (*e.g.*, with the *ad equate* basis set).
- To have an accurate ground state exchange-correlation functional to assess the eigenvalues and eigenfunctions for the KS orbitals.
- To have an accurate exchange-correlation kernel to assess excitation energies.

Bibliography

[1]   Schrödinger, E., *An Undulatory Theory of the Mechanics of Atoms and Molecules.* Physical Review, 1926. **28**: p. 1049-1070.

[2]   Cramer, C.J., *Essentials of computational chemistry* 2004, Chichester: Wiley.

[3]   Szabo, A. and N.S. Ostlund, *Modern quantum chemistry* 1989, New York: Dover Publications.

[4]   Møller, C. and M.S. Plesset, *Note on an Approximation Treatment for Many-Electron Systems.* Physical Review, 1934. **46**: p. 618-622.

[5]   Grimme, S., *Improved second-order M[o-slash]ller--Plesset perturbation theory by separate scaling of parallel- and antiparallel-spin pair correlation energies.* Journal of Chemical Physics, 2003. **118**: p. 9095-9102.

[6]   Jung, Y.*, et al.*, *Scaled opposite-spin second order Moller-Plesset correlation energy: an economical electronic structure method.* Journal of Chemical Physics, 2004. **121**: p. 9793-9802.

[7]   Riley, K.E.*, et al.*, *Assessment of the Performance of MP2 and MP2 Variants for the Treatment of Noncovalent Interactions.* Journal of Physical Chemistry A, 2012. **116**: p. 4159-4169.

[8]   Hohenberg, P. and W. Kohn, *Inhomogeneous Electron Gas.* Physical Review, 1964. **136**: p. B864-B871.

[9]   Kohn, W. and L.J. Sham, *Self-Consistent Equations Including Exchange and Correlation Effects.* Physical Review, 1965. **140**: p. A1133-A1138.

[10]   Lee, C., W. Yang, and R.G. Parr, *Development of the Colle-Salvetti correlation-energy formula into a functional of the electron density.* Physical Review B, 1988. **37**: p. 785-789.

[11]   Perdew, J.P., *Density-functional approximation for the correlation energy of the inhomogeneous electron gas.* Physical Review B, 1986. **33**: p. 8822.

[12]   Parr, R.G. and W. Yang, *Density-functional theory of atoms and molecules* 1989, New York; Oxford [England]: Oxford University Press ; Clarendon Press.

[13]   Koch, W. and M.C. Holthausen, *A chemist's guide to density functional theory* 2001, Weinheim; New York: Wiley-VCH.

[14]   Vosko, S.H., L. Wilk, and M. Nusair, *Accurate spin-dependent electron liquid correlation energies for local spin density calculations: a critical analysis.* Canadian Journal of Physics, 1980. **58**: p. 1200-1211.

[15]   Becke, A.D., *Density-functional thermochemistry. III. The role of exact exchange.* Journal of Chemical Physics, 1993. **98**: p. 5648-5652.

[16]   Becke, A.D., *A new mixing of Hartree--Fock and local density-functional theories.* Journal of Chemical Physics, 1993. **98**: p. 1372-1377.

[17] Zhao, Y. and D.G. Truhlar, *Hybrid Meta Density Functional Theory Methods for Thermochemistry, Thermochemical Kinetics, and Noncovalent Interactions: The MPW1B95 and MPWB1K Models and Comparative Assessments for Hydrogen Bonding and van der Waals Interactions.* Journal of Physical Chemistry A, 2004. **108**: p. 6908-6918.

[18] Perdew, J.P. and A. Zunger, *Self-interaction correction to density-functional approximations for many-electron systems.* Physical Review B, 1981. **23**: p. 5048-5079.

[19] Heaton, R.A., J.G. Harrison, and C.C. Lin, *Self-interaction correction for density-functional theory of electronic energy bands of solids.* Physical Review B, 1983. **28**: p. 5992-6007.

[20] Cortona, P., *Self-interaction correction: The transition-metal atoms.* Physical Review A, 1988. **38**: p. 3850-3856.

[21] KÜMmel, S. and J.P. Perdew, *Two avenues to self-interaction correction within Kohn—Sham theory: unitary invariance is the shortcut.* Molecular Physics, 2003. **101**: p. 1363-1368.

[22] Grimme, S., *Accurate description of van der Waals complexes by density functional theory including empirical corrections.* Journal of Computational Chemistry, 2004. **25**: p. 1463-1473.

[23] Grimme, S., *Semiempirical GGA-type density functional constructed with a long-range dispersion correction.* Journal of Computational Chemistry, 2006. **27**: p. 1787-1799.

[24] Grimme, S.*, et al.*, *A consistent and accurate ab initio parametrization of density functional dispersion correction (DFT-D) for the 94 elements H-Pu.* Journal of Chemical Physics, 2010. **132**.

[25] Wu, Q. and W. Yang, *Empirical correction to density functional theory for van der Waals interactions.* Journal of Chemical Physics, 2002. **116**: p. 515-524.

[26] Chai, J.-D. and M. Head-Gordon, *Long-range corrected hybrid density functionals with damped atom-atom dispersion corrections.* Physical Chemistry Chemical Physics, 2008. **10**: p. 6615-6620.

[27] Grimme, S., S. Ehrlich, and L. Goerigk, *Effect of the damping function in dispersion corrected density functional theory.* Journal of Computational Chemistry, 2011. **32**: p. 1456-1465.

[28] Dion, M.*, et al.*, *Van der Waals Density Functional for General Geometries.* Physical Review Letters, 2004. **92**: p. 246401.

[29] Lee, K.*, et al.*, *Higher-accuracy van der Waals density functional.* Physical Review B, 2010. **82**: p. 081101.

[30] Vydrov, O.A. and T. Van Voorhis, *Nonlocal van der Waals Density Functional Made Simple.* Physical Review Letters, 2009. **103**: p. 063004.

[31] Vydrov, O.A. and T.V. Voorhis, *Nonlocal van der Waals density functional: The simpler the better.* Journal of Chemical Physics, 2010. **133**: p. 244103.

[32] Zhao, Y. and D. Truhlar, *The M06 suite of density functionals for main group thermochemistry, thermochemical kinetics, noncovalent interactions, excited states, and transition elements: two new functionals and systematic testing of four M06-class functionals and 12 other functionals.*

Theoretical Chemistry Accounts: Theory, Computation, and Modeling (Theoretica Chimica Acta), 2008. **120**: p. 215-241.

[33]   Gráfová, L.*, et al.*, *Comparative Study of Selected Wave Function and Density Functional Methods for Noncovalent Interaction Energy Calculations Using the Extended S22 Data Set.* Journal of Chemical Theory and Computation, 2010. **6**: p. 2365-2376.

[34]   Řezáč, J., K.E. Riley, and P. Hobza, *S66: A Well-balanced Database of Benchmark Interaction Energies Relevant to Biomolecular Structures.* Journal of Chemical Theory and Computation, 2011. **7**: p. 2427-2438.

[35]   Grimme, S., *Density functional theory with London dispersion corrections.* Wiley Interdisciplinary Reviews: Computational Molecular Science, 2011. **1**: p. 211-228.

[36]   Tao, J.*, et al.*, *Climbing the Density Functional Ladder: Nonempirical Meta–Generalized Gradient Approximation Designed for Molecules and Solids.* Physical Review Letters, 2003. **91**: p. 146401.

[37]   Grimme, S., *Semiempirical hybrid density functional with perturbative second-order correlation.* Journal of Chemical Physics, 2006. **124**: p. 034108.

[38]   Chai, J.-D. and S.-P. Mao, *Seeking for reliable double-hybrid density functionals without fitting parameters: The PBE0-2 functional.* Chemical Physics Letters, 2012. **538**: p. 121-125.

[39]   Schwabe, T. and S. Grimme, *Double-hybrid density functionals with long-range dispersion corrections: higher accuracy and extended applicability.* Physical Chemistry Chemical Physics, 2007. **9**: p. 3397-3406.

[40]   Atkins, P.W. and J. de Paula, *Atkins' physical chemistry* 2006, Oxford: Oxford University Press.

[41]   Barone, V., *Computational strategies for spectroscopy : from small molecules to nano systems* 2012, Hoboken, N.J.: John Wiley & Sons.

[42]   Chai, J.-D. and M. Head-Gordon, *Systematic optimization of long-range corrected hybrid density functionals.* Journal of Chemical Physics, 2008. **128**: p. 084106.

Chapter III. Optical properties of polyphenols: from the simple polyphenols to copigmentation complexes

Introduction

To theoretically study electronic spectroscopy for polyphenols is a relatively new field of research with very promising applications. This is one of the main projects under development in our lab. The article of Anouar et *al.* validated the use of the B3P86 functional within the TD-DFT formalism to describe the electronic vertical transition of simple flavonoids.[1] In this publication structure-property relationship was established for a series of thirty-three different polyphenols, mainly flavonoids. This method succeeded to rationalize the influence of substitution pattern on UV/Vis spectra. Quantum calculations also provide an accurate molecular orbital picture of the electronic transitions. In future, such methodologies would allow to tune optical properties of natural compounds. This chapter collects three new publications, corresponding to the three different sections:

Section A is a joint experimental and theoretical study which aims at describing the UV-absorption properties of original polyphenols extracted from lichens to assess the UV-screen potential. [26]

Section B proposes an adapted theoretical methodology to rationalize the copigmentation phenomenon on a simple model (*i.e.*, [3-*O*-methylcyanidin: quercetin]).[27] New refinements of DFT (*i.e.*, DFT-D and range-separated hybrid - RSH - functionals) were used and the parameterization of B3P86-D2 was assessed, comparing experimental data issued from the literature and high-level calculations.

Section C uses a combined DFT-D/RSH strategy to evaluate the optical properties of bigger and more realistic copigmentation complexes (flavanol-anthocyanin adducts / flavanol

---

[26] This section was published in Journal of Photochemistry and Photobiology B (Millot, M. *et al.*, J. Photochem. Photobiol. B, 2012, 111, 17-26). I only managed the theoretical part but the entire manuscript is incorporated in this PhD for the sake of clarity.

[27] This section was published in Journal of Chemical Theory and Computation (Di Meo *et al.*, J. Chem. Theo. Comp., 2012, 8, 2034-2043).

dimers).[28] This theoretical work supports experimental data obtained in the group of Pr. Victor Freitas in Porto.


Section A. Photoprotective capacities of lichen metabolites: A joint theoretical and experimental study

1. Introduction

UV-B (280–315 nm) radiations primarily cause photocarcinogenesis due to direct interaction with cellular DNA and subsequent formation of pyrimidine dimers but the role of UV-A (315–400 nm) is also to be considered. Major consequence of cumulative UV-A radiation is the generation of reactive oxygen species which can also induce cancer, generating oxidized DNA base derivatives and altering tumor suppressor genes like p53.[2] It has been suggested that UV-A may be the primary cause of sunlight-induced melanoma. Hence, sunscreens with a good absorption in the UV-A spectral range need to be developed as only a poor number of commercialized sunscreens are absorbing in the UV-A range with a good efficacy and photostability.[3]

Lichen fungi exposed to high light intensities are recognized to accumulate various pigments in the cortical layers overlying the algal cells.[4-7] Consequently, several lichen metabolites such as calycin, rhizocarpic acid, usnic acid and mycosporine-like amino acids have demonstrated some photoprotective capacities.[8-10] Looking for new photoprotective compounds, twelve lichen species particularly exposed to strong UV radiations (rocks on the seashore, rocks in mountain) were studied in the present work. *n*-Heptane, dichloromethane and THF extracts were chromatographed with high performance thin layer chromatography (HPTLC) and analysed with a spectrophotodensitometer CAMAG® at six different wavelengths. Eight compounds (five depsidones: diploicin **1**, dechlorodiploicin **2**, 4-*O*-methyldiploicin **3**, 4-*O*-methyldechlorodiploicin **4**, scensidin **5**, one diphenylether: buellin **6**, and two bisxanthones: secalonic acids B **7** and D **8**, see Scheme III.1) have deserved a special attention for a thorough evaluation as UV-absorbers. All these eight compounds were recently isolated (3–120mg from 155g of the dry lichen) and their chemical structures were elucidated in our group.[11] In the present work, their experimental spectra were measured and fully rationalized by time-dependent density functional theory (TD-DFT) calculations, providing a complete molecular orbital (MO) picture of their UV-absorption spectra.
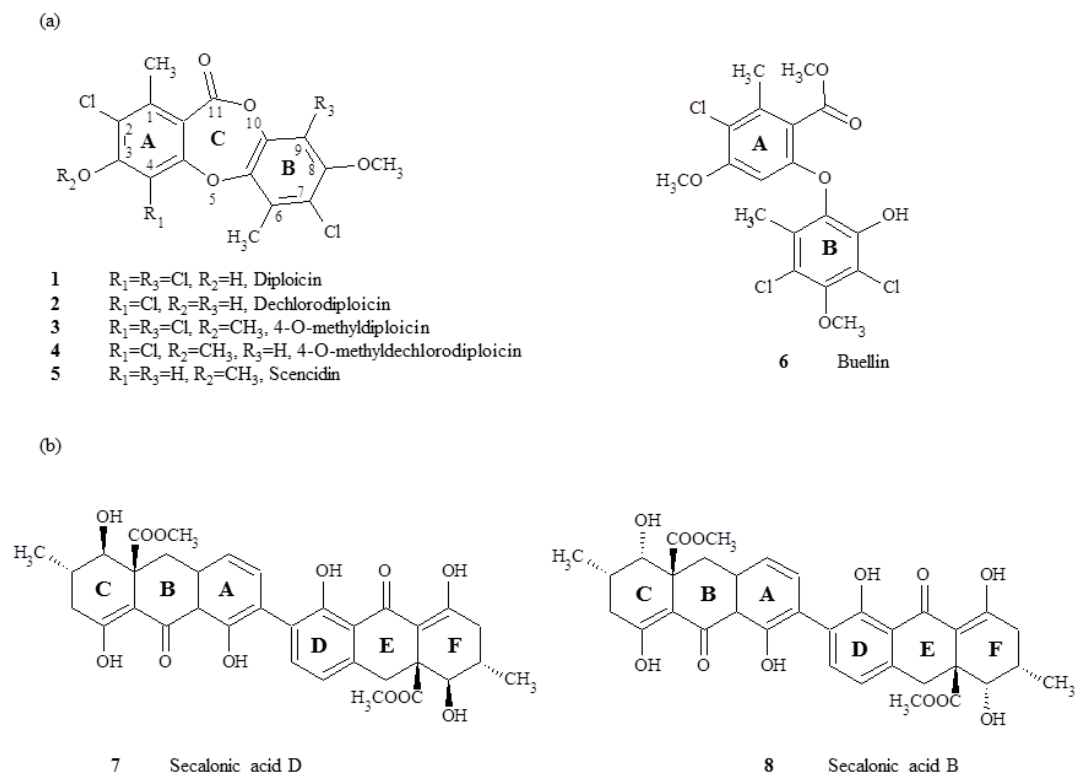
**Scheme III.1.** Chemical structures of (a) depsidones **1-5** and the diphenylether **6** and (b) secalonic acids **7-8**.

2. Materials and methods

2.1. General experimental procedures

UV-absorber molecules were supplied by Acros Organics for octylmethoxycinnamate (OMC) (UV-B absorbent), Sigma Aldrich for 2-hydroxy-4-methoxybenzophenone (UV-A&B absorbent) and Merck for avobenzone (UV-A absorbent) (Scheme III.2).
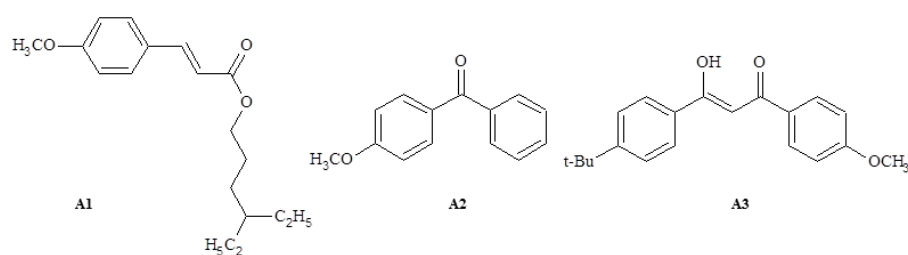
Scheme III.2. Chemical structure of the referent sunscreens: octylmethoxycinnamate (**A1**), 2-hydroxy-4-methoxybenzophenone (**A2**) and avobenzone (**A3**).

2.2. HPTLC

Sample solutions were applied with the Automatic TLC Sampler 4 (ATS 4, CAMAG) using the following settings: band length 2 mm, distance from left plate edge 10 mm and from the lower plate edge 10 mm, resulting 12 tracks per plate, sample application volumes 10 µl of a 1 mg/mL solution (Fig. III.1).
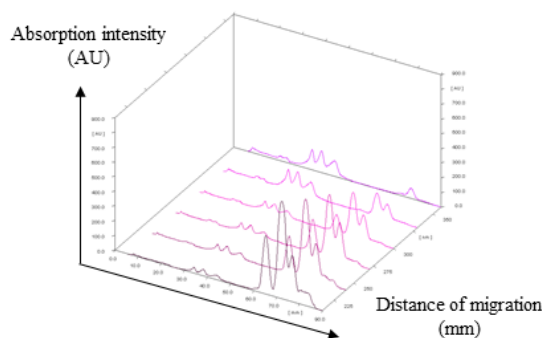

Figure III.1. UV profile of CH2Cl2 extract of *D. canescens* at six wavelenghts (220 nm→360 nm)

Chromatography was performed in a 10x10 cm plate developed in the Automated Developing Chamber (ADC2, CAMAG) up to a migration distance of 80 mm using a mixture of toluene-ethyl acetate-formic acid (70/20/5) for dichloromethane and THF extracts and *n*-hexane, ethyl ether, acetic acid (130/80/20), for *n*-heptane extracts. Then, the plate was dried for 3 min in a stream of warm air. UV spectra were recorded using the TLC scanner 3 (CAMAG). Multi-wavelength detection was performed by TLC Scanner 3 at 210, 240, 270, 300, 330 and 360 nm. All instruments were controlled via the software platform winCats 1.4.1. Planar Chromatography Manager (CAMAG).

2.3. Lichen material

Diploicia canescens (Dicks.) Massal., *Lichina pygmea* (Lightf) Agardh., *Ochrolechia parella* (L.) Massal. and *Tephromela atra* (Hudson) Hafellner, were collected on the seashore rocks near Dinard, Brittany and *Diploschistes scruposus* (Schreber) Norman, *Flavoparmelia caperata* (L.) Hale and *Pertusaria pseudocorallina* (Lilj.) Arnold, near Rennes, Brittany. *Teloschistes chrysophtalmus* (L.) Th. Fr. and *Usnea rubicunda* were collected on trees along the seashore in Brittany near Cancale, *Umbillicaria deusta* (L.) Baumg, *Umbillicaria cylindrica* (L.) Delise and *Cetraria islandica* (L.) Ach., were collected on rocks in the mountain chain Pyrénées near Font-Romeu.

Diploicia canescens (Dicks.) Massal. thalli were collected in larger amount on the rocks of the sea coast near Dinard, Ille et Vilaine, France, in September 2006. Voucher specimens have been deposited at the herbarium of Pharmacognosy and Mycology, Rennes, France (REN-ABB) with the reference number JB/06/10. The identification of the lichen material was supported by thalline chemical tests (K+ yellow, UV-).

2.4. Preparation of lichen extracts

500 mg of dried and powdered lichens were extracted successively with *n*-heptane, dichloromethane and tetrahydrofurane (5 mL, 3 times) using an automatic robot Heidolph Synthesis1. Extracts were filtered and evaporated to dryness. The residues were diluted in acetone to reach a concentration of 5 mg/mL.

2.5. *In vitro* photoprotection capacity

Molecular extinction coefficients ε_m were obtained from the measured absorbances (A) according to the Beer–Lambert law:

$$A = \varepsilon_m lc \qquad \text{(III. 1)}$$

where l is the light path length of the cell (l = 1 cm) and c the concentration of the solution (2.5x10^{-5} M).

Estimated $SPF_{in\,vitro}$ is calculated according to the Mansur equation:

$$SPF_{in\,vitro} = 10 \sum_{\lambda=290nm}^{320nm} EE(\lambda)I(\lambda)A(\lambda) \qquad \text{(III. 2)}$$

where $EE(\lambda)$ is the erythemal effect spectrum at wavelength λ, $I(\lambda)$ is the light intensity at wavelength λ and $A(\lambda)$ the absorbance at wavelength λ.

To calculate the critical wavelength (λ_c), the area under the absorbance curve (ACU) is set at 100%. λ_c is the wavelength at which 90% of the ACU is reached in the range 290–400 nm. According to FDA, a five-point scale ranging from 0 to 4 is used to classify products: 0 ($\lambda_c <$ 325 nm); 1 ($325 \leq \lambda_c < 335$); 2 ($335 \leq \lambda_c < 350$); 3 ($350 \leq \lambda_c < 370$); 4 ($370 < \lambda_c$). Springsteen *et al.* have classified products exhibiting λ_c values higher than 370 nm as broad spectrum sunscreens.[12] The following equation is applied:

$$\int_{290nm}^{\lambda_c} A(\lambda)d\lambda = 0.9 \int_{290nm}^{400nm} A(\lambda)d\lambda \qquad \text{(III. 3)}$$

The UV-A/UV-B ratio (R) is a criterion reflecting the broadness of the UV spectra and hence the capacity of a pure product to protect against UV-B and UV-A. When R is lower than 1.5, the product can be considered as a UV-B filter. When R is higher than 1.5, the product can be considered as a UV-A filter. For its determination, the following equation, corresponding to the ratio between the surface under the curve of the spectra in the UV-A and UV-B ranges, is employed:

$$R = \frac{\left.\int_{320nm}^{400nm} A(\lambda)d\lambda \middle/ \int_{320nm}^{400nm} d\lambda\right.}{\left.\int_{290nm}^{320nm} A(\lambda)d\lambda \middle/ \int_{320nm}^{320nm} d\lambda\right.} \qquad \text{(III. 4)}$$

2.6. Methods of calculation

In order to provide a full comparison to theoretical spectra, experimental absorbances were recast in oscillator strengths (f). The $f_{\text{experimental}}$ were extracted from the experimental UV/Vis peak at λ_{max} according to the following formula in a given solvent:

$$f = 4.319 \times 10^{-9} [\text{mol. cm}^2 . \text{dm}^{-3}] \int \varepsilon_m(\nu) d\nu \qquad (\text{III.} 5)$$

The integration was performed over the frequency ν, after decomposition of the peak using Gaussian functions.

The UV/Vis absorption is attributed to $\pi \rightarrow \pi^*$ electronic transitions. The maximum wavelength and intensity of the UV/Vis absorption peaks correspond to the energy and the oscillator strength of the vertical transitions, respectively. These parameters can be evaluated by different methods allowing excited state evaluation (*e.g.*, configuration interaction and time dependent-Hartree–Fock). TD-DFT[13, 14] has appeared reliable to provide accurate estimates of the UV/Vis absorption spectra of π-conjugated compounds.[15] While keeping reasonable computational time, TD-DFT turned out to be the only method to accurately describe the impact of substituents *e.g.*, fluorine,[16] hydroxyl and methoxy groups[1]. The B3P86 functional has allowed reaching high accuracy to reproduce UV/Vis absorption spectra of a series of 33 different polyphenols.[1] In order to benchmark the most appropriate methodology to evaluate UV/Vis spectra of the compounds studied here (Scheme III.1), different DFT functionals pure (BP86 and PBEPBE), hybrid including more or less Hartree–Fock (HF) exchange (B3P86 (20% HF), B3LYP (20% HF), BHandH (50% HF) and BHandHP86 (50% HF), and Coulomb-attenuating method (CAMB3LYP) were used.[17-21]

The Pople-type triple-f basis set 6-311+g(d,p) is a good compromise between accuracy and time consuming.[1] The addition of diffuse function is mandatory to better evaluate electron distribution on these highly conjugated systems. The use of LANL2DZ basis set for the core electrons of Cl-atoms does not change λ_{max} and only slightly influence the oscillator strength (*ca.* 2%, data not shown).

The calculations were performed with or without solvent effects taken account with the implicit solvent model IEFPCM (Integral Equation Formalism Polarizable Continuum

Model).[22, 23] In this case, the solute is embedded in a shape-adapted cavity surrounded by a dielectric continuum, which is characterized by a dielectric constant. Following the experimental data, the calculations were performed in methanol (ε = 32.61) and dichloromethane (ε = 8.93) for compounds **1**, **2**, **7**–**8** and compounds **3**–**6**, respectively. PCM has allowed providing a satisfactory solvent effect evaluation for polyphenol compounds.[1]

The ground states (GS) geometries were optimized using (IEFPCM)-B3P86/6-311+g(d,p). Frequency analysis was performed at the same level of theory and confirmed the absence of imaginary frequency. The excited states (ES) were calculated within the TDDFT formalism using the GS geometries, thus giving the vertical transition.

All calculations including GS geometries, frequency analysis and ES energies have been performed with the Gaussian09 package.[24] The theoretical UV/Visible spectra [200–400 nm] are plotted as the combination of Gaussian functions, each of them (i) centered on wavelengths of the different allowed-absorption bands, (ii) with an intensity equals to the oscillator strength and (iii) with an arbitrary width of 3 eV, small enough to distinguish the different electronic transitions.

2.7. Functional choice for the theoretical evaluation of UV/Vis absorption for compounds 1-8

Compound **1** was chosen as prototype of the depsidone derivative for benchmarking. In this case, the best evaluation of λ_{max} (E_{max}) was relatively well assessed with the pure BP86 and PBEPBE functionals (Table III.1 and Figs. S3 and S4). However, the major peak above 5 eV (below 250 nm) and intensities (*i.e.*, oscillator strengths f) were better reproduced by hybrid functionals including a moderate HF percentage (B3P86 and B3LYP, see Figs. III.2a and S3). A too high HF percentage (BHandH and BHandHP86) or the long-range correction (CAM-B3LYP) dramatically overestimated and underestimated f and λ_{max}, respectively (Table III.1 and Figs. S3 and S4).

For secalonic acids, compound **8** was chosen for benchmarking. The pure DFT functionals (BP86 and PBEPBE) overestimated λ_{max} by around 20 nm (Table III.1). Including 20% HF exchange (B3P86 and B3LYP) allowed reaching accuracy for λ_{max} and f, as well (Table III.1 and Figs. S3 and S4). The entire spectrum is also well reproduced with B3P86 (Figs. III.2b and

126

S3). Again in this case the oscillator strengths are well reproduced giving an accurate picture of the entire spectra of secalonic acids. For compound **8**, $f_{experimental}$ equals 0.14, 0.53 and 0.21 while $f_{theoretical}$ equals 0.20, 0.66 and 0.24 for the three main electronic transitions, respectively, which constitute the maximum absorption band ($\lambda_{theoretical}$ = 385 nm, 340 nm and 323 nm) (Fig. III.2b). Again BHandH, BHandHP86 and CAM-B3LYP dramatically overestimated and underestimated f and λ_{max}, respectively (Table III.1 and Figs. S3 and S4). Moreover CAM-B3LYP totally neglected the shoulder of the maximum absorption band.

Table III.1 Experimental and theoretical λ_{max}^{a} (nm) for compounds **1-6** and **7-8,** with the 6-311+g(d,p) basis set.

Compound	Exp	BP86	B3P86	BHandHP86	B3LYP	BHandH	PBEPBE	CAM-B3LYP
1[b]	320	314.5	279.5	241.4	280.5	251.7	340.7	249.4
2[b]	315	308.1	281.6	244.9	-	-	-	-
3[c]	326	323	285.9	255.4	-	-	-	-
4[c]	342	316.6	283.5	248.1	-	-	-	-
5[c]	288	309.3	265.6	238.1	-	-	-	-
6[c]	289	318	278.1	248.5	-	-	-	-
7[b]	337	-	343.2	316.8	-	-	-	-
8[b]	338	358.8	340.4	307.8	341.4	320.3	359.4	329.7

[a] *Allowed transition was estimated as possible for a oscillator strength f higher than 0.02.*
[b] *Performed in CH_3OH using IEFPCM for theoretical UV/Vis spectra.*
[c] *Performed in CH_2Cl_2 using IEFPCM for theoretical UV/Vis spectra.*

For the rest of the study, the B3P86 hybrid functional was chosen as (i) it includes the appropriate HF exchange percentage to reach accuracy with respect to experimental data and (ii) it is consistent with our recent results on a large series of other polyphenols.[1] It is important to note that the functional choice does not influence the MO picture because, for all compounds, the assignment of the MOs involved in transitions is unambiguously similar whatever the functional that was used.
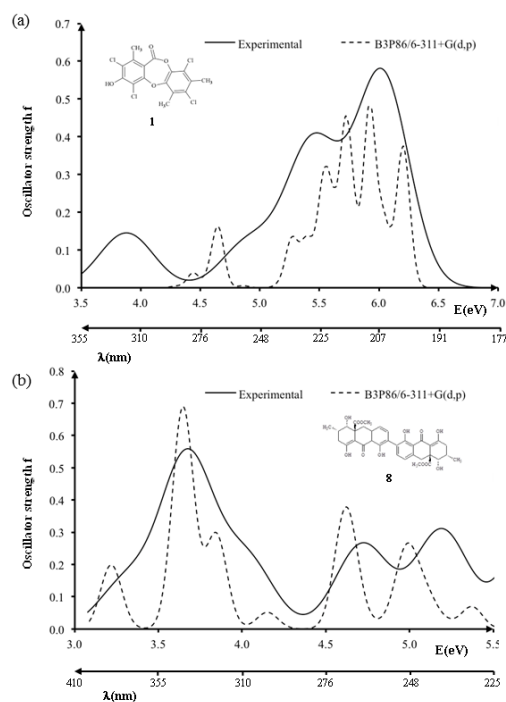
Figure III.2. Experimental and theoretical UV/Visible spectra of compounds (a) **1** and (b) **8**.

3. Results

3.1. HPTLC screening

THF extracts of all the samples contained one or two polar compounds absorbing in the UV-B and/or UV-A ranges. Regarding dichloromethane extracts, UV-absorbents were observed only in the following species: *P. pseudocorallina*, *T. atra* and *D. canescens*. A few absorbing compounds were observed in *n*-heptane extracts of all the species. Nevertheless, the common depside atranorin and its derivative product (methyl-*β*-orcinolcarboxylate) were predominants in these apolar extracts, especially in *D. canescens*, *F. caperata*, *T. atra* and *U. rubicunda*.

According to the criteria defined above, the lichen *D. canescens* can be clearly distinguished from the others, containing several compounds absorbing in the UV-B and/or UV-A ranges. In the dichloromethane extract, three major nonpolar metabolites ($0.7 < R_f < 0.9$), absorbing mainly in the UV-B range, were observed in the chromatogram (Fig. III.1). Three more polar metabolites ($0.3 < R_f < 0.5$), absorbing in the UV-A range, were also present in this extract.

3.2. Primary photophysical properties of *D. canescens* metabolites

The "gold standard" of sunscreen measurement is the SPF. This parameter is used to evaluate quality of UV-B sunscreens. However, SPF measures an endpoint that is sensitive to UV-B, and not the UV-A protection of sunscreens. λ_c straightforwardly characterizes the UV-A protection capacity. By this assessment, a given sun-care product may be qualified as broad-spectrum sunscreen, according to a minimum value of λ_c.

The UV spectra of compounds **1**, **2**, **7** and **8** were recorded in methanol while dichloromethane was used for compounds **3–6**, providing λ_{max}, ε_m, R and *SPF* or λ_c. All these parameters were compared to those of commercialized sunscreens (Table III.2).

Table III.2. Photophysical parameters of compounds **1-8** and UV-absorbers (**A1**-**A3**).

Lichens compounds	λ_{max} (ε)	UV-A/UV-B	λ_c	*SPF*
1	320 (11 000)	0.67	-	0.21
2	288 (6 800); 315 (6 000)	0.68	-	0.15
3	342 (200)	1.20	-	0.01
4	326 (6 500)	1.07	-	0.16
5	289 (8 500)	0.09	-	0.15
6	288 (6 600)	0	-	0.06
7	338 (36 000)	3.37	374	-
8	337 (37 000)	2.79	372	-
UV-absorbers	λ_{max} (ε)	UV-A/UV-B	λ_c	*SPF*
A1	309 (22 000)	0.3	-	0.60
A2	287 (15 000) ; 328 (9 600)	1.00	-	0.27
A3	359 (35 000)	6.98	378	-

Among the potential candidates as UV-B-absorbers, most of the extracted products exhibited low molar extinction values (ε_m < 10 000). Only compounds **1**, **7** and **8** exhibited ε_m higher than 10 000 in the 280–400 nm range to be considered as potential sunscreen agents. With one main band at 320 nm and a UV-A/UV-B ratio close to 1, compound **1** offers a protection against both UV-B and UV-A. Despite a good protection and similarities for in vitro UV measurements with the referent sunscreen **A2**, diploicin exhibited a low in vitro *SPF* value (0.21). Secalonic acid isomers **7** and **8** exhibited a main band at 338 nm with a high em around (36000, as seen in Table III.2). As for avobenzone, these two compounds exhibited λ_c higher than 370 nm and a UV-A/UV-B ratio higher than 1.5. Therefore, they are good candidates as potential sunscreens with respect to avobenzone (Fig. III.3).

With the aim of finding new sunscreens, a deep understanding of electronic transitions is mandatory to propose a future rational design of new compounds based on natural products.
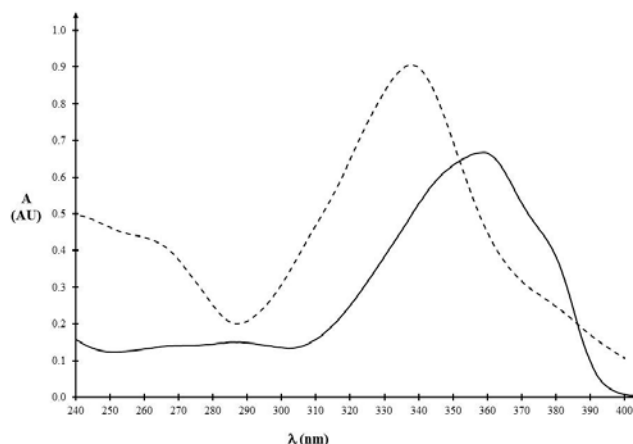

Figure III.3. UV-absorption spectra of avobenzone (—) (UV-A sunscreen) and secalonic acid B (--) (**8**) (2.5 10^{-5} M in MeOH).

3.3. Structure-property relationships

3.3.1. Depsidones and diphenylether

The UV/Vis spectra of depsidone and diphenylether compounds (**1–6**) consist of two absorption bands above 250 nm (low-energy bands) and one apparent large band (high-energy bands) ranging between 200 and 250 nm.

The low-energy bands are mainly described by the HOMO→LUMO, HOMO-1→LUMO and HOMO-2→LUMO transitions (Table III.3a). These absorption peaks appear relatively weak. The overlapping between the π and π^* orbitals involved in the electronic transitions is a major requirement to increase oscillator strengths (*i.e.*, to increase band intensities) and in those peaks the corresponding MO overlapping is relatively weak (Fig. III.4). As illustrated for compound **1**, the contribution of the HOMO→LUMO transition is low since HOMO is mainly on the B-ring and LUMO on the A-ring (Fig. III.4a). In this case, λ_{max} is described by the HOMO-1→LUMO transition. For this transition the overlapping between both MOs is located on a non-extended region (*i.e.*, on the A-ring), explaining the relatively low oscillator strength ($f = 0.04$).

130

Table III.3. Theoretical and experimental maximum absorption wavelength (respectively λ_{max} and λ_{exp}, nm), related theoretical excitation energy (E_{max}, eV) and oscillator strengths f (a) for compounds **1**-**8** in solvent and (b) for compounds **1**-**6** in the gas phase (used to compare the value in a given environment) at the B3P86/6-311+G(d,p) level of theory.

(a)

Compound	λ_{max}	E_{max}	f	Electronic transition contribution[a]	λ_{exp}
1	279.5	4.4	0.04	HOMO-1→LUMO (54%)	320 (0.04)
2	281.6	4.4	0.03	HOMO→LUMO (50%)	315
3	285.9	4.3	0.05	HOMO-1→LUMO (62%)	326
4	283.5	4.4	0.06	HOMO→LUMO (54%) HOMO-1→LUMO (38%)	324
5	278.1	4.6	0.09	HOMO-1→LUMO (62%)	289
6	265.6	4.7	0.08	HOMO→LUMO+1 (51%) HOMO→LUMO (38%)	288
7	343.2	3.6	0.64	HOMO-1→LUMO+1 (66%)	337 (0.47)
	383.3 sh [b]	3.2 sh	0.22	HOMO→LUMO (70%)	375 (0.11)
8	340.4	3.6	0.66	HOMO-1→LUMO+1 (67%)	338 (0.50)
	385.4 sh [b]	3.2 sh	0.2	HOMO→LUMO (70%)	375 (0.14)

[a] *Electronic transition contributions correspond to the different percentages of MO transitions describing the excited state*

[b] *λ_{max} shoulder observed on experimental and theoretical spectra.*

(b)

Compound	λ_{max}	E_{max}	f	Electronic transition contribution[a]		λ_{exp}
1	282.3	4.4	0.02	HOMO-1→LUMO	61%	320
2	265.2	4.7	0.03	HOMO-2→LUMO	52%	315
3	287.1	4.3	0.03	HOMO-1→LUMO	62%	326
4	279.3	4.4	0.02	HOMO-1→LUMO	63%	324
5	275.8	4.5	0.05	HOMO-1→LUMO	60%	289
6	272.8	4.5	0.08	HOMO→LUMO	62%	288

[a] *Electronic transition contributions correspond to the different percentages of MO transitions describing the excited state*

The high-energy absorption bands ($\lambda < 250$ nm) are significantly more intense. Again, this is very well explained by the orbital scheme. First, these bands are described not only by one, but by a combination of several transitions involving unoccupied MOs higher in energy than LUMO (Table III.4 and Fig. III.2a). Among these transitions some of them exhibit relatively high oscillator strengths mainly due to a better overlapping of the orbitals involved in these transitions *e.g.*, (i) HOMO→LUMO+5 and HOMO→LUMO+3 ($f = 0.47$) for compound **1** (Fig. III.5a), (ii) HOMO-1→LUMO+5 and HOMO→LUMO+3 ($f = 0.44$) for compound **2** (Fig. III.5b) and (iii) HOMO-1→LUMO+3 ($f = 0.56$) for compound **3** (Fig. III.5c).
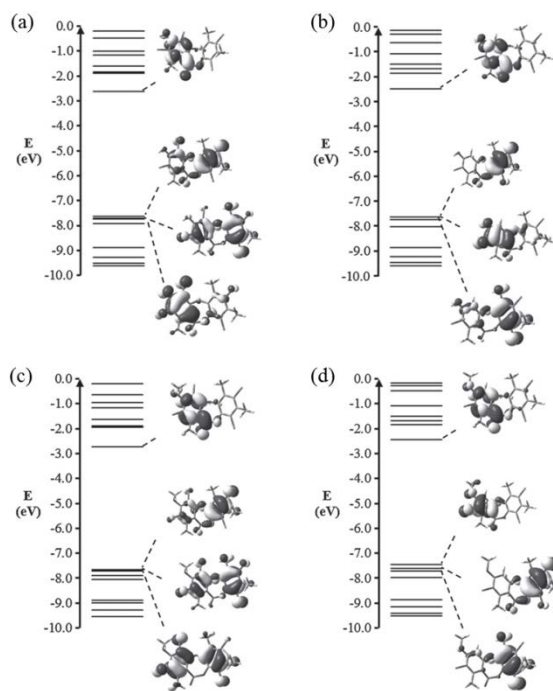
Figure III.4. Electronic scheme showing the topology of frontier orbitals involved in the first $\pi \rightarrow \pi^*$ transitions for compounds (a) **1**, (b) **2**, (c) **3** and (d) **4**.
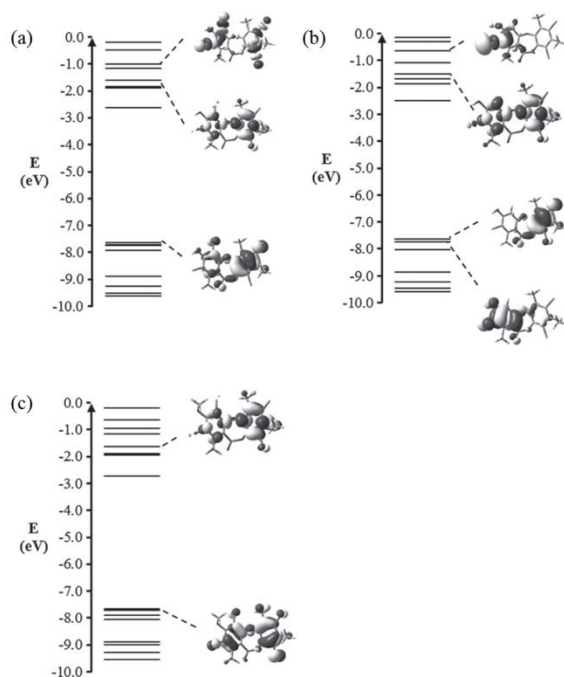

Figure III.5. Electronic scheme showing the topology of frontier orbitals involved in the main absorption band for compounds (a) **1**, (b) **2**, (c) **3**.

Controlling substituent effects at the molecular level is of great importance and can be achieved by TD-DFT calculations. It has been shown that the effects of alkaline substituents is a subtle combination of both inductive (-I) and mesomeric (+M) characters of these atoms.[16] The former stabilizes HOMO more than LUMO, which induces an increase of the HOMO–LUMO gap and hypsochromic (blue-) shifts. The latter destabilizes HOMO more than LUMO, which induces a decrease of the HOMO–LUMO gap and bathochromic (red-) shifts.

Substitution pattern mainly affects the low-energy bands, changing HOMO, HOMO-1 and HOMO-2 topologies. The presence of a Cl-atom at C4 extends π-delocalization over the A-ring, *e.g.*, from compounds **2–1** (Fig. III.4a and b) and from **4** and **5** to **3** (Figs. III.4c and d and S5). A systematic hypsochromic shift is observed when increasing the number of Cl-atoms (Fig. S6), which is consistent with the experimental observations. At C3, the presence of an OCH3 group rather than an OH group modifies π-delocalization and may interchange HOMO and HOMO-1. This is clearly observed from compound **2** to compound **4** (Fig. S5), inducing bathochromic shifts (Table III.3) since the HOMO→LUMO transition is favoured for **4**. From **1** to **3**, the effect of the OCH3 group is screened by the effect of the Cl-atom at C4. A slighter bathochromic shift is thus observed (Table III.3b). All the substitution effects only induce slight shifts since HOMO-2, HOMO-1 and HOMO are relatively close in energy and the corresponding bands appear in the same energetic range.

It is difficult to fully rationalize the influence of substitution on the high-energy bands since the substitution effects may decrease the oscillator strength of one transition but increase for another. So all effects are compensated and the same global band (combination of several bands) is experimentally observed.

In the special case of the diphenylether (compound **6**), the C-ring opening at O10-C11 induces a destabilisation of LUMO that becomes closer in energy to LUMO+1. The contribution of the HOMO→LUMO+1 transition to the maximum absorption band is high, thus inducing a significant hypsochromic shift (Table III.3). Again for the high-energy band the difference in the global peak is not significant.

Table III.4. Theoretical wavelength (λ, nm) and corresponding electronic transitions of the maximum absorbance band for compounds **1**-**6** in solvent.

Compound	λ_{max}	E_{max}	f	Electronic transition contribution[a]	
	224.4	5.5	0.23	HOMO-2→LUMO+3	46%
	221.8	5.6	0.12	HOMO→LUMO+4	43%
	217.3	5.7	0.28	HOMO-2→LUMO+4	30%
				HOMO-1→LUMO+4	24%
	216.1	5.7	0.17	HOMO-2→LUMO+4	37%
1				HOMO-2→LUMO+5	34%
	209.6	5.9	0.47	HOMO→LUMO+5	29%
				HOMO→LUMO+3	29%
	205.6	6	0.17	HOMO-3→LUMO+3	43%
	200.1	6.2	0.22	HOMO→LUMO+5	29%
				HOMO-3→LUMO+4	28%
	219.1	5.7	0.15	HOMO-2→LUMO+4	35%
	209.9	5.9	0.3	HOMO-2→LUMO+3	32%
				HOMO-3→LUMO+2	21%
	209.7	5.9	0.14	HOMO-4→LUMO	56%
2	207.6	6.0	0.26	HOMO-1→LUMO+5	45%
	206.6	6.0	0.44	HOMO-1→LUMO+5	40%
				HOMO→LUMO+3	31%
	201.4	6.2	0.19	HOMO-4→LUMO+1	38%
	199.3	6.2	0.1	HOMO-6→LUMO	52%
	223.4	5.5	0.45	HOMO-3→LUMO+1	33%
				HOMO-2→LUMO+2	31%
	221.3	5.6	0.14	HOMO-3→LUMO+2	38%
3	218	5.7	0.31	HOMO-1→LUMO+4	43%
	210.3	5.9	0.56	HOMO-1→LUMO+3	30%
	206	6.0	0.18	HOMO-2→LUMO+3	43%
	200	6.2	0.15	HOMO→LUMO+5	44%
	229.7	5.4	0.19	HOMO→LUMO+3	40%
	222	5.6	0.15	HOMO-3→LUMO+1	60%
	210.6	5.9	0.36	HOMO-2→LUMO+3	36%
4	208.7	5.9	0.23	HOMO-4→LUMO	46%
	208.1	6.0	0.33	HOMO-4→LUMO	41%
	206.9	6.0	0.13	HOMO→LUMO+5	59%
	202.8	6.1	0.31	HOMO-3→LUMO+3	42%
	229.3	5.4	0.21	HOMO-4→LUMO	39%
	227.3	5.5	0.13	HOMO-2→LUMO+1	41%
	209.9	5.9	0.40	HOMO-3→LUMO+2	47%
5	207.1	6.0	0.34	HOMO-1→LUMO+5	49%
	205.2	6.0	0.24	HOMO-2→LUMO+2	34%
	193.6	6.4	0.34	HOMO-2→LUMO+3	42%
	209.7	5.9	0.16	HOMO-4→LUMO+1	37%
	207.3	6.0	0.35	HOMO-1→LUMO+5	43%
	204.8	6.1	0.50	HOMO-3→LUMO	37%
	204.6	6.1	0.15	HOMO→LUMO+7	52%
	202.5	6.1	0.19	HOMO-1→LUMO+5	37%
6				HOMO-1→LUMO+7	28%
	201.5	6.2	0.29	HOMO-2→LUMO+3	34%
				HOMO-2→LUMO+4	33%
	200.7	6.2	0.19	HOMO-1→LUMO+7	50%
	194.5	6.3	0.21	HOMO-2→LUMO+5	45%

[a] *Electronic transition contributions correspond to the different percentages of MO transitions describing the excited state.*

3.3.2. Secalonic acids

The UV/vis spectra of secalonic acids consist of two main absorption bands (Fig. III.2b). The highest absorption band is experimentally located at 343.2 and 340.4 nm for 7 and 8, respectively. This band is mainly assigned to the HOMO-1→LUMO+1 electronic transitions (contributions of 66% and 67% for **7** and **8**, respectively, see Table III.3). Due to the symmetry of the molecules, LUMO and LUMO+1 are degenerated. This transition is highly probable ($f =$ 0.64 and 0.66 for both compounds, respectively) since HOMO-1 and LUMO/LUMO+1 overlap on a relatively extended region *i.e.*, almost the entire molecule (Fig. III.6). For π-conjugated systems, λ_{max} is usually attributed to the HOMO→LUMO electronic transition. However, for both secalonic acids the oscillator strength of the HOMO→LUMO electronic transition is relatively weak (f = 0.22 and 0.20, respectively) (Table III.3a). This originates from the relatively weak overlapping between both molecular orbitals, HOMO and LUMO being located on the central moiety (C and Drings) and the B-, C- D-, E- and F-rings, respectively (Fig. III.6). This electronic transition thus appears as a shoulder of the first major absorption band (Fig. III.1b). As a consequence, the first major UV-absorption band is not only located in the UV-A region but half&half UV-A and B.
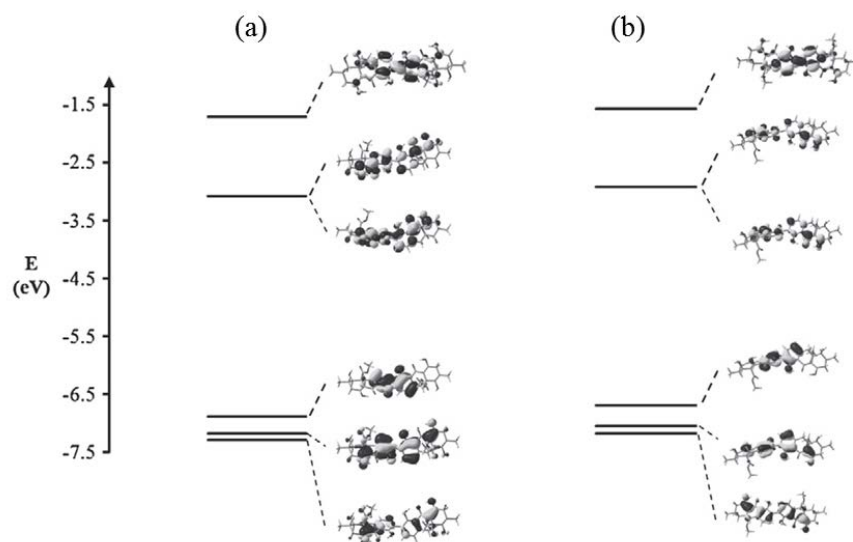
Figure III.6. Electronic scheme showing the topology of frontier orbitals involved in the first $\pi \rightarrow \pi^{*}$ transitions for compounds (a) **7** and (b) **8**.

The second absorption band observed experimentally is actually attributed to two electronic transitions (mainly assigned to HOMO→LUMO+2). The oscillator strengths are lower than for

the first absorption band ($f = 0.24$ and 0.21 for compounds **7** and **8**, respectively). LUMO+2 is located in the central moiety and the carboxylic moiety (Fig. III.6).

As expected stereochemistry of the C&E rings has no significant impact of the optical properties. This is particularly true for these compounds since the asymmetrical C-atoms possess very weak LCAO coefficients in the frontier orbitals involved in the electronic transitions described above (Fig. III.6).

Even if secalonic acids have some chemical similarities with avobenzone (phenyl-β-diketo moiety), there is a main difference distinguishing both optical behaviours. The ground state of avobenzone presents keto-enol equilibrium. The enol form shows a strong absorption band around 340–350 nm, while the keto form absorbs in the 260–280 nm range. Avobenzone can thus efficiently behaves as a photoprotector under conditions favouring the intramolecular hydrogen bonded enol "chelated" form.[25] One may imagine similar keto-enol equilibrium for secalonic acids; four different isomers existing in this case. Nonetheless the isomer presented in Scheme III.1 is much more stable than the other three forms (relative calculated $\Delta G°$ ranging from 9 to 22 kcal.mol^{-1}) and is thus the only form participating in the UV/Vis absorption properties.

4. Conclusion

HPTLC screening has allowed us to select the lichen *D. canescens* as a potential source of photo absorbing compounds. Photophysical properties of these lichen metabolites were evaluated using in vitro methods. Except a low absorption band in the UV-A range (λ_{max} at 322 nm) for **1**, depsidones and diphenylether (**2–6**) do not exhibit the required UV profiles between 280 and 400 nm to be considered as a potent UV-A protectors. In the case of secalonic acids, π-delocalization and stabilized enol form by intramolecular H-bonds partially explain the high absorption in the UV-A range. TD-DFT provides an accurate picture of the optical absorption of depsidones and secalonic acids. Structure–property relationship is relatively well understood for the maximum absorption wavelengths. The influence of substitution on frontier orbitals is clearly rationalized, even for Cl-atoms for which *-I* and *+M* effects compete. Quantum chemistry offers a powerful guideline to tune absorption shifts. These theoretical studies will lead us an easy selection of lichen metabolites as photoprotective agents focused on xanthone derivatives and no chlorinated compounds.

Photostability of compounds **1** and **8** were assessed and demonstrated non-optimum stability under UV irradiation[26] (15% product degradation measured as the decrease of the UV signature before and after irradiation)[29]. Future developments would aim at improving (i) photostability and (ii) UV-absorption using the quantum guideline proposed here. For the latter point we should slightly increase π-delocalization of frontier orbitals with appropriate substitution (electron donor or acceptor depending on the position) to increase oscillator strength while staying in the same absorption band.

Sunscreen penetration and safety assessment should be considered together in order to ensure that cytotoxicity studies examine relevant doses.[27] The preliminary evaluation of the *in vitro* cytotoxicity for the different compounds studied here indicated that their toxicity towards the HaCaT cell line varies according to their stereochemistry.[11] Due to the lower toxicity of **8** (secalonic acid B) with respect to the other compounds, it appears as a good candidate for the development of new sunscreens. The present work would be systematically extended to other synthetic secalonic acid B derivatives. Other in vitro evaluations (antioxidant capacities, activation of melanogenesis pathway) and appropriate in vivo studies would fully rationalize the sunscreen capacity of this promising series of compounds.

---

[29] UV spectra were recorded after 2 h of irradiation at 650 W/m^2 using a doublebeam spectrophotometer (Hitachi UV–Vis., model U-2000) and the areas under curve were calculated.

Section B. Highlights on Anthocyanin Pigmentation and Copigmentation: A Matter of Flavonoid π-Stacking Complexation To Be Described by DFT-D[30]

1. Introduction

More than 8,000 different natural polyphenols (*e.g.*, flavonoids, lignans, depsides, coumarins, oligomers and polymers) have been isolated from the plant kingdom; all plant organs being concerned (*e.g.*, leaves, fruit, roots and flowers). Therefore they are relatively abundant in human diets (*e.g.*, fruit, vegetables, spices and beverages including tea, wine, beer). Apart from their important biological activities in plants and potential health benefits in humans (*e.g.*, prevention of cardiovascular,[28] neurodegenerative[29] and hepatic diseases,[30, 31] and possibly some cancers[32]), some polyphenols are responsible for fruit/beverage/flower/leaf colouration.[33, 34] The UV/Vis absorption characteristics of polyphenols taking part in plant colours are well established from both experimental and theoretical points of view.[1, 35]

Anthocyanins belong to the flavonoid subclass and are responsible for red, blue and purple colours of many flowers (*e.g.*, orchids, tulips, roses and many blue flowers), leaves (*e.g.*, veins of tobacco leaves), fruit (*e.g.*, grapes, berries, tomatoes) and vegetables (*e.g.*, tomatoes, aubergines). Around one thousand of such pigments have been evidenced so far. Anthocyanins are glycosides of so-called anthocyanidins, which are flavylium (2-phenyl-1-benzopyrylium) ions substituted by several OH and OMe groups.[36, 37] Additionally, the sugar moieties are frequently acylated by a variety of aliphatic and aromatic carboxylic acids including acetic, *p*-coumaric and caffeic acids (as in *Vitis vinifera* L. grape). The red colour of anthocyanins is mainly attributed to the flavylium cation (AH^+), which prevails at pH < 4. At pH 4 - 6, the most acidic groups of AH+ (positions 4', 5 and 7) are deprotonated, thus giving a mixture of neutral tautomeric quinoid bases A (purple). At pH > 6, a second deprotonation can take place forming anionic quinoid bases A^- (blue). Besides fast proton transfer equilibria, AH+ also undergoes water addition at position 2 with formation of a colourless hemiketal (B), itself in equilibrium with minor amounts of pale yellow (*Z*)- and (*E*)-chalcones (C).[38] Although water addition is much slower than proton transfer, the colourless hemiketal is typically the thermodynamic most

---

stable form in mildly acidic solutions (pH > 2 - 3), in the case of common anthocyanins. Thus, the persistence of bright colours in plants under such conditions (non extreme low pH) clearly suggests that natural mechanisms of colour stabilization operate. The flat polarizable chromophores of the coloured forms (mainly AH+) are quite prone to π-stacking interactions with themselves (self-association) and with the pool of colourless polyphenols (especially, flavones, flavonols and hydroxycinnamic acids) coexisting with anthocyanins in the vacuoles of plant cells.[39-43] The latter binding phenomenon is so-called copigmentation, being evidenced *e.g.*, by the diamagnetic shifts of NMR signals pertaining to the aromatic protons of the pigment and copigment molecules when they associate.[44] Being maximized in aqueous solution (weakened by organic cosolvents) and weakly affected by the ionic strength, copigmentation must be mainly driven by van der Waals interactions and hydrophobic effects, although H-bonding between the pigment and copigment molecules may contribute.[45, 46]

π-Stacking was suggested as the major contribution to molecular complexation of aromatic ligands. An offset geometry for the two partners within the complex is usually favoured so as to minimize unfavourable repulsions of π-electrons.[47] π-Stacking may be important i) in organic chemistry contributing to regio- and stereoselectivity,[48, 49] ii) in material science explaining charge transfer (CT) phenomena[50, 51] and supramolecular organization issues[47] or iii) in biology contributing to ligand-protein and ligand-nucleic acid interactions.[52] Although the major role of π-stacking interactions in copigmentation has sound experimental support,[53-57] it is still unclear how they take part in colour variation. Indeed, copigmentation, not only displaces the hydration equilibrium toward the flavylium ion, thereby resulting in a hyperchromic shift, but is also known to shift the visible absorption band of anthocyanins to higher wavelengths. The role of π-stacking interactions in this typical bathochromic(red)-shift is still incompletely understood.

The present work aims at describing and rationalizing π-stacking interactions and the subsequent light absorption properties using state-of-the-art computational methods *i.e.*, time dependent density functional theory (TD-DFT) with functionals accurately describing dispersive effects and CT. For this purpose we used a prototypical couple of flavonoid pigment/co-pigment that may form π-stacking complexes. 3-*O*-Methylcyanidin and quercetin, a very common flavonol (Scheme III.3), were chosen as the anthocyanin-pigment and copigment, respectively; the methyl group being chosen to model the electronic effect of the

sugar moiety at a lower computational cost. Both compounds can be considered as the two interacting moieties of many pigment and copigment couples found in Nature.[39, 56, 58] When both quercetin and cyanidin derivatives are present in aqueous solution, they can in principle bind (copigmentation) or self-associate (formation of non-covalent dimers). A large set of relevant properties such as interaction energies, CT and UV/Vis properties were investigated for the copigmentation complex [3-*O*-methylcyanidin:quercetin] (**C:Q**) and both dimers [3-*O*-methylcyanidin]$_2$ (**C:C**) and [quercetin]$_2$ (**Q:Q**). Copigmentation has thus been rationalized by comparing the UV/Vis properties of the complexes with those of the free flavonoids.
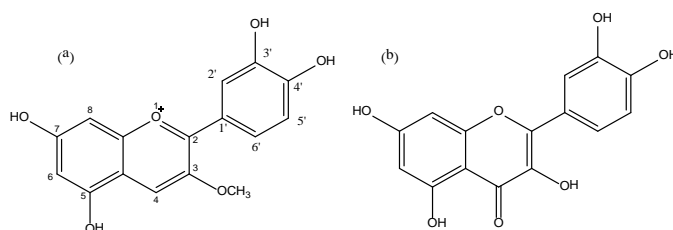
Scheme III.3. Chemical structures of (a) 3-*O*-methylcyanidin and (b) quercetin.

To achieve these goals, the manuscript is structured as follows: Section 2 carefully describes the computational methodology employed. Section 3 shows further computational details concerning the choice of the theoretical method after a detailed benchmark study. Section 4.1 first describes geometries and energies of all stable complexes. A detailed analysis of the different binding contributions (*i.e.*, dispersive, H-bonding and electrostatic) is next proposed. The CT excited-state and UV/Vis properties are then discussed in Section 4.2 to rationalize copigmentation by flavonols. Note that throughout text, as well as within the concluding section, the robustness of the cost-effective theoretical methodology used is discussed with respect to both high-level calculations and experimental observations.

2. Methodology

Over the past years, quantum chemistry calculations have emerged as a relevant tool to provide accurate pictures of both π-stacking complexes[59] and optical properties.[51] DFT is particularly well adapted for medium-sized molecular systems and hybrid functionals permit accurate descriptions of many different chemical systems. For instance, B3P86 is particularly well adapted to calculate both thermodynamic[60, 61] and UV/Vis absorption properties[1] of isolated polyphenols. However, standard hybrid functionals are known to poorly reproduce i)

non-covalent weak interactions such as π-stacking of conjugated systems and ii) charge transfer (CT) in excited states. Both properties are of particular importance to understand copigmentation and must be therefore accurately described. Fortunately, new methods have been recently developed to correct these two generalized drawbacks of common functionals.[62, 63]

Dispersion interaction arises from instantaneous fluctuations of locally induced dipole moments. To accurately model this system, the so-called van der Waals correlation functionals explicitly incorporate non-locality (*i.e.*, kernels depending simultaneously on *r* and *r′*) effects in an accurate way.[64] Parameterized functionals have also been developed to calculate these non-bonded interactions, M06-2X being possibly among the most advanced fine-tuned expressions.[65] Another successful approach circumvents the use of these sophisticated correlation kernels by adding a dispersion correction based on the well-known dependence of the interactions between weakly overlapping systems as a function of the interatomic distance R:

$$E_{disp} = -\frac{C_6}{R^6} - \frac{C_8}{R^8} - \frac{C_{10}}{R^{10}} \qquad (III.6)$$

which is normally truncated after the first (or eventually the second) term and properly renormalized. The approach, originally developed by Grimme and called DFT-D[66] can be efficiently coupled with any existing DFT-based method. It appears particularly relevant to calculate non-covalent interactions within an acceptable accuracy/computational time ratio.[66, 67] Pairwise-like dispersion energy (E_{disp}) is thus calculated separately in a post self-consistent field fashion:

$$E = E_{DFT} + E_{disp} \qquad (III.7)$$

where E_{disp} is a dispersion correction having the expected R_{AB}^{-6} dependent decay:

$$E_{disp} = -s_6 \sum_{A}^{N-1} \sum_{B>A}^{N} \frac{C_6^{AB}}{R_{AB}^6} f_{dmp}(R_{AB}) \qquad (III.8)$$

where s_6 is a functional-dependent scaling factor, C_6^{AB} is the dispersion coefficient for the atomic pair AB, R_{AB} is the interatomic distance for atoms A and B, and $f_{dmp}(R_{AB})$ is a damping

function that avoids near-singularities for small interatomic distances.[67] The refined version DFT-D2 has been widely used over the past years.[67] More recently the DFT-D3 version included atom pairwise-specific dispersion coefficients and a new set of cutoff radii as defined in the damping function.[68]

As quoted above, the uncorrected B3P86 method has been repeatedly applied before to the flavonoids tackled here with great success;[1, 60, 69] however, the copigmentation issue requires an accurate evaluation of the non-covalent interactions dominating the final shape of the dimers. To keep consistency with the previous studies, the specific parameterization of s_6 for the B3P86-D2 functional was achieved (see Section 3).

Once the ground state structure of the complexes has been elucidated, its excited-state description can be done through the use of Range-Separated Hybrid (RSH) functionals (*e.g.*, CAM-B3LYP and ωB97).[70, 71] This new family of functionals has been recently developed for an improved description of mainly Rydberg and CT excitations within the time dependent (TD)-DFT framework. The key point of RSH functionals is to split the $1/r_{ij}$ particle-particle operator entering into the Hamiltonian into controlled short- and long-range components, using the standard error function:

$$\frac{1}{r_{ij}} = \frac{1 - \mathrm{erf}(\omega r_{ij})}{r_{ij}} + \frac{\mathrm{erfc}(\omega r_{ij})}{r_{ij}} \qquad (\mathrm{III}.\,9)$$

where r_{ij} is the interelectronic distance and ω is a parameter defining the range separation. Different combinations of density-based and exact-like exchange functionals as a function of the inter-electronic distance can be used. RSH functionals including ωB97 and ωB97X are known to definitely improve excited state CT predictions.[50, 72] Since the CT properties are known to be dramatically affected by the self-interaction error of standard hybrid functionals, this strategy is also known to partly tackle this problem. The ωB97 functional were also corrected to better describe non-covalent interactions, including empirical dispersion terms (ωB97X-D).[73]

Therefore geometry optimizations were performed using both B3P86-D2 and ωB97X-D functionals with the ORCA[74] and Gaussian09[24] packages, respectively. Excited states (ES) and the corresponding energies were obtained in the TD-DFT framework (with B3P86 and

ωB97X-D). In order to assess the most adapted functional to describe copigmentation, in which CT may play an important role, results obtained with B3P86 were carefully compared to those obtained with the RSH functional ωB97X (see notes in text below).

The cc-pVDZ basis set has been used as it provides a good compromise between accuracy and computational time, regarding the size of the systems studied here. All DFT-D calculations (except those performed with ωB97X-D) have been achieved within the RIJCOSX approximation largely decreasing the computational time with a negligible error. This approach consists in using auxiliary basis sets to efficiently calculate exchange and coulomb matrices in the framework described by Neese *et al.*.[75]

The intermolecular interaction energies were calculated as follow:

$$\Delta E_{int} = E_{complex} - \sum_{i}^{\substack{\text{Free} \\ \text{Partner}}} E_i \quad \text{(III.10)}$$

where $E_{complex}$ denotes the energy of the complex, and the summation runs over the two free partners. $E_{complex}$ included basis set superposition error (BSSE), estimated using the traditional counterpoise method:

$$BSSE = [E_{AB}^{AB}(A) - E_A^{AB}(A)] + [E_{AB}^{AB}(B) - E_B^{AB}(B)] \quad \text{(III.11)}$$

where $E_{AB}^{AB}(A)$ and $E_{AB}^{AB}(B)$ are the energies of two given free partners A and B, respectively as obtained in the AB complex geometry with the AB basis set; $E_A^{AB}(A)$ and $E_B^{AB}(B)$ are the energies of A and B, respectively as obtained in the AB complex geometry with the A and B basis sets, respectively.

A comparison between Mulliken, ESPdipole[76, 77] and CHelpG[78, 79] population analysis is also done in Section 3, to avoid any possible CT overestimation provided by Mulliken densities.

Solvent effects were taken into account using implicit solvent models, in which the solute is embedded in a shape-adapted cavity surrounded by a dielectric continuum, which is characterized by a dielectric constant. Water ($\varepsilon = 78.35$) was used to reproduce the polar

compartment (vacuoles) in which anthocyanins are concentrated in plant. Conformational analysis and interaction energies performed with the B3P86-D2 functional were performed using COSMO (COnductor-like Screening Model)[80] model, while PCM[22, 81] (Polarizable Continuum Model) was used with the other functionals. For TD-DFT calculations, the classical use of implicit solvent can be applied but may suffer from a fundamental problem, ignoring the time dependence of solvent relaxation (in particular the fast electron response, corresponding to the non-equilibrium solvent regime). An effective state specific (SS) approach has been developed and has been showed to accurately describe the solvation free energy of a specific excited state.[82]

3. Computational Details

3.1. s_6 Grimme's parameter assessment

The dispersion correction of B3P86 mainly depends on s_6 as defined in Eq. (III.8). There is no assessed s_6 value available for B3P86-D2. An optimum value is found for the non-hybrid form, namely BP86 ($s_6 = 1.05$). However it may slightly deviate from the optimum value when a fraction of exact HF-like exchange is introduced (20% HF, in the case of B3P86). The s_6 optimization procedure is usually assessed on model systems including i) the potential energy curve for some rare-gas dimer dissociation and/or ii) the S22 database[83, 84] that includes non-covalent complexes. A set of s_6 values ranging from 1.05 to 0.65 were tested on S22 (see supporting information, Table S1). This range was motivated because s_6 decreases by 0.15 from BLYP to B3LYP (20% HF).[67] The standard mean average deviation (MAD) obtained with the entire S22 set was largely reduced, reaching chemical accuracy (MAD of 0.87 kcal.mol^{-1}) for the optimum 0.780 value (see supporting information, Table S1). The S22 database can be decomposed into three subgroups namely H-bond, true dispersion and mixed electrostatic interactions.[84] The s_6 optimization procedure only slightly MAD decreased for the H-bond subgroup, while it was dramatically improved for the other two subgroups. The basis set employed (cc-pVTZ) is believed to be close to the asymptotic region, additional calculations with the nearly exact def2-QZVP basis set provided a very similar MAD (0.76 kcal.mol^{-1}).

To validate the entire model the potential energy curve of the **C:Q** complex was assessed with B3P86-D2 (default and optimized s6 parameter) and compared to B3P86, BP86-D2, BP86-D3(BJ), ωB97X-D, B3LYP-D2, B3LYP-D3(BJ), B3LYP-D3, M06-2X and SCS-

144

MP2[85, 86] (Fig. III.7a). The cc-pVDZ basis set was chosen to reach enough accuracy at a reasonable computational cost, regarding the size of the system. The SCS-MP2/cc-pVDZ potential curve (taken here as an accurate reference) exhibited a minimum of -19.1 kcal.mol^{-1} at 3.3 Å (Fig. III.7a). As expected, the uncorrected B3P86 functional failed to qualitatively describe this potential energy curve (Fig. III.7a), exhibiting a dramatic underestimation of non-covalent interaction energies (ΔE_{int} of -0.6 kcal.mol^{-1}). The use of a too high s_6 parameter (*i.e.*, $s_6 = 1.05$) stressed a minimum of -23.3 kcal.mol^{-1} at 3.1 Å (Fig. III.7a), which suggests the overestimation of non-covalent interaction energies and the corresponding underestimation of optimum intermolecular distances. The decrease of the s_6 parameter to the optimum value (0.780) significantly improved the π-π complex stabilization exhibiting a minimum of -17.0 kcal.mol^{-1} at 3.3 Å (Fig. III.7a).[31] BP86-D2, BP86-D3(BJ) and B3LYP-D3(BJ) significantly overestimated the non-covalent interaction energies (ΔE_{int} of -22.2, -26.5 and -22.8 kcal.mol^{-1} at 3.1, 3.3 and 3.3 Å, for the three functionals respectively). The RSH functional ωB97X-D provided a too low interaction energy (-10.1 kcal.mol^{-1} at 3.4 Å, see Fig. III.7a). B3LYP-D3 and M06-2X provide a relatively accurate evaluation of the minimum (-20.6 and -17.3 kcal.mol^{-1} at 3.3 and 3.3 Å, for both functionals respectively, as seen in Fig. III.7a).

---

[31] Due to the size of the basis set (cc-pVDZ), the energy difference between the optimized B3P86-D2 and SCS-MP2 is (mainly) attributed to BSSE. For this comparison, interaction energies were not counterpoise corrected here, considering that BSSE effects were later incorporated.
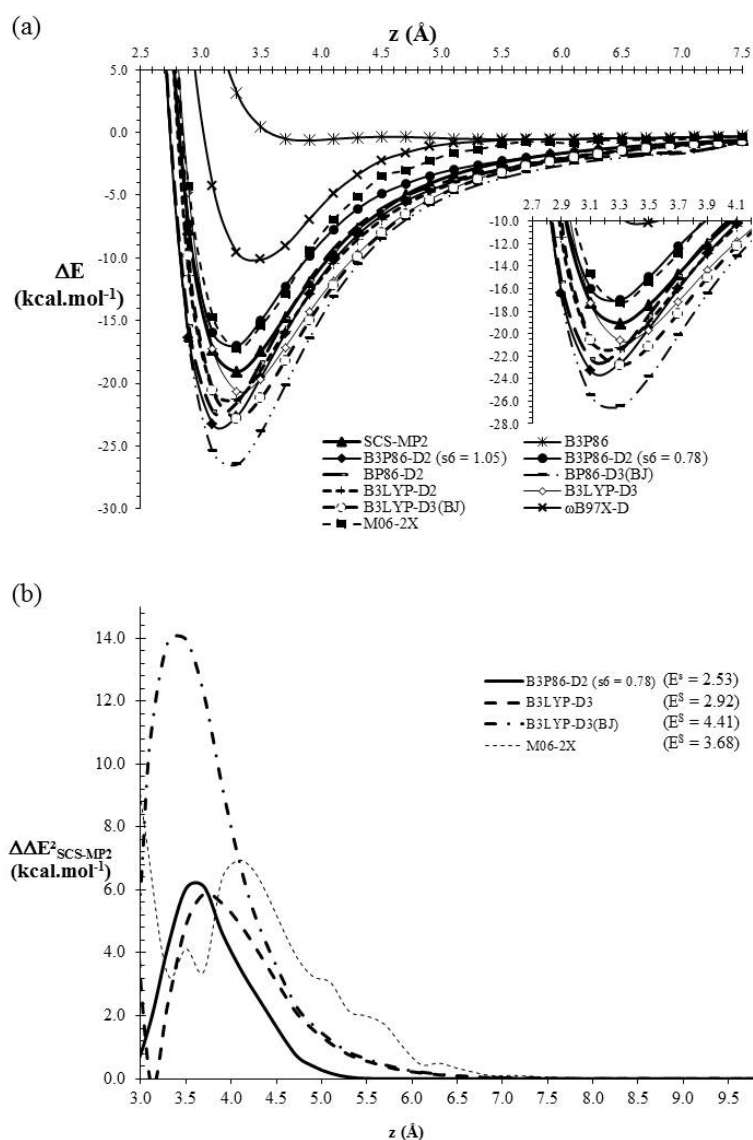
Figure III.7. (a) Potential energy curves of the C:Q complex as obtained with different functionals. (b) Square differences ($[\Delta\Delta E_{int}]^2$) between the DFT and SCS-MP2 energies.

A thorough comparison of B3P86-D2($s_6 = 0.780$), B3LYP-D3 and M06-2X was performed with respect to SCS-MP2 (Fig. III.7b). The most accurate methods appear to be B3P86-D2($s_6 = 0.780$) and B3LYP-D3, as judged for instance by the surface error E^S,[32] which turns to be 2.5 and 2.9 kcal.mol^{-1} (Fig. III.7b). Note that the agreement between these two methods and the SCS-MP2 results is better around the equilibrium region (*i.e.*, at 3.3 Å) although deteriorates for longer distances in favour of B3P86-D2($s_6 = 0.780$). On the other hand, M06-2X provided

---

[32] The surface error (E^S) is obtained in a statistical manner by integrating energy differences between the DFT functional under evaluation and the SCS-MP2 value (taken here as reference), as a function of the intermolecular distance.

a 'noisy' potential energy curve, which has already been described in certain cases and attributed to the high number parameters used to define this functional.[62]

3.2. Charge transfer assessment

Ground state CT between interacting partners is a main characteristic of π-π molecular complexes. It is well admitted that for aromatic systems, charge analysis is better described by Class III methods such as CHelpG.[87] Therefore this method was consequently used here to evaluate charge transfer (q_{GS}^{CT}) with B3P86-D2, ωB97X-D and SCS-MP2/cc/pVDZ. SCS-MP2/cc-pVDZ exhibited q_{GS}^{CT} of 0.09 |e| at the optimum intermolecular distance (*i.e.*, z = 3.3 Å) (Fig. III.8), while both functionals provided very satisfactory results (0.12 and 0.08 |e| for B3P86-D2 and ωB97X-D, respectively).
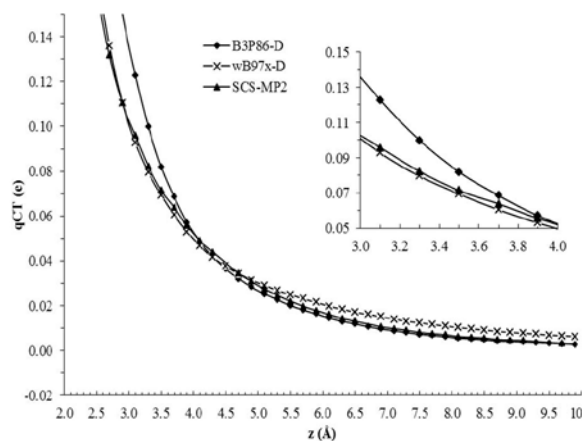
Figure III.8. Ground-state CT for the antiparallel **C:Q** at the B3P86, B3P86-D2 (with default and optimum s_6 parameters), and ωB97X-D. The SCSMP2 curve is shown as a reference. The cc-pVDZ was used for calculations shown here.

All-in-all, these results showed that B3P86-D2 with an optimized s_6 parameter (0.780) might well serve as a reliable method to systematically explore potential energy surfaces of π-π flavonoid complexation, whereas ωB97X-D is expected to accurately deal with CT excitations as we will show next.

4. Results and Discussions

4.1. Geometry of π-π complexes

4.1.1. Potential Energy Surface Exploration

Due to the asymmetry of the 2-phenyl-1-benzopyrane nuclei of quercetin and 3-*O*-methycyanidin (see Scheme III.3), two possible orientations were investigated *i.e.*, parallel and antiparallel (also called head-to-head or head-to-tail, respectively). In the aim of exploring the entire potential energy surface for both orientations, the potential energy curve was first studied along the *z*-axis *i.e.*, following the distance separating both flavonoids. The minimum energy distance (z_{min}) appears higher for the parallel than for the antiparallel orientations (*e.g.*, for **C:Q**, z_{min} = 3.5 Å and 3.3 Å for both orientations, respectively). The (x,y) potential energy surface was then explored at zmin (see supporting information, Fig. S2). Five, four and four orientations were obtained for **C:Q**, **Q:Q** and **C:C**, respectively (Fig. III.9).
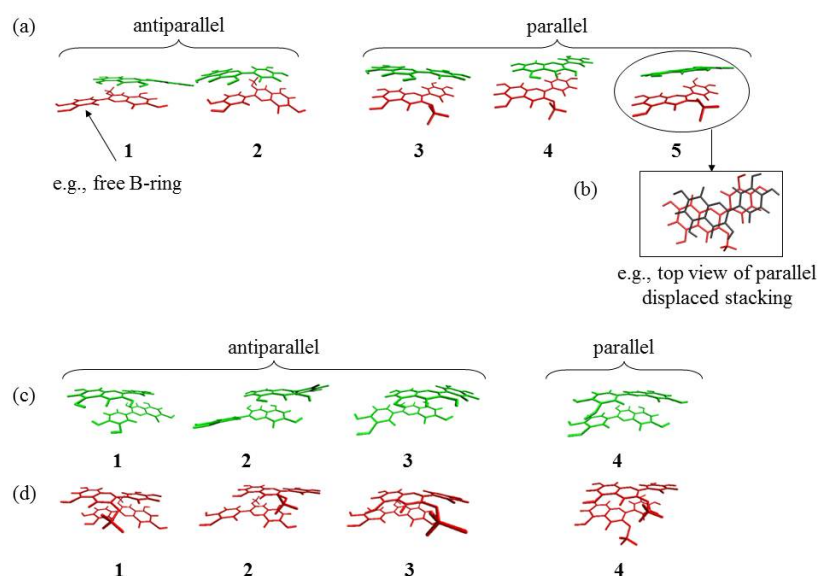
Figure III.9. Optimized (COSMO-B3P86-D2(s_6 = 0.780)/cc-pVDZ) geometries for (a,b) **C:Q**, (c) **Q:Q**, and (d) **C:C**.

4.1.2. Optimized geometries

For the antiparallel π-π complexes, C-ring interacts either with B-ring (orientation **2** of **C:Q**, orientation **1** of **Q:Q** and orientation **1** of **C:C**) or with A-ring (orientation **1** of **C:Q**,

orientations **2**-**3** of **Q:Q** and orientations **2**-**3** of **C:C**) (Fig. III.9). In the latter case (interaction between A and C-rings), B-ring only interacts with the solvent (Fig. III.9). For the parallel π-π complexes (orientations **3**-**5** of **C:Q**, orientation **4** of **Q:Q** and orientation **4** of **C:C**), the whole tricyclic nuclei of both flavonoids interact with each other (Fig. III.9). As usually observed in π-π complexes, no strict cofacial (face-to-face) arrangement occurs[88] but only the so-called parallel-displaced one (orientations **3**-**5** of **C:Q**, orientation **4** of **Q:Q** and orientation **4** of **C:C**) (Fig. III.9).

4.1.3. Binding energies

All the thirteen orientations exhibit considerable binding energies (Table III.5); **C:Q** being more stable than both dimers (by 1 to 3 kcal.mol^{-1}). **Q:Q** is more stabilized than **C:C** by around 1 kcal.mol^{-1} (Table III.5). The five conformers of **C:Q** are very similar in energy, orientation **5** being slightly more probable according to the Boltzmann distribution (44.0%, see Table III.5). These energies are in perfect agreement with the -13.9 kcal.mol^{-1} experimental binding enthalpy obtained for the **C:Q** complex.[33][46] This agreement confirms again the robustness of the BSSE corrected B3P86-D2(s_6 = 0.780)/cc-pVDZ method to evaluate stability of polyphenol π-stacking complexes.

Taking all possible orientations into account for copigmentation complexes and both non-covalent dimers, the global Boltzmann distribution is 81%, 1% and 18% for **C:Q**, **Q:Q** and **C:C**, respectively. Anthocyanin self-association is also a mechanism that competes with water addition on the flavylium ion, thereby resulting in colour stabilization. The relative contribution of anthocyanin copigmentation and self-association to colour stability is of course dependent on the relative concentrations of pigment and copigment. With a potent copigment such as quercetin, the higher stability of the **C:Q** copigmentation complex in comparison to the **C:C** anthocyanin dimer obtained in this work suggests that at equal pigment and copigment concentrations, copigmentation is the prevalent mechanism.

---

[33] It must be stressed that Dimitric *et al.* used the cyaniding aglycone, while we used 3-*O*-methylcyanidin as a slightly better model of natural anthocyanins (see Section B.1). Nonetheless we have also performed the calculation with the cyanidin:quercetin complexes, and we have obtained very similar results, as shown in the Supporting Information.

Table III.5. Counterpoise-corrected binding energies (ΔE_{int}, kcal.mol^{-1}) and Boltzmann weights (D_{bolz}) calculated for the most stable geometries of (a) **C:Q**, (b) **Q:Q** and (c) **C:C** with COSMO-B3P86-D2($s_6 = 0.780$)/cc-pVDZ.

	Complex	Orientation	ΔE_{int}	D_{bolt}
(a)	**C:Q**	1	-13.3	16.2%
		2	-13.1	12.9%
		3	-12.8	7.0%
		4	-13.4	19.9%
		5	-13.9	44.0%
(b)	**Q:Q**	1	-11.1	27.1%
		2	-9.1	0.9%
		3	-10.6	11.6%
		4	-11.6	60.4%
(c)	**C:C**	1	-12.7	30.5%
		2	-12.9	41.7%
		3	-11.9	7.7%
		4	-12.5	20.2%

4.1.4. Contributions to total binding energy

Our calculations suggest that hydrogen bonding subtly participates in copigmentation. All intermolecular H-bonds observed in the copigmentation complex are relatively weak, with distances higher than 2.0 Å. Although weak, the H-bonds significantly change the planarity of 3-*O*-methylcyanidin (*e.g.*, the dihedral angle between the C- and B-rings is -175.5° for free 3-*O*-methylcyanidin while it is -159.0 and -161.3° for orientations **2** and **5** of **C:Q**, respectively). Nonetheless, H-bonding is not the most important contribution to the intermolecular interactions between quercetin and 3-*O*-methylcyanidin. Several orientations (orientations **1**, **3** and **4** of **C:Q**, orientation **3** of **Q:Q** and orientations **1** and **2** of **C:C**) do not present any H-bond while their binding energies are in the same range as for the other orientations (see Table III.5). The dispersive contribution is definitely the most important contribution to copigmentation complex formation with quercetin. The relative Grimme's dispersive energies are -25.6, -23.4 and -24.7 kcal.mol^{-1}, for **C:Q**, **Q:Q** and **C:C**, respectively, which is attributed to the large π-electron delocalization in each partner allowing strong London forces.

Finally, quantum calculations also shed light on the paradox of **C:C** dimers. As already described for other molecular systems,[89] there exist four optimal π-π rearrangements in which dispersion compensates the strong Coulomb repulsion: taking the first-order terms, the average Coulomb and dispersion energies are +27.2 and -24.7 kcal.mol^{-1}, respectively.

4.1.5. Ground-State charge transfer

At equilibrium distance, ground state CT is observed from quercetin to 3-*O*-methylcyanidin (q_{GS}^{CT} around 0.06 |e|, see Table III.6a). As a powerful free radical scavenger, quercetin is indeed an effective electron donor and is thus able to transfer some electron density to the positively charged 3-*O*-methylcyanidin. This efficient electron coupling decreases the positive charge of 3-*O*-methylcyanidin, thus stabilizing again the complex, decreasing Coulomb repulsion. Moreover, the ground state CT allows stabilization of low-lying unoccupied orbitals of 3-*O*-methylcyanidin, a precursor effect of the Vis absorption shift typical of copigmentation. Only slight or even non-significant CTs are expected in the dimer ground states (Tables III.6b and c). However, for the **Q:Q** dimers, the parallel orientation (orientation **4**) presents a significant CT (q_{GS}^{CT} around 0.04 e, see Table III.6a). In this specific case corresponding to the so-called parallel displaced stacking, the arrangement of dipole moments on each monomer favours CT (Scheme III.4). On the contrary, for the antiparallel orientations (orientations **1-3**), CT is unfavourable (Scheme III.4b). CT is definitely unlikely for the **C:C** dimers as both monomers are positively charged, thus dramatically decreasing their electron-donating capacity.
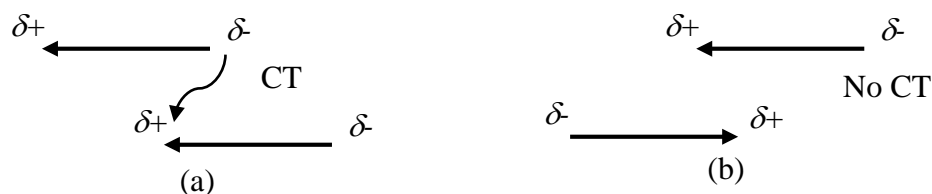
Scheme III.4. (a) Parallel and (b) antiparallel dipole displaced stacking, allowing and not allowing CT, respectively in Q:Q complexes.

Table III.6. Charge transferred in ground state (q_{GS}^{CT}, |e|) and in excited state (q_{ES}^{CT}, |e|), total charge transfer (q^{CT}, |e|), Dipole moment of ground state (μ_{GS}, D) and excited state (μ_{ES}, D) and absolute dipole variation ($|\Delta\mu|$, D) of optimized (a) **C:Q**, (b) **Q:Q** and (c) **C:C** complexes. The electronic population analysis was achieved with the CHELPG formalism.

	Complex	Orientation	q_{GS}^{CT}	q_{ES}^{CT}	q^{CT}	μ_{GS}	μ_{ES}	$|\Delta\mu|$
(a)	**C:Q**	1	0.07	0.02	0.09	8.3	7.8	0.5
		2	0.06	0.00	0.06	16.2	16.6	0.4
		3	0.05	0.08	0.13	9.1	7.8	1.3
		4	0.05	0.25	0.30	9.9	4.8	5.1
		5	0.05	0.68	0.73	9.0	6.5	2.4
(b)	**Q:Q**	1	0.00	0.00	0.00	0.0	0.0	0.0
		2	0.00	0.00	0.00	0.0	0.0	0.0
		3	0.00	0.00	0.00	0.1	0.0	0.1
		4	0.05	-0.04	0.00	13.2	7.6	5.5
(c)	**C:C**	1	0.00	0.00	0.00	0.1	0.0	0.0
		2	0.00	0.00	0.00	0.0	0.0	0.0
		3	0.00	0.00	0.00	0.0	0.1	0.1
		4	0.01	0.17	0.17	6.9	0.1	6.8

4.2. UV/Vis properties

In the copigmentation complex studied here, both Highest Occupied Molecular Orbital (H or HOMO) and H-1 correspond to H of quercetin and 3-*O*-methylcyanidin, respectively; while Lowest Unoccupied Molecular Orbital (L or LUMO) and L+1 correspond to L of 3-*O*-methylcyanidin and quercetin, respectively (Fig. III.10). According to the Linear Combination of Atomic Orbital (LCAO) analysis, H is equally on A&C rings and half on B-ring of the quercetin moiety; L is mainly located on the A&C rings of the 3-*O*-methylcyanidin moiety (*ca.* 77%, see supporting information, Table S11).

As a direct consequence of this redistribution in the frontier orbitals, the H→L gap (E_{gap}) of the complex (*e.g.*, 5.8 eV in orientation **5** of **C:Q**) is dramatically and slightly reduced compared to quercetin (E_{gap} = 7.1 eV) and 3-*O*-methylcyanidin (E_{gap} = 6.1 eV), respectively (Fig. III.10).

For orientations **4** and **5** of **C:Q**, the maximum absorption wavelength is mainly assigned to the H→L electronic transition, corresponding to a CT excited state. As for the ground state, CT occurs from quercetin to 3-*O*-methylcyanidin.[34] This CT absorption band corresponds to the

---

[34] The differences in CT energies between B3P86 and ωB97X-D were evaluated for **C:Q** for which the B3P86-D geometry was used (see Supporting Information, Table S7). Both functionals provided the same wavelength for the main electronic transition, *i.e.*, the H-1→L transition having the highest oscillator strength f (E_{max} = 2.76 and 2.44 eV with ωB97X-D and B3P86, respectively). Nonetheless, the CT excited state corresponding to the H→L vertical transition is dramatically underestimated with B3P86 (f = 3.0 × 10^{-3}). The ωB97X-D functional appeared

observed bathochromic shift typical of copigmentation. We must insist that it is not strictly a Vis absorption band shift but actually a new band that appears, corresponding to the CT excited state that can only occur in π-stacking complexes. The oscillator strength of this new band can be relatively high (f being up to 0.41, see Table III.7).
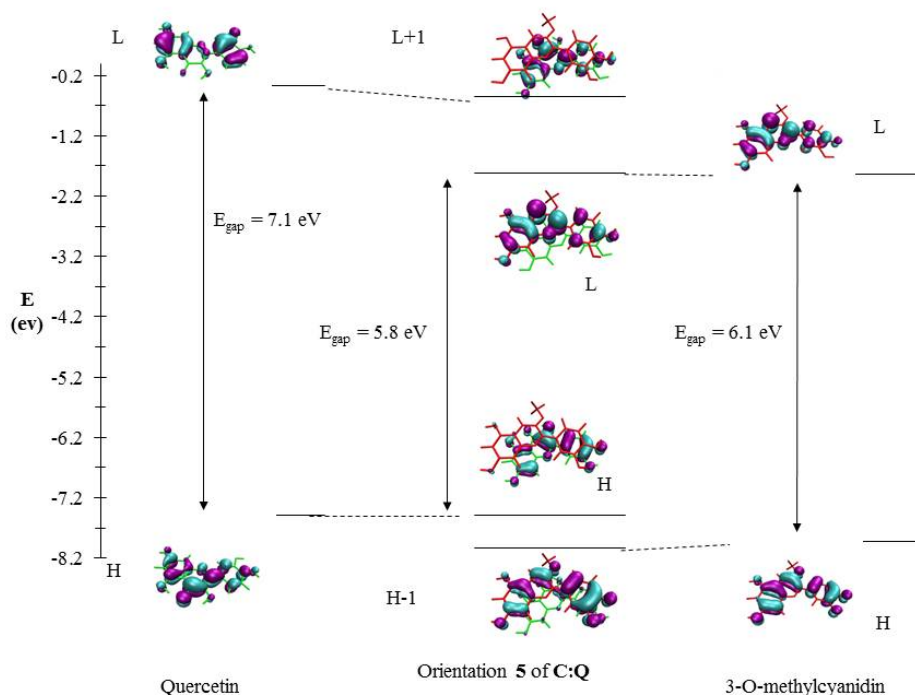
Figure III.10. MO correlation diagram of quercetin, orientation **5** of **C:Q** and 3-O-methylcyanidin.

Nonetheless this strongly depends on the orientation. On the one hand, when CT is important (see Table III.6 for *e.g.*, orientation **5** for which q^{CT} is 0.73), the CT excited state contribution is high and the bathochromic reaches -0.23 eV (37.8 nm). This is attributed to an efficient overlap between H and L, involving A&C and B-rings of both partners. The importance of CT is also correlated to the change in the dipole moment from the ground to the excited states (Table III.6). On the other hand, when the H-1→L transition (*i.e.*, involving only the 3-O-methylcyanidin fragment) contributes to the maximum absorption band, the oscillator strength is increased while the CT contribution decreases (Table III.7). *E.g.*, for orientation **1**, both B-

---

much more relevant to study UV−vis absorption of π−π polyphenol complexes as it exhibited an oscillator strength ($f = 0.28$) higher and more accurate with respect to experimental data.

rings do not interact, decreasing H and L overlap between both partners, making the H→L electronic transition improbable. The CT excited state contribution is weak and the maximum absorption energy (E_{max}) is similar to that of 3-O-methylcyanidin, preventing bathochromic shift (ΔE_{max} = -0.02 eV, see Table III.7).

Table III.7. Maximum vertical excitation energies (E_{max}, eV), absorption wavelengths (λ_{max}, nm), oscillator strengths (f), MO descriptions, excitation energy shifts (ΔE_{max}, eV), absorption wavelength shifts ($\Delta\lambda_{max}$, nm) and Boltzmann weighted bathochromic shift ($\Delta\lambda_{bolt}$, nm) of **C:Q**, **Q:Q** and **C:C** at the TD-ωB97X-D/cc-pVDZ level of theory using SS-PCM implicit solvent model. The energy and wavelength shifts are calculated with respect to the corresponding free flavonoid for **Q:Q** and **C:C** and with respect to 3-O-methylcyanidin for **C:Q**.

Complex	Orientation	E_{max}	λ_{max}	f	MO description	ΔE_{max}	$\Delta\lambda_{max}$	$\Delta\lambda_{bolt}$
	1	2.81	441.7	0.41	H-1→L (65.0%)	-0.02	3.7	
	2	2.79	443.7	0.33	H-1→L (66.3%)	-0.04	5.7	
C:Q	3	2.76	448.7	0.27	H-1→L (66.3%)	-0.07	10.8	22.9
	4	2.70	458.9	0.33	H→L (56.8%)	-0.13	20.9	
	5	2.61	475.8	0.05	H→L (66.1%)	-0.23	37.8	
	1	3.73	332.8	0.82	H-1→L (59.5%)	0.01	-1.1	
	2	3.73	332.5	0.95	H→L (52.7%)	0.02	-1.5	
Q:Q	3	3.74	331.7	0.89	H-1→L (40.5%) H→L+1 (53.5%)	0.03	-2.3	-4.1
	4	3.78	328.3	0.86	H-1→L (37.6%)	0.06	-5.7	
	1	2.89	429.1	0.72	H→L (59.5%)	0.06	-8.8	
	2	2.88	430.9	1.07	H-1→L (54.7%)	0.05	-7.1	
C:C	3	2.88	430.3	0.79	H-1→L (56.7%)	0.05	-7.7	-8.3
	4	2.90	427.9	0.53	H-1→L (49.6%) H→L (34.7%)	0.07	-10.0	

The bathochromic shift experimentally observed thus appears as a global effect that must be attributed to the different orientations of the copigmentation complexes. The Boltzmann weighted bathochromic shift (16.2%. $\lambda_{max}^{Orientation1}$ + 12.9%. $\lambda_{max}^{Orientation2}$ + 7.0%. $\lambda_{max}^{Orientation3}$ + 19.9%.$\lambda_{max}^{Orientation4}$ + 44.0%. $\lambda_{max}^{Orientation5}$) is 0.14 eV (23 nm) (Table III.7). This correctly fits with the experimental bathochromic shift obtained with the cyanidin/quercetin couple, *i.e.* 11.7 nm.[46] The theoretical evaluation slightly overestimated this shift,[35] however it has been discussed that under these experimental conditions the complete complexation cannot be reached, which may slightly induce underestimation of $\Delta\lambda_{max}$.[56] This confirms again the robustness of the methodology described above. The non-covalent dimers exhibit slight hypsochromic shifts with respect to the monomers (quercetin and 3-O-methylcyanidin) *i.e.*,

---

[35] PCM seemed to be in better agreement with ref. 20 (see Supporting Informations, Table S9). However, as explained in text the corresponding shift maybe slightly underestimated, showing that the trend obtained with SS-PCM appears in better agreement with most of experimental observations, which appear very consistent with the improvement proposed by this method.

lower than 0.06 eV (-5.7 nm) and up to 0.07 eV (-10 nm) for **Q:Q** and for **C:C**, respectively (Table III.7). The maximum wavelengths are not assigned to H→L only, as in the monomers (Table III.7), but to a mixture of H-1→L, H→L and H→L+1 transitions. This partially explains the hypsochromic shifts. Due to symmetry between both monomers, mainly in the parallel orientations, H and H-1 on one hand and L and L+1 on the other hand are very close in energy; confirming that the shift is slight. Such hypsochromic shifts have been observed in self-association of anthocyanins. However it may only slightly affect the global UV/Vis spectra of pigment/copigment mixtures because of the small occurrence of dimers and the low shift values when averaged over all possible orientations.

5. Conclusion

The present work has adopted, after a careful benchmarking, a theoretical methodology to reliably evaluate the formation of π-stacking complexes, as demonstrated for the copigmentation of anthocyanins by flavonols. The evaluation of π-stacking complexes is achieved by the BSSE-corrected B3P86 DFT functional including the Grimme's dispersive term (with the s_6 parameter adjusted to a value of 0.780). The robustness of this method was cross-checked according to high-level SCS-MP2 calculations for the evaluation of the binding energies. By using the former and less-costly method, different possible π-stacking complexes of flavonoids can be predicted in solution or in plant cells. The driving force in the formation of cyanidin:flavonol complexes appears to be π-π interactions, H-bonding only slightly contributing to the stabilizing energies. This observation agrees with experimental data. The careful evaluation of the potential energy surface highlighted several possible orientations with significant Boltzmann weight. The weighted complexation energies also fit well with experimental values.

It must be stressed that in most in vitro studies in which UV/Vis absorption properties are evaluated, the 1:1 binding definitely obtained.[90] Therefore in the present study only two-partner association (self-association and copigmentation complexes) has been considered. The formation of complexes of higher stoichiometry (tri-, tetra- or pentamers) cannot be excluded in plant cell vacuoles where the pigment and copigment concentrations maybe quite high. Moreover in this case, pigments and copigments can be more complex,[91] providing large-scale molecular architectures, for which the optical properties cannot be achieved at the

quantum level. Moreover, under strongly acidic solutions (typically used to measure bathochromic shift typical of copigmentation), the presence of coloured quinonoid bases (pK_h *ca.* 4) is neglected, also because neutral quinonoid bases typically bind flavonols less strongly than the corresponding flavylium ion (*e.g.*, a factor *ca.* 3 for malvidin 3,5-di-*O*-glucoside and quercetin 3-*O*-rutinoside).[92]

The bathochromic shift typical of copigmentation, a major mechanism of colour variation in plants, has been also accurately evaluated using the ωB97X-D range-separated hybrid functional. In particular, the expected bathochromic shift experimentally observed with the cyanidin:quercetin pair is perfectly reproduced by theoretical calculations. It actually corresponds to the appearance of a new Vis absorption band corresponding to a CT excited state. Again, taking all possible geometries into account together with their corresponding Boltzmann weights appeared mandatory to accurately reproduce the UV/Vis absorption spectra. Quantum-chemical calculations have thus allowed providing a detailed molecular orbital picture and thus a complete spectroscopic understanding of anthocyanin:flavonol copigmentation. We are confident that this methodology can be successfully applied in the near future to firmly rationalize the mechanism causing colour variation in polyphenols, which occurs in plant and food. Indeed, controlling natural colours in the food industry and in modern "*haute cuisine*" such as molecular gastronomy is a crucial point in the appreciation of quality by consumers.

Section C. The influence of a flavan-3-ol substituent on the affinity of anthocyanins (pigments) toward vinylcatechin dimers and procyanidins (copigments)

1. Introduction

Flavanol-anthocyanin adducts, such as catechin-(4→8)-oenin, result from the direct condensation between flavan-3-ols (catechin monomers and condensed tannins) and anthocyanins.[93, 94] Such adducts, which were evidenced in wine[94, 95] and fruit[96-98], and their copigmentation complexes could contribute to the colour of mature red wines, a point largely undocumented so far.

Although the anthocyanin moiety is obviously responsible for the colour of flavanol-anthocyanin adducts, slight alterations (a λ_{max} blue shift of 8 nm) in the UV/Vis spectrum can be attributed to the flavan-3-ol moiety.[99, 100] In aqueous and hydroalcoholic solutions, as the pH is raised, the cationic flavylium form (AH$^+$, red) is very rapidly converted into neutral purple quinonoid bases (A, kinetic products) by deprotonation of one of the most acidic OH groups, and more slowly into a colourless hemiketal (B, thermodynamic product, itself in equilibrium with small concentrations of *cis*- and *trans*-chalcones, C_c and C_t), by water addition onto the pyrylium ring of the residual red cation (Scheme III.5). At mildly acidic pH, the colourless hemiketal is the dominant species.[101] This frame of structural transformations applies to all common anthocyanins. A previous work by some of the authors[101] has reported the thermodynamic and kinetic parameters of these reversible transformations for the flavanol-anthocyanin adduct (catechin-(4→8)-oenin) and has showed that the flavanol nucleus only marginally affects the anthocyanin behaviour.

Despite the thermodynamic tendency of anthocyanins to form colourless hemiketals, natural colours expressed by anthocyanins are fairly stable. This evidences natural occurring stabilization mechanisms, copigmentation being one of the most important. Copigmentation mainly refers to interactions between colourless phenols (copigments) and the planar polarizable nuclei of anthocyanins' coloured forms.[102] The binding is promoted by the hydrophobic effects, mainly dispersive π-π stacking interactions between the polarizable orbitals of the aromatic rings.[34, 102-104]
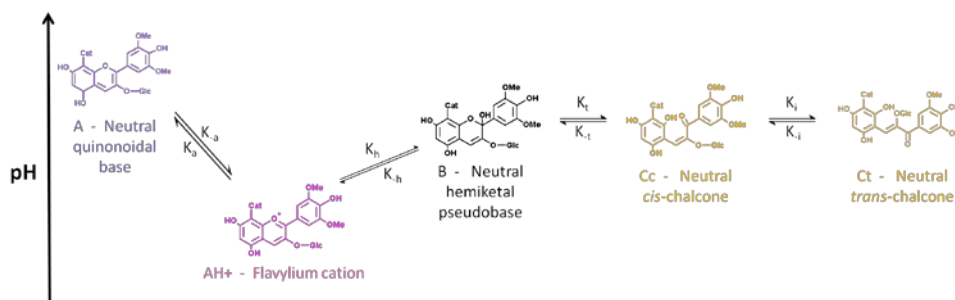
Scheme III.5. Anthocyanin (cat-mv3glc) pH dependent interconversion scheme.

CP1 - 9S11R vinylcatechin dimer

CP2 - 9R11S vinylcatechin dimer

CP3 - procyanidin B3 (dimer)

Pigment - catechin-(4,8)-malvidin-3-glucoside
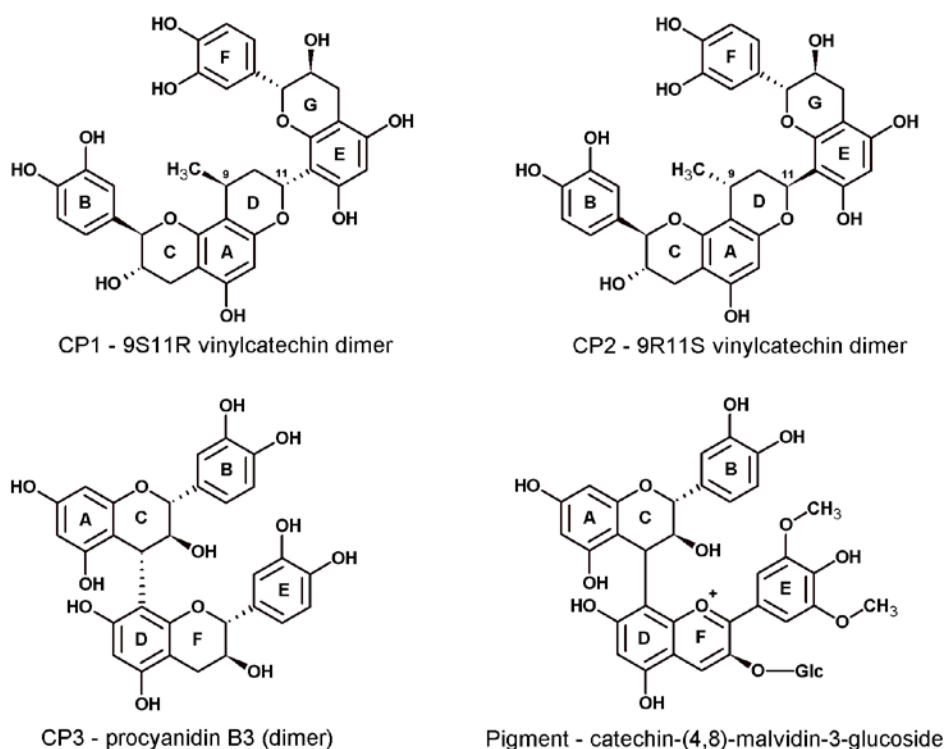
Scheme III.6. Chemical structures of the pigment and the three copigments CP1, CP2 and CP3.

Procyanidins and vinylcatechin dimers (originated in wine by the cleavage of methylmethine-bridged flavan-3-ol oligomers and by the reaction between flavan-3-ols and acetaldehyde)[105] were shown to act as copigments.[103] In the present work, three of these copigments were tested for their capacity to form complexes with catechin-(4→8)-oenin (Scheme III.6). To the authors' knowledge, this is the first work dealing with the copigmentation of flavanol-anthocyanin adducts.

/…/

Finally, the consequences of the pigment-copigment on the visible spectrum of the pigment were also theoretically analyzed, thus providing a complete picture of the electronic transitions describing the excited states (involved in visible light absorption). The theoretical investigation includes: a description of copigmentation for a prototype pigment/copigment pair, the optimal geometries of the three copigmentation complexes studied (evaluated by combining molecular dynamics and quantum calculations), and an analysis of the spectral shifts on the basis of time-dependent density functional theory (TD-DFT) calculations.

2. Materials and methods

/…/ *Note for the readers: This part refers to experimentals details and methods used to rationalize copigmentation process.*

2.1. Molecular dynamics simulations[36]

The starting geometries of the copigment and pigment molecules were obtained at the HF/6-31G(d) level of calculation, using the Gaussian09 package.[106] Atomic charges were further recalculated using the RESP procedure.[107] MD simulations were performed with GAFF (Generalized Amber Force Field) and the TIP3P model for the solute and water, respectively. Explicit solvation was included as a truncated octahedral box with a 12 Å distance between the box faces and any atom of the compound. Energy minimization occurred in two stages: first, the solute was kept fixed, and only the position of the water molecules was optimized, second the full system was optimized. Following a 100 ps equilibration procedure, 10 ns MD simulations were carried out. The Langevin thermostat was used[108, 109], and all the simulations were carried out in the *NPT* ensemble with periodic boundary conditions. All MD simulations were carried out using the Sander module, implemented in the Amber 10.0 simulations package[110], with the Cornell force field.[111] Bond lengths involving H-atoms were constrained using the SHAKE algorithm[112], and the equations of motion were integrated with a 2 fs time step using the Verlet leapfrog algorithm. Nonbonded interactions were truncated with a 12 Å cutoff. The temperature of the system was maintained at 303.15 K.

---

[36] This part has been performed by Pr. Victor Freitas in Porto. Geometries obtained by using MD calculations were the starting geometries for the quantum investigation.

2.2. Quantum calculations for complexation and corresponding optical properties

Over the past decade, the Density Functional Theory (DFT) has been well validated to evaluate conformational/electronic/optical properties of polyphenols. TD-DFT has appeared relevant to evaluate UV/Vis absorption spectra of π-conjugated compounds. However the choice of functionals is a determinant criterion to reach accuracy. In the present work long-range interaction is a key parameter. Classical DFT functionals fail in the description of i) long-range electron correlation for non-covalent interactions such as π-stacking interactions as observed in copigmentation complexes[113-115] [116-118], and ii) intra- and intermolecular charge transfer (CT) as observed in excited states involving non-bonding interaction. New functionals have been recently developed to better describe the former point (long-range electron correlation). *E.g.*, the DFT-D approaches introduce the dispersive contribution in DFT calculations by an empirically-parameterized R_{AB}^{-6} potential, as a perturbation post self-consistent field term.[66-68] The latter point (intra- and inter-CT) is better described by range-separated hybrid (RSH) functionals, in which the two-particle operator R_{ij} is split into short- and long-range exchange components (*e.g.*, ωB97).[119] The ωB97X-D functional hence appears relevant to correctly describe both π-stacking interactions and CT[73], which are expected to play a crucial role in copigmentation.[37]

Due to the system size (mainly for complexes), the Pople-type double-ζ basis set 6-31+G(d) was chosen as a relevant compromise between accuracy and time demand.

The ground states (S_0) were optimized using ωB97X-D/6-31+G(d,p) from the average geometries of each complex as obtained from the MD simulations. Excited states were calculated within the TD-DFT formalism from S_0 geometries, thus providing the vertical transition, at the ωB97X-D/6-31G+(d,p) level of theory.

Quantum calculations were performed using the Gaussian09 package.[106]

---

[37] It was shown that ωB97X-D failed to exactly reproduce the absolute experimental wavelengths of polyphenols, however in this case this is an appropriate method to allow an accurate i) assignment of the different bands, ii) description of the corresponding electronic transitions and iii) evaluation of the bathochromic shift attributed to copigmentation

3. Results and discussion

/.../ Important note for the readers: Experimental details and results are available on demand. Experiments exhibited the well-known bathochromic shift due to copigmentation. Moreover, CP1 and CP3 exhibit new bands in the range 440 - 460 nm. The theoretical investigation below aims at rationalizing both experimental observations.

3.1. Quantum rationalization of a prototype pigment/copigment system

Due to the size of the pigment/copigment system we first proposed a full rationalization of copigmentation on a prototype system, namely the [catechin:3-*O*-methylmalvidin] complex (Scheme III.5), smaller in size and thus easier to fully analyze at the quantum level. The entire potential energy surface was explored and three geometries were obtained (orientations **1**, **2** and **3**). In orientation **1**, the two partners are parallel to each other, the A and C-rings of catechin interacting with the A-ring of malvidin (Fig. III.11a). The other two orientations are head-to-head, the A-ring of catechin interacting with the C-ring of malvidin (orientation **2**, see Fig. III.11b) or the A and B-rings of catechin interacting with A and B-rings of malvidin (orientation **3**, see Fig. III.11c). The highest π-overlap is obtained for orientation **3**. As usually observed in π-π complexes, no strict cofacial (face-to-face) arrangement occurs but only the so-called parallel-displaced one (orientations **3**) (Fig. III.11).
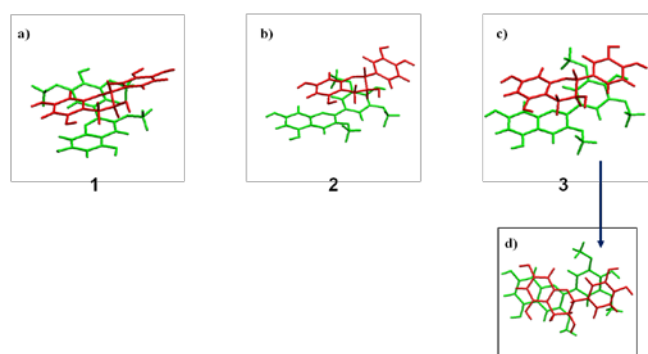
Figure III.11. Optimized (B3P86-D/cc-pVDZ) geometries for the [catechin:3-*O*-methylmalvidin] prototype complex for the three more favourable *i.e.*, a) orientation 1, b) orientation 2, c) orientation 3, showing d) the parallel displaced stacking on a top view.

The orientations exhibit considerable negative binding energies[38] (Table III.8) in which the dispersive contribution is high (ΔE^{disp} = -37.1, 38.4 and -42.5 kcal.mol^{-1} for the three orientations, respectively). π-Stacking appears definitely as the major contribution whereas H-bonding is relatively weak since the distances are higher than 2.3 Å. The Boltzmann distribution is 55%, 2% and 43% for the three conformers, respectively (Table III.8). In these complexes, charge transfer (from catechin to malvidin) is possible in ground state S_0 (q^{CT} = 0.08, 0.11 and 0.13 |e|, respectively).

Table III.8. Binding energies (ΔE, kcal.mol^{-1}), Boltzmann weights (D_{bolz}) and S_0 q^{CT} (e) calculated for all the most stable geometries of [catechine:3-O-methylmalvidin] with B3P86-D(s_6 = 1.05)/cc-pVDZ.

Orientation	ΔE	D_{bolz}	q^{CT}
1	-36.5	55%	0.08
2	-34.3	2%	0.13
3	-36.3	43%	0.11

For the three orientations, the classically described bathochromic shift attributed to copigmentation is observed (Table III.9). The intensity of this shift is however very dependent on the orientation: -0.09 eV (14.9 nm), -0.09 eV (14.9 nm) and -0.22 eV (40.5 nm) for the three orientations, respectively. In this prototype copigmentation complex, the absorption maximum wavelength corresponds to the first excited state S_1, which is constituted of electronic transitions involving HOMO (Highest Occupied Molecular Orbital), HOMO-1 and LUMO (Lowest Unoccupied Molecular Orbital). LUMO is mainly localized on the entire malvidin moiety and, depending on the orientation, the distribution of HOMO and HOMO-1 may significantly differ. In orientation **1**, HOMO is mainly localized on the malvidin moiety (as for LUMO), which allows an efficient MO (molecular orbital) overlap. In orientations **2** and **3**, HOMO is mainly localized on the B-ring of catechin. In this case, the contribution to the excited state of charge transfer (CT) from copigment to pigment increases and this is responsible of the bathochromic shift. Therefore the electronic transitions are tuned by i) MO overlap and the classical electronic transition contribution and ii) CT, which may occur in the excited state. Both contributions are more or less important depending on the orientation. Here it is possible to confirm, as previously

---

[38] Binding energies are expected to be overestimated since (i) the s_6 parameter of B3P86-D is not optimized, (ii) calculations have been performed in the gas phase, which probably leads to a significant overestimation of the stabilization attributed to intra-H bonding, and (iii) binding energies are compared to experimental binding Gibbs energies, thus including entropic effects that cannot be calculated here. To tackle the second point, solvent effects should be taken into account not only implicitly but also explicitly, as inter-H bonding is probably crucial in aqueous solutions. Due to the size of the systems studied here, the corresponding calculations are not feasible.

shown for the flavanol - anthocyanidin copigment complex, that the optical properties must be rationalized after a careful analysis of the potential hypersurface. The spectral shifts are obtained by averaging over all the possible copigmentation complex geometries, according to the Boltzmann distribution.

Table III.9. Maximum vertical excitation energies (E_{max}, eV), absorption wavelengths (λ_{max}, nm), oscillator strengths (*f*), MO descriptions, excitation energy shifts (ΔE_{max}, eV) and absorption wavelength shifts ($\Delta\lambda_{max}$, nm). The energy and wavelength shifts are calculated with respect to the 3-*O*-methylmalvidin.

Compound		E_{max}	λ_{max}	*f*	MO description
3-*O*-methylmalvidin		2.72	456.2	0.78	H→L (67%)
	1	2.63	471.1	0.49	H→L (66%)
		3.1	400.1	0.05	*H-1→L (30%)
		3.23	383.6	0.08	*H-1→L (34%)
[catechin:3-*O*-methylmalvidin]	**2**	2.63	471.2	0.43	H-1→L (52%)
		3.27	379.2	0.01	*H→L (55%)
	3	2.5	496.7	0.45	H→L (64%)
		2.76	448.7	0.01	*H-1→L (43%)

3.2. Theoretical conformation of the three pigment/copigment complexes

/…/

As noticed for the prototype system, the rationalization of optical properties strongly depends on the conformation. Hence, using a series of MD averaged geometries of complexes as starting geometries, DFT-D optimization was performed and allowed identifying 3, 3 and 4 geometries for the three complexes [CP1:catechin-(4→8)-oenin], [CP2: catechin-(4→8)-oenin] and [CP3: catechin-(4→8)-oenin], respectively (Fig. III.12). Unlike the prototype system, the number of degrees of freedom is very large and steric hindrance does not allow optimized π-stacking arrangements. However, due to the numerous OH groups, H-bonding now plays a major role in the binding. Anyway, even if π-interactions are no longer the only driving force, they still take place in all complexes. In most conformers, the D and F-rings of the pigment make π-type interactions with i) C, A and D-rings of CP1 and CP2 and ii) C and A-rings with CP3 (Table III.10). Then depending on the complex, the B- or E-ring of the pigment interacts with C, A, D and F-rings of the copigments (Table III.10). All these interactions occur at a distance of around 3.5 Å, which is typically observed for π-stacking interactions. Again, no cofacial arrangement is observed but, as expected, parallel-displaced stacking occurs.
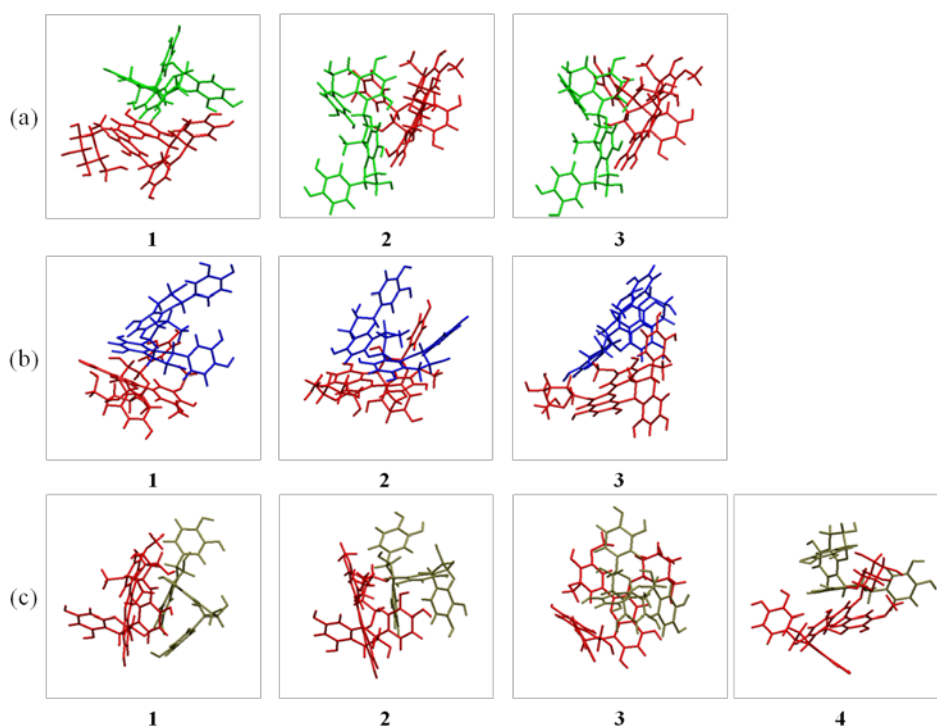
Figure III.12. All optimized (ωB97XD/cc-pVDZ) geometries for a) [CP1:catechin-(4→8)-oenin], b) [CP2:catechin-(4→8)-oenin] and c) [CP3:catechin-(4→8)-oenin] complexes. The pigment catechin-(4→8)-oenin is in red, CP1, CP2 and CP3 are in green, blue and brown, respectively.

Table III. 9. Geometrical characteristics for each complex obtained from the DFT-D calculations.

Complex	Conformer	Pigment moiety*	Copigment moiety*	Minimal π-stacking distance	Number of intermolecular H-bond	Mean H-bond distance	ΔE^{CP}
[CP1:cat-oenin]	**1**	DF	CAD	3.23	3	1.88	-57.6
		B	F	3.17			
	2	DF	CAD	3.41	3	1.87	-64.9
		B	F	3.23			
	3	DF	CAD	3.46	3	1.82	-50.1
		B	F	3.13			
[CP2:cat-oenin]	**1**	DF	GE	3.11	1	2.26	-24.1
		B	CAD	3.46			
	2	DF	CAD	3.45	3	2.21	-31
	3	DF	GE	3.93	5	1.92	-26
		B	CAD	3.21			
[CP3:cat-oenin]	**1**	DF	A	3.35	5	1.98	-46
		E	C	3.61			
	2	DF	A	3.24	3	2.02	-49.6
		E	C	3.88			
	3	DF	A	3.25	4	2	-41.6
	4	E	AC	3.21	1	1.85	-30.5

* involved in π-stacking

164

3.3. The classical bathochromic shift in pigment/copigment complexes

As for the prototype, the visible absorption band is attributed to the first excited state S_1. However, the structure of S_1 is much more complex, which requires a careful analysis. The visible absorption band is basically constituted of electronic transitions from different MOs (HOMO, HOMO-1, HOMO-2, HOMO-3, HOMO-4 etc… down to even HOMO-10) to LUMO (Table III.11). Again, the description of the excited state strongly depends on the conformer. In most cases a more or less pronounced bathochromic shift is observed. However, a hypsochromic shift is observed in one conformer (Table III.11).

The [CP1: catechin-(4→8)-oenin] complex perfectly exemplifies the optical behaviour of these complexes. In this case, the bathochromic shift is observed with conformers **1** and **3** whereas a hypsochromic shift is obtained with conformer **2** (ΔE_{max} = -0.13, 0.05 and -0.07 eV for conformers **1**, **2** and **3**, respectively, see Table III.11). The bathochromic shift is mainly attributed to the contribution of a CT excited state (see Fig. III.13), which occurs from the A, C and D-rings of the copigment to the E-ring of the pigment, for both conformers **1** and **3**. The CT allows a global stabilization of S_1, inducing a lower energy for the $S_0 \rightarrow S_1$ transition and a higher absorption wavelength (Table III.11). For the conformer **2**, no CT is observed in S_1, in agreement with the absence of bathochromic shift. Concomitantly to the decrease in CT, the classical contribution to the transition may increase, thus increasing oscillator strengths (f = 0.30 for conformer **2**).

Table III.10. Maximum vertical excitation energies (E_{max}, eV), absorption wavelengths (λ_{max}, nm), oscillator strengths (f), MO descriptions, excitation energy shifts (ΔE_{max}, eV) and absorption wavelength shifts ($\Delta\lambda_{max}$, nm) of the different complexes. The energy and wavelength shifts are calculated with respect to stand-alone pigment.

Compound		E_{max}	λ_{max}	f	MO description	ΔE_{max}	$\Delta\lambda_{max}$
Pigment	Conformer	2.87	432.6	0.46	H-2→L (59%)	-	-
[CP1:cat-oenin]	**1**	2.74	453.3	0.25	H-2→L (47%) H→L (30%)	-0.13	20.6
	2	2.91	425.7	0.3	H→L (39%)	0.05	-6.9
	3	2.8	443.5	0.25	H-1→L (47%)	-0.07	10.8
[CP2:cat-oenin]	**1**	2.64	470	0.1	H-4→L (65%)	-0.23	37.4
	2	2.72	455.3	0.19	H-4→L (44%) H-3→L (38%)	-0.14	22.6
	3	2.76	449.3	0.35	H-10→L (42%)	-0.11	16.6
[CP3:cat-oenin]	**1**	2.63	470.7	0.09	H→L (45%)	-0.23	38.1
	2	2.67	463.6	0.2	H-2→L (45%)	-0.19	31
	3	2.78	445.4	0.19	H-2→L (60%)	-0.08	12.8
	4	2.62	473	0.31	H-2→L (51%)	-0.24	40.3

The bathochromic shift in copigmentation complexes appears as a subtle effect, which is strongly influenced by the conformations and orientations of both pigment and copigment. At the quantum level, the sampling is not sufficient[39] to exactly reproduce the experimental UV/Vis spectra. However, quantum calculations allow providing an accurate MO description of the visible absorption band. From the quantum calculations we can firmly conclude that the broadening of the experimental visible absorption band is not only attributed to solvent effects, as usually, but also comes from the presence of different conformers with different optical properties.

---

[39] Quantum calculations are not able to reproduce experimental values because i) calculations have been carried out *in vacuo* without taking solvent effects into account, ii) the MD approach used to generate the starting geometries for QM calculations is not sufficient to allow the complete exploration of the potential energy surface (PES).
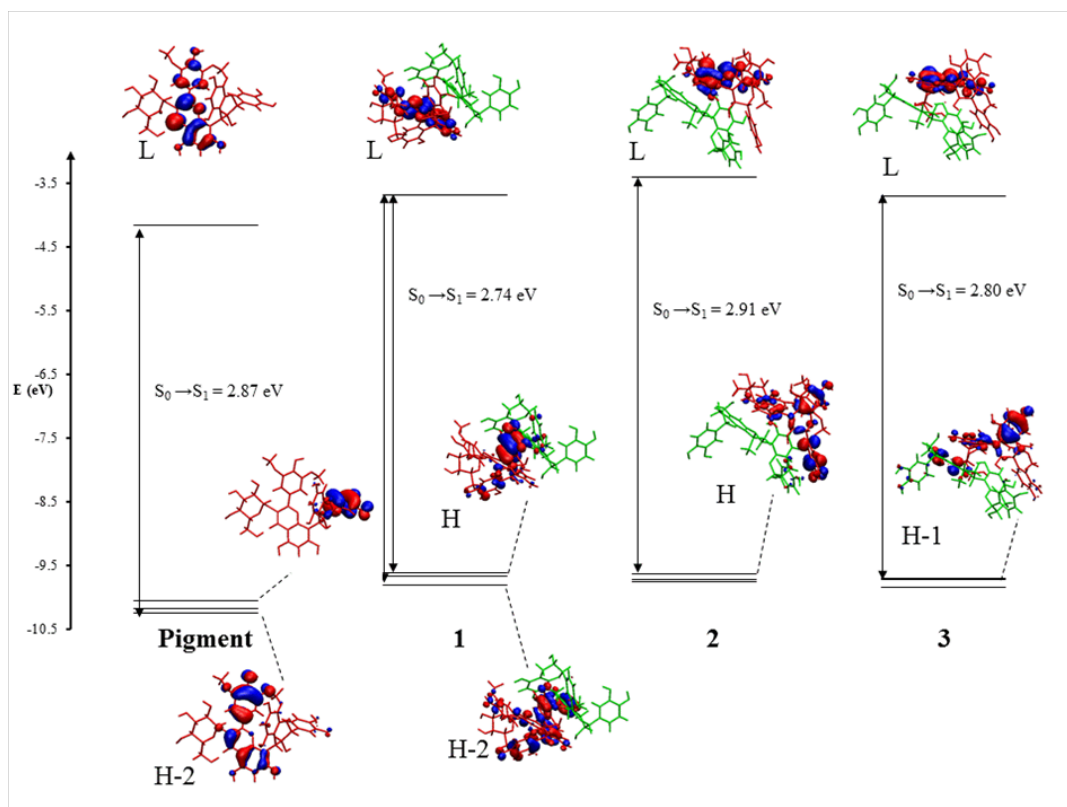
Figure III.13. MO correlation diagram of pigment and conformers **1**, **2** and **3** of the [CP1: catechin-(4→8)-oenin] copigmentation complex.

3.4. Rationalization of the new bands in the 400-500 nm range

The new bands observed for [CP1:catechin-(4→8)-oenin] and [CP3:catechin-(4→8)-oenin] are mainly attributed excited states S_2 and/or S_3. Again, these excited states are complex *i.e.*, constituted of different electronic transitions from different MOs (from H-1 to H-11) but always to the LUMO. However, even if the description of S_2 and S_3 is complex, most of the electronic transitions involved in these two excited states exhibit a contribution of intramolecular CT within in the pigment. Such CT mainly occurs from the C and A-rings of the catechin moiety to the malvidin moiety (as seen in Fig. III.14 for *e.g.*, conformer **3** of [CP1:catechin-(4→8)-oenin]).
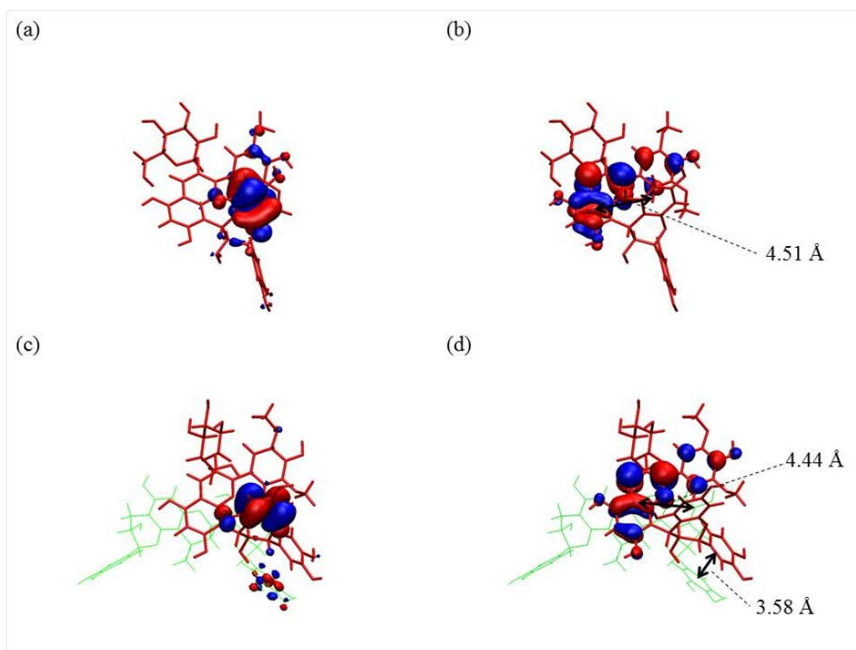
Figure III.14. Spatial distribution of the MOs involved in the transition corresponding to the band ranging between 400 and 500 nm a) HOMO-3 and (b) LUMO of the pigment catechin-(4→8)-oenin in the absence of copigment and c) HOMO-4 and d) LUMO of conformer 3 of [CP1:catechin-(4→8)-oenin]. The pigment is in red while the copigment is in green. Here we can see that HOMO-3(4) and LUMO are on two separated moieties, so the corresponding transition requires CT.

This intramolecular CT is definitely characteristic of the new band in the 400-500 nm range, which actually exists in the free pigment itself but only with a very low oscillator strength. In the copigmentation complexes, this band can be amplified due to conformational changes in the pigment brought about by the copigment (Fig. III.14). This enhancement of CT within the pigment depends on the conformer and complex. In the case of [CP2:catechin-(4→8)-oenin], this effect is weak for most conformers while it is more important for [CP3:catechin-(4→8)-oenin] (Fig. III.15) in very good agreement with the experimental data: for CP3, a double band arises around 440 nm, and for CP2 a single band arises at 450 nm amplifies the shoulder of the anthocyanic spectra at this wavelength.
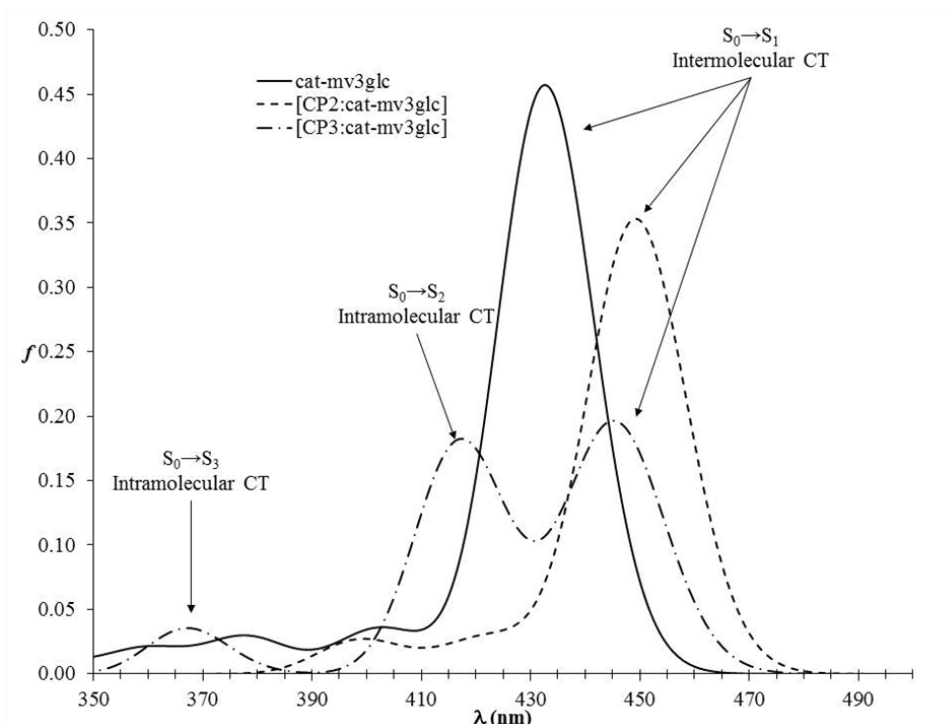
Figure III.15. Theoretical UV/Vis absorption spectra of catechin-(4→8)-oenin and both complexes [CP1:catechin-(4→8)-oenin] and [CP2:catechin-(4→8)-oenin]. The former complex exhibits the enhancing of the second and third absorption bands, corresponding to the S2 and S3 excited states. These bands are lower (almost hidden) for the pigment itself and the latter complex. Note that the absorption wavelengths are shifted compared to the experimental spectra.

4. Conclusion

This work has shown that the flavan-3-ol substituent of catechin-(4,8)-oenin weakens the affinity of the pigment for vinylcatechin dimers and procyanidins because of steric constrains. In these copigmentation complexes, the driving force is a combination of π-stacking interactions and H-bonding. The theoretical investigation of the copigmentation complexes by a combination of molecular dynamics and DFT approaches has allowed valuable spatial representations of the complexes and a deep insight in the description of their absorption properties in the visible range. The shift in the pigment's visible band brought about by the copigment appears strongly dependent on the copigment's structure and orientations of the two partners within the complex. Although bathochromism is usually observed, this effect can be cancelled out by averaging over all the stable geometries. The quantum calculations have also succeeded in interpreting absorption bands in the 400 - 500 nm range, which are attributed to intramolecular CT within the pigment.

Bibliography

[1]   Anouar, E.H.*, et al.*, *UV/Visible spectra of natural polyphenols: A time-dependent density functional theory study.* Food Chemistry, 2012. **131**: p. 79-89.

[2]   Zhang, H., *p53 plays a central role in UVA and UVB induced cell damage and apoptosis in melanoma cells.* Cancer Letters, 2006. **244**: p. 229-238.

[3]   Gonzalez, S., M. Fernandez-Lorente, and Y. Gilaberte-Calzada, *The latest on skin photoprotection.* Clinics in Dermatology, 2008. **26**: p. 614-626.

[4]   Gauslaa, Y. and M. McEvoy, *Seasonal changes in solar radiation drive acclimatation of the sun-screening compound parietin in the lichen Xanthoria parietina.* Basic and Applied Ecology, 2005. **6**: p. 75-82.

[5]   Lawrey, J.D., *Biological Role of Lichen Substances.* The Bryologist, 1986. **89**: p. 111-122.

[6]   Legaz, M.E.*, et al.*, *Pigment Analysis of Sun and Shade Populations of Cladonia Verticillaris.* Biochemical Systematics and Ecology, 1986. **14**: p. 575-582.

[7]   Solhaug, K.G., Y. Nybakken, L. Biger, W., *UV-induction of sun-screening pigments in lichens.* New Phytologist, 2003. **158**: p. 91-100.

[8]   Rancan, F.R., S. Boehm, K. Fernandez, E. Hidalgo, E. Quihot, W. Boehm, F. Piazena, H. Oltmanns, U., *Protection against UVB irradiation by natural filters extracted from lichens.* Journal of Photochemistry and Photobiology, 2002. **68**: p. 133-139.

[9]   Hidalgo, M.E.*, et al.*, *Photophysical, photochemical, and thermodynamic properties of shikimic acid derivatives: calycin and rhizocarpic acid (lichens).* Journal of Photochemistry and Photobiology, B, 2002. **66**: p. 213-217.

[10]   Roullier, C.*, et al.*, *Characterization and identification of mycosporines-like compounds in cyanolichens. Isolation of mycosporine hydroxyglutamicol from Nephroma laevigatum Ach.* Phytochemistry, 2011. **72**: p. 1348-1357.

[11]   Millot, M.*, et al.*, *Cytotoxic constituents of the lichen Diploicia canescens.* Journal of Natural Products, 2009. **72**: p. 2177-2180.

[12]   Springsteen, A.*, et al.*, *In vitro evaluation of subn protection factor of sunscreens by diffuse transmittance.* Analytica Chimica Acta, 1999. **380**: p. 155-164.

[13]   Runge, E. and E.K.U. Gross, *Density-Functional Theory for Time-Dependent Systems.* Physical Review Letters, 1984. **52**: p. 997-1000.

[14]   Ipatov, A.*, et al.*, *Excited-state spin-contamination in time-dependent density-functional theory for molecules with open-shell ground states.* Journal of Molecular Structure: THEOCHEM, 2009. **914**: p. 60-73.

[15]   Perpète, E.A.*, et al.*, *Toward a Theorical Quantitative Estimation of the λ_{max} of Anthraquinones-Baased Dyes.* Journal of Chemical Theory and Computation, 2006. **2**: p. 434-440.

[16]   Medina, B.M., *et al.*, *Effect of fluorination on the electronic structure and optical excitations of pi-conjugated molecules.* Journal of Chemical Physics, 2007. **126**: p. 111101-111106.

[17]   Becke, A.D., *Density-functional exchange-energy approximation with correct asymptotic behavior.* Physical Review A, 1988. **38**: p. 3098-3100.

[18]   Becke, A.D., *A new mixing of Hartree-Fock and local-density-functional theories.* Journal of Chemical Physics, 1993. **98**: p. 1372-1377.

[19]   Becke, A.D., *Density-functional thermochemistry. III. The role of exact exchange.* Journal of Chemical Physics, 1993. **98**: p. 5648-5652.

[20]   Perdew, J.P., *Density-functional approximation for the correlation energy of the inhomogeneous electron gas.* Physical Review B, 1986. **33**: p. 8822.

[21]   Perdew, J.P., K. Burke, and M. Ernzerhof, *Generalized gradient approximation made simple.* Physical Review Letters, 1996. **77**: p. 3865-3868.

[22]   Tomasi, J., B. Mennucci, and R. Cammi, *Quantum Mechanical Continuum Solvation Models.* Chemical Reviews, 2005. **105**: p. 2999-3093.

[23]   Amovilli, C., *et al.*, *Recent Advances in the Description of Solvent Effects with the Polarizable Continuum Model*, in *Advances in Quantum Chemistry*, L. Per-Olov, Editor 1998, Academic Press. p. 227-261.

[24]   Frisch, M.J., *et al.*, *Gaussian 09, Revision A.02*, 2009: Wallingford CT.

[25]   Aspée, A., C. Aliaga, and J.C. Scaiano, *Transient enol isomers of dibenzoylmethane and avobenzone as efficient hydrogen donors toward a nitroxide pre-fluorescent probe.* Photochemistry and Photobiology, 2007. **83**: p. 481-485.

[26]   Choquenet, B., *et al.*, *Quercetin and Rutin as Potential Sunscreen Agents: Determination of Efficacy by an in Vitro Method.* Journal of Natural Products, 2008. **71**: p. 1117-1118.

[27]   Hayden, C.G.J., *et al.*, *Sunscreen penetration of human skin and related keratinocyte toxicity after topical apllication.* Skin Pharmacology and Physiology, 2005. **18**: p. 170-174.

[28]   Hertog, M.G., *et al.*, *Dietary antioxidant flavonoids and risk of coronary heart disease: the Zutphen Elderly Study.* Lancet, 1993. **342**: p. 1007-1011.

[29]   Commenges, D., *et al.*, *Intake of flavonoids and risk of dementia.* European Journal of Epidemiology, 2000. **16**: p. 357-363.

[30]   Saller, R., R. Meier, and R. Brignoli, *The use of silymarin in the treatment of liver diseases.* Drugs, 2001. **61**: p. 2035-2063.

[31]   Gazak, R., *et al.*, *Large-scale separation of silybin diastereoisomers using lipases.* Process Biochemistry, 2010. **45**: p. 1657-1663.

[32]   Rice-Evans, C.A., L. Packer, and Editors, *Flavonoids in Health and Disease.*1998, New York: Dekker. 541 pp.

[33]   Ballester, A.-R.*, et al.*, *Biochemical and molecular analysis of pink tomatoes: deregulated expression of the gene encoding transcription factor S1MYB12 leads to pink tomato fruit color.* Plant Physiology, 2010. **152**: p. 71-84.

[34]   Yoshida, K., M. Mori, and T. Kondo, *Blue flower color development by anthocyanins: from chemical structure to cell physiology.* Natural Product Reports, 2009. **26**: p. 884-915.

[35]   Quartarolo, A.D. and N. Russo, *A Computational Study (TDDFT and RICC2) of the Electronic Spectra of Pyranoanthocyanins in the Gas Phase and Solution.* Journal of Chemical Theory and Computation, 2011. **7**: p. 1073-1081.

[36]   Harbone, J.B., *Comparative Biochemistry of the Flavonoids.* Academic Press, London and New York, 1967.

[37]   Markakis, P. and Editor, *Anthocyanins as Food Colors*1982: Academic Press. 263 pp.

[38]   Timberlake, C.F. and P. Bridle, *Flavylium salts, anthocyanidins and anthocyanins. I.— Structural transformations in acid solutions.* Journal of the Science of Food and Agriculture, 1967. **18**: p. 473-478.

[39]   Brouillard, R. and O. Dangles, *Anthocyanin molecular interactions: the first step in the formation of new pigments during wine aging?* Food Chemistry, 1994. **51**: p. 365-371.

[40]   Bayer, E.*, et al.*, *Complex Formation and Flower Colors.* Angewandte Chemie International Edition, 1966. **5**: p. 791-798.

[41]   Raymond, B., *The in vivo expression of anthocyanin colour in plants.* Phytochemistry, 1983. **22**: p. 1311-1323.

[42]   Boulton, R., *The Copigmentation of Anthocyanins and Its Role in the Color of Red Wine: A Critical Review.* American Journal of Enology and Viticulture, 2001. **52**: p. 67-87.

[43]   Rustioni, L.*, et al.*, *Copigmentation and anti-copigmentation in grape extracts studied by spectrophotometry and post-column-reaction HPLC.* Food Chemistry, 2012. **132**: p. 2194-2201.

[44]   Stephen J, B., *Novel pigments and copigmentation in the blue marguerite daisy.* Phytochemistry, 1999. **50**: p. 1395-1399.

[45]   Brouillard, R., ed. *Anthocyanins as Food Colors.* 1982

[46]   Dimitric, M.J.M., J.M. Baranac, and T.P. Brdaric, *Electronic and infrared vibrational analysis of cyanidin-quercetin copigment complex.* Spectrochimica Acta A, 2005. **62A**: p. 673-680.

[47]   Hunter, C.A. and J.K.M. Sanders, *The nature of .pi.-.pi. interactions.* Journal of the American Chemical Society, 1990. **112**: p. 5525-5534.

[48]   Velu, S.S.*, et al.*, *Regio- and Stereoselective Biomimetic Synthesis of Oligostilbenoid Dimers from Resveratrol Analogues: Influence of the Solvent, Oxidant, and Substitution.* Chemistry – A European Journal, 2008. **14**: p. 11376-11384.

[49]   Rezazgui, O.*, et al.*, *One-pot and catalyst-free amidation of ester: a matter of non-bonding interactions.* Tetrahedron Letters, 2011. **52**: p. 6796-6799.

[50]   Aragó, J.*, et al.*, *Ab Initio Modeling of Donor–Acceptor Interactions and Charge-Transfer Excitations in Molecular Complexes: The Case of Terthiophene–Tetracyanoquinodimethane.* Journal of Chemical Theory and Computation, 2011. **7**: p. 2068-2077.

[51]   Gierschner, J., J. Cornil, and H.-J. Egelhaaf, *Optical bandgaps of π-conjugated organic materials at the polymer limit: experiment and theory.* Advanced Materials, 2007. **19**: p. 173-191.

[52]   Zondlo, N.J., *Non-covalent interactions: Fold globally, bond locally.* Nature Chemical Biology, 2010. **6**: p. 567-568.

[53]   Malien-Aubert, C., O. Dangles, and M.J. Amiot, *Color Stability of Commercial Anthocyanin-Based Extracts in Relation to the Phenolic Composition. Protective Effects by Intra- and Intermolecular Copigmentation.* Journal of Agricultural and Food Chemistry, 2000. **49**: p. 170-176.

[54]   Alluis, B.*, et al.*, *Water-soluble flavonol (= 3-hydroxy-2-phenyl-4H-1-benzopyran-4-one) derivatives: chemical synthesis, coloring, and antioxidant properties.* Helvetica Chimica Acta, 2000. **83**: p. 428-443.

[55]   Ferreira, d.S.P.*, et al.*, *Charge-Transfer Complexation as a General Phenomenon in the Copigmentation of Anthocyanins.* Journal of Physical Chemistry A, 2005. **109**: p. 7329-7338.

[56]   Alluis, B. and O. Dangles, *Quercetin (=2-(3,4-dihydroxyphenyl)-3,5,7-trihydroxy-4H-1-benzopyran-4-one) glycosides and sulfates: chemical synthesis, complexation, and antioxidant properties.* Helvetica Chimica Acta, 2001. **84**: p. 1133-1156.

[57]   Baranac, J.M., N.A. Petranovic, and J.M. Dimitric-Markovic, *Spectrophotometric study of anthocyanes copigmentation reactions.* Journal of Agricultural and Food Chemistry, 1996. **44**: p. 1333-1336.

[58]   Brouillard, R. and O. Dangles. *Flavonoids and flower color.* 1994. Chapman and Hall.

[59]   Riley, K.E.*, et al.*, *Stabilization and Structure Calculations for Noncovalent Interactions in Extended Molecular Systems Based on Wave Function and Density Functional Theories.* Chemical Reviews, 2010. **110**: p. 5023-5063.

[60]   Trouillas, P.*, et al.*, *A theoretical study of the conformational behavior and electronic structure of taxifolin correlated with the free radical-scavenging activity.* Food Chemistry, 2004. **88**: p. 571-582.

[61]   Anouar, E.*, et al.*, *New aspects of the antioxidant properties of phenolic acids: a combined theoretical and experimental approach.* Physical Chemistry Chemical Physics, 2009. **11**: p. 7659-7668.

[62]   Grimme, S., *Density functional theory with London dispersion corrections.* Wiley Interdisciplinary Reviews: Computational Molecular Science, 2011. **1**: p. 211-228.

[63]   Janesko, B.G., T.M. Henderson, and G.E. Scuseria, *Screened hybrid density functionals for solid-state chemistry and physics.* Physical Chemistry Chemical Physics, 2009. **11**: p. 443-454.

[64]   Vydrov, O.A. and T.V. Voorhis, *Nonlocal van der Waals density functional: The simpler the better.* Journal of Chemical Physics, 2010. **133**: p. 244103.

[65]   Zhao, Y. and D. Truhlar, *The M06 suite of density functionals for main group thermochemistry, thermochemical kinetics, noncovalent interactions, excited states, and transition elements: two new functionals and systematic testing of four M06-class functionals and 12 other functionals.* Theoretical Chemistry Accounts: Theory, Computation, and Modeling (Theoretica Chimica Acta), 2008. **120**: p. 215-241.

[66]   Grimme, S., *Accurate description of van der Waals complexes by density functional theory including empirical corrections.* Journal of Computational Chemistry, 2004. **25**: p. 1463-1473.

[67]   Grimme, S., *Semiempirical GGA-type density functional constructed with a long-range dispersion correction.* Journal of Computational Chemistry, 2006. **27**: p. 1787-1799.

[68]   Grimme, S.*, et al.*, *A consistent and accurate ab initio parametrization of density functional dispersion correction (DFT-D) for the 94 elements H-Pu.* Journal of Chemical Physics, 2010. **132**.

[69]   Trouillas, P.*, et al.*, *A DFT study of the reactivity of OH groups in quercetin and taxifolin antioxidants: The specificity of the 3-OH site.* Food Chemistry, 2006. **97**: p. 679-688.

[70]   Yanai, T., D.P. Tew, and N.C. Handy, *A new hybrid exchange–correlation functional using the Coulomb-attenuating method (CAM-B3LYP).* Chemical Physics Letters, 2004. **393**: p. 51-57.

[71]   Chai, J.-D. and M. Head-Gordon, *Systematic optimization of long-range corrected hybrid density functionals.* Journal of Chemical Physics, 2008. **128**: p. 084106.

[72]   Jacquemin, D.*, et al.*, *Assessment of the ωB97 family for excited-state calculations.* Theoretical Chemistry Accounts: Theory, Computation, and Modeling (Theoretica Chimica Acta), 2011. **128**: p. 127-136.

[73]   Chai, J.-D. and M. Head-Gordon, *Long-range corrected hybrid density functionals with damped atom-atom dispersion corrections.* Physical Chemistry Chemical Physics, 2008. **10**: p. 6615-6620.

[74]   Neese, F., *The ORCA program system.* Wiley Interdisciplinary Reviews: Computational Molecular Science, 2012. **2**: p. 73-78.

[75]   Neese, F.*, et al.*, *Efficient, approximate and parallel Hartree-Fock and hybrid DFT calculations. A 'chain-of-spheres' algorithm for the Hartree-Fock exchange.* Chemical Physics, 2009. **356**: p. 98-109.

[76]   Singh, U.C. and P.A. Kollman, *An approach to computing electrostatic charges for molecules.* Journal of Computational Chemistry, 1984. **5**: p. 129-145.

[77]   Besler, B.H., K.M. Merz, Jr., and P.A. Kollman, *Atomic charges derived from semiempirical methods.* Journal of Computational Chemistry, 1990. **11**: p. 431-439.

[78]   Breneman, C.M. and K.B. Wiberg, *Determining atom-centered monopoles from molecular electrostatic potentials. The need for high sampling density in formamide conformational analysis.* Journal of Computational Chemistry, 1990. **11**: p. 361-373.

[79] Chirlian, L.E. and M.M. Francl, *Atomic charges derived from electrostatic potentials: a detailed study.* Journal of Computational Chemistry, 1987. **8**: p. 894-905.

[80] Sinnecker, S.*, et al.*, *Calculation of Solvent Shifts on Electronic g-Tensors with the Conductor-Like Screening Model (COSMO) and Its Self-Consistent Generalization to Real Solvents (Direct COSMO-RS).* Journal of Physical Chemistry A, 2006. **110**: p. 2235-2245.

[81] Cossi, M.*, et al.*, *New developments in the polarizable continuum model for quantum mechanical and classical calculations on molecules in solution.* Journal of Chemical Physics, 2002. **117**: p. 43-54.

[82] Improta, R.*, et al.*, *A state-specific polarizable continuum model time dependent density functional theory method for excited state calculations in solution.* Journal of Chemical Physics, 2006. **125**: p. 054103.

[83] Jurecka, P.*, et al.*, *Benchmark database of accurate (MP2 and CCSD(T) complete basis set limit) interaction energies of small model complexes, DNA base pairs, and amino acid pairs.* Physical Chemistry Chemical Physics, 2006. **8**: p. 1985-1993.

[84] Gráfová, L.*, et al.*, *Comparative Study of Selected Wave Function and Density Functional Methods for Noncovalent Interaction Energy Calculations Using the Extended S22 Data Set.* Journal of Chemical Theory and Computation, 2010. **6**: p. 2365-2376.

[85] Grimme, S., *Improved second-order M[o-slash]ller--Plesset perturbation theory by separate scaling of parallel- and antiparallel-spin pair correlation energies.* Journal of Chemical Physics, 2003. **118**: p. 9095-9102.

[86] Antony, J. and S. Grimme, *Is Spin-Component Scaled Second-Order Møller−Plesset Perturbation Theory an Appropriate Method for the Study of Noncovalent Interactions in Molecules?* Journal of Physical Chemistry A, 2007. **111**: p. 4862-4868.

[87] Jacquemin, D., *et al.*, *What is the "best" atomic charge model to describe through-space charge-transfer excitations?* Physical Chemistry Chemical Physics, 2012. **14**: p. 5383-5388.

[88] Grimme, S., *Do Special Noncovalent π–π Stacking Interactions Really Exist?* Angewandte Chemie International Edition, 2008. **47**: p. 3430-3434.

[89] Grimme, S. and J.-P. Djukic, *Cation−Cation "Attraction": When London Dispersion Attraction Wins over Coulomb Repulsion.* Inorganic Chemistry, 2011. **50**: p. 2619-2628.

[90] Brouillard, R.*, et al.*, *The copigmentation reaction of anthocyanins - a microprobe for the structural study of aqueous-solutions.* Journal of the American Chemical Society, 1989. **111**: p. 2604-2610.

[91] Gonzalez-Manzano, S.*, et al.*, *Influence of the degree of polymerization in the ability of catechins to act as anthocyanin copigments.* European Food Research and Technology, 2008. **227**: p. 83-92.

[92] Dangles, O. and R. Brouillard, *Polyphenol interactions. The copigmentation case: thermodynamic data from temperature variation and relaxation kinetics. Medium effect.* Canadian Journal of Chemistry, 1992. **70**: p. 2174-2189.

[93]   Salas, E.*, et al.*, *Reactions of anthocyanins and tannins in model solutions.* Journal of Agricultural and Food Chemistry, 2003. **51**: p. 7951-7961.

[94]   Salas, E.*, et al.*, *Demonstration of the occurrence of flavanol-anthocyanin adducts in wine and in model solutions.* Analytica Chimica Acta, 2004. **513**: p. 325-332.

[95]   Vivar-Quintana, A.M.*, et al.*, *Formation of anthocyanin-derived pigments in experimental red wines.* Food Science and Technology International, 1999. **5**: p. 347-352.

[96]   Fossen, T., S. Rayyan, and O.M. Andersen, *Dimeric anthocyanins from strawberry (Fragaria ananassa) consisting of pelargonidin 3-glucoside covalently linked to four flavan-3-ols.* Phytochemistry, 2004. **65**: p. 1421-1428.

[97]   Gonzalez-Paramas, A.M.*, et al.*, *Flavanol-anthocyanin condensed pigments in plant extracts.* Food Chemistry, 2006. **94**: p. 428-436.

[98]   Gonzalez-Manzano, S.*, et al.*, *Flavanol-anthocyanin pigments in corn: NMR characterisation and presence in different purple corn varieties.* Journal of Food Composition and Analysis, 2008. **21**: p. 521-526.

[99]   Williamson, G. and C. Santos-Buelga, eds. *Methods in polyphenol analysis.* 2003, Royal Society of Chemistry: Cambridge.

[100]   Salas, E.*, et al.*, *Structure determination and colour properties of a new directly linked flavanol-anthocyanin dimer.* Tetrahedron Letters, 2004. **45**: p. 8725-8729.

[101]   Nave, F.*, et al.*, *Thermodynamic and kinetic properties of a red wine pigment: catechin-(4,8)-malvidin-3-O-glucoside.* Journal of Physical Chemistry B, 2010. **114**: p. 13487 - 13496.

[102]   Galland, S.*, et al.*, *Chemical synthesis of hydroxycinnamic acid glucosides and evaluation of their ability to stabilize natural Colors via anthocyanin copigmentation.* Journal of Agricultural and Food Chemistry, 2007. **55**: p. 7573-7579.

[103]   Cruz, L.*, et al.*, *Vinylcatechin Dimers Are Much Better Copigments for Anthocyanins than Catechin Dimer Procyanidin B3.* Journal of Agricultural and Food Chemistry, 2010. **58**: p. 3159-3166.

[104]   Gonzalez-Manzano, S.*, et al.*, *Studies on the copigmentation between anthocyanins and flavan-3-ols and their influence in the colour expression of red wine.* Food Chemistry, 2009. **114**: p. 649-656.

[105]   Cruz, L.*, et al.*, *Synthesis and Structural Characterization of Two Diasteroisomers of Vinylcatechin Dimers.* Journal of Agricultural and Food Chemistry, 2009. **57**: p. 10341-10348.

[106]   Gaussian 09, R.A., Frisch, M. J.; Trucks, G. W.; Schlegel, H. B.; Scuseria, G. E.; Robb, M. A.; Cheeseman, J. R.; Scalmani, G.; Barone, V.; Mennucci, B.; Petersson, G. A.; Nakatsuji, H.; Caricato, M.; Li, X.; Hratchian, H. P.; Izmaylov, A. F.; Bloino, J.; Zheng, G.; Sonnenberg, J. L.; Hada, M.; Ehara, M.; Toyota, K.; Fukuda, R.; Hasegawa, J.; Ishida, M.; Nakajima, T.; Honda, Y.; Kitao, O.; Nakai, H.; Vreven, T.; Montgomery, Jr., J. A.; Peralta, J. E.; Ogliaro, F.; Bearpark, M.; Heyd, J. J.; Brothers, E.; Kudin, K. N.; Staroverov, V. N.; Kobayashi, R.; Normand, J.; Raghavachari, K.; Rendell, A.; Burant, J. C.; Iyengar, S. S.; Tomasi, J.; Cossi, M.; Rega, N.; Millam, N. J.; Klene, M.; Knox, J. E.; Cross, J. B.; Bakken, V.; Adamo, C.; Jaramillo,

J.; Gomperts, R.; Stratmann, R. E.; Yazyev, O.; Austin, A. J.; Cammi, R.; Pomelli, C.; Ochterski, J. W.; Martin, R. L.; Morokuma, K.; Zakrzewski, V. G.; Voth, G. A.; Salvador, P.; Dannenberg, J. J.; Dapprich, S.; Daniels, A. D.; Farkas, Ö.; Foresman, J. B.; Ortiz, J. V.; Cioslowski, J.; Fox, D. J. Gaussian, Inc., Wallingford CT, 2009.

[107]   Bayly, C.I.*, et al.*, *A Well-Behaved Electrostatic Potential Based Method Using Charge Restraints for Deriving Atomic Charges - the Resp Model.* Journal of Physical Chemistry, 1993. **97**: p. 10269-10280.

[108]   Izaguirre, J.A.*, et al.*, *Langevin stabilization of molecular dynamics.* Journal of Chemical Physics, 2001. **114**: p. 2090-2098.

[109]   Loncharich, R.J., B.R. Brooks, and R.W. Pastor, *Langevin Dynamics of Peptides - the Frictional Dependence of Isomerization Rates of N-Acetylalanyl-N'-Methylamide.* Biopolymers, 1992. **32**: p. 523-535.

[110]   Case, D.A., Darden, T. A., Cheatham, III T. E., Simmerling, C. L., Wang, J., Duke, R. E., Luo, R., Crowley, M., Ross C. Walker, Zhang, W., Merz, K.M., Wang, B., Hayik, S., Roitberg, A., Seabra, G., Kolossváry, I., Wong, K.F., Paesani, F., Vanicek, J., Wu, X., Brozell, S.R., Steinbrecher, T., Gohlke, H., Yang, L., Tan, C., Mongan, J., Hornak, V., Cui, G., Mathews, D.H., Seetin, M.G., Sagui, C., Babin, V. and Kollman P.A., *AMBER 10, University of California, San Francisco*, 2008.

[111]   Cornell, W.D.*, et al.*, *A 2nd Generation Force-Field for the Simulation of Proteins, Nucleic-Acids, and Organic-Molecules.* Journal of the American Chemical Society, 1995. **117**: p. 5179-5197.

[112]   Ryckaert, J.P., G. Ciccotti, and H.J.C. Berendsen, *Numerical-Integration of Cartesian Equations of Motion of a System with Constraints - Molecular-Dynamics of N-Alkanes.* Journal of Computational Physics, 1977. **23**: p. 327-341.

[113]   Brouillard, R. and B. Delaporte, *Chemistry of anthocyanin pigments .2. Kinetic and thermodynamic study of proton-transfer, hydration, and tautomeric reactions of malvidin-3-glucoside.* Journal of the American Chemical Society, 1977. **99**: p. 8461-8468.

[114]   Malien-Aubert, C., O. Dangles, and M.J. Amiot, *Influence of procyanidins on the color stability of oenin solutions.* Journal of Agricultural and Food Chemistry, 2002. **50**: p. 3299-3305.

[115]   Markovic, J.M.D., N.A. Petranovic, and J.M. Baranac, *A spectrophotometric study of the copigmentation of malvin with caffeic and ferulic acids.* Journal of Agricultural and Food Chemistry, 2000. **48**: p. 5530-5536.

[116]   Kristyan, S. and P. Pulay, *Can (semi)local density-functional theory account for the london dispersion forces?* Chemical Physics Letters, 1994. **229**: p. 175-180.

[117]   Hobza, P., J. šponer, and T. Reschel, *Density functional theory and molecular clusters.* Journal of Computational Chemistry, 1995. **16**: p. 1315-1325.

[118]   Allen, M.J. and D.J. Tozer, *Helium dimer dispersion forces and correlation potentials in density functional theory.* Journal of Chemical Physics, 2002. **117**: p. 11113-11120.

[119]   Chai, J.D. and M. Head-Gordon, *Systematic optimization of long-range corrected hybrid density functionals.* Journal of Chemical Physics, 2008. **128**.

Chapter IV. Oxidative processes in polyphenols: from antioxidant to pro-oxidant effects

Introduction

Over the past decade, the free radical scavenging properties of polyphenols has been fully described from the thermodynamic point of view. Physico-chemical descriptors (*e.g.*, geometry, BDE, IP, electronic distributions) have been assessed allowing the establishment of robust thermodynamic structure-activity-relationships. However, the kinetics of free radical scavenging is still under debate for a full understanding. From the experimental point of view, the discrimination between the different mechanisms is a challenging task *e.g.*, between SPLET and PCET. Only indirect proofs can be obtained. From the theoretical point of view, the theoretical methodologies are still under development to fully and accurately calculate free radical scavenging rate constants.

Another important issue is the consequence of free radical scavenging by polyphenols. As shown in Chapter I, whatever the mechanism of action, phenoxyl radicals are formed. These radicals cannot be considered without substantial effects. They are reactive and by this way can undergo further reactions to produce new compounds, which can be anti- or pro-oxidants. For example, Kosinova *et al.* theoretically studied the dimerization process of quercetin under oxidative stress. Chemists also use this natural oxidative coupling as a source of new polyphenols with potent biological activities.[1]

The present chapter is divided as follows:

Section A is the theoretical evaluation of rate constants of free radical scavenging.[40] The three main mechanisms (CPET, ET-PT and SPLET) are studied by using the transition state and Marcus' theories.

Section B aims at rationalizing the post-oxidative processes producing stilbene oligomers.[41] It was observed that the pterostilben oligomerization is a regio- and stereo-selective process.[2] DFT calculations provide an elegant rationalization of this regio- and stereo-selectivity, within an electronic picture.

---

[40] This section has been recently submitted.

[41] This section has been recently submitted.

Section A. Free radical scavenging by natural polyphenols: Atom versus electron transfer

1. Introduction

Oxidative stress is ubiquitous in the human organism where it can induce various diseases *e.g.*, atherosclerosis,[3] inflammation,[4] Alzheimer disease,[5] lung diseases,[6] liver diseases[7, 8] and cancer.[9] It results from an imbalance between the production of reactive oxygen species (ROS), mainly free radicals, and protective effects (inhibition of free radical production, direct free radical scavenging or detoxification). Free radicals are produced by endogenous (*e.g.*, production of $O_2^{•-}$ which is rapidly transformed into other reactive oxygen species like hydrogen peroxide and $^•OH$ radicals in the presence of metal ions) or exogenous (ionizing radiations, UV light or pollution) processes. Different cascades of events like the oxidation of lipids (LH) in cell membranes produce a huge variety of free radical species including carbon-centered ($R^•$ and $L^•$), alkoxyl ($RO^•$ and $LO^•$) and peroxyl ($ROO^•$ and $LOO^•$) radicals. These free radicals can act on DNA, proteins and lipids, in both polar and non-polar compartments.

Antioxidant molecular systems are endogenous (*e.g.*, catalase and glutathione peroxidase) or provided exogenously (*e.g.*, vitamins and polyphenols largely found in human diets *i.e.*, fruit, vegetables, spices and beverages made from plants such as tea, wine, beer, infusions, fruit juices and food supplements). Polyphenols (ArOH) are divided in various subclasses including phenolic acids, lignans, flavonoids and tannins. The large variety of their chemical structures allows for a wide range of biological (including antioxidant) activities.[10, 11]

Flavonoid derivatives (natural, metabolized or hemisynthetic) are a large subclass of polyphenols. They are powerful free radical scavengers acting by H-atom transfer from their OH groups to the free radicals ($R^•$):

$$ArO\text{-}\mathbf{H} + R^• \longrightarrow ArO^• + R\text{-}\mathbf{H} \qquad (IV.1a)$$

Structure-activity relationships of their antioxidant capacity have been experimentally established over the past years and rationalized on the basis of quantum-chemical studies.[12-25] The calculated thermodynamic descriptors (*e.g.*, O-H bond dissociation enthalpies (BDEs) and π-electron conjugation) fit perfectly with the free radical scavenging activities, particularly

when calculated at the DFT (density functional theory) level using hybrid functionals. Those calculations confirm: i) the important role of the 3-OH group of quercetin derivatives; ii) the important role of the 2,3 double bond and the catechol moiety in the B-ring; iii) the passive role of the 5-OH group, because it is engaged in a strong H-bond with the keto group at C4; iv) the minor direct role of the 7-OH group (see Fig. IV.1 for numbering).[42] and v) the important role of intramolecular H-bonding.[12, 16, 26] These thermodynamic descriptors are now validated to predict the capacity of polyphenols to act as antioxidants *in vitro*.
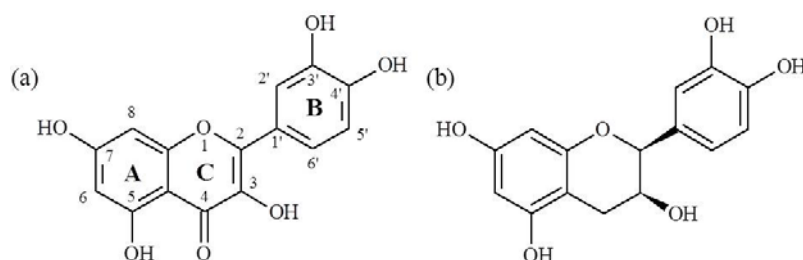
Figure IV.1. Chemical structures of (a) quercetin and (b) (-)-epicatechin

However, the thermodynamic approach is not sufficient to accurately predict free radical scavenging activity in physiological environments. To be fully active, a polyphenol (or its active metabolites) must react by H-atom transfer faster than at least one of the reactions of the free-radical-production cascade (*e.g.*, the limiting propagation step in lipid peroxidation). An accurate description of the kinetics of H-atom transfer between polyphenols and free radicals is crucial to predict biological activities *in vivo*. Kinetic measurements (*e.g.*, pulse radiolysis, laser flash photolysis, styrene oxidation essays) have been performed over the past years for phenol derivatives and many radicals.[24, 25, 27-30] The experimental exploration of antioxidant kinetics is somewhat delicate to be systematically performed for large series of compounds and under various conditions (different solvents and pH). Quantum-chemistry appears as a relevant alternative to evaluate kinetics. Calculated intrinsic BDEs or Gibbs energies of free radical scavenging reactions provide an indirect way to estimate kinetics *e.g.*, phenol substitution influence.[31] The rate constants can also be truly calculated. Nonetheless, to reach accuracy, the *ad equate* theoretical methodology must be carefully chosen. An accurate qualitative description would allow providing a relevant tool to establish structure-activity

---

[42] A detailed analysis of the thermodynamic aspects of the HAT-type reaction between the flavonoid quercetin (Fig. 1a) and ROO• radicals is presented in the Supplementary Information section, available by mail.

relationship in term of kinetics. An accurate quantitative description would allow to perfectly predict antioxidant activity in vivo.

To deal with kinetics of polyphenol free-radical-scavenging, three possible H-atom transfer mechanisms must be considered:

(i) HAT (H-atom transfer) and PCET (proton-coupled electron transfer). HAT is somehow the pure H-atom transfer in which the proton and the electron of the H-atom are transferred to the same atomic orbital of the free radical. PCET is distinguished from the pure HAT as in this case the proton and the electron are transferred PCET is more a concerted mechanism in which the proton transfer occurs to a lone pair of the free radical, while the electron transfer occurs from a lone pair of the antioxidant to the SOMO (singly occupied molecular orbital) of the free radical.[32, 33] This latter mechanism is well-adapted to describe H-atom transfer form polyphenols to free radicals: [28, 29, 34, 35] In both mechanisms, the proton and the electron are transferred in one kinetic step.[43]

$$ArO\text{-}\mathbf{H} + R^{\bullet} \longrightarrow ArO^{\bullet} + R\text{-}\mathbf{H} \qquad (IV.1b)$$

(ii) ET-PT (electron transfer-proton transfer) is a two-step mechanism initiated by an electron transfer (Eq. (IV.2)) and followed by a proton release (Eq. (IV.3)). PT is so fast that ET-PT can be considered as a HAT process:[36, 37]

$$ArOH + R^{\bullet} \longrightarrow ArOH^{+\bullet} + R^{-} \qquad (IV.2)$$

$$ArO\mathbf{H}^{+\bullet} + R^{-} \longrightarrow ArO^{\bullet} + R\text{-}\mathbf{H} \qquad (IV.3)$$

(iii) SPLET (sequential proton loss-electron transfer, Eq. (IV.4-6)) is the reverse mechanism with respect to ET-PT: it is initiated by proton loss (Eq. (IV.4)). The polyphenol anion then undergoes an electron transfer (Eq. (IV.5)). SPLET is favoured when the anion (ArO⁻) is stable enough to allow electron transfer before re-

---

[43] K.M.Mayer recently proposes to use the same terminology (HAT), which makes sense in a global quantum picture.

protonation. This is unambiguously a three-step mechanism which is not strictly considered as HAT:[25, 27, 35, 38]

$$ArO\text{-}\mathbf{H} \longrightarrow ArO^- + \mathbf{H}^+ \qquad (IV.4)$$

$$ArO^- + R^\bullet \longrightarrow ArO^\bullet + R^- \qquad (IV.5)$$

$$R^- + H^+ \longrightarrow R\text{-}\mathbf{H} \qquad (IV.6)$$
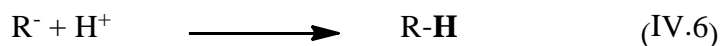
These three mechanisms have the same thermodynamic balance since the reactants and products are the same ($\Delta G^{PCET} = \Delta G^{ET\text{-}PT} = \Delta G^{SPLET}$). The competition between the different mechanisms is governed by the kinetics of the limiting step of each mechanism (atom transfer for PCET and electron transfer for both ET-PT and SPLET).[39]

The present work evaluates the rate constants for the antioxidant quercetin (Fig. IV.1a), a prototypical representative of flavonoids. It is a relevant model to deal with structure antioxidant-activity relationship. Even if it can be toxic (*i.e.*, pro-oxidant at high concentration)[6, 40] and not efficiently absorbed by the organism,[41] quercetin is widely distributed in fruit and vegetables in its glycoside form and possesses most of the chemical characteristics responsible for the free radical scavenging capacity of flavonoid-type compounds. It has extensively been studied over the past decades.

Section 2 describes the DFT-based theoretical methodology we have used; to be *ad equate*, predictive and an efficient complementary tool of experimental data, this methodology had been carefully chosen. Section 3 describes the reaction of each OH group of quercetin with different types of free radicals (*i.e.*, peroxyl (ROO$^\bullet$), hydroxyl ($^\bullet$OH), alkoxyl (RO$^\bullet$) and carbon centered (R$^\bullet$) radicals) produced by oxidative processes (*e.g.*, lipid peroxidation). Flavonoids are known to act poorly as peroxyl free radical scavenger during the propagation phase of lipid peroxidation in membranes or in micelles.[42-45] They appear more efficient to scavenge free radicals during the initiation phase rather than the propagation phase. Thus their capacity to inhibit different sorts of free radicals is of crucial importance to tackle their behaviour directly in living organisms. Our first goal is to provide a qualitative description, establishing structure-activity relationships based on kinetics, complementary to those derived from thermodynamic studies. The second aim is to compare the atom and electron transfer processes; both being

184

presented in Sections 3.1 and 3.2, respectively. This requires a detailed analysis of the electronic properties of the pre-reaction complexes formed by the quercetin molecule and the free radicals. Concluding remarks (Section 4) complete the comparison between the two processes in different environments (polar vs. non-polar).

2. Theoretical methodology

2.1. Models and methods for ground states

$CH_3OO^•$, $CH_3O^•$, and $^•CH_2OH$ were used as prototypes for lipid (L) or small (R) peroxyl ($LOO^•$ and $ROO^•$), alkoxyl ($LO^•$ and $RO^•$) and carbon centered ($L^•$) radicals,[44] respectively. Flavonoid derivatives (ArOH) and their corresponding radicals ($ArO^•$) were found to be accurately described by DFT calculations.[24, 46] The B3P86 functional has been shown to be particularly well-adapted to evaluate the thermodynamics of the reaction between polyphenols and free radicals.[12, 47] The 6-31+G(d,p) basis set is used since it provides very similar results compared to the larger and more computationally demanding 6-311+G(2d,3pd) basis set.[12, 48] Geometries, energies including the zero-point correction (V), enthalpies (H) and Gibbs energies (G) at 298K of the reactants, and products were determined at the (U)B3P86/6-31+G(d,p) level. Ground-state geometries were confirmed by a vibrational frequency analysis that indicated the absence of imaginary frequency.

2.2. Pre-reaction complexes and non-covalent interaction description

The pre-reaction complexes are crucial in the different mechanisms. They drive the bimolecular approach. These complexes involve non-covalent interactions (H-bonding and π-stacking interactions), which are poorly described by classical hybrid functionals. The dispersion corrected DFT-D is a successful approach to circumvent the use of high-costing post-HF methods.[49] We recently re-parameterized the B3P86-D2 functional, reaching accuracy to evaluate dispersive complexation of flavonoid derivatives.[50] The geometries of the pre-reaction complexes were obtained with B3P86-D2 after a complete scan of possible approaches *i.e.*, either towards the OH groups (for the [**HBi**]-type complexes which form H-bond between

---

[44] Carbon centered free radicals are radical intermediates produced by HAT from the lipid chains during the lipid peroxidation process. They are also produced *e.g.*, in liver intoxication to alcohol.

the free radical and the i-OH group, see Fig. IV.2) or towards the aromatic rings (for the [ν−π]-type complexes having non covalent lone-pair/aromatic-ring interactions, see Fig. IV.2).
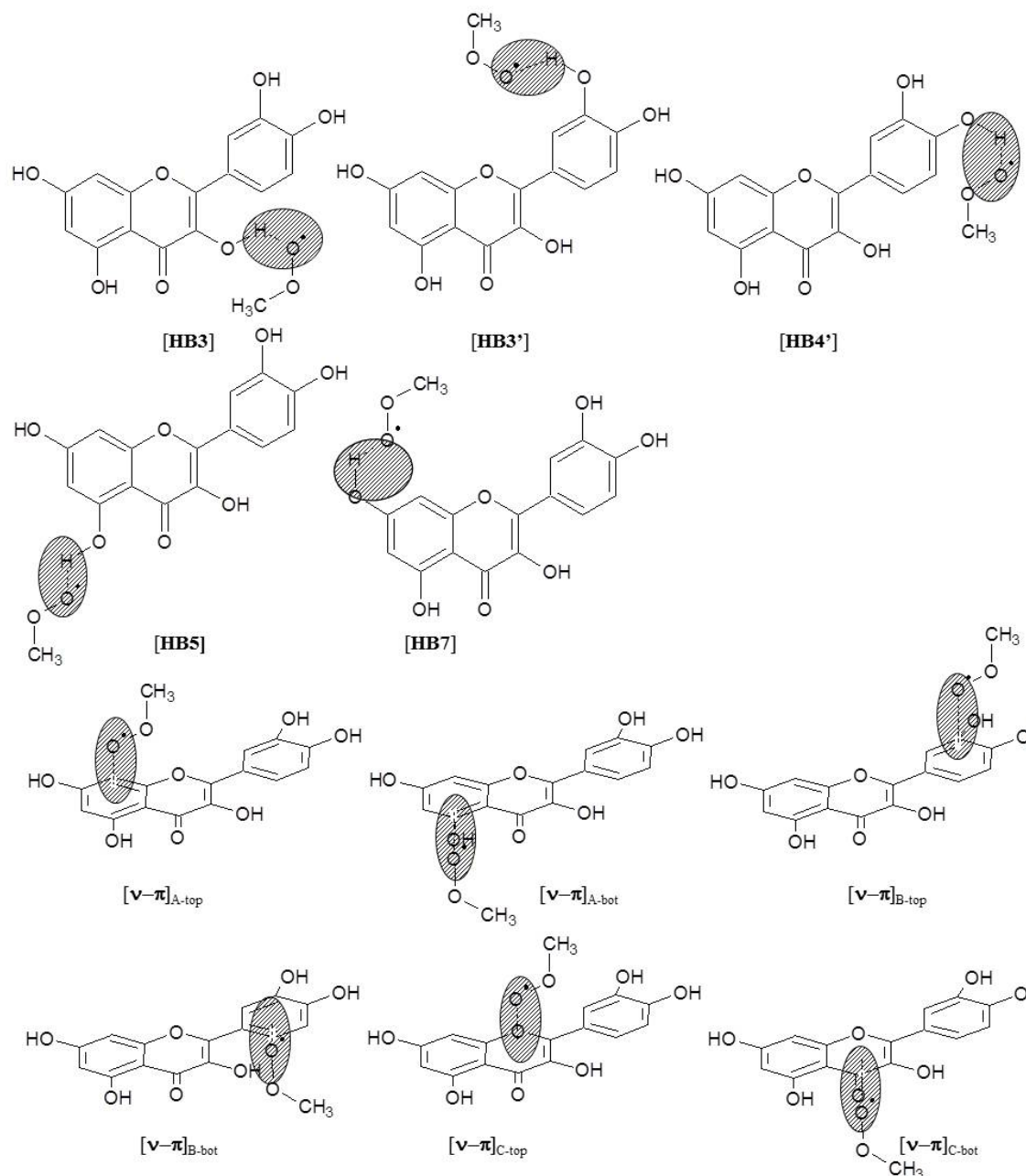
Figure IV.2. Structures of the different complexes-of-approach with H bond ([**HB3**], [**HB3'**], [**HB4'**], [**HB5**] and [**HB7**]) and $\nu-\pi$ type interactions

2.3. Kinetics and transition state description

Concerning PCET, the transition states (TSs) were confirmed by the presence of one imaginary frequency assigned to the normal mode corresponding to the reaction studied (*i.e.*, O-H bond cleavage and the concomitant O-H or C-H bond formation in the polyphenol and the free radical, respectively). TSs were also confirmed by the calculation of the minimum energy

path (MEP) evaluated with the IRC (intrinsic reaction coordinate) algorithm as implemented in the Gaussian03 program.[51] The vibrational analysis was performed using a scaling factor of 0.9537.[52]

Hybrid functionals (*e.g.*, B3P86) are known to underestimate the energy of the transition states (TSs) corresponding to the cleavage of O-H bonds. This was observed for various molecular systems including HAT reactions.[52] Meta hybrid functionals such as MPWB1K appear to be more accurate to reproduce $\varDelta G^{\#}_{PCET}$ values.[52] Therefore, all the activation barriers involving HAT(PCET) were evaluated at the (U)MPWB1K/6-31+G(d,p) level.[45] To validate this choice, the rate constants of HAT(PCET) were calculated with (U)B3P86/6-31+G(d,p) and (U)MPWB1K/6-31+G(d,p) and were compared to the robust (U)CCSD(T)/cc-pVDZ//(U)MPWB1K/6-31+G(d,p) level of theory (See Supplementary materials) for the following two prototype reactions from phenol (PhOH) and propane (CH$_3$-CH$_2$-CH$_3$) to CH$_3$OO$^{\bullet}$:

$$PhOH + CH_3OO^{\bullet} \longrightarrow PhO^{\bullet} + CH_3OOH \quad (IV.7)$$

$$CH_3\text{-}CH_2\text{-}CH_3 + CH_3OO^{\bullet} \longrightarrow CH_3\text{-}\overset{\bullet}{C}H\text{-}CH_3 + CH_3OOH \quad (IV.8)$$

The free energy barriers of reaction (IV.7) are 14.9, 22.7 and 25.9 kcal.mol^{-1} with B3P86, MPWB1K, and CCSD(T), respectively; the corresponding values for reaction (IV.8) are 23.5, 29.5 and 30.2 kcal.mol^{-1} (See Table IV.1). As expected and firmly confirmed by several theoretical works for many HAT(PCET) prototype reactions,[32, 33] the free energy barriers are underestimated with classical hybrid functionals (*e.g.*, B3P86) whereas those obtained with MPWB1K are closer to those obtained at the CCSD(T) level.

---

[45] We have checked that the thermodynamics is similar with both (U)B3P86/6-31+G(d,p) and (U)MPWB1K/6-31+(d,p).

Table IV.1. Gibbs energy of activation $\Delta G^{\#}_{PCET}$ (in kcal.mol^{-1}), tunneling transmission coefficients obtained according to the Skodje & Truhlar formalism $\kappa(T)$, transition rate constants k^{TST} and k^{PCET} (M^{-1}.s^{-1}) with B3P86 and MPWB1K functional and coupled B3P86/MPWB1K.

Eq.	$\Delta G^{\#}_{PCET}$			$\kappa(T)$		k^{TST}		k^{PCET}		
	B3P86	MPWB1K	CCSD(T)^a	B3P86	MPWB1K	B3P86	MPWB1K	B3P86	MPWB1K	Mixed^b
IV.1b^c	15.06	28.7	-	2.83	5.97×10^5	5.8×10^1	6.0×10^{-9}	1.6×10^2	3.6×10^{-3}	3.5×10^7
IV.7	14.9	22.7	25.9	1.00	2.75×10^3	7.6×10^1	1.5×10^{-4}	7.6×10^1	4.1×10^{-1}	2.1×10^5
IV.8	23.5	29.5	30.2	4.46	5.81×10^1	3.8×10^{-5}	1.6×10^{-9}	1.7×10^{-4}	9.0×10^{-8}	2.2×10^{-3}
IV.12^d	-	15.8	-	-	8.79×10^1	-	1.6×10^1	-	1.4×10^3	-
IV.13^e	12.2		-	1.09	-	6.7×10^3	-	7.3×10^3	-	-

^{a} *Performed on the MPWB1K geometry;* ^{b}*.following* $k^{PCET} = \kappa_{MPWB1K} \times k^{PCET}_{B3P86}$; ^{c} *with ArOH = QOH and concerning the 4'-OH group in water;* ^{d} *in benzene;* ^{e} *concerns 4'-OH in chlorobenzene*

2.4. Solvent effects

Solvent effects were taken into account during optimization implicitly by a PCM (polarizable continuum model) method. The IEFPCM (integral equation formalism PCM) method coupled to UA0 radii was used.[53, 54] The PCET, ET-PT and SPLET mechanisms have been studied in media corresponding to benzene ($\varepsilon = 2.27$) and water ($\varepsilon = 78.35$). The former solvent simulates the behaviour in non-polar environments (*e.g.*, lipid bilayer membranes) and the latter describes the behaviour in a polar environment. DFT as well as other quantum-chemistry methods badly reproduce the energy of isolated protons. For all the reactions that include protons, the $\Delta G_{water}(H^+)$ value of -264.61 kcal.mol^{-1} was used here; this value was derived from electrochemical experiments and has largely been used in the literature.[55-57] All calculations were carried out using Gaussian03[51] and Orca.[58]

3. Results and Discussion

The free radical scavenging action is driven either by atom transfer (PCET) or by electron transfer (ET-PT and SPLET). These two physical mechanisms are treated by two different theories. The former is well-described by the transition state theory (TST) and the corresponding refinements, while for the latter, Marcus theory and related formalisms offer an appropriate description. These three processes can take place by overcoming the free energy barrier or by tunneling along the reaction coordinate. Therefore, rate constants rather than Gibbs activation energies ($\Delta G^{\#}$) must be evaluated to compare the kinetics of these three mechanisms.

3.1. Atom transfer processes (PCET)

As already described, PCET occurs when [**HBi**]-type pre-reaction complexes are formed;[35, 59] H-bonds being formed between the free radical and one of the OH groups of quercetin. Therefore the H-atom transfer is seen within a classical electronic picture as involving one proton and five electrons.[35]

The rate constants of PCET were calculated within the conventional TST framework:[60, 61]

$$k^{PCET} = \kappa(T)\frac{k_b T}{h} exp\left(-\frac{\Delta G^{\#}_{PCET}}{RT}\right) \quad (IV.9)$$

$\Delta G^{\#}_{PCET}$ is calculated as the difference in Gibbs energy between the TS and the reactants. $\kappa(T)$ is the transmission coefficient, k_b is the Boltzmann constant and T is the temperature (298K).

It has been shown for the flavonoid epicatechin (Fig. IV.1b) that results based on CVT (canonical variational transition state theory) and TST were very similar, confirming the relevance of TST to evaluate rate constants of PCET.[62]

The $\kappa(T)$ transmission coefficient associated to quantum tunneling along the reaction coordinate was evaluated by the Skodje & Truhlar (S/T) method.[63] To describe the MEP and tunneling, the S/T method uses the TS imaginary frequency and the height of the potential energy barrier including the zero-point correction. The transmission coefficients are given by the following expressions (Eq. (IV.10-11)):

- $\beta < \alpha$:

$$\kappa(T) = \frac{\beta\pi/\alpha}{sin\left(\beta\pi/\alpha\right)} - \frac{\beta}{\beta - \alpha}exp[(\beta - \alpha)(\Delta V^{\#} - V)] \quad (IV.10)$$

- $\beta > \alpha$:

$$\kappa(T) = \frac{\beta}{\beta - \alpha}\{exp[(\beta - \alpha)(\Delta V^{\#} - V)] - 1\} \quad (IV.11)$$

where $\alpha = 2\pi/[h \times Im(v^\#)]$, $\beta = 1/k_b T$, $\Delta V^\#$ is the zero-point-corrected potential energy difference between TS and reactants, and V is either zero (for an exoergic reaction) or the zero-point-corrected energy difference between products and reactants (for an endoergic reaction). $v^\#$ is the TS imaginary frequency.

3.1.1. Reactivity of quercetin with peroxyl radicals

The $CH_3OO^\bullet$-scavenging reaction strongly depends on the OH group.[46] In the non-polar and polar environment the hierarchies are 4'-OH > 3'-OH > 3-OH > 7-OH >> 5-OH (Table IV.2a) and 4'-OH ~ 3'-OH ~ 3-OH > 7-OH ~ 5-OH (Table IV.2b), respectively. These hierarchies are very consistent with the experimental knowledge, confirming the robustness of the methodology to provide an accurate qualitative description of the free radical scavenging kinetics of polyphenols.

From the quantitative point of the view the values obtained here (up to 1.7×10^1 $M^{-1}.s^{-1}$, see Table IV.2) are in agreement with the few theoretical studies at similar level of calculation (around 10^3 $M^{-1}.s^{-1}$ for the 4'-OH group of epicatechin in non-polar solvent at the ONIOM(CCSD(T)/6-31G(d,p):MPWB1K/6-31G(d,p))//MPWB1K/6-31G(d,p) level within the CVT formalism[62] and around 10^{-2} $M^{-1}.s^{-1}$ for quercetin in polar-solvent with PCM-MPWB1K/6-311G(d,p))//MPWB1K/6-311G(d,p)[59]). This appeared encouraging to validate the choice of the methodology to evaluate atom transfer, allowing comparison between i) free radicals and ii) mechanisms of action. There exist no experimental value for $CH_3OO^\bullet$ radical scavenging by flavonoids, however this value has appeared relatively weak with respect to the rate constants of $e.g.$, DPPH-scavenging by flavonoids (around 10^3 $M^{-1}.s^{-1}$ in methanol). We evaluated the rate constant of the following two reactions, for which experimental data are available in non-polar solvents:[29, 35]

$$PhOH + t\text{-}BuO^\bullet \longrightarrow PhO^\bullet + t\text{-}BuOH \qquad (IV.12)$$

---

[46] This process has recently been studied for the scavenging reaction between quercetin and $CH_3OO^\bullet$.(See Ref. 58) Here we reproduced the calculation with this free radical as our methodolgy slightly differs from the methodology used in this publication. As seen in this section, results obtained with both methodologies are similar, however these new calculations are mandatory to ensure consistency throughout the text (all other sections) and to allow all comparisons i) between the different free radicals and ii) between the atom-transfer and electron-transfer processes.

$$(k \sim 10^8 \text{ M}^{-1}.\text{s}^{-1} \text{ in benzene})$$

$$QOH + Ph_2CHOO\cdot \longrightarrow QO\cdot + Ph_2CHOOH \qquad (IV.13)$$
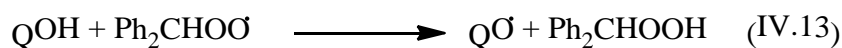
$$(k \sim 10^7 \text{ M}^{-1}.\text{s}^{-1} \text{ in chlorobenzene[64]})$$

The B3P86 rate constants appeared significantly underestimated (*e.g.*, $k \sim 10^4 \text{ M}^{-1}.\text{s}^{-1}$ for Eq. (IV.13), Table IV.1), while they are $\sim 10^4$ higher than those obtained from MPWB1K. This poor description of PCET rate constants has already been pointed out with Eq. (IV.12), being attributed to "a poor description of the charge separation in the PCET transition state"[32] It must be pointed out that both functionals B3P86 and MPWB1K provide a similar qualitative description (same structure activity relationship). Both values are presented in Table IV.1 but the discussions are based on the B3P86 set of values.[47]

---

[47] The better agreement of B3P86 with experimental values is more probably attributed to a compensation of errors rather than to fundamental reasons. B3P86 thus appears adapted for π-conjugated phenol systems. All in all, the qualitative description of PCET is definitely accurate, but the quantitative description must be carefully considered and should be shifted according to a correcting factor.

Table IV.2. Gibbs energies of activation $\Delta G^{\#}_{PCET}$ (kcal.mol^{-1}), tunneling transmission coefficients obtained according to the Skodje & Truhlar formalism $\kappa(T)$ and rate constants k^{PCET} (M^{-1}.s^{-1}) for PCET in (a) non-polar and (b) polar environments.

(a) Non-polar solvent

Radical	OH group	$\Delta G^{\#}_{PCET}$	$\kappa(T)$	k^{PCET}
	3-OH	24.6	1.71×10^4	9.7×10^{-2}
	3'-OH	21.1	1.51×10^3	3.6
CH$_3$OO$^{\bullet}$	4'-OH	19.7	7.12×10^2	1.7×10^1
	5-OH	37.0	1.40×10^5	7.1×10^{-10}
	7-OH	27.7	9.26×10^2	3.1×10^{-5}
CH$_3$O$^{\bullet}$		17.8	2.63×10^2	6.4×10^1
$^{\bullet}$CH$_2$OH	3-OH	21.1	3.80×10^3	8.9
$^{\bullet}$OH		8.2	1.00	6.3×10^6

(b) Polar solvent

Radical	OH group	$\Delta G^{\#}_{PCET}$	$\kappa(T)$	k^{PCET}
	3-OH	28.4	1.95×10^5	2.0×10^{-3}
	3'-OH	29.2	7.17×10^5	1.8×10^{-3}
CH$_3$OO$^{\bullet}$	4'-OH	28.7	5.97×10^5	3.6×10^{-3}
	5-OH	40.3	3.13×10^{11}	6.4×10^{-6}
	7-OH	34.3	2.67×10^5	1.3×10^{-7}
CH$_3$O$^{\bullet}$		19.3	1.42×10^2	6.2
$^{\bullet}$CH$_2$OH	3-OH	23.7	3.45×10^3	8.9×10^{-2}
$^{\bullet}$OH		7.3	1.00	2.9×10^7

3.1.2. Reactivity of quercetin with other free radicals

As expected, the reaction with the $^{\bullet}$OH free radicals is much faster than with CH$_3$OO$^{\bullet}$ (k^{PCET} = 6.3×10^6 and 2.9×10^7 M^{-1}.s^{-1} in the non-polar and polar solvents, respectively, see Table IV.2). According to the quantitative underestimation of k by DFT, this process can clearly be considered diffusion-controlled, being almost barrierless.

The rate constants with the CH$_3$O$^{\bullet}$ free radical are much smaller than with $^{\bullet}$OH (k^{PCET} = 6.4x10^1 and 6.2 M^{-1}.s^{-1} in the non-polar and polar solvents, respectively, see Table IV.2), which is consistent with the lower reactivity of alkoxyl radicals compared to $^{\bullet}$OH free radicals. The presence of the CH$_3$ group considerably increases the stability of the free radical, which in turn decreases its reactivity.

The rate constants with $^{\bullet}$CH$_2$OH are even smaller than with the CH$_3$O$^{\bullet}$ free radicals. This is due to the fact that the PCET reaction with the carbon-centered free radical $^{\bullet}$CH$_2$OH implies a strong reorganization, from sp^2 to sp^3 hybridization. This reorganization requires a large activation free energy (21.1 and 23.7 kcal.mol^{-1} in the non-polar and polar solvents, respectively), which is somewhat mitigated by a sizable tunneling transmission coefficient in both the non-polar and the polar solvents (Table IV.2). Furthermore, no H-bond is observed in the complex-of-approach with $^{\bullet}$CH$_2$OH, decreasing the stability and implying a much less favourable scavenging event.

3.1.3. Empirical correction attributed to kinetic (specific) solvent effects

The PCET mechanism is known to exhibit kinetic solvent effects (KSE). It has been well-described that intermolecular interaction, namely between phenolic OH groups and solvent may decrease rate constants. Rate constants in HBA (H bond acceptor) solvents can be efficiently corrected according to the following equation:[29, 35, 65]

$$log\big(k_{ArOH/R^{\bullet}}^{solvent}\big) = log\big(k_{ArOH/R^{\bullet}}^0/M^{-1}s^{-1}\big) - 8.3\alpha_2^H\beta_2^H \quad (IV.14)$$

where k^0 is the rate constant in a non HBA solvent, α_2^H predicts H-bonding capacity of ArOH and β_2^H describes the HBA capacity of the solvent.[29, 65] In polar solvents, β_2^H is around 0.5 (e.g., 0.4 for alcohol); and for phenol α_2^H is around 0.6. Therefore according to Eq. (IV.14) the KSE-corrected rate constant can be reduced by more than 10^2. However in our case, most of the OH groups, except 7-OH, are involved in strong intramolecular H-bonding (with the neighbouring group for 3'-OH and 4'-OH, and with the keto group for 3-OH and 5-OH).[12, 26] It has been shown that in such cases, KSE is lowered[29, 31] since intermolecular interactions with solvent are weakened. E.g. α_2^H is around 0.25 for guaiacol (2-methoxyphenol). [29] Taking a value of 0.5 for β_2^H, the rate constant of PCET from guaiacol would only be

divided by 10. In non-polar solvents, β_2^H is much lower and KSE is of minor importance in our case. Taking explicitly the solvent into account would have required a huge computational effort. Therefore PCM-type solvent is a perfect choice for non-polar solvents. For polar solvents it properly takes polarizable effects into account but we are aware that KSE is not fully determined, inducing a slight overestimation of PCET rate constants in our case.

3.2. Electron transfer processes (ET-PT and SPLET)

While PCET from a given OH group can only take place when the corresponding [**HBi**]-type complex-of-approach is formed, ET can occur when either the [**HBi**]-type (complexes [**HB3**], [**HB3'**], [**HB4'**], [**HB5**] and [**HB7**] with the 3-OH, 3'-OH, 4'-OH, 5-OH and 7-OH groups, respectively) or [**ν–π**]-type (complexes [**ν–π**]$_A$, [**ν–π**]$_B$ and [**ν–π**]$_C$, with the A-, B- and C-rings, respectively) pre-reaction complexes are formed. The [**HBi**]-type pre-reaction complexes are globally more stable by about 2-3 kcal.mol^{-1} than the [**ν–π**]-type complexes (Table IV.3&4).

Within the Marcus-Levich-Jortner formalism, the rate constant of the electron transfer (for the ET-PT and SPLET mechanisms) between the donor (quercetin) and the acceptor (the free radical) is expressed as:[66]

$$k^{LJ-Marcus} = \frac{4\pi}{h} V_{RP}^2 \sqrt{\frac{1}{4\pi\lambda_s k_b T}} \sum_{\nu'} \left\{ \exp(-S) \frac{S^{\nu'}}{\nu'!} exp\left[-\frac{(\Delta G° + \lambda_s + \nu'\hbar\langle\omega\rangle)^2}{4\lambda_s k_b T} \right] \right\} \quad (IV.15)$$

where $\Delta G°$ is the Gibbs energy difference of reactions (IV.2) or (IV.5), λ_s the external reorganization energy, V_{RP} the electronic coupling, S the Huang-Rhys factor and ν' a vibrational level.

$\Delta G°$ estimation has been made by considering the total Gibbs energies of the isolated species (reactants and products), neglecting the entropy effects for the electrostatic interaction between the species as accounted by a classical Coulomb term:[67]

$$\Delta G° = [G_{298K}(ArOH^{\bullet+}) + G_{298K}(R^-)] - [G_{298K}(ArOH) + G_{298K}(R^\bullet)]$$
$$+ E_{coulomb} \qquad \text{for ET} - \text{PT (IV.16a)}$$

$$\Delta G° = [G_{298K}(ArO^\bullet) + G_{298K}(R^-)] - [G_{298K}(ArO^-) + G_{298K}(R^\bullet)]$$
$$+ E_{coulomb} \qquad \text{for SPLET (IV. 16b)}$$

where $G_{298K}(ArOH^{\bullet+})$, $G_{298K}(ArO^\bullet)$, $G_{298K}(R^-)$, $G_{298K}(ArOH)$, $G_{298K}(R^\bullet)$ and $G_{298K}(ArO^-)$ are the total free energies of the equilibrated isolated species ArOH$^{\bullet+}$, ArO$^\bullet$, R$^-$, ArOH, R$^\bullet$ and ArO$^-$ respectively.

Electron transfer is a multi-path process since in principle the electron can be transferred from each MO (molecular orbital) of quercetin having energy higher than that of the SOMO (Singly Occupied Molecular Orbital) of the free radical. For quercetin, MO is a member of {HOMO-HOMO-n}, with n ranging from 1 to 9 depending on the radical (see supplementary materials). $\Delta G°$ and thus $k^{LJ-Marcus}$ were estimated for each path, correcting $G_{298K}(ArOH^{\bullet+})$ by the difference in energy between HOMO and the corresponding HOMO-n levels.[48] The term $E_{coulomb}$ is defined as the difference in electrostatic interactions between reactants and products, calculated in first approximation in the geometries of the pre-reaction complexes.

$$E_{coulomb} = \frac{1}{4\pi\varepsilon_0\varepsilon_s}\left(\sum_i^{ArOH^{+\bullet}}\sum_j^{R^-}\frac{q_i q_j}{r_{ij}} - \sum_k^{ArOH}\sum_l^{R^\bullet}\frac{q_k q_l}{r_{kl}}\right) \text{ for ET} - \text{PT (IV. 17a)}$$

$$E_{coulomb} = \frac{1}{4\pi\varepsilon_0\varepsilon_s}\left(\sum_i^{ArO^\bullet}\sum_j^{R^-}\frac{q_i q_j}{r_{ij}} - \sum_k^{ArO^-}\sum_l^{R^\bullet}\frac{q_k q_l}{r_{kl}}\right) \text{ for SPLET (IV. 17b)}$$

where q_i and q_j (q_k and q_l) are atomic charges on the donor and acceptor units, respectively, and r_{ij} (r_{kl}) is the interatomic distance after (before) ET. All atomic charges were obtained within the ESPdipole[68, 69] formalism in our computational scheme; ε_s is the static dielectric constant.

$\Delta G°$ thus depends on both the nature of the solvent and pre-reaction complexes. In the polar solvent, $\Delta G°$ is similar for the different complexes. On the other hand, in the non-polar solvent,

---

[48] The differences in energy between HOMO and the corresponding HOMO-n levels were performed at IEFPCM CCSD(T)/cc-pVDZ//MPWB1K/6-31+G(d,p) level of theory to overcome the poor description of MO energies at DFT level of theory.

$\Delta G°$ and therefore $k^{LJ-Marcus}$ strongly depend on the different free radical approaches (Tables IV.3&4).

λ_s is the external reorganization energy (*i.e.*, related to the electronic and nuclear polarization of the solvent), which can be expressed as:[70]

$$\lambda_s = \frac{1}{8\pi\varepsilon_0}\left(\frac{1}{\varepsilon_{opt}} - \frac{1}{\varepsilon_s}\right)\left(\frac{1}{r_{ArOH}} + \frac{1}{r_{R^\bullet}} + 2\sum_i^{ArOH}\sum_j^{R^\bullet}\frac{\Delta q_i\Delta q_j}{r_{ij}}\right) \quad \text{for ET} - \text{PT (IV. 18a)}$$

$$\lambda_s = \frac{1}{8\pi\varepsilon_0}\left(\frac{1}{\varepsilon_{opt}} - \frac{1}{\varepsilon_s}\right)\left(\frac{1}{r_{ArO^-}} + \frac{1}{r_{R^\bullet}} + 2\sum_i^{ArO^-}\sum_j^{R^\bullet}\frac{\Delta q_i\Delta q_j}{r_{ij}}\right) \quad \text{for SPLET (IV. 18b)}$$

where ε_{opt} is the optical dielectric constant. Δq_i and Δq_j are the charge difference along the reaction of the electron donor (i.e., ArOH and ArO⁻ for ET-PT and SPLET, respectively) and the free radical R$^\bullet$, respectively. The radii (r_{ArO^-}, r_{ArOH} and $r_{R^\bullet}$) were calculated as:

$$r_{R^\bullet} \text{ or } r_{ArO^-} \text{ or } r_{ArOH} = \frac{1}{N}\sum_A^N |r_A - r_q| \quad \text{(IV. 19)}$$

where the sum runs over all atoms; r_A is the atomic position and r_q is the charge-weighted barycenter of the molecule. This definition allows using a radius that is averaged according to its electrostatic significance.

The electronic coupling V_{RP} is estimated at the semi-empirical Hartree-Fock Intermediate Neglect of Differential Overlap (INDO) level.[71] The electronic coupling term has been directly calculated between quercetin MOs and the free radical SOMO, in the geometry of the pre-reaction complexes.[67] The coupling V_{ij} between two orbitals ϕ_i and ϕ_j (belonging to molecules i and j, respectively) can be classically recast in an atomic orbital basis set (Eq. (IV.20)):

$$V_{ij} = \langle\phi_i|h|\phi_j\rangle = \sum_\mu\sum_\nu c_{i\mu}c_{j\nu}\langle\chi_\mu|h|\chi_\nu\rangle \quad \text{(IV. 20)}$$

where $c_{i\mu}$ and $c_{j\nu}$ are the LCAO (linear combination of atomic orbitals) coefficients of the atomic orbitals χ_μ and χ_ν in the molecular orbitals ϕ_i and ϕ_j, respectively. In our case the coupling is calculated for each path *i.e.*, for each electron transition from all the HOMO-n having an energy higher than that of the SOMO of the free radical.[49] It must be stressed that MO shapes are very similar at both the INDO and DFT levels of calculation.

In Eq. (IV.15) the summation runs over all vibrational levels of effective modes, which are in our case the aromatic C-C and phenolic C-O bond stretchings; the elongation of these bonds being the most probable reaction coordinate involved during the electron transfer. The corresponding energy is taken as their average energy ($\hbar\langle\omega\rangle = 4.6$ kcal.mol^{-1}). The Huang-Rhys factor S is directly related to the internal reorganization energy λ_i (*i.e.*, the geometry reorganization along the reaction coordinate[72]):

$$S = \frac{\lambda_i}{\hbar\langle\omega\rangle} \quad \text{(IV.21)}$$

The global rate constant is the sum of the rate constants calculated for each accessible pathway. Even though many pathways exhibit large electronic couplings, the electron transfer is mainly dominated by the HOMO to SOMO pathway. When the electron is transferred from HOMO-n rather than from HOMO, the large increase in $\Delta G°$ makes the pathways really unlikely.

The robustness of such an application of Marcus theory has been largely shown on various systems.[67, 72]

3.2.1. ET-PT: pure electron transfer

Whatever the pre-reaction complex, the calculated rate constants of ET between quercetin and $CH_3OO^\bullet$ radicals are very small, lower 10^{-100} M^{-1}.s^{-1} in the non-polar solvent (Table IV.3a). This definitely makes this process unfeasible in such an environment. Such extremely low rate constants are attributed to the high instability of the $ArOH^{\bullet+}$ radical cation in non-polar solvents.

---

[49] The electronic coupling term V_{RP} does not strongly depend on the nature of the complexes. Electronic coupling does not depend on the solvent since the geometries of the complexes are very similar with both non-polar and polar solvents.

Moreover, due to the large positive value of $\Delta G°$, tunneling is not an efficient physical event that could compensate for the height of the activation barrier. An increase in polarity of the solvent induces a dramatic increase in the radical cation stability (Table IV.3b). ΔG^{ET} is 29.0 kcal.mol^{-1} but the corresponding rate constants are still very low (k^{ET-PT} ranging from 10^{-14} to 10^{-59} M^{-1}.s^{-1}).

The ET step is followed by PT (reaction (IV.3)). This reaction is very exothermic (ΔG^{PT} lower than -25 and -70 kcal.mol^{-1} in the polar and non-polar solvent, respectively). Nonetheless, ET exhibits too low rate constants, whatever the solvent polarity, making the whole process totally inefficient in both hydrophilic and lipophilic environments.

The ET-PT process with $^{•}CH_2OH$ is even slower than with $CH_3OO^{•}$ (k^{ET-PT} lower than 10^{-100} M^{-1}.s^{-1} in both the polar and non-polar solvents). Such low values are again attributed to the high instability of the radical cation but also to the higher instability of $^{-}CH_2OH$ with respect to CH_3OO^{-}, due to a reduced charge delocalization: the charge is around -1.72 on the C-atom of $^{-}CH_2OH$ vs. -0.75 on the O-atom of CH_3OO^{-}. Electron transfer to the $CH_3O^{•}$ free radical is still not competitive as compared to PCET in the non-polar solvent (k^{ET-PT} being very low).

No pre-reaction complex with $^{•}OH$ free radical was obtained at the level of theory suggesting a direct PCET reaction. The ET-PT reaction is thus not expected to occur.

Table IV.3. Interaction energy ΔE_{int} (kcal.mol^{-1}) of pre-reaction complex, internal λ_i and external λ_s reorganization energies (kcal.mol^{-1}), electronic coupling V_{RP} (kcal.mol^{-1}), Gibbs energy of the reaction $\Delta G°$(kcal.mol^{-1}), rate constants $k^{ET\text{-}PT}$ (M^{-1}.s^{-1}) including the tunneling transmission coefficient κ^{LJ} obtained within the Marcus-Levich-Jortner formalism of the electron transfer reaction in the ET-PT mechanism in (a) non-polar and (b) polar solvents.

(a) Non-polar solvent

Free radical	Pre-reactant complex	ΔE_{int}	λ_i	λ_s	V_{RP}	$\Delta G°$	$k^{ET\text{-}PT}$
	[HB3]	-2.8	13.9	0.1	0.1	55.6	-
	[HB3']	-6.4	13.9	0.1	0.1	43.5	-
	[HB4']	-6.6	13.9	0.0	-1.8	45.1	-
	[HB5]	-1.2	13.9	0.1	-0.2	65.6	-
	[HB7]	-6.2	13.9	0.1	0.0	48.1	-
CH$_3$OO$^{\bullet}$	[ν−π]$_{A\text{-bot}}$	-3.8	13.9	0.1	-1.8	56.3	-
	[ν−π]$_{A\text{-top}}$	-3.8	13.9	0.1	1.9	56.2	-
	[ν−π]$_{B\text{-bot}}$	-4.2	13.9	0.1	-1.4	56.2	-
	[ν−π]$_{B\text{-top}}$	-3.5	13.9	0.1	0.5	56.1	-
	[ν−π]$_{C\text{-bot}}$	-3.8	13.9	0.1	1.9	56.2	-
	[ν−π]$_{C\text{-top}}$	-4.0	13.9	0.1	2.2	56.0	-
CH$_3$O$^{\bullet}$		-2.2	7.4	0.1	-5.1	45.2	-
$^{\bullet}$CH$_2$OH	**[HB3]**	-3.4	22.8	0.1	-3.2	89.2	-
$^{\bullet}$OH		-	4.3	-	-	-	-

(b) Polar solvent

Free radical	Pre-reactant complex	ΔE_{int}	λ_i	λ_s	V_{RP}	$\Delta G°$	$k^{ET\text{-}PT}$
	[HB3]	-1.8	13.3	4.9	0.0	28.2	2.9x10^{-32}
	[HB3']	-4.0	13.3	6.8	-0.2	27.7	6.7x10^{-22}
	[HB4']	-3.6	13.3	3.4	1.6	27.8	8.2x10^{-40}
	[HB5]	-0.2	13.3	10.7	0.2	28.5	3.4x10^{-16}
	[HB7]	-3.9	13.3	11.3	-0.5	27.9	7.9x10^{-14}
CH$_3$OO$^{\bullet}$	[ν−π]$_{A\text{-bot}}$	-2.2	13.3	8.0	0.9	28.2	2.7x10^{-18}
	[ν−π]$_{A\text{-top}}$	-2.6	13.3	8.7	-2.4	28.2	3.2x10^{-16}
	[ν−π]$_{B\text{-bot}}$	0.5	13.3	2.5	0.0	28.1	5.2x10^{-59}
	[ν−π]$_{B\text{-top}}$	-2.9	13.3	5.0	0.0	28.1	4.7x10^{-31}
	[ν−π]$_{C\text{-bot}}$	-2.3	13.3	8.2	-1.9	28.2	2.8x10^{-17}
	[ν−π]$_{C\text{-top}}$	-2.8	13.3	6.1	0.8	28.1	1.1x10^{-23}
CH$_3$O$^{\bullet}$		-3.3	6.3	5.6	-6.2	21.0	1.6x10^{-12}
$^{\bullet}$CH$_2$OH	**[HB3]**	-2.2	22.2	4.4	-3.2	71.9	-
$^{\bullet}$OH		-	4.3	-	-	-	-

3.2.2. SPLET: activated electron transfer

In SPLET, the electron transfer occurs from a deprotonated form of quercetin (Eq. (IV.5)). It means that the initiation of this mechanism strongly depends on pH of the medium and the acidity of the different OH groups of quercetin. It is known that the pH influences the antioxidant activity: the higher the pH, the higher the free radical scavenging activity of various polyphenols (*e.g.*, flavonoids and curcuminoids).[27, 73-75] From the free energies of deprotonation of the different OH groups of quercetin (Table IV.5), the 7-OH group appears to be the most acidic site and the following hierarchy is obtained 7-OH > 4'-OH > 3-OH > 5-OH > 3'-OH. This confirms the experimental pK_A values of 7.7, 8.8, 9.8 $\pm$ 0.2 obtained for the three most acidic groups: 7-OH, 4'-OH and 3-OH, respectively.[74] The deprotonation is naturally very unfavourable in non-polar solvents ($\Delta G_{deprot} > 200$ kcal.mol^{-1}) due to the ionic nature of the products, which cannot be stabilized in a non-polar environment. The SPLET process can thus only occur in polar environments and under certain pH conditions (*i.e.*, alkaline or neutral conditions).

The electron transfer occurs after the formation of the pre-reaction complex, in which quercetin is deprotonated, *i.e.*, H$^+$ is released from one of the most acidic groups 7-OH, 4'-OH or 3-OH. The rate constants were calculated with all pre-reaction complexes formed with quercetin deprotonated at 7-OH (complexes [**HB3**]-7H+, [**HB3'**]-7H+, [**HB4'**]-7H+, [**HB5**]-7H+ and all [$\nu-\pi$]-7H+) and with three other pre-reaction complexes with quercetin deprotonated at 4'-OH and 3-OH (complexes [**HB7**]-4'H+, [**HB7**]-3H+ and [**HB3'**]-3H+) (Table 4).

Table IV.4. Interaction energy ΔE_{int} (kcal.mol^{-1}) of pre-reaction complex, internal λ_i and external λ_s reorganization energies (kcal.mol^{-1}), electronic coupling V_{RP} (kcal.mol^{-1}), Gibbs energy of the reaction $\Delta G°$ (kcal.mol^{-1}), rate constants k^{SPLET} (M^{-1}.s^{-1}) including the tunneling transmission coefficient κ^{LJ} obtained within the Marcus-Levich-Jortner formalism of the electron transfer reaction in SPLET and rate constant ratio K with respect to the fastest reaction in polar solvent.

Free radical	Pre-reactant complex	ΔE_{int}	λ_i	λ_s	V_{RP}	$\Delta G°$	K^{SPLET}	K
CH$_3$OO$^\bullet$	[**HB3**]-7H+	-1.2	11.6	8.7	0.1	17.9	1.3x10^5	1x10^{-12}
	[**HB3'**]-7H+	-4.0	11.6	9.4	0.1	17.5	5.5x10^{-5}	4x10^{-12}
	[**HB4'**]-7H+	-3.5	11.6	12.7	-1.3	17.5	4.0x10^{-1}	3x10^{-8}
	[**HB5**]-7H+	-3.4	11.6	4.3	-0.8	17.9	2.8x10^{-9}	2x10^{-16}
	[ν−π]$_{Atop}$-7H+	-2.3	11.6	8.7	2.0	18.0	1.6x10^{-2}	1x10^{-9}
	[ν−π]$_{Atop}$-7H+	-2.3	11.6	9.6	2.0	18.0	4.9x10^{-2}	4x10^{-9}
	[ν−π]$_{Bbot}$-7H+	-2.8	11.6	8.3	0.4	17.9	3.4x10^{-4}	3x10^{-11}
	[ν−π]$_{Btop}$-7H+	-2.2	11.6	14.0	0.5	17.9	3.6x10^{-2}	3x10^{-9}
	[ν−π]$_{Cbot}$-7H+	-1.8	11.6	8.5	-1.8	18.0	1.0x10^{-2}	8x10^{-10}
	[ν−π]$_{Ctop}$-7H+	-2.7	11.6	10.0	0.5	17.9	5.4x10^{-3}	4x10^{-10}
	[**HB7**]-4'H+	-8.9	12.6	12.9	-0.8	9.1	2.3x10^5	2x10^{-2}
	[**HB7**]-3H+	-3.6	13.0	10.6	-0.2	4.9	8.7x10^6	7x10^{-1}
	[**HB3'**]-3H+	-3.8	13.0	9.0	-0.2	4.8	1.3x10^7	1
CH$_3$O$^\bullet$	[**HB3**]-7H+	-2.8	4.6	47.2	1.0	-1.9	2.3x10^{12}	-
$^\bullet$CH$_2$OH	[**HB3**]-7H+	-1.7	20.5	46.0	-0.9	49.0	1.3x10^{-52}	-

Table IV.5. Gibbs energy of deprotonation ΔG_{deprot} (kcal.mol^{-1}) for the different OH groups of quercetin in the polar solvent.

OH group	3-OH	3'-OH	4'-OH	5-OH	7-OH
ΔG_{deprot}	25.8	28.5	24.9	26.7	21.7

One of the major results gained by quantum calculations is that rate constants strongly depend on both the pre-reaction complex and the site of deprotonation. For quercetin scavenging CH$_3$OO$^\bullet$, they are ranging from 10^{-9} to 10^7 M^{-1}.s^{-1}. When quercetin is deprotonated at 7-OH, the highest rate constant is obtained with the pre-reaction complex [**HB4'**]-7H+ (k^{SPLET} is 4.0x10^{-1} M^{-1}.s^{-1}, see Table 4). When quercetin is deprotonated at 3-OH and 4'-OH, high rate constants are observed, *e.g.*, k^{SPLET} is 1.3x10^7 M^{-1}.s^{-1} for the [**HB3'**]-3H+ pre-reaction complex (Table 4). The deprotonation induces a decrease in the polyphenol stability, which somewhat activates the electron transfer process, which then becomes highly competitive with respect to PCET.

The SPLET reaction with $^\bullet CH_2OH$ appears to be totally inefficient in non-polar and polar environments. The rate constant in the polar solvent is around 10^{-52} $M^{-1}.s^{-1}$ (Table 4). This very small value is partly attributed to the poor stability of the products formed after electron transfer: ($\Delta G° = 49.0$ kcal.mol^{-1}, Table IV.4). In this case, the rate constant is further strongly affected by the internal reorganization energy ($\lambda_i= 20.5$ kcal.mol^{-1}) when going from the $^\bullet CH_2OH$ free radical to the $^-CH_2OH$ anion, due to the hybridization change of the C-atom from sp^2 to sp^3.

SPLET with the alkoxyl radicals is also an activated-ET process. The rate constants increase from 2.3×10^{-12} to 2.3×10^{12} $M^{-1}.s^{-1}$ going from ET-PT to SPLET (Tables 3 & 4). In the polar solvent, SPLET is faster than PCET (Tables 2&4) making SPLET the most likely process to scavenge alkoxyl free radicals in polar solvents, being diffusion-controlled.

In the case of the $^\bullet OH$ free-radical, no pre-reaction complex was obtained at the theoretical level. A barrier-less reaction is suspected since the electron transfer systematically occurs from all starting geometries for these complexes. This radical is very reactive and whatever the mechanism of action (PCET or SPLET), its scavenging is diffusion-controlled.

4. Concluding Remarks

Whatever the polarity of the solvent, ET-PT is totally inefficient due to the high instability of the ArOH$^{\bullet+}$ radical cation, except for the specific case of the $^\bullet OH$ free-radical. To rationalize the competition between the other two mechanisms, the rate constants of H-atom transfer from quercetin can thus be estimated by a linear combination of the rate constants of PCET and SPLET:

$$k^{Hatom\ tranfer} = \sum_{i} \sum_{j=7,4',3} a_{ij} k^{SPLET}_{[HBi]-jH^+} + \sum_{L=A,B,C}^{bot} \sum_{j=7,4',3} b_{Lj} k^{SPLET}_{[v-\pi]_L-jH^+}$$

$$+ \sum_{L=A,B,C}^{top} \sum_{j=7,4',3} b'_{Lj} k^{SPLET}_{[v-\pi]_L-jH^+} + \sum_{i=4',3,3'} c_i k^{CPET}_{[HBi]} \quad (IV.22)$$

in which i) all coefficients are 0 for i = 5; ii) a_{ij}, b_{Lj} and b'_{Lj} are 0 for carbon centered radicals; and iii) for the other type of radicals, the coefficients depend on the solvent polarity and pH,

according to the rate constants calculated for the different mechanisms and pre-reaction complexes.

In non-polar environments (*e.g.*, lipid bilayer membranes), PCET is the only active process since the deprotonation of quercetin is highly unlikely, making SPLET infeasible. In other words, when possible, PCET is the major process to break the chain reaction in lipid peroxidation, *i.e.*, LOO$^\bullet$ free radical scavenging inside the membrane.

In polar solvents, *e.g.*, in plasma, the pH is ranging from 7.35 to 7.45, so that quercetin is partially deprotonated (mainly at 7-OH). Both PCET (from the neutral form) and SPLET (from the deprotonated form) are in competition, the latter appearing as the major process in agreement with the literature[35] (Tables 2b&4). Nonetheless an important point highlighted in the present work is that this competition strongly depends on the pre-reaction complex and the deprotonation site. From a statistical point of view, SPLET offers much more possibilities since the number of approaches by free radicals associated to high rate constants is higher with SPLET than with PCET. For an effective scavenging by H-atom abstraction, the free radicals should approach: i) all OH groups and the aromatic rings to form $\nu-\pi$ complexes (*e.g.*, $[\nu-\pi]_C$) with SPLET, or ii) only the OH groups with a low BDE (*i.e.*, 3-OH, 3'-OH and 4'-OH) with PCET. The competition also depends on the pH: the higher the pH, the higher the number of deprotonated sites and the higher the contribution of SPLET (having high to very high rate constants). This is in very good agreement with the increase of the free radical scavenging with the pH experimentally observed for flavonoids.[27, 73, 74] So as previously suggested from experimental studies under such conditions, SPLET is probably the fastest and major mechanism until all deprotonated forms are depleted, afterwards PCET becomes again the major mechanism.[35] This picture, involving both mechanisms as it, is probably the most adapted to rationalize scavenging of peroxyl radicals (and also 2,2-diphenyl-1-picryl-hydrazyl, DPPH radical that has shown a similar behaviour[35] and widely used in antioxidant evaluations). For the free radical scavenging of carbon-centered and alkoxyl radicals, the major process is PCET and SPLET, respectively. To scavenge $^\bullet$OH radicals, both mechanisms are diffusion-controlled and even if ET-PT is relatively fast, this is probably a rare event.

These conclusions are drawn out for quercetin, which is a relevant model of antioxidant highly representative of flavonoids. However, it must be stressed that these results can easily be

extrapolated to a large class of compounds including other antioxidants, bioavailable metabolites and new hemi synthetic derivatives.

Section B. Region- and stereoselective synthesis of oligostilbenoids: the theoretical highlights using refinements of density functional theory

1. Introduction

Naturally occurring oligostilbenoids form a specific group of polyphenolic compounds. In spite of their relatively small number, they have a significant economic impact as they are constituents of widely used plant species *e.g.*, dipterocarp timber trees from South East Asia and grapevine.[76, 77] Their attractiveness originates from their structural diversity that includes rings of unusual sizes, various types of fused rings with or without oxygen atoms as well as numerous stereogenic centers. Biogenetically, oligostilbenoids result from homogenous or heterogeneous coupling of monomeric stilbenoid units (*i.e.* resveratrol, isorhapontigenin, pterostilbene) into dimeric to octameric species (Fig. IV.3). The compounds from this group exhibit diverse biological activities including anti-bacterial,[76] antifungal,[77] antioxidant, anti-HIV, cytotoxic, anti-inflammatory.[78] Over the past decade, the synthesis of oligostilbenoids has deserved particular attention; a seminal work concerning the "programmable synthesis design" of resveratrol oligomers was recently proposed.[79-81]

$R^1=R^2=R^3=H$: stilbene
$R^1=R^2=R^3=OH$: resveratrol
$R^1=OH, R^2=R^3=OMe$: pterostilbene

R=H: ampelopsin F
R=Me: ampelopsin F analogue

R=H: pallidol
R=Me: pallidol analogue

R=H: tricuspidatol
R=Me: tricuspidatol analogue
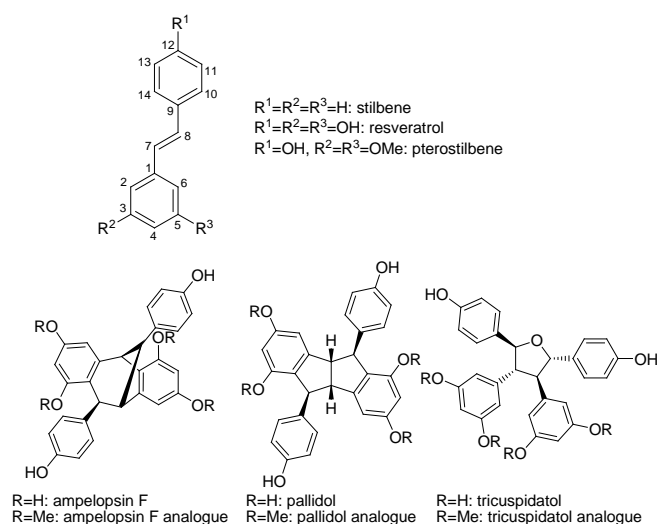
Figure IV.3. Chemical structures of stilbenoid monomers and dimers.

The literature usually describes stilbenoid oligomerisation as a classical phenolic oxidative coupling. This approach is globally correct but not sufficient to understand the apparent inconsistencies concerning regio- and stereo-selectivity, leading to the formation of the various specific skeletons under different reaction conditions (*e.g.*, solvents and/or metal oxidants). An

206

in-depth analysis of the outcome of stilbene oxidative coupling[2, 78] led us to derive a key hypothesis:[2] π-stacking interaction is the driving force to regio- and stereo-selectivity, allowing self-association of two stilbenoid partners in solution, thus orienting further reactions.

π-π Interactions are involved in many natural processes including i) copigmentation in plants,[82] ii) ligand-protein and ligand-nucleic acid interactions,[83] iii) solid state arrangements[84] and iv) charge transfer[85, 86]. π-Stacking has already been suggested as an important contribution in chemical reactions contributing to regio- and stereo-specificity.[2, 87] π-Stacking interactions in solid state allow controlling the photodimerisation of olefins.[88] In a similar way on how benzene and hexafluorobenzene produce face-to-face stacks, (*E*)-pentafluorostilbene crystallizes with long stacks of alternating phenyl and pentafluorophenyl rings.[88] These stacks produce a single isomer of the cyclobutane photodimer.

Stilbenoids are fully π-conjugated systems and may in principle interact non-covalently through π-π interactions when in solution. An NMR-based dynamical and structural study of resveratrol in DMSO-d6/D$_2$O showed that the molecule can engage in strong auto-stacking interactions.[89] In stilbenoid oligomerisation, π-π interactions would play a crucial role in the self-assembly of stilbenoids prior to the oxidation and phenolic radical coupling, which then would determine the type of skeletons that are produced.

In an attempt to validate this hypothesis, the present work provides a quantum-calculation-based description of π-stacking interactions involved in the pterostilbene dimerisation into analogues of ampelopsin F and pallidol. Section 2 justifies the choice of the method of calculation to properly describe π-π interaction (Section 2.2), density functional theory (DFT) including dispersive correction being recommended in this case. Section 3.1 describes the oxidative initiation and the formation of the subsequent phenoxyl radical. Section 3.2 proposes a molecular description of the π-stacking complexes, showing the different stabilizing contributions. The coupling may occur after oxidative initiation of at least one monomer and the presence of the subsequent phenoxyl radical (see Scheme IV.1).[2] Then, two types of reaction pathway are suggested in solution (Section 3.3): the oxidative coupling of one phenoxyl radical monomer with i) a native monomer (*i.e.*, radical-neutral reaction) or ii) another phenoxyl radical monomer (*i.e.*, radical-radical reaction). Section 3.3 also provides

thermodynamics of the entire mechanism of action and the initial bond formation is kinetically rationalized.

2. Methods of calculation

2.1. Mechanism of reaction

Over the past decades, DFT methods have been widely used to study the electronic structure of natural compounds, allowing high accuracy at a relatively reasonable computational time with respect to post-Hartree Fock (HF) methods. Oxidative reactions of polyphenols (*i.e.*, oxidation by H-atom transfer and radical coupling) were accurately evaluated within the classical hybrid DFT framework, the B3P86 functional being particularly well adapted.[90-92] The 6-31+G(d,p) basis set is used since it provides very similar results to the larger and more computational demanding 6-311+g(2d,3pd) basis set.[90]

Geometries and energies including the zero-point correction (V), enthalpies (H) and Gibbs energies (G) at 298K of reactants, intermediates and products were calculated at the B3P86/6-31+G(d,p) level of theory. The ground-state geometries are confirmed by vibrational analysis that indicated the absence of imaginary frequencies. Transition states (TSs) are confirmed by the presence of one imaginary frequency assigned to the normal mode of the corresponding reaction coordinate.

The capacities of H-atom transfer (HAT) from a given compound R-**H** and inducing the formation of the radical issued from pterostilbene, **RNA3** and **RNP3** (Scheme IV.1) are evaluated by the bond dissociation enthalpy (BDE) calculated as follows:

$$BDE(\text{R} - \textbf{H}) = H^{298}[\text{R} - \textbf{H}] - (H^{298}[\text{R}^\bullet] + H^{298}[\text{H}^\bullet]) \quad (\text{IV. } 22)$$

where H^{298K} refers to the electronic plus the corrections to enthalpy obtained at 298K.

The hard and soft (Lewis) acids and bases (HSAB) principle can be quantified by the chemical hardness (η), which is calculated as follows:

$$\eta = \frac{I - A}{2} \quad (\text{IV. } 23)$$

where *I* and *A* are the adiabatic ionization potential and the adiabatic electron affinity, respectively. This is a global parameter obtained to quantify the hardness or softness of a given molecular system in term of its acid and base behaviour. It allows rationalizing the global capacity of a compound to react according to the HSBA principle. The Fukui function $f_k(r)$ was developed to provide the atomic picture of this reactivity.[93] For a given atom *k*, it is calculated as follows:

$$f_k(r) = f_k^+(r) + f_k^-(r) \qquad (IV.24)$$

where $f_k^+(r)$ and $f_k^-(r)$ are the electrophilic and nucleophilic contributions of the Fukui function:

$$f_k^+(r) = q_k(N+1) - q_k(N) \qquad (IV.25a)$$

$$f_k^-(r) = q_k(N) - q_k(N-1) \qquad (IV.26b)$$

where $q_k(N)$, $q_k(N-1)$ and $q_k(N+1)$ are the electronic populations of atom *k* in its neutral, radical-cation and radical-anion forms, respectively. In the present study, the Fukui nucleophilic contribution is used to rationalize the reactivity of stilbenoids with $FeCl_3.6H_2O$; the higher the $f_k^-(r)$ value, the higher the atomic nucleophilicity. All these calculations were performed with Gaussian09.[94]

2.2. Description of π–stacking interactions

Classical hybrid functionals are known to poorly describe non-covalent weak interactions such as π-stacking interactions of conjugated systems. Among new DFT refinements, DFT-D is a successful approach to circumvent the use of sophisticated and high-costing post-HF methods, has been originally developed by Grimme.[50][49] It consists in the addition of dispersion correction based on the well-known dependence of the interactions between weakly overlapping systems as a function of R^{-6}.[95, 96] It appears particularly relevant to calculate non-covalent interactions within an acceptable accuracy/computational time ratio. The pairwise-like dispersion energy (E_{disp}) is thus calculated in a post self-consistent field fashion:

$$E = E_{DFT} + E_{disp} \qquad (IV.27)$$

where E_D is the dispersive energy having the aforesaid R_{AB}^{-6} dependent decay:[95]

$$E_{disp} = -s_6 \sum_{A}^{N-1} \sum_{B>A}^{N} \frac{C_6^{AB}}{R_{AB}^6} f_{dmp}(R_{AB}) \qquad (IV.28)$$

where s_6 is a functional-dependent scaling factor, C_6^{AB} is the dispersion coefficient for the atomic pair AB, R_{AB} is the interatomic distance for atoms A and B, and $f_{dmp}(R_{AB})$ is a damping function that avoids near-singularities for small interatomic distances.[95] The refined version DFT-D2 has been widely used over the past years.[51] We recently re-parameterized a new s_6 value (0.78) for the B3P86-D2 functional providing accuracy to evaluate π-stacking complexation in flavonoid derivatives.[82] Geometries of π-stacking complexes were thus obtained at the B3P86-D2($s_6 = 0.78$)/6-31+G(d,p) level. The robustness of this methodology was tested on flavonol and anthocyanidin self-association and flavonol:anthocyanidin complexation, with respect to high level calculations and experimental evidences of these chemical arrangements.[82]

The intermolecular interaction energies are calculated as follow:

$$\Delta E_{int} = E_{complex} - \sum_{i}^{\substack{Free \\ Partner}} E_i \qquad (IV.29)$$

where $E_{complex}$ denotes the energy of the complex, and the summation runs over both free partners. $E_{complex}$ includes basis set superposition error ($BSSE$), estimated using the traditional counterpoise method:

$$BSSE = [E_{AB}^{AB}(A) - E_A^{AB}(A)] + [E_{AB}^{AB}(B) - E_B^{AB}(B)] \qquad (IV.30)$$

---

[51] We are aware that that the new generation DFT-D3 has been developed including atom pairwise-specific dispersion coefficients and a new set of cutoff radii as defined in the damping function. The re-parameterized s_6 = 0.78 provided better accuracy for interaction energies in p-stacking complexes than DFT-D3.

where $E_{AB}^{AB}(A)$ and $E_{AB}^{AB}(B)$ are the energies of two given free partners A and B, respectively as obtained in the AB complex geometry with the AB basis set; $E_{A}^{AB}(A)$ and $E_{B}^{AB}(B)$ are the energies of A and B, respectively as obtained in the AB complex geometry with the A and B basis sets, respectively.

All these calculations were performed with ORCA.[58]

2.3. Solvent description

Solvent effects were taken into account implicitly. The integral equation formalism-polarizable continuum model (IEF-PCM)[53, 97] and conductor-like screening (COSMO[98])[52] models were used for thermodynamics of oxidative coupling and π-staking complexation, respectively. In these types of models the solute is embedded in a shape-adapted cavity surrounded by a dielectric continuum, which is characterized by its dielectric constant ε. Calculations were performed in benzene (ε = 2.27, n_D = 1.50), methanol (ε = 32.63, n_D = 1.33), dichloromethane (ε = 9.08, n_D = 1.42) and water (ε = 80.40, n_D = 1.33). Implicit PCM models are known to provide very reasonable descriptions of solvent effects. The general trend is globally accurate enough with polyphenols.[48] The only general weakness occurs for solvent having high H bonding capacities (mainly water). To improve accuracy, empirical corrections should be added, *e.g.* for HAT reactions, because adding explicitly water molecules would be too much computational resources consuming. In the present work, the discussion is mainly based on calculations performed in dichloromethane to be compared to experimental data. Calculations with other solvents were mostly performed to evaluate the global influence of the solvent polarity.[2]

3. Results and Discussion.

3.1. Initiation process: pterostilbene oxidation

Oxidation of polyphenols (ArOH) has extensively been rationalized, showing the importance of HAT from the OH groups of ArOH to the oxidative agent. Four different

---

[52] The default atom-sphere radii (*i.e.*, Van der Waals radii increased by 20%) as implemented in the ORCA package are used.

chemical pathways exist: i) HAT-PCET (Proton-Coupled Electron Transfer) (ArOH + R$^\bullet$ → ArO$^\bullet$ + RH);[28, 34] ii) electron transfer proton transfer (ET-PT) (ArOH + R$^\bullet$ → ArOH$^{+\bullet}$ + R$^-$ → ArO$^\bullet$ + RH);[36, 37] iii) sequential proton loss electron transfer (SPLET) mechanism (ArOH → ArO$^-$ + H$^+$; ArO$^-$ + R$^\bullet$ → ArO$^\bullet$ + R$^-$; R$^-$ + H$^+$ → RH);[25, 27, 38] and iv) adduct formation (ArOH + R$^\bullet$ → ArOH-R → other metabolites or ArO$^\bullet$ + RH in the presence of water).[48] The ArO-**H** BDE appeared as a relevant thermodynamic descriptor to evaluate the capacity of HAT, disregarding the mechanism of action.

BDEs of resveratrol and pterostilbene were re-calculated with the same methodology for the sake of comparison and were found in agreement with previous determination performed for resveratrol.[99] The 12-OH BDE is similar for both compounds, being 81.7 and 81.4 kcal.mol^{-1}, respectively (Table IV.6). The 3-OH BDE of resveratrol is much higher (88.1 kcal.mol^{-1}) and no OH group exists at this position in pterostilbene. This indicates that the HAT mechanism would preferentially take place at the 12-OH. However these BDE values are relatively high compared to those of strong H-atom donors such as quercetin or catechin.[12] Thus, the HAT requires the presence of a strong oxidant such as FeCl$_3$.6H$_2$O. Moreover, FeCl$_3$ is a strong Lewis acid while pterostilbene is a relatively strong base ($\eta = 4.3$ eV as seen in Table IV.6), showing that according to the HSBA principle the reaction between both compounds is very likely. The complexation with FeCl$_3$.6H$_2$O mainly occurs at O12. Indeed, the highest Fukui nucleophilic contribution is obtained for this group, $f_k^-(r)$ being 0.030 and 0.017 at the O-atom of the 12-OH and 1(3)-OCH$_3$ groups, respectively (Table IV.6).
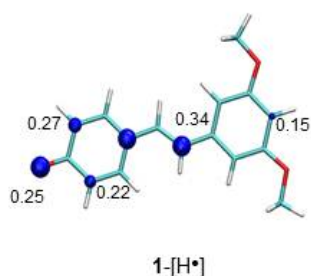
Figure IV.4. Spatial spin density distribution of the phenoxyl radical obtained after HAT from the 12-OH group of pterostilbene. Only atomic values higher than 0.1 are reported.

The spin density distribution of the phenoxyl radical generated after HAT from the native stilbene is delocalized over almost the entire molecule (Fig. IV.4).[53] This distribution highlights different reactive sites (mainly at O12, C9, C11, C13 and C7) for further reactions such as radical coupling. In principle this allows several different C-C or C-O combinations leading to several dimers. However all the possible dimers are not observed experimentally and the dimerisation appears strongly regio-selective as only compounds obtained from the C7-C7' and C7-C8' bond formation are observed, namely pallidol and ampelopsin F analogues (Fig. IV.3).

Table IV.6. Bond dissociation enthalpies (BDE, kcal.mol^{-1}), nucleophilic function ($f_k^-(r)$, |e|) and chemical hardness (η, eV) of pterostilbene, resveratrol, **RNA2** and **RNP2**.

Compound	Position	BDE	$f_k^-(r)$	η
Pterostilbene	1(3)-OMe	-	0.017	4.3
	12-OH	81.4	0.030	
Resveratrol	1(3)-OH	88.1	-	-
	12-OH	81.7		
RNA2	C6	28.9	-	-
RNP2	C6	30.8	-	-

3.2. π-Stacking complexation

Based on our previous hypothesis involving the formation of π-stacking self-association between two pterostilbene partners,[2] here we explore the different possibilities for π-stacking arrangements, namely Head-to-Head or Head-to-Tail with both possible approaches Re/Re or Re/Si (Fig. IV.5a). For all four possibilities the complexes were found to be stabilized by around 8 kcal.mol^{-1}: ΔE_{int} is -7.8, -8.1, -7.9 and -6.2 kcal.mol^{-1} for Head-to-Head (Re/Re), Head-to-Head (Re/Si), Head-to-Tail (Re/Re) and Head-to-Tail (Re/Si), respectively (Table IV.7). The differences in stabilizing energies between the different orientations appeared not significant, indicating that all possibilities may occur in solution with very similar Boltzmann ratio, *i.e.*, 25 % for each conformation.

---

[53] The spin density delocalization of the resveratrol radical obtained after HAT from O3 is less extended than from O12, the radical being not planar. This explains the higher BDE obtained for 3OH compare to 12OH. It must also be stressed that in this case, the spin density is very low at C7.

Table IV.7. Stabilizing energies (ΔE_{int}, kcal.mol^{-1}) of the self-association complexes of stilbene, pterostilbene and the mono-oxidized pterostilbene.

Orientation	stilbene		pterostilbene		mono-oxidized pterostilbene	
	Re/Re	*Re/Si*	*Re/Re*	*Re/Si*	*Re/Re*	*Re/Si*
Head-to-Tail	-3.2	-4.8	-7.9	-6.2	-7.4	-7.7
Head-to-Head	-3.2	-3.2	-7.8	-8.1	-	-
T-Shape	-7.3		-		-	

The minimum distance in these complexes is around 3.5 Å (Fig. IV.5a), as usually observed in π-stacking complexes. However, the π-stacking alignments are not ideal (Fig. IV.5a) as rings are displaced but not in a classical manner (so-called parallel-displaced stacking in which the center of one partner exactly faces a C-atom of the other partner). In these complexes intermolecular H-bonding slightly distorts the structures (the parallel alignment) but reinforces the stabilization.

As described in the literature[100] and confirmed here (at our level of calculation), the self-association is more likely of the T-shaped rather than co-facial π-stacked type in the absence of any substituent (*i.e.*, stilbene, Fig. IV.3 and IV.5b). The former arrangement is stabilized by around 7 kcal.mol^{-1} while the stabilizing energy of the latter re-arrangement is around 4 kcal.mol^{-1} (Fig. IV.5b and Table IV.7). The presence of OH and OMe groups, as in pterostilbene, induces i) an increase of π-conjugation due to their electron donor capacity, thus increasing the capacity for dispersive interactions between both partners, and ii) the capacity of intermolecular H-bond formation between both partners. As a consequence, the co-facial π-stacking between two pterostilbene units is dramatically favoured (ΔE_{int} ranging from -6.2 to -8.1 kcal mol^{-1}), no T-shaped arrangement being stabilized (Table IV.7). This surprisingly high stability of this substituted-stilbenoid self-association is attributed to the combination of both intermolecular H-bonding and π-stacking. The latter contribution remains crucial since no energetic potential well (*i.e.*, no stabilized complex) was found when using classical hybrid functionals that do not include dispersion (*e.g.*, B3P86).

The stabilizing energies are slightly higher than those we recently computed (at the same level of calculation) for quercetin self-association (ranging from -9.1 to -11.6 kcal mol^{-1}) and significantly higher than those obtained for cyanidin:quercetin complexes (-13.9 kcal mol^{-1}).[82] Quercetin self-association involves π-type interaction with three conjugated aromatic

rings vs. two for pterostilbene. This is however compensated by intermolecular H-bonding that is stronger in pterostilbene than in quercetin self-association complexes (averaged H-bond lengths of 2.1 and 2.7 Å, respectively).[54]

The solvent effect slightly influences stabilization when increasing the dielectric permittivity from 2.27 to 80.4. A usual asymptotic behaviour was observed (Fig. IV.6), showing that for ε higher than 10, the stabilizing energy remained unchanged. Specific interactions like intermolecular H-bonding with solvent cannot be taken into account here. This would require using explicit solvent (at least for the first solvation shell), which is unfeasible for these molecular systems at this level of theory. However this would be mainly critical in the case of water, while most of the experiments on which our previous study was based were performed in CH_2Cl_2 or CH_2Cl_2/MeOH 7:3 mixtures.[2]

---

[54] The Head-to-Tail Re/Si orientation presents both the highest p-stacking alignment and the lowest H-bond distance (2.3 Å) but also exhibits the lowest interaction energy (ΔE_{int} = -6.2 kcal.mol-1) with respect to the other geometries.

(a)

Head-to-Head orientations   Head-to-Tail orientations

Re/Re   *Re/Si*   *Re/Re*   *Re/Si*

(b)

T-shape   T/π-mixed shape   π-Shape

Re/Re   *Re/Si*
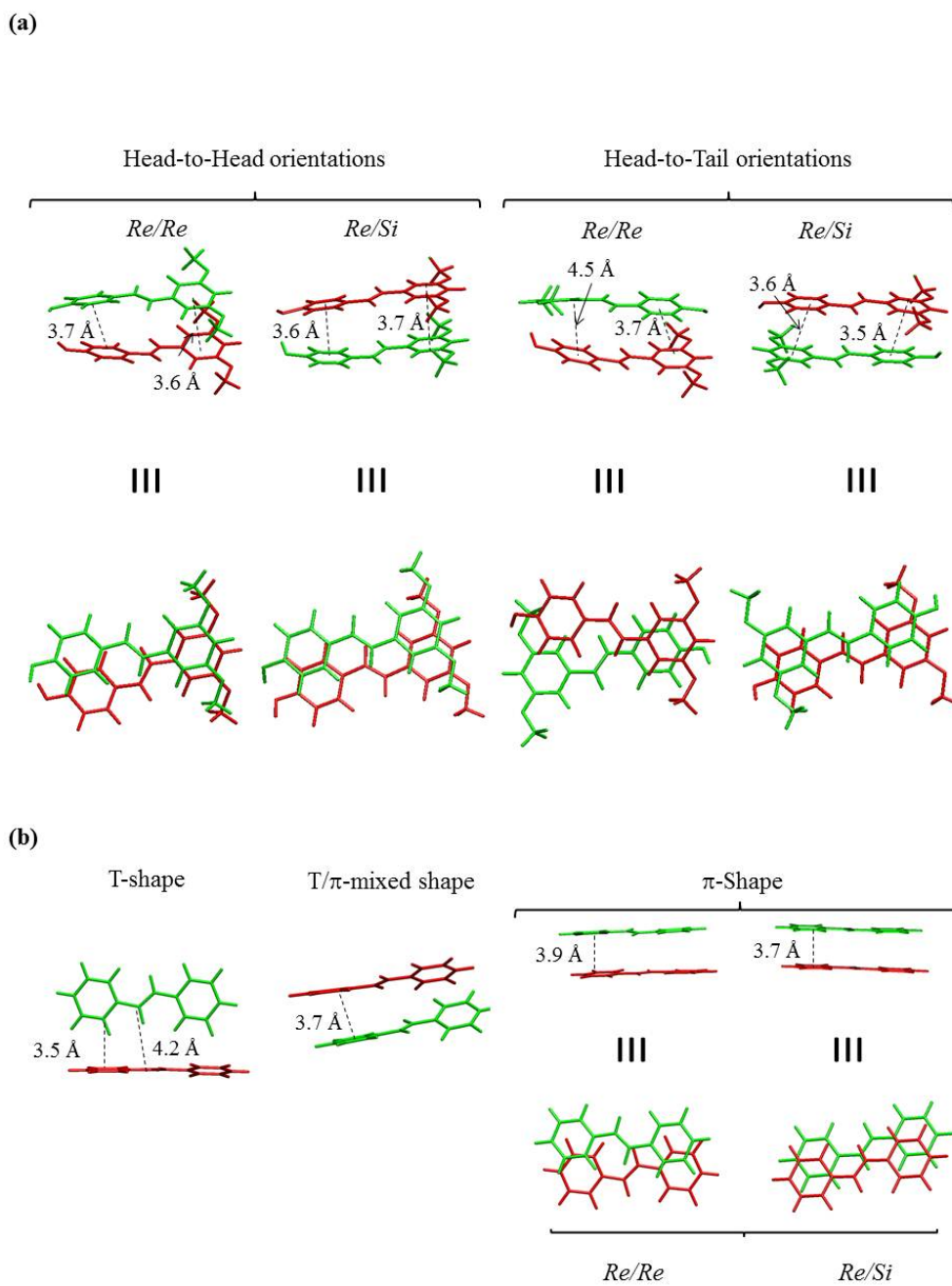
Figure IV.5. Optimized geometries for self-association complexes for a) pterostilbene and b) stilbene. Side (up) and top (bottom) views are proposed here for all π-stacking complexes.
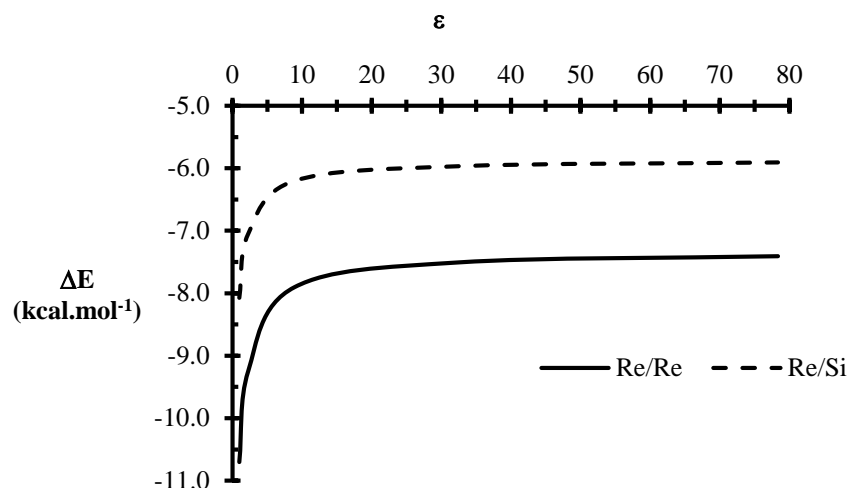
Figure IV.6. Impact of the solvent polarity on the binding energies of the Head-to-Tail π–π pterostilbene self-association complexes.

Such π-stacking arrangements make the atoms of the 7,8-double bond of both partners close to each other (C7-C7' distance is ranging from 3.4 Å to 4.6 Å, while that of C7-C8' from 3.6 Å to 4.0 Å, see Table IV.8). According to the spin density distribution occurring in the phenoxyl monomer (obtained after oxidation), it clearly appears that the easiest bond formations are C7-C7' or C7-C8' giving rise to pallidol and ampelopsin F analogues, respectively. Based on an accurate molecular picture of these complexes we confirm here that favourable arrangements are possible prior to oxidation in order to rationalize the regio-selective formation of pallidol and ampelopsin F.

Table IV.8. Bond distances (in Å) in Re/Re and Re/Si alignments for both head-to-tail and head-to-head orientations in the pterostilbene self-association complexes.

Alignment	Head-to-Tail		Head-to-Head	
	C7-C7	C7-C8	C7-C7	C7-C8
Re/Re	4.4	3.6	3.4	4.0
Re/Si	4.6	3.7	3.7	3.5

π-Stacking complexes in which one H-atom is removed from the OH group of one unit, namely neutral:radical complexes, can also exist in solution. The stabilizing energies of these complexes are very similar to those obtained for the neutral:neutral complexes (Table IV.7). This confirms that π-stacking complexation is not only a reactant-complex that would be

formed just before the bond formation and after oxidation of one partner, but truly exists in solution prior to oxidation.

3.3. The complete dimerisation mechanism: a matter of de-aromatization and re-aromatization

In principle, the bond formation that initiates the formation of pallidol and ampelopsin F types of compounds occurs either between one phenoxyl radical and the other native unit engaged in the π-stacking complex (radical-neutral reaction), or between two phenoxyl radicals (radical-radical reaction).

3.2.1. Radical-neutral reaction

It is of major importance to note that, contrary to our previous hypothesis,[2] the Re/Si and Re/Re (or Si/Si) approaches do not favour C7-C8' and C7-C7' bond formations, respectively. The bond formation is more likely driven by the Head-to-Tail or Head-to-Head orientations, C7-C7' and C7-C8' being slightly favoured by the Head-to-Head and Head-to-Tail, respectively (Table IV.8). However, when the bond is formed, the subsequent intermediates **RNA1** or **RNP1** (Scheme IV.1) can flip-flop around the torsion angle defined by this bond. The Gibbs energy of activation for such a torsion re-arrangement is around 8 kcal mol^{-1}, meaning that this step is not limiting in solution. In both cases, the lone pair electron, mainly located on C7 (Fig. IV.7), attacks C8' or C7', respectively. This bond formation is endergonic, with a Gibbs energy of 28.9 and 27.8 kcal mol^{-1}, respectively (Table IV.9).
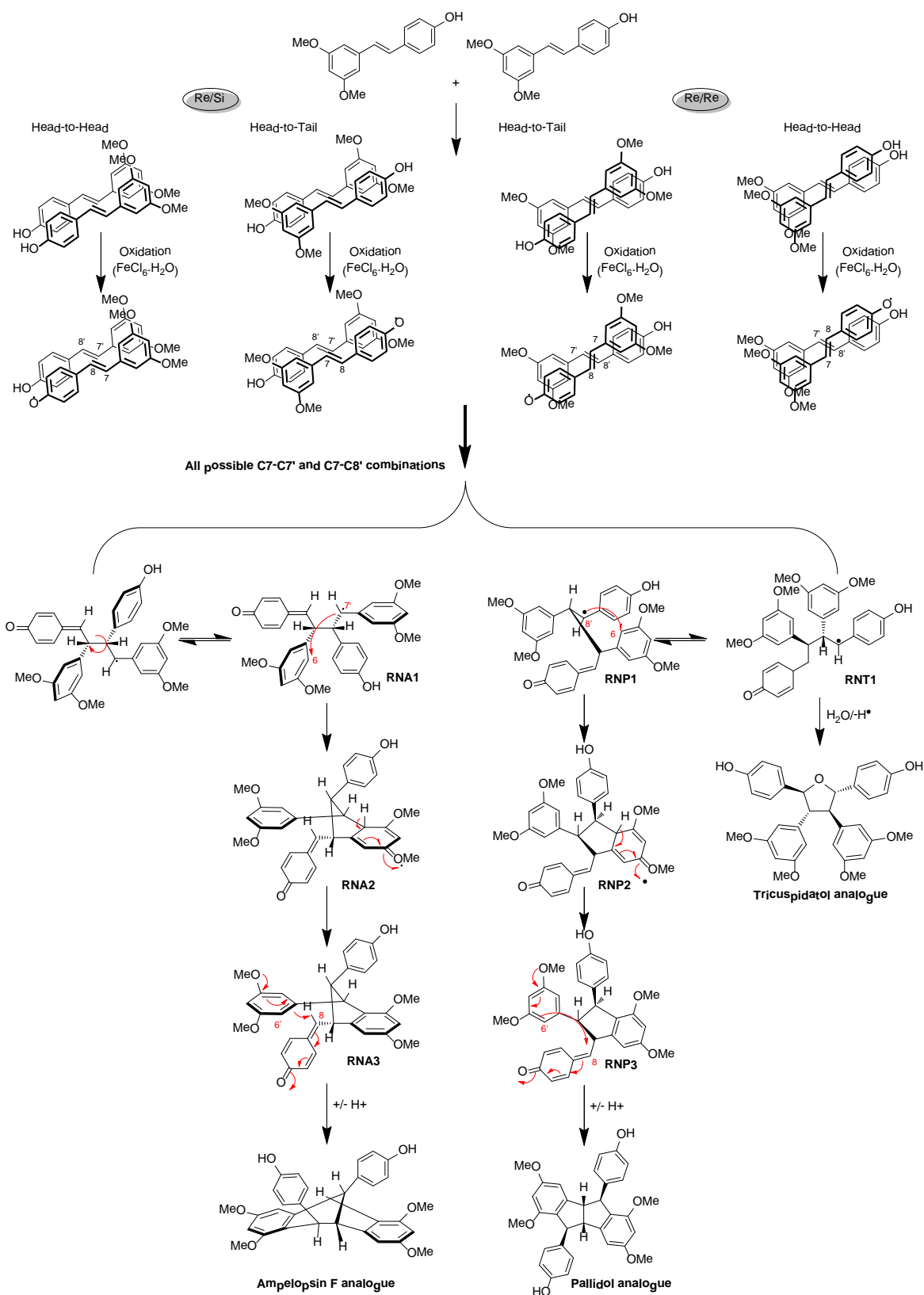
Scheme IV.1. Radical-neutral chemical pathway of the oxidative-coupling dimerisation process of pterostilbene.

Table IV.9. Gibbs energy ($\Delta G°$, kcal.mol^{-1}) of the radical-neutral and radical-radical mechanisms following schemes 1 and 2.

	Synthesis	Mechanism	Reaction	$\Delta G°$	$\Delta G^{\#}$	$\Delta\Delta G°$
(a)	Ampelopsin	Radical-Neutral	**RNA1** formation[a]	28.9	37.7	5.5[a]
			RNA1 → RNA2	-1.3	-	
			RNA3 → Ampelopsin F	-16.7	-	
(b)	Pallidol	Radical-Neutral	**RNP1** formation[a]	27.8	35.8	0.0[a]
			RNP1 → RNP2	5.5	-	
			RNP3 → Pallidol	-29.5	-	
		Radical-Radical	**RRP1** formation[b]	8.3	-	
			RRP1 → RNP2	-24.1	-	
(c)	Tricuspidatol	Radical-Neutral	**RNT1** formation[a]	28.0	-	
			RNP1 → RNT1	0.0	8.1	
		Radical-Radical	**RRT1** formation[b]	9.5	-	

[a] refers to Scheme 1
[b] refers to Scheme 2

This indicates that the energy consumed to break the π-conjugated system is higher than the energy released to establish the C7-C8' or C7-C7' covalent bonds. The spin distributions of **RNA1** and **RNP1** are poorly delocalized, less than in the phenoxyl radical partner, thus confirming the destabilization of the products (Fig. IV.7). Moreover, this reaction exhibits a very similar Gibbs energy of activation for both pathways (37.7 and 35.8 kcal mol^{-1}, respectively). This shows that the bond formation is the limiting step, also confirming that the torsion re-arrangement is not limiting.
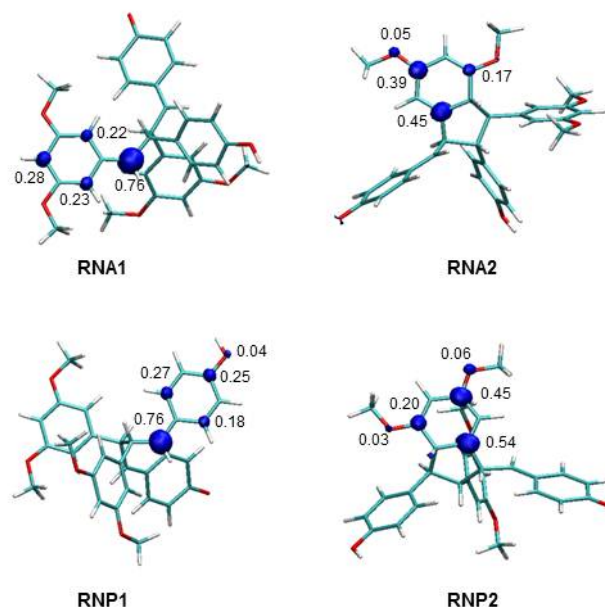
Figure IV.7. Spin density distributions of the radical intermediates involved in the different chemical pathways. Only atomic values higher than 0.1 are quoted here.

After the establishment of the bond between C7 and C8' (**RNA1**) or C7 and C7' (**RNP1**), the electron enriched atom C7' attacks C6 (-1.3 kcal mol^{-1}) or C8' (5.5 kcal mol^{-1}) to produce semi fused ring systems (**RNA2** and **RNP2**, respectively, see Scheme IV.1). The Gibbs energies of these reactions are close to 0 (slightly negative and positive, respectively) due to the loss of aromaticity in the methide quinone group, only partially compensated by spin delocalization (Fig. IV.7). The formation of **RNA2** appears easier than that of **RNP2** as in the former product, the spin is better delocalized (spin densities on the atom C6' of 0.45 and 0.54 for both intermediates, respectively, see Fig. IV.7). Further dissociation of H-atom from **RNA2** and **RNP2** (Scheme IV.1), leading **RNA3** and **RNP3**, respectively, is highly favoured as the corresponding C-H BDEs are very low *i.e.*, 34.2 and 35.2 kcal mol^{-1}, respectively (Table IV.6). The HAT from these intermediates (**RNA2** and **RNP2**) is so easy (highly labile H-atom) that these species can be reduced by any surrounding molecules including other FeCl$_3$ molecules or other intermediates present in the solution. Both intermediates **RNA3** and **RNP3** complete the semi-fused ring systems by nucleophilic attack of C6' onto C8 followed by re-aromatization leading to ampelopsin F and pallidol analogues, respectively. This step is crucial to rationalize the entire process, exhibiting Gibbs energies of -16.7 and -29.5 kcal mol^{-1}, respectively. Following the radical-neutral process, the overall formation of pallidol analogue thus appears

221

thermodynamically favoured with respect to that of ampelopsin F ($\Delta\Delta G° = 5.5$ kcal.mol^{-1}, see Table IV.7).

3.2.2. Radical-radical reaction

In principle this reaction may occur between C7 and C7' or C8' depending on the complex-of-approach. However, when the second unit is oxidised, two phenoxyl radicals face each other, both having a high spin density on C7 and C7' atoms. This leads to a reaction that occurs "spontaneously",[55] that is following a potential energy surface as described for other polyphenol dimerisations.[56][92] In this case, the reaction is exothermic (ΔH of -6.3 kcal mol^{-1}) with a very low energetic barrier. Taking entropy into account, this reaction appears endergonic (Gibbs energy of 8.3 kcal mol^{-1}), suggesting that the formation of the closed-shell system **RRP1** (from two radicals) does not compensate the loss of aromaticity of both phenolic rings. This means that the reaction can only occur if it continues to evolve to a more stable molecular system (Scheme IV.2). This step of the radical-radical process is however much more favourable than that of the radical-neutral reaction. The subsequent nucleophilic attack of C6' on C8, leading to **RNP3** (Scheme IV.2) is highly favourable (Gibbs energy of -24.1 kcal.mol^{-1}), leading to the pallidol analogue.

---

[55] When optimizing a radical-radical complex, the C7-C7' bond is automatically formed, meaning that i) no radical-radical complex may exist in solution and ii) the double oxidation systematically produces the C7-C7' bond formation.

[56] This is a typical radical-radical reaction in which the system is i) a triplet state when both units are far from each other, ii) a singlet when the bond is formed and iii) a complex mixture of both triplet and singlet states.
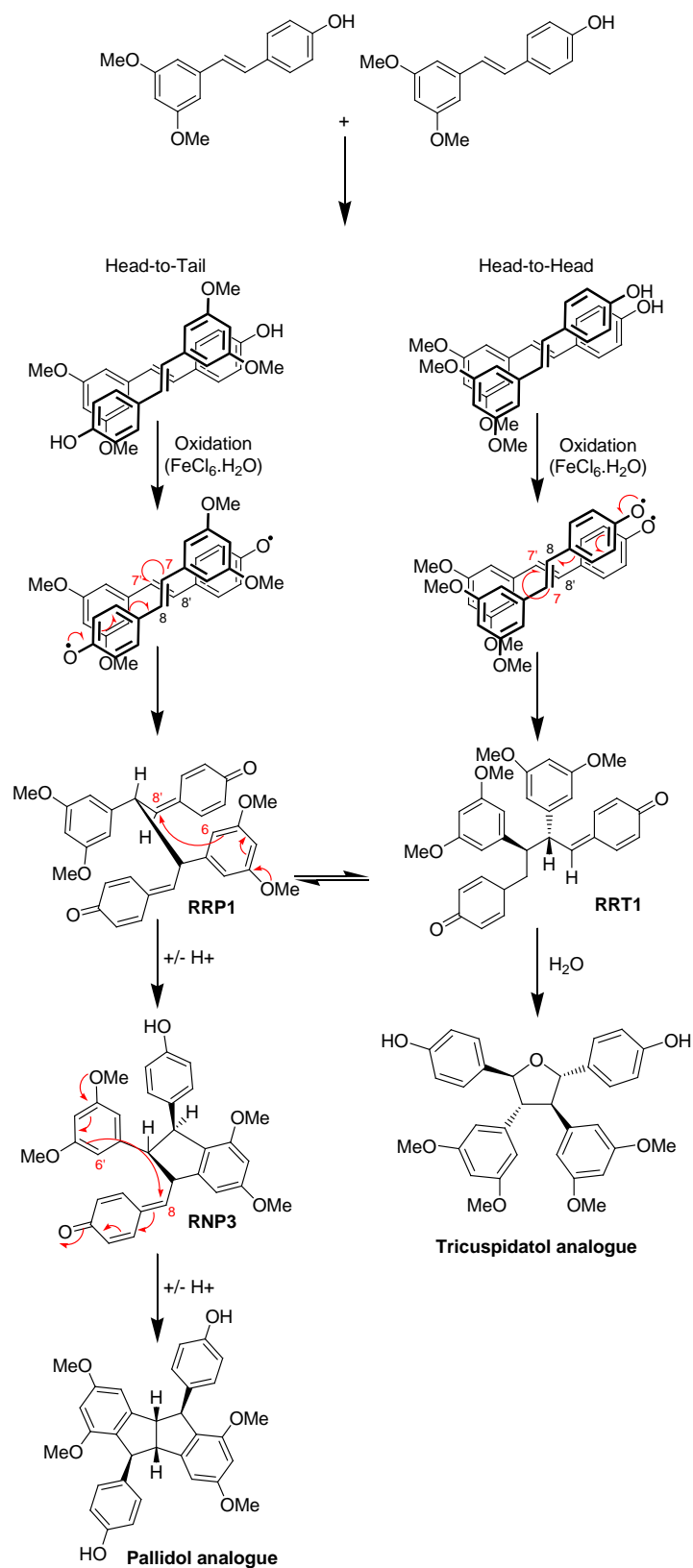
Scheme IV.2. Radical-Radical chemical pathway of the oxidative-coupling dimerisation process of pterostilbene.

The C7-C8' bond formation is highly improbable with respect to the C7-C7' bond formation, mainly due to the very low spin density at C8', making this site much less reactive than the neighbouring C7' atom. Thus the radical-radical pathway intrinsically avoids the formation of the ampelopsin F analogue, only providing the pallidol analogue.

4. Concluding remarks

Based on an accurate quantum methodology (in particular taking dispersive effects into account) the present work has addressed many of the concerns hypothesized from experimental data on silbenoid oligomerisation.[2]

First, the occurrence of π-stacking complexes made of substituted stilbenoid derivatives is definitely confirmed; they may exist in solution, prior to oxidation. These complexes are stabilized by intermolecular H-bonding and π-stacking interactions. Solvent effects, substitution pattern or metal oxidant coordination are expected to profoundly influence these interactions, as all these factors tend to alter the electronic distribution in the system. One of the clearest case concerns addition of Ag-atom in solution. In the presence of AgOAc, pallidol and ampelopsin F analogues are not formed; only ε-vinferifin derivatives are formed.[2] The production of this type of compounds involves neither C7-C7' nor C7-C8' bond formation, but C7-C11'. These Ag atoms efficiently bind the 7,8-double bond (probably giving 2:1 stilbenoid:Ag coordination complexes), breaking planarity and making π-stacking complexation very unlikely.

The presence of non-covalent stacks prior to oxidation fully explains the regio-selectivity that was observed in pterostilbene dimerisation.[2] Supramolecular chemistry appears here mandatory to tackle all concerns of silbenoid oligomerisation.

Second, the distinction between radical-neutral and radical-radical reactions is rationalized. It is clear that an ampelopsin F analogue comes from the C7-C8' bond formation while a pallidol structure derives from the C7-C7' bond formation. The formation of π-stacking complexes fully explains the regio-selectivity at the 7,8-double bond but does not drive the regio-selectivity of the C7-C7' or C7-C8' bond formations. However the thermodynamics of the entire process is clearly in favour of the formation of pallidol derivatives, which is in perfect agreement with the 1:2 ratio obtained for ampelopsin F:pallidol analogues.[2] It must be

stressed that the C7-C7' bond formation can also provide the well stabilized tricuspidatol-like product, in the presence of water according to the mechanism reported on Schemes IV.1 and IV.2.

The radical-radical reaction may only provide pallidol-like derivatives and cannot appear as the major mechanism. If that was the case, the pallidol analogue concentration would be much higher than that of ampelopsin F when considering the thermodynamics and kinetics of this process.

Bibliography

[1]   Kosinova, P., *et al.*, *Dimerisation process of silybin-type flavonolignans: insights from theory.* ChemPhysChem, 2011. **12**: p. 1135-1142.

[2]   Velu, S.S., *et al.*, *Regio- and Stereoselective Biomimetic Synthesis of Oligostilbenoid Dimers from Resveratrol Analogues: Influence of the Solvent, Oxidant, and Substitution.* Chemistry – A European Journal, 2008. **14**: p. 11376-11384.

[3]   Hertog, M.G., *et al.*, *Dietary antioxidant flavonoids and risk of coronary heart disease: the Zutphen Elderly Study.* Lancet, 1993. **342**: p. 1007-1011.

[4]   Blake, D.R., R.E. Allen, and J. Lunec, *Free radicals in biological systems - a review orientated to inflammatory processes.* British Medical Bulletin, 1987. **43**: p. 371-385.

[5]   Commenges, D., *et al.*, *Intake of flavonoids and risk of dementia.* European Journal of Epidemiology, 2000. **16**: p. 357-363.

[6]   Boots Agnes, W., *et al.*, *The quercetin paradox.* Toxicology and Applied Pharmacology, 2007. **222**: p. 89-96.

[7]   Saller, R., R. Meier, and R. Brignoli, *The use of silymarin in the treatment of liver diseases.* Drugs, 2001. **61**: p. 2035-2063.

[8]   Gazak, R., *et al.*, *Large-scale separation of silybin diastereoisomers using lipases.* Process Biochemistry (Amsterdam, Netherlands), 2010. **45**: p. 1657-1663.

[9]   Rice-Evans, C.A. and S.A.B. Van Acker, *Flavonoids in health and disease*, ed. M. Decker1998, New York.

[10]   Rice-Evans, C., N.J. Miller, and G. Paganga, *Structure-antioxidant activity relationships of flavonoids and phenolic acids.* Free Radical Biology & Medicine, 1996. **20**: p. 933-956.

[11]   Cos, P., *et al.*, *Structure-Activity Relationship and Classification of Flavonoids as Inhibitors of Xanthine Oxidase and Superoxide Scavengers.* Journal of Natural Products, 1998. **61**: p. 71-76.

[12]   Trouillas, P., *et al.*, *A DFT study of the reactivity of OH groups in quercetin and taxifolin antioxidants: The specificity of the 3-OH site.* Food Chemistry, 2006. **97**: p. 679-688.

[13]   Kozlowski, D., *et al.*, *Density Functional Theory Study of the Conformational, Electronic, and Antioxidant Properties of Natural Chalcones.* Journal of Physical Chemistry A, 2007. **111**: p. 1138-1145.

[14]   Trouillas, P., *et al.*, *Mechanism of the Antioxidant Action of Silybin and 2,3-Dehydrosilybin Flavonolignans: A Joint Experimental and Theoretical Study.* Journal of Physical Chemistry A, 2008. **112**: p. 1054-1063.

[15]   Anouar, E., *et al.*, *Free Radical Scavenging Properties of Guaiacol Oligomers: A Combined Experimental and Quantum Study of the Guaiacyl-Moiety Role.* Journal of Physical Chemistry A, 2009. **113**: p. 13881-13891.

[16]   Leopoldini, M., *et al.*, *Structure, Conformation, and Electronic Properties of Apigenin, Luteolin, and Taxifolin Antioxidants. A First Principle Theoretical Study.* Journal of Physical Chemistry A, 2004. **108**: p. 92-96.

[17]   Leopoldini, M., *et al.*, *Density functional computations of the energetic and spectroscopic parameters of quercetin and its radicals in the gas phase and in solvent.* Theoretical Chemistry Accounts, 2004. **111**: p. 210-216.

[18]   Lucarini, M., G.F. Pedulli, and M. Guerra, *A Critical Evaluation of the Factors Determining the Effect of Intramolecular Hydrogen Bonding on the O   □H Bond Diss Catechol and of Flavonoid Antioxidants.* Chemistry – A European Journal, 2004. **10**: p. 933-939.

[19]   Priyadarsini, K.I., *et al.*, *Role of phenolic O-H and methylene hydrogen on the free radical reactions and antioxidant activity of curcumin.* Free Radical Biology & Medicine, 2003. **35**: p. 475-484.

[20]   Fiorucci, S., *et al.*, *DFT Study of Quercetin Activated Forms Involved in Antiradical, Antioxidant, and Prooxidant Biological Processes.* Journal of Agricultural and Food Chemistry, 2007. **55**: p. 903-911.

[21]   Fiorucci, S., *et al.*, *Oxygenolysis of flavonoid compounds: DFT description of the mechanism for quercetin.* ChemPhysChem, 2004. **5**: p. 1726-1733.

[22]   Russo, N., M. Toscano, and N. Uccella, *Semiempirical Molecular Modeling into Quercetin Reactive Site: Structural, Conformational, and Electronic Features.* Journal of Agricultural and Food Chemistry, 2000. **48**: p. 3232-3237.

[23]   Kong, L., L.-F. Wang, and H.-Y. Zhang, *Theoretical elucidation on mechanism and reactivity of bisphenol A derivatives as inhibitors and radical scavengers in methacrylate polymerization.* Journal of Molecular Structure: THEOCHEM, 2005. **716**: p. 27-31.

[24]   Foti, M.C., *et al.*, *Reaction of Phenols with the 2,2-Diphenyl-1-picrylhydrazyl Radical. Kinetics and DFT Calculations Applied To Determine ArO-H Bond Dissociation Enthalpies and Reaction Mechanism.* Journal of Organic Chemistry, 2008. **73**: p. 9270-9282.

[25]   Foti, M.C., C. Daquino, and C. Geraci, *Electron-Transfer Reaction of Cinnamic Acids and Their Methyl Esters with the DPPH.bul. Radical in Alcoholic Solutions.* Journal of Organic Chemistry, 2004. **69**: p. 2309-2314.

[26]   Leopoldini, M., *et al.*, *Antioxidant Properties of Phenolic Compounds: H-Atom versus Electron Transfer Mechanism.* Journal of Physical Chemistry A, 2004. **108**: p. 4916-4922.

[27]   Litwinienko, G. and K.U. Ingold, *Abnormal solvent effects on hydrogen atom abstractions. 1. The reactions of phenols with 2,2-diphenyl-1-picrylhydrazyl (dpph*) in alcohols.* Journal of Organic Chemistry, 2003. **68**: p. 3433-3438.

[28]   De Heer, M.I., *et al.*, *Hydrogen Atom Abstraction Kinetics from Intramolecularly Hydrogen Bonded Ubiquinol-0 and Other (Poly)methoxy Phenols.* Journal of the American Chemical Society, 2000. **122**: p. 2355-2360.

227

[29]   Snelgrove, D.W.*, et al.*, *Kinetic Solvent Effects on Hydrogen-Atom Abstractions: Reliable, Quantitative Predictions via a Single Empirical Equation for.* Journal of the American Chemical Society, 2001. **123**: p. 469-477.

[30]   MacFaul, P.A., K.U. Ingold, and J. Lusztyk, *Kinetic Solvent Effects on Hydrogen Atom Abstraction from Phenol, Aniline, and Diphenylamine. The Importance of Hydrogen Bonding on Their Radical-Trapping (Antioxidant) Activities1.* Journal of Organic Chemistry, 1996. **61**: p. 1316-1321.

[31]   Foti, M.C.*, et al.*, *Influence of "Remote" Intramolecular Hydrogen Bonds on the Stabilities of Phenoxyl Radicals and Benzyl Cations.* Journal of Organic Chemistry, 2010. **75**: p. 4434-4440.

[32]   DiLabio, G.A. and E.R. Johnson, *Lone Pair−π and π−π Interactions Play an Important Role in Proton-Coupled Electron Transfer Reactions.* Journal of the American Chemical Society, 2007. **129**: p. 6199-6203.

[33]   Lingwood, M.*, et al.*, *MPW1K Performs Much Better than B3LYP in DFT Calculations on Reactions that Proceed by Proton-Coupled Electron Transfer (PCET).* Journal of Chemical Theory and Computation, 2006. **2**: p. 740-745.

[34]   Burton, G.W.*, et al.*, *Autoxidation of biological molecules. 4. Maximizing the antioxidant activity of phenols.* Journal of the American Chemical Society, 1985. **107**: p. 7053-7065.

[35]   Litwinienko, G. and K.U. Ingold, *Solvent Effects on the Rates and Mechanisms of Reaction of Phenols with Free Radicals.* Accounts of Chemical Research, 2007. **40**: p. 222-230.

[36]   Jovanovic, S.V.*, et al.*, *Flavonoids as Antioxidants.* Journal of the American Chemical Society, 1994. **116**: p. 4846-4851.

[37]   Jovanovic, S.V.*, et al.*, *Reduction potentials of flavonoid and model phenoxyl radicals. Which ring in flavonoids is responsible for antioxidant activity?* Journal of the Chemical Society, Perkin Transactions 2: Physical Organic Chemistry, 1996: p. 2497-2504.

[38]   Zhang, H.-Y. and H.-F. Ji, *How vitamin E scavenges DPPH radicals in polar protic media.* New Journal of Chemistry, 2006. **30**: p. 503-504.

[39]   Brede, O.*, et al.*, *Localized Electron Transfer in Nonpolar Solution: Reaction of Phenols and Thiophenols with Free Solvent Radical Cations.* Journal of Physical Chemistry A, 2001. **105**: p. 3757-3764.

[40]   Galati, G. and P.J. O'Brien, *Potential toxicity of flavonoids and other dietary phenolics: significance for their chemopreventive and anticancer properties.* Free Radical Biology & Medicine, 2004. **37**: p. 287-303.

[41]   Crozier, A., D. Del Rio, and M.N. Clifford, *Bioavailability of dietary flavonoids and phenolic compounds.* Molecular Aspects of Medicine, 2010. **31**: p. 446-467.

[42]   Goupy, P.*, et al.*, *Dietary antioxidants as inhibitors of the heme-induced peroxidation of linoleic acid: Mechanism of action and synergism.* Free Radical Biology and Medicine, 2007. **43**: p. 933-946.

[43]   Roche, M*., et al.*, *Antioxidant activity of olive phenols: mechanistic investigation and characterization of oxidation products by mass spectrometry.* Organic & Biomolecular Chemistry, 2005. **3**: p. 423-430.

[44]   Vulcain, E*., et al.*, *Inhibition of the metmyoglobin-induced peroxidation of linoleic acid by dietary antioxidants: Action in the aqueous vs. lipid phase.* Free Radical Research, 2005. **39**: p. 547-563.

[45]   Sánchez-Moreno, C., J. A. Larrauri, and F. Saura-Calixto, *Free radical scavenging capacity and inhibition of lipid oxidation of wines, grape juices and related polyphenolic constituents.* Food Research International, 1999. **32**: p. 407-412.

[46]   Feng, Y*., et al.*, *Assessment of Experimental Bond Dissociation Energies Using Composite ab Initio Methods and Evaluation of the Performances of Density Functional Methods in the Calculation of Bond Dissociation Energies.* Journal of Chemical Information and Computer Sciences, 2003. **43**: p. 2005-2013.

[47]   Kosinova, P*., et al.*, *H-atom acceptor capacity of free radicals used in antioxidant measurements.* International Journal of Quantum Chemistry, 2011. **111**: p. 1131-1142.

[48]   Anouar, E*., et al.*, *New aspects of the antioxidant properties of phenolic acids: a combined theoretical and experimental approach.* Physical Chemistry Chemical Physics, 2009. **11**: p. 7659-7668.

[49]   Grimme, S., *Accurate description of van der Waals complexes by density functional theory including empirical corrections.* Journal of Computational Chemistry, 2004. **25**: p. 1463-1473.

[50]   Di Meo, F*., et al.*, *Highlights on Anthocyanin Pigmentation and Copigmentation: A Matter of Flavonoid π-Stacking Complexation To Be Described by DFT-D.* Journal of Chemical Theory and Computation, 2012. **8**: p. 2034-2043.

[51]   Frisch, M.J*., et al.*, *Gaussian 03, Revision C.02*, ed. I. Gaussian2004, Wallingford CT.

[52]   Zhao, Y. and D.G. Truhlar, *Hybrid Meta Density Functional Theory Methods for Thermochemistry, Thermochemical Kinetics, and Noncovalent Interactions: The MPW1B95 and MPWB1K Models and Comparative Assessments for Hydrogen Bonding and van der Waals Interactions.* Journal of Physical Chemistry A, 2004. **108**: p. 6908-6918.

[53]   Cossi, M*., et al.*, *New developments in the polarizable continuum model for quantum mechanical and classical calculations on molecules in solution.* Journal of Chemical Physics, 2002. **117**: p. 43-54.

[54]   Tomasi, J., B. Mennucci, and R. Cammi, *Quantum Mechanical Continuum Solvation Models.* Chemical Reviews (Washington, DC, United States), 2005. **105**: p. 2999-3093.

[55]   Liptak, M.D. and G.C. Shields, *Accurate pKa Calculations for Carboxylic Acids Using Complete Basis Set and Gaussian-n Models Combined with CPCM Continuum Solvation Methods.* Journal of the American Chemical Society, 2001. **123**: p. 7314-7319.

[56]   Liptak, M.D*., et al.*, *Absolute pKa Determinations for Substituted Phenols.* Journal of the American Chemical Society, 2002. **124**: p. 6421-6427.

[57] Brown, T.N. and N. Mora-Diez, *Computational Determination of Aqueous pKa Values of Protonated Benzimidazoles (Part 1)*. Journal of Physical Chemistry B, 2006. **110**: p. 9270-9279.

[58] Neese, F., *The ORCA program system*. Wiley Interdisciplinary Reviews: Computational Molecular Science, 2012. **2**: p. 73-78.

[59] Chiodo, S.G.*, et al.*, *The inactivation of lipid peroxide radical by quercetin. A theoretical insight*. Physical Chemistry Chemical Physics, 2010. **12**: p. 7662-7670.

[60] Eyring, H., *The Activated Complex in Chemical Reactions*. Journal of Chemical Physics, 1935. **3**: p. 107-115.

[61] Truhlar, D.G., W.L. Hase, and J.T. Hynes, *Current status of transition-state theory*. The Journal of Physical Chemistry, 1983. **87**: p. 2664-2682.

[62] Tejero, I.*, et al.*, *Tunneling in Green Tea: Understanding the Antioxidant Activity of Catechol-Containing Compounds. A Variational Transition-State Theory Study*. Journal of the American Chemical Society, 2007. **129**: p. 5846-5854.

[63] Skodje, R.T. and D.G. Truhlar, *Parabolic tunneling calculations*. Journal of Physical Chemistry, 1981. **85**: p. 624-628.

[64] Belyakov, V.A., V.A. Roginsky, and W. Bors, *Rate constants for the reaction of peroxyl free radical with flavonoids and related compounds as determined by the kinetic chemiluminescence method*. Journal of the Chemical Society, Perkin Transactions 2, 1995: p. 2319-2326.

[65] Abraham, M.H.*, et al.*, *Hydrogen bonding. Part 10. A scale of solute hydrogen-bond basicity using log K values for complexation in tetrachloromethane*. Journal of the Chemical Society, Perkin Transactions 2: Physical Organic Chemistry, 1990: p. 521-529.

[66] Bixon, M. and J. Jortner, *Electron Transfer—from Isolated Molecules to Biomolecules*. Advances in Chemical Physics2007: John Wiley & Sons, Inc. 35-202.

[67] Van Vooren, A.*, et al.*, *Impact of Bridging Units on the Dynamics of Photoinduced Charge Generation and Charge Recombination in Donor–Acceptor Dyads*. ChemPhysChem, 2007. **8**: p. 1240-1249.

[68] Singh, U.C. and P.A. Kollman, *An approach to computing electrostatic charges for molecules*. Journal of Computational Chemistry, 1984. **5**: p. 129-145.

[69] Besler, B.H., K.M. Merz, Jr., and P.A. Kollman, *Atomic charges derived from semiempirical methods*. Journal of Computational Chemistry, 1990. **11**: p. 431-439.

[70] Marcus, R.A., *Theory of electron-transfer reactions. VI. Unified treatment for homogeneous and electrode reactions*. Journal of Chemical Physics, 1965. **43**: p. 679-701.

[71] Ridley, J. and M. Zerner, *An intermediate neglect of differential overlap technique for spectroscopy: Pyrrole and the azines*. Theoretical Chemistry Accounts: Theory, Computation, and Modeling (Theoretica Chimica Acta), 1973. **32**: p. 111-134.

[72]   Lemaur, V.*, et al.*, *Photoinduced Charge Generation and Recombination Dynamics in Model Donor/Acceptor Pairs for Organic Solar Cell Applications: A Full Quantum-Chemical Treatment.* Journal of the American Chemical Society, 2005. **127**: p. 6077-6086.

[73]   Galano, A.*, et al.*, *Role of the reacting free radicals on the antioxidant mechanism of curcumin.* Chemical Physics, 2009. **363**: p. 13-23.

[74]   Musialik, M.*, et al.*, *Acidity of hydroxyl groups: an overlooked influence on antiradical properties of flavonoids.* Journal of Organic Chemistry, 2009. **74**: p. 2699-2709.

[75]   Musialik, M. and G. Litwinienko, *Scavenging of dpph.bul. Radicals by Vitamin E Is Accelerated by Its Partial Ionization: the Role of Sequential Proton Loss Electron Transfer.* Organic Letters, 2005. **7**: p. 4951-4954.

[76]   Gorham, J., *The Biochemistry of the Stilbenoids*1995: Chapman & Hall. 262 pp.

[77]   Weber, J.F.F.*, et al.*, *Heimiol A, a new dimeric stilbenoid from Neobalanocarpus heimii.* Tetrahedron Letters, 2001. **42**: p. 4895-4897.

[78]   Velu, S.S., N.F. Thomas, and J.-F.F. Weber, *Strategies and methods for the syntheses of natural oligomeric stilbenoids and analogues.* Current Organic Chemistry, 2012. **16**: p. 605-662.

[79]   Snyder, S.A., A. Gollner, and M.I. Chiriac, *Regioselective reactions for programmable resveratrol oligomer synthesis.* Nature, 2011. **474**: p. 461-466.

[80]   Snyder, S.A.*, et al.*, *Total synthesis of diverse carbogenic complexity within the resveratrol class from a common building block.* Journal of the American Chemical Society, 2009. **131**: p. 1753-1765.

[81]   Snyder, S.A., A.L. Zografos, and Y. Lin, *Total synthesis of resveratrol-based natural products: a chemoselective solution.* Angewandte Chemie International Edition, 2007. **46**: p. 8186-8191.

[82]   Di Meo, F.*, et al.*, *Highlights on Anthocyanin Pigmentation and Copigmentation: A Matter of Flavonoid π-Stacking Complexation To Be Described by DFT-D.* Journal of Chemical Theory and Computation, 2012. **8**: p. 2034-2043.

[83]   Zondlo, N.J., *Non-covalent interactions: Fold globally, bond locally.* Nature Chemical Biology, 2010. **6**: p. 567-568.

[84]   Hunter, C.A. and J.K.M. Sanders, *The nature of .pi.-.pi. interactions.* Journal of the American Chemical Society, 1990. **112**: p. 5525-5534.

[85]   Aragó, J.*, et al.*, *Ab Initio Modeling of Donor–Acceptor Interactions and Charge-Transfer Excitations in Molecular Complexes: The Case of Terthiophene–Tetracyanoquinodimethane.* Journal of Chemical Theory and Computation, 2011. **7**: p. 2068-2077.

[86]   Gierschner, J., J. Cornil, and H.-J. Egelhaaf, *Optical Bandgaps of π-Conjugated Organic Materials at the Polymer Limit: Experiment and Theory.* Advanced Materials, 2007. **19**: p. 173-191.

[87]   Rezazgui, O.*, et al.*, *One-pot and catalyst-free amidation of ester: a matter of non-bonding interactions.* Tetrahedron Letters, 2011. **52**: p. 6796-6799.

[88]   Coates, G.W.*, et al.*, *Phenyl-perfluorophenyl stacking interactions: a new strategy for supermolecule construction.* Angewandte Chemie International Edition, 1997. **36**: p. 248-251.

[89]   Bonechi, C.*, et al.*, *Stacking interaction study of trans-resveratrol (trans-3,5,4'-trihydroxystilbene) in solution by Nuclear Magnetic Resonance and Fourier Transform Infrared Spectroscopy.* Magnetic Resonance in Chemistry, 2008. **46**: p. 625-629.

[90]   Trouillas, P., Marsal, P., Siri, D., Lazzaroni, R., Duroux, J. L. , *A DFT study of the reactivity of OH groups in quercetin and taxifolin antioxydants : The specificity of the 3-OH site.* Food Chemistry, 2006. **97**: p. 10.

[91]   Anouar, E.*, et al.*, *Free Radical Scavenging Properties of Guaiacol Oligomers: A Combined Experimental and Quantum Study of the Guaiacyl-Moiety Role.* Journal of Physical Chemistry A, 2009. **113**: p. 13881-13891.

[92]   Kosinova, P.*, et al.*, *Dimerization Process of Silybin-Type Flavonolignans: Insights from Theory.* ChemPhysChem, 2011. **12**: p. 1135-1142.

[93]   Yang, W. and W.J. Mortier, *The use of global and local molecular parameters for the analysis of the gas-phase basicity of amines.* Journal of the American Chemical Society, 1986. **108**: p. 5708-5711.

[94]   Frisch, M.J.*, et al.*, *Gaussian 09, Revision A.02*, 2009: Wallingford CT.

[95]   Grimme, S., *Semiempirical GGA-type density functional constructed with a long-range dispersion correction.* Journal of Computational Chemistry, 2006. **27**: p. 1787-1799.

[96]   Grimme, S.*, et al.*, *A consistent and accurate ab initio parametrization of density functional dispersion correction (DFT-D) for the 94 elements H-Pu.* Journal of Chemical Physics, 2010. **132**: p. 154104-154119.

[97]   Tomasi, J., B. Mennucci, and R. Cammi, *Quantum Mechanical Continuum Solvation Models.* Chemical Reviews, 2005. **105**: p. 2999-3094.

[98]   Sinnecker, S.*, et al.*, *Calculation of Solvent Shifts on Electronic g-Tensors with the Conductor-Like Screening Model (COSMO) and Its Self-Consistent Generalization to Real Solvents (Direct COSMO-RS).* Journal of Physical Chemistry A, 2006. **110**: p. 2235-2245.

[99]   Cao, H.*, et al.*, *Density functional theory calculations for resveratrol.* Bioorganic and Medicinal Chemistry Letters, 2003. **13**: p. 1869-1871.

[100]   Gierschner, J. and D. Oelkrug. *Optical properties of oligophenylenevinylenes*. 2004. American Scientific Publishers.

Conclusion

The present work aimed at studying to main properties of natural polyphenols *i.e.*, UV-visible absorption and free radical scavenging. The idea was to provide new insights from a theoretical point of view. We have clearly demonstrated how theoretical chemistry is a powerful tool to rationalize the mechanisms of action at the molecular scale, supporting experimental results and elucidating experimental unknowns.

In chapter III, the structure UV-absorption property relationship was investigated for six depsides and two secalonic acids extracted from *Diploicia canescens*. Theoretical investigations showed that Cl-atom substitution pattern mainly affect (hypsochromic shifts) the low-energy bands. Secalonic acids proved to be promising candidates as sunscreens with respect to reference molecules (*i.e.*, avobenzone present in many cosmetic preparations). The quantum calculations showed that the absorption capacity in the UV region was attributed to the biphenyl moiety. Chemical modulations on the biphenyl ring of secalonic acid should improve those UV-screen properties.

All these theoretical absorption wavelengths were in perfect agreement with the experimental data. Using classical hybrid functionals appeared particularly efficient to rationalize UV-visible absorption properties of single polyphenols. The effects of substitution pattern were qualitative and even quantitatively well reproduced. To go further, we investigated polyphenol aggregation and the following colour modulation. This was first performed on a small model system and extended to bigger and more realistic molecular assemblies. The copigmentation process is driven by non-covalent interactions between the pigment and the copigment. *Ad equate* theoretical methods are mandatory to fully explain this phenomenon; DFT-D2 and RSH functionals (for geometry and ES energies, respectively) provides results in very good agreement with experiments. We also showed that copigmentation is driven by the electron transfer capacity from the copigment to the pigment. In bigger molecular systems, the copigment may also play an important geometrical role, constraining specific geometries for the pigment in which intramolecular charge transfers become possible. Therefore it must be stressed that a careful geometry analysis is mandatory to rationalize the properties of ES. The validation of those specific methodologies opens a new large field of investigation. Recently, Rustioni *et al.* proposed anticopigmentation effects, highlighting the competition between different copigments. A copigment may take the place of another inducing colour loss. To

theoretically establish a series of parameters correlating with binding and electron donor capacities would allow classifying copigments with respect to ability to induce anti- and pro-copigmentation effects.

Chapter IV is a study of the free radical scavenging kinetics, which was investigated with quercetin as an antioxidant of reference. Free radical can be scavenged by electron or atom transfer. The Marcus theory within the Levich-Jortner formalism was used for the former transfer process. The latter was studied within the classical transition state theory (TST) in which the tunnelling contribution was assessed by using the Skodje & Truhlar (S/T) coefficient. The free radical scavenging is a complicated process in which the key factors are (i) pre-reaction complex geometries driven by non-covalent interaction, (ii) solvent polarities, (iii) pH conditions and (iv) acid-base properties of the antioxidant.

In non-polar solvents, the atom transfer is the only possible mechanism whereas both atom and electron transfers are in competition in polar solvents. It must be stressed that electron transfer in polar solvent is possible if and only if (i) the free radical scavenger is activated by deprotonation and (ii) if the pH conditions allow this deprotonation. If both conditions are met, electron transfer appears even faster than atom transfer.

Whichever the transfer mechanism, free radical scavenging leads to the formation of radical species. Usually stabilized by π-conjugation, these species are more stable than the free radicals. Nonetheless, even if more stable, as radicals they may react in solutions. This reactivity originates new compounds and possibly pro-oxidant effects. The end of chapter IV proposes to study the oxidative coupling of stilbenoid derivatives after the free radical attack. Experiments showed that both the solvent and the oxidant drive the structure of dimers formed after oxidation. Here, the theoretical calculations fully rationalized the experimental observations. First, the existence of π-stacking complexes made of substituted stilbenoids was definitely confirmed by using DFT-D2 methods. Their geometries are profoundly influenced by (i) the solvent polarity, (ii) the substitution pattern and (iii) the nature of the oxidant. Long-range interaction is the key parameter to initiate regio-selectivity of the process. Then, the competition between the formation of ampelopsin and pallidol analogues was elucidated from both the thermodynamic and kinetic points of view. Quantum calculation showed that pallidol is the thermodynamic product while the ampelopsin is the kinetic product. Currently, our group is

studying the further step of oxidative coupling, *i.e.*, the tetramer formation from the oxidative coupling of dimers in a joint experimental and theoretical study.

This manuscript has participated in establishing recommendations for the description of polyphenol properties. Classical hybrid DFT functionals are *ad equate* at describing most of thermodynamic properties and related trends. The use of B3P86-D2 is recommended to describe all phenomena related to non-covalent interactions. The use of ωB97XD is required to describe the UV-visible properties of non-covalent complexes in which electron transfer have a key role. The use of adequately parameterized Marcus theory within the Levich-Jortner formalism is sufficient to qualitatively and quantitatively rationalize electron transfer from polyphenols to free radicals. Also the kinetics of H-atom transfer is qualitatively well evaluated.

Theoretical chemistry thus appears more than ever as a crucial tool to rationalize the numerous chemical and biological actions of natural compounds. The electronic answer to experimentalist questions was an exotic, has become an original and is now a very practical issue. It gives a new dimension to sciences of natural compounds, deeply exploring the limit of knowledge at the atomic scale. However, theoretical chemistry still proposes models that are perfectible. The method, the basis set and the formalism must be carefully chosen and are still dependent on the available computer facilities. The models proposed in this manuscript can and should be improved over the next few years. Future refinements should be the centre of interest to be developed by our group.

Throughout this manuscript, we have shown that dispersive interactions play an important role in many polyphenol-containing systems. The use of a post-SCF correction may be improved with the non-local functionals. Recently, Di Labio *et al*. have also proposed a new dispersion correction based on the definition of modified basis sets (DCP dispersion-correction potential). A systematic comparison with all new method refinements including B3P86-D2/DCP, VdW-DF, SCS-S66-MP2 and higher level methods should be considered to definitely validate B3P86-D2 as a reference functional. The parameterization of B3P86-D3 could also be envisaged even if the accuracy gain from this formalism is probably too small accounting the dramatic increase of computational time to assess DFT-D3 parameterization.

Another major refinement concerns the second main methodology proposed in this manuscript, namely the use of the Marcus framework to describe electron transfer in antioxidant

actions. To improve the quantitative description, this formalism could be improved. The solvent reorganisation could be explicitly calculated by using QM/MM methods in which the solvent is explicitly described. The second main limit is the description of the electron transfer Gibbs energy which fails at accurately describing (i) the free energy profile and (ii) the multi-pathway reaction (*i.e.*, the electron transfer from {HOMO;HOMO-n} to SOMO). The former failure may be improved by using the constrained DFT which could impose specific spin multiplicities and charges to each fragment of a complex. The last costing perspective would be to separately calculate electron transfer Gibbs energies of each pathway with multi-reference methods *e.g.*, CASPT2 or CASSCF. However, such refinements constitute a huge task in which the computational time/accuracy compromise must be reached.

Annexes

A- The Resolution of Identity (RI) approximation[57]

The calculation of four-index-two electron integrals is the most time-consuming. These integrals appear during the resolution of Coulomb and Exchange terms. For example, the Coulomb term is written in HF theory on the basis of orbitals:

$$(\mu\nu|\lambda\sigma) = \iint \varphi_\mu(r_1)\varphi_\nu(r_1)\frac{1}{r_{12}}\varphi_\lambda(r_2)\varphi_\sigma(r_2)dr_1dr_2 \qquad (A.1)$$

where r_1 and r_2 refer to electrons 1 and 2, respectively. Based on the basis of primitives functions the equation is:

$$(\mu\nu|\lambda\sigma)$$
$$= \sum_{a_\mu=1}^{A_\mu}\sum_{a_\nu=1}^{A_\nu}\sum_{a_\lambda=1}^{A_\lambda}\sum_{a_\sigma=1}^{A_\sigma} c_{a_\mu}c_{a_\nu}c_{a_\lambda}c_{a_\sigma} \int \phi_{a_\mu}(r_1)\phi_{a_\nu}(r_1)\frac{1}{r_{12}}\phi_{a_\lambda}(r_2)\phi_{a_\sigma}(r_2)dr_1dr_2 \quad (A.2)$$

The integral term is complicated to be evaluated since each individual function ϕ_a is made up of many primitive functions. Neese *et al.* have proposed to approximate these integrals by using auxiliary basis sets $\{Q\}$ since they are highly linear dependent:

$$\phi_{a_\mu}(r)\phi_{a_\nu}(r) \approx \sum_Q c_{Q,\mu\nu}Q(r) \qquad (A.3a)$$

$$\phi_{a_\lambda}(r)\phi_{a_\sigma}(r) \approx \sum_P c_{Q,\lambda\sigma}P(r) \qquad (A.3b)$$

The four-center-two-electrons integrals are thus reduced to two- and three-center-two-electrons integrals by including Eqs. (A.3) in Eq. (A.2) where the integral term becomes:

---

[57] Further details are available in *Journal of Computational Chemistry*, **2003**, 24, 1740-1747

$$(\mu\nu|\lambda\sigma) = \sum_{PQ} (\mu\nu|P)V^{-1}(Q|\lambda\sigma) \qquad (A.4)$$

with

$$(Q|P) = \iint Q(r_1)\frac{1}{r_{12}}P(r_2)dr_1dr_2 \qquad (A.5a)$$

$$(Q|\lambda\sigma) = \sum_{a_\lambda=1}^{A_\lambda} \sum_{a_\sigma=1}^{A_\sigma} c_{a_\lambda}c_{a_\sigma} \iint Q(r_1)\frac{1}{r_{12}}\phi_{a_\lambda}(r_2)\phi_{a_\sigma}(r_2)dr_1dr_2 \qquad (A.5b)$$

RI approximation significantly decreases computational time providing negligible numerical errors if the optimized auxiliary basis set is carefully chosen with respect to the used basis set. It must be stressed that RI approximation is sometimes named density fitting (DF).

B- Implicit solvent effects and electronic excited-state description[58]

Static and dynamic properties of molecular systems are of particular importance for biological systems in which the external environment (mainly the solvent) plays a crucial role. The "natural" and ideal way to model solvent is to explicitly surround the solute by the solvent molecules (first and second solvation shells). This approach dramatically increases the number of basis functions used for the MO description as well as the degrees of freedom. The direct consequence is a dramatic increase of computational time. Full explicit solvation is thus rarely used nowadays at the quantum level. One can imagine describing explicitly the first solvation shell on relatively small molecular systems, which is rather limited for most of natural compounds. Implicit solvents have been developed over the past two decades to allow taking solvent effects into account at a reasonable computational time.

1. Basic description of continuum model

The total Hamiltonian $\mathcal{H}_{tot}$ for a solute-solvent system is given by:

$$\mathcal{H}_{tot} = \mathcal{H}_{solute}(r_1) + \mathcal{H}_{solvent}(r_2) + \mathcal{H}_{int}(r_1, r_2) \qquad (A.6)$$

where $\mathcal{H}_{solute}$, $\mathcal{H}_{solvent}$ are both solute and solvent Hamiltonians, respectively. $\mathcal{H}_{int}$ is the Hamiltonian describing the interaction between the solvent and the solute. r_1 and r_2 refer to the coordinates of the solvent and the solute, respectively.

Implicit solvent models postulate that the most important solvent effects are related to electrostatic interactions between solvent and solute, which is perfectly true as far as no specific interaction exists (H-bonding and π-stacking). This electrostatic contribution can be elegantly and efficiently taken into account from classical electrostatics. In implicit models, the solvent is described by a dielectric continuum so that $\mathcal{H}_{solvent}$ vanishes. In such formalism, the solute is embedded in a cavity (shape-adapted for more recent models) surrounded by a dielectric continuum, which is characterized by its dielectric constant. The solute is described by its charge distribution ρ_M. It polarizes the continuum which in turn polarizes the solute; this effect is globally account by the reaction potential V_R, acting on the solute. In the apparent surface

---

[58] Further details are available in *Chemical Review*, **2005**, 105, 2999-3093.

charge (ASC) methods like PCM (polarizable continuum models), V_M is described by the potential induced by surface charges V_σ, calculated on the cavity surface (usually divided into tesserae to which a point charge is assigned). The total potential $V(r)$ is thus:

$$V(r) = V_M(r) + V_R(r) \qquad (A.7)$$

Even if providing all connections between the quantum and electrostatic problems is far beyond the scope of this manuscript, it is noteworthy to mention that the interaction energy (or free energy of solvation), is related to the reaction field as follows:[59]

$$E_{int} = \int \rho_M(r)V_\sigma(r)dr \qquad (A.8)$$

where: $V_\sigma(r) = \int_\Gamma \frac{\sigma(s)}{|r-s|}d^2s$, the integral being performed over the whole cavity surface;[60] σ(s) is the surface charge calculated at point s.

In the implicit solvent models, the Hamiltonian is an effective Hamiltonian given by:

$$\mathcal{H}_{tot}^{eff} = \mathcal{H}_{solute}(r_1) + H_{int}(r_1, r_2) \qquad (A.9)$$

To eliminate r_2 that has no meaning in an implicit model, the Hamiltonian is written as follows:

$$\mathcal{H}_{tot}^{eff} = \mathcal{H}_{solute} + \mathcal{V}_{int}[\mathcal{Q}(s, s')] \qquad (A.10)$$

where $\mathcal{Q}(r, r')$ is the solvent-response function, which allows connecting the potential in different points of the cavity. It allows providing another formulation of the solute-solvent interaction energy:

$$G = \frac{1}{2}\int_\Gamma \int_\Gamma V(s)\mathcal{Q}(s, s')V(s')dsds' \qquad (A.11)$$

---

[59] This formulation appears rather trivial, but the rigorous demonstration is not.

[60] The resolution is self-consistent as the potential depends on ρ_M.

Many different implicit solvent models have been developed based on different formalisms (*e.g.*, multipole expansion MPE, apparent surface charge ASC or generalized born – GB-methods). The two most used being COSMO (COnductor-like Screening MOdel) and PCMs, mainly IEFPCM.

2. Non-equilibrium, time-dependent DFT and continuum models[61]

The combination of continuum models with excited-state (ES) calculation methods has become very challenging over the past years. Due to the success of TD-DFT, allowing a very competitive accuracy/computational ratio, the application of PCM together with TD-DFT has deserved particular attention. The effective Hamiltonian (Eq. A.10) is defined in a static way, while electronic vertical transition is a dynamical problem. According to the TD-DFT formalism, the PCM contribution to the time dependent KS equation explicitly depends on the electron density variation associated with the electronic transition ($\delta\rho_{el}$):

$$v_{non-eq}^{PCM}[\delta\rho_{el}(r)] = \int_{\Gamma} \int_{\Gamma} \int_{R^3} \frac{\delta\rho_{el}(r',\omega)}{|s'-r'|} Q(\varepsilon_{opt}, s, s') \frac{1}{|s-r|} dr'dsds' \qquad (A.12)$$

for non-equilibrated solution *i.e.*, only the environment dynamic (electronic) response (fast degrees of freedom are equilibrated) is equilibrated.[62] This corresponds to the vertical transition, which is usually enough when tackling absorption properties.

And:

$$v_{eq}^{PCM}[\delta\rho_{el}(r)] = \int_{\Gamma} \int_{\Gamma} \int_{R^3} \frac{\delta\rho_{el}(r',\omega)}{|s'-r'|} Q(\varepsilon, s, s') \frac{1}{|s-r|} dr'dsds' \qquad (A.13)$$

for equilibrated solvation *i.e.*, molecular relaxation of the solvent (slow degrees of freedom).[63]

---

[61] Further details are available in *Chemical Review*, **2005**, 105, 2999-3093.

[62] For non-equilibrated solution, the solvent-response depends on the optical dielectric constant ε_{opt}.

[63] Contrary to non-equilibrated solution, the solvent response of equilibrated solution depends on the dielectric constant ε.

Here, the response of the solvent to the excitation is obtained using a transition density[64] and not a state density. The calculation of ES with continuum model is a complex non-linear problem. The solvent reaction field depends on the variation of the solute density along the electronic excitation while the electronic excitation in turn depends on the solvent reaction field.

Different approaches have been recently developed to overcome this weakness. They may be divided into two families that are state-specific (SS) and linear-response (LR) methods. SS methods solve the effective Schrödinger equation for each state of interest. LR-methods aim at directly calculating the vertical excitation energies: the time-dependent wave function is described by a linear perturbation on the time-independent wave function. LR-methods are not discussed in this annex.

In SS-PCM,[65] the solvent contribution to the vertical electronic transition (ΔG_{abs}) can be simply calculated by:

$$\Delta G_{abs} = \mathcal{G}_{non-eq}^{ES} - \mathcal{G}_{eq}^{GS} \qquad (A.14)$$

where $\mathcal{G}_{eq}^{GS}$ is the equilibrium solvation free energy of the GS and $\mathcal{G}_{non-eq}^{ES}$ is the ES non-equilibrium solvation free energy. The former is easily achieved by a classical PCM calculation on the GS. The latter is calculated using:

$$\mathcal{G}_{non-eq}^{ES} = \frac{1}{2}\sum_i q_{i,f}^{ES}V_{i,\rho}^{ES} + \left(\sum_i q_{i,s}^{GS}V_{i,\rho}^{ES} - \frac{1}{2}\sum_i q_{i,s}^{GS}V_{i,\rho}^{GS}\right)$$
$$+ \frac{1}{2}\left(\sum_i q_{i,s}^{GS}V_{i,f}^{ES} - \sum_i q_{i,s}^{GS}V_{i,f}^{GS}\right) \qquad (A.15)$$

where $q_{i,f}$, $q_{i,s}$ are the polarization charges relative to the "fast" and "slow" solvent degrees of freedom. $V_{i,f}$ is the potential corresponding to the $q_{i,f}$ polarization charge. $V_{i,\rho}^{GS}$ and $V_{i,\rho}^{ES}$ are the

---

[64] This depends on the GS density and the calculated corrections to density and orbitals due to the GS→ES electronic transition.

[65] SS-PCM formalism is fully described in *Journal of Chemical Physics*, **2006**, 125, 054103-1-9 and *Computational strategies for spectroscopy: from small molecules to nano systems*; **Chap. I**, John Wiley & Sons, **2012**

potential generated by the GS and ES densities, respectively. The GS density is thus explicitly involved in the expression of $\mathcal{G}_{non-eq}$.

Without entering into the mathematical details, the SS-PCM iterative multistep procedure can be sum up as follow:

(1) Energy calculation of GS within the classical PCM approach *i.e.*, including the free energy of solvation $\mathcal{G}_{eq}^{GS}$.

(2) TD-DFT calculation to evaluate all ES within a classical PCM approach.

(3) SS response calculation for a given ES according to Eq. (A.14) giving a first set of polarization charges.

(4) TD-DFT calculation in the presence of the solvent defined by the corresponding first set of polarization charges issued from (3), leading to an updated (and improved according to variational principle) ES density.

(5) Iterative procedure until convergence.

(6) Addition of the solvation correction to the ES energy obtained *in vacuo.*

Contents

Figures

Schemes

Chapter I

Chapter II

Chapter III

Chapter IV

Tables

Articles

Accepted or published

- Anouar, E.; Calliste, C. A.; Kosinova, P.; <u>Di Meo, F.</u>; Duroux, J.-L.; Champavier, Y.; Marakchi, K.; Trouillas, P. Free radical scavenging properties of guaiacol Oligomers: A Combined experimental and quantum study of the guaiacyl-moiety role, J. Phys. Chem. A 2009, 113, 13881-13891.
- Košinová, P.; <u>Di Meo, F.</u>; El Hassane, A.; Duroux, J.-L.; Trouillas, P. H-atom acceptor capacity of free radicals used in antioxidant measurements (e.g. DPPH and peroxyradicals ROO$^\bullet$ and LOO$^\bullet$), Int. J. Quantum Chem. 2009, 111, 1131-1142.
- Millot, M.; <u>Di Meo, F.</u>, Tomasi, S.; Boustie, J.; Trouillas, P. Photoprotective capacities of lichen metabolites: A joint theoretical and experimental study, J. Photochem. Photobiol. B, 2012, 111, 17-26
- <u>Di Meo, F.</u>; Sancho-Garcìa, J.-C.; Dangles, O.; Trouillas, P. Highlights on anthocyanin pigmentation and copigmentation: a matter of flavonoid π-stacking complexation to be described by DFT-D, J. Chem. Theo. Comp., 2012, 8, 2034-2043.
- Nave, F.; Bràs, N. F.; Cruz, L.; Teixeira, N; Mateus, N.; Galembeck, S. E.; <u>Di Meo, F.</u>; Trouillas, P.; Dangles, O.; De Freitas, V. The influence of a flavan-3-olic substituent in the copigmentation ability of anthocyanins towards vinylcatechin dimers and procyanidins, J.Phys. Chem B, 2012, 116, 14089-14099
- Ruiz, A.; Coro, J.; Almagro, L.; Ruiz, J. A.; Molero, D.; Maroto, E. E.; Filippone, S.; Herranz, M. A.; Martìnez-Àlvarez, R.; Sancho-Garcìa, J.-C.; <u>Di Meo, F.</u>; Suàrez, M.; Martìn, N.; Diastereoselective synthesis of C60/Steroid conjugates, J. Org. Chem., 2013, *DOI: 10.1021/jo302528t*.
- <u>Di Meo, F.</u>; Steel, M.; Picard, N.; Marquet, P.; Duroux, J.-L; Trouillas, P. Acylglucuronide in alkaline conditions: Migration vs. Hydrolysis, J. Mol. Mod., 2013, *DOI: 10.1007/s00894-013-1790-3*. [66]
- <u>Di Meo, F.</u>; Lemaur, V.; Cornil J.; Lazzaroni, R.; Duroux, J.-L; Olivier, Y.; Trouillas, P. Free radical scavenging by natural polyphenols: Atom versus Electron transfer, J. Phys. Chem. A, 2013, *DOI: 10.1021/jp3116319*.
- Velue, S.* & <u>Di Meo, F.*</u>; Sancho-Garcìa, J.-C.; Trouillas, P.; Weber, J.-F. Regio- and Stereoselective synthesis of oligostilbenoids: The Theoretical Point of View using Refinements of Density Functional Theory, J. Nat. Prod., 2013, DOI: 10.1021/np300705p - *These authors contributed equally.*

In Preparation

- Gazak R.; <u>Di Meo F.</u>; Biedermann D.; Trouillas, P.; Kren, V. Silybin isomerization: a matter of solvent effect, *In preparation*.[67]
- <u>Di Meo, F.</u>; Trouillas, P. ; Magdelaine, C. ; Nizou, A.; Funalot, B.; Sturtz, F.; Lienhardt, A.; Lia-Baldini, A.-S.; Structural Elucidation of the Calcium-Sensing Receptor highlighting spatial location of mutations observed in hyper- and hypocalcaemic patients, *In preparation*.[68]

---

[66] This project is not related to the main project of my PhD. In this paper, we compared both alkaline hydrolysis and transacylation reactions from the theoretical point of view.

[67] This project is directly related to my PhD since it focuses on the reactivity of natural polyphenol. The stereo-isomerization of silybin A and B is rationalized from both experimental and theoretical points of view.

[68] This project is not related to the main project of my PhD. In this paper, we elucidated the three-dimensional structure of the calcium-sensible receptor by using homology modeling and molecular dynamics calculations. Then the locations of several mutations are studied and compared to experimental observations.

Le dernier mot de ce manuscrit de thèse sera Kamoulox.

Abstract

Nature provides a huge armamentarium of original compounds having a broad range of activities. The deep understanding of the physico-chemical processes responsible for their biological actions is of great importance to improve these actions. The present PhD focuses on UV-visible and antioxidant properties of natural polyphenols from a theoretical point of view. Density functional theory (DFT) was mainly used with modern refinements.

Chapter I is a presentation of natural compounds and related properties including pigmentation and antioxidant properties. Chapter II presents some theories on which this work is based. In chapter III UV-visible absorption of single polyphenols is studied with time-dependent (TD)-DFT; classical hybrid functional being used. Then, the role of non-covalent interactions is investigated with a combined DFT-D/RSH-functional methodology to rationalize colour modulation in copigmentation complexes. In chapter IV, the oxidative mechanisms of polyphenols are studied. The kinetics of free radical scavenging is evaluated and described with new theoretical protocols. The competition between atomic and electron transfer is discussed. In another section, the formation of stilbenoid oligomers by oxidative coupling is studied, highlighting the crucial role of π-π complexation on regio- and stereoselectivity of these reactions.

Keywords: DFT – POLYPHENOLS – π-STACKING INTERACTION – UV-VISIBLE ABSORPTION – REACTIVITY – FREE RADICAL SCAVENGING

Approches moléculaires et supramoléculaires sur la réactivité et l'optoélectronique des polyphénols naturels

La Nature est une fantastique source de composés originaux ayant un large champ d'activité biologique. La compréhension des phénomènes physico-chimiques correspondants est capitale afin d'améliorer les propriétés thérapeutiques des composés naturels. Cette thèse s'intéresse théoriquement aux propriétés d'absorption UV/Vis et antioxydantes de polyphénols naturels. La théorie de la fonctionnelle de la densité (DFT) et ses récentes améliorations ont été principalement utilisées.

Le chapitre I est une présentation des composés naturels et de leurs propriétés incluant les phénomènes de pigmentation et les propriétés antioxydantes. Le chapitre II présente les théories utilisées dans ce travail. Dans le chapitre III, les propriétés d'absorption UV/Vis de polyphénols simples sont étudiées en utilisant les fonctionnelles hybrides classiques de la DFT dépendante du temps (TD-DFT). Ensuite, le rôle des interactions non-covalentes dans la modulation de la couleur par le phénomène de copigmentation est élucidé en combinant la DFT-Dispersive et fonctionnelles RSH (range-separated hybrid). Dans le chapitre IV, les mécanismes oxydatifs des polyphénols sont étudiés. La cinétique du piégeage des radicaux libres est décrite et évaluée à l'aide de nouveaux protocoles théoriques. La compétition entre le transfert d'atome et d'électrons est alors discutée. Dans une autre section, la formation des oligomères de stilbenoïdes par un couplage oxydatif est étudiée, soulignant le rôle capital de l'empilement $\pi-\pi$ dans la régio et la stéréosélectivité de ces réactions.

Mot-clés : DFT – POLYPHENOLS – COMPLEXE π - ABSORPTION UV/VISIBLE – REACTIVITE – PIEGEAGE DES RADICAUX LIBRES